NASA
Technical
Paper
2256

June 1984

Natural Laminar Flow Experiments on Modern Airplane Surfaces

Bruce J. Holmes,
Clifford J. Obara,
and Long P. Yip

NASA

NASA Technical Paper 2256

1984

Natural Laminar Flow Experiments on Modern Airplane Surfaces

Bruce J. Holmes
Langley Research Center
Hampton, Virginia

Clifford J. Obara
Kentron International, Inc.
Hampton, Virginia

Long P. Yip
Langley Research Center
Hampton, Virginia

National Aeronautics and Space Administration

Scientific and Technical Information Branch

Use of trademarks or names of manufacturers in this report does not constitute an official endorsement of such products or manufacturers, either expressed or implied, by the National Aeronautics and Space Administration.

CONTENTS

SUMMARY 1

INTRODUCTION 1

SYMBOLS AND ABBREVIATIONS 3

REVIEW OF PAST NATURAL LAMINAR FLOW RESEARCH 5

AIRPLANE DESCRIPTIONS AND CORRESPONDING EXPERIMENTS 7
Airplanes 7
Rutan VariEze 8
Rutan Long-EZ 8
Rutan Laser Biplane Racer 9
Gates Learjet Model 28/29 Longhorn 9
Cessna P-210 Centurion 9
Beech 24R Sierra 9
Bellanca Skyrocket II 9
Beech T-34C gloves 10
Testing Procedures 10
Sublimating chemical detection of boundary-layer transition 10
Acoustic detection of boundary-layer transition 11
Other testing procedures 11

RESULTS 12
Wind-Tunnel VariEze Experiments 12
Transition locations 12
Effect of fixed transition on canard 12
Flight Experiments 13
Rutan VariEze 13
Rutan Long-EZ 14
Rutan Laser Biplane Racer 15
Gates Learjet Model 28/29 Longhorn 16
Cessna P-210 Centurion 16
Beech 24R Sierra 17
Bellanca Skyrocket II 17
Beech T-34C gloves 19

DISCUSSION 20
Transition Locations 20
Effects of Precipitation and Cloud Particles 21
Effects of Fixed Transition 22
Propeller Slipstream Effects 23
Waviness 24
Sweep Effects 24
Insect Debris Contamination 25

CONCLUSIONS 26

APPENDIX - SURFACE WAVINESS ON RESEARCH MODELS 28

REFERENCES 48

TABLES 52

FIGURES 73

SUMMARY

Flight and wind-tunnel natural laminar flow experiments have been conducted on various lifting and nonlifting surfaces of several airplanes at unit Reynolds numbers between 0.63×10^6 ft^{-1} and 3.08×10^6 ft^{-1}, at Mach numbers from 0.1 to 0.7, and at lifting surface leading-edge sweep angles from 0° to 63°. The airplanes tested were selected to provide relatively stiff skin conditions, free from significant roughness and waviness, on smooth modern production-type airframes. The observed transition locations typically occurred downstream of the measured or calculated pressure peak locations for the test conditions involved. No discernible effects on transition due to surface waviness were observed on any of the surfaces tested. None of the measured heights of surface waviness exceeded the empirically predicted allowable surface waviness. Experimental results consistent with spanwise contamination criteria were observed. Large changes in flight-measured performance and stability and control resulted from loss of laminar flow by forced transition. Simulated rain effects on the laminar boundary layer caused stick-fixed nose-down pitch-trim changes in two of the airplanes tested. No effect on transition was observed for flight through low-altitude liquid-phase clouds. These observations indicate the importance of fixed-transition tests as a standard flight testing procedure for modern smooth airframes. The results taken as a whole indicate that significant regions of natural laminar flow exist and that this boundary-layer behavior is more durable and persistent on certain modern practical production airplane surfaces than previously expected.

INTRODUCTION

In decades past, the achievement of extensive regions of natural laminar flow (NLF) was sought as a means of increasing airplane speed and range. However, early methods of wing manufacture and maintenance produced rough, wavy surfaces; therefore, the successful application of laminar-flow airfoils for increased performance on production aircraft was never achieved.

In recent years, two major trends in airplane fabrication and operations have developed which are favorable to NLF. First, modern airframe construction materials and fabrication methods offer the potential for the production of aerodynamic surfaces without critical roughness and waviness. These modern techniques include composites, milled aluminum skins, and bonded aluminum skins. The second modern trend favorable to NLF is the lower range of both chord and unit Reynolds numbers at which current high-performance business airplanes operate. Most of these airplanes cruise at unit Reynolds numbers less than 1.5×10^6 ft^{-1} and at chord Reynolds numbers less than 20×10^6. Therefore, the achievement of NLF-compatible surface quality is relatively easy. These lower Reynolds numbers result from the shorter airfoil chord lengths (wing loadings and aspect ratios are larger) and from the much higher cruise altitudes for modern airplanes.

It is significant that NLF has been a practical reality for one category of aircraft - sailplanes. The achievement of laminar flow on sailplanes has been facilitated by the lower chord Reynolds numbers ($<4 \times 10^6$ typically) at which they operate, relative to most power airplanes, and by the use of composite construction methods to produce smooth complex shapes.

This report presents the results of several NLF wind-tunnel and flight experiments recently conducted by NASA to determine the maximum Reynolds number, Mach number, and sweep-angle ranges over which the smoothness of modern, practical airframe construction techniques fail to meet requirements for NLF in favorable pressure gradients. These experiments were designed to address the issues of achievability and maintainability of NLF on production-quality airframe surfaces in typical operating environments. The significant factor that distinguishes these recent flight experiments from those of the 1930's and 1940's is the difference in preflight preparation of the surfaces tested. The recent experiments were conducted on production-quality surfaces, that is, on surfaces which received no modification by filling and sanding to meet the airfoil contour or waviness requirements for NLF (minor exceptions are described in the text).

Full-scale flight and wind-tunnel experiments were conducted with the following specific objectives:

1. Examine the effect of increasing Reynolds numbers and Mach numbers on laminar flow for production airframe surfaces.

2. Observe transition locations on a large variety of aerodynamic surfaces (including wings, fuselage nose, wheel fairings, horizontal and vertical stabilizers, and propeller spinner and blade airfoil surfaces), and, where possible, correlate measured transition with empirical predictions.

3. Measure the effect of total loss of laminar flow (fixed transition due to transition grit or simulated rain) on airfoil behavior, airplane performance, and stability and control.

4. Observe the effect of a propeller slipstream on laminar flow.

5. Document the effect of flight through clouds on transition.

6. Observe the practical effects of wing leading-edge sweep on spanwise contamination of the attachment line.

7. Investigate the nature of insect contamination on an NLF airfoil in flight.

Eight different airplane types were used in the flight experiments: two high-aspect-ratio canard, pusher-propeller configurations (the Rutan VariEze and Long-EZ); a large negative-stagger biplane, tractor-propeller configuration (the Rutan Biplane Racer); a business jet (Gates Learjet Model 28/29 Longhorn); two low-wing airplanes (Beech 24R Sierra and Bellanca Skyrocket II); and a high-wing single-engine general-aviation airplane (Cessna P-210 Centurion). The eighth airplane, a Beech T-34C, was equipped with laminar-flow gloves on which experiments were conducted to provide additional data to support the findings of the other flight experiments. The wind-tunnel experiments used only the VariEze airplane.

Based on the results of these flight and wind-tunnel experiments, this paper provides a new appreciation for the achievability and maintainability of NLF on modern airplane surfaces at chord Reynolds numbers representative of business and commuter transport aircraft. The implications of these results to further airplane designs, flight testing procedures, and further studies are also discussed.

SYMBOLS AND ABBREVIATIONS

a	airfoil mean-line designation
avg	average
BL	butt line
b	airplane wing span, ft
C_D	airplane drag coefficient
C_d	section drag coefficient
C_L	airplane trimmed lift coefficient
C_{L_α}	lift-curve slope, deg^{-1}
C_ℓ	section lift coefficient
C_m	airplane pitching-moment coefficient (referenced to $\bar{c}/4$)
C_p	pressure coefficient, $(p_t - p)/q_\infty$
c	local chord, ft
$\bar{c}$	mean aerodynamic chord, in.
d	propeller diameter, ft
FS	fuselage station
h	indicated double-amplitude wave height, in.
h_d	density altitude, ft
J	advance ratio, V/nd
L.E.	leading edge
L.S.	lower surface
M	Mach number
n	propeller rotational speed, rps
P_s	vapor pressure, mm Hg
p	static pressure, psf
p_t	total pressure, psf
q	dynamic pressure, psf
R	free-stream unit Reynolds number, ft^{-1}

R_c chord Reynolds number

R_θ attachment-line boundary-layer momentum thickness Reynolds number (see eq. (1))

r radius, ft

S lifting surface reference area, sq ft

s surface length, in.

T temperature, °C

t/c wing thickness ratio

U.S. upper surface

u/u_e local-to-edge velocity in boundary layer

V free-stream true airspeed, knots or mph

V_c calibrated airspeed (local flow field and indicator errors removed), knots or mph

V_i indicated airspeed, knots or mph

WL water line

x/c location in percent local chord

$(x/\ell)_t$ transition location in percent body length

y semispan location, ft

z vertical dimension, ft

α angle of attack, deg (relative to longitudinal reference axis)

δ boundary-layer thickness, in.

δ_e elevator deflection, deg (positive trailing edge down)

η nondimensional semispan position, $\frac{y}{b/2}$

Λ sweep angle, deg

λ wavelength, in.

Subscripts:

a allowable

c canard

L lower

le	leading edge
max	maximum
min	minimum
t	transition location
U	upper
w	wing
∞	free stream

Notation:

i.d.	inside diameter
NLF	natural laminar flow
o.d.	outside diameter
psf	pounds (force) per square foot

REVIEW OF PAST NATURAL LAMINAR FLOW RESEARCH

The achievement and maintenance of NLF are the two principal challenges to its use for performance improvement on airplanes today. Natural laminar flow is achieved on airfoil surfaces with small sweep angles (≈15°) by designing long runs of favorable pressure gradients (accelerating flow) which limit the growth of two-dimensional disturbances (Tollmien-Schlichting (T-S) waves) in the boundary layer. The growth of T-S waves can be aggravated, on the other hand, by the effects of surface waviness on local pressure gradients and on boundary-layer velocity profiles. These effects reduce boundary-layer stability and can lead to premature transition. Thus, favorable pressure gradients "protect" the laminar boundary layer from the effects of limited amounts of surface waviness by counteracting the destabilizing influences of waviness. Similar influences govern the critical sizes of other two-dimensional protuberances such as steps and gaps in laminar boundary layers. On wings with significant sweep, NLF is achieved by compromise between the above pressure distribution consideration and the conflicting design requirement for less favorable pressure gradients which limit the growth of three-dimensional disturbances (crossflow vortices) in the boundary layer. The growth rate of crossflow vortices is rapid in the region of rapidly falling pressure near the leading edge. It is not presently well understood how the interaction between crossflow vortices and T-S waves affects transition on swept wings at free-stream conditions of interest for business, commuter, or airline transport airplanes. The technical challenge to the successful design of such airplane wings will be to meet both of the conflicting pressure gradient design requirements for avoidance of these two- and three-dimensional instabilities.

The maintenance of wing surface conditions compatible with NLF requires that the surfaces be kept free, in an operating environment, from critical amounts of surface contamination (e.g., insect debris or ice), free-stream disturbances (e.g., noise and turbulence), and surface damage. Compared with phenomena affecting the achievability of NLF, less is understood about the maintainability of NLF under the wide ranges of

Reynolds numbers, Mach numbers, meteorological conditions, flight profiles, and aircraft configurations which characterize the potential applications for NLF. It is generally true, however, that ease in maintenance of NLF surfaces improves as Reynolds number decreases. In summary, the critical issues concerning the practicality of NLF for drag reduction are twofold: (1) Can practical production surfaces meet the roughness and waviness requirements for achievement of NLF under high-speed conditions, and (2) can laminar-flow benefits be maintained in typical aircraft operating environments in a cost-effective manner.

Past research left a mixture of positive and negative conclusions concerning these questions. A significant consensus from early research (circa 1950) was that the airframe surface quality required for NLF could not be achieved in the metal airframe mass production methods of that time. (See ref. 1, chapter 5.) Close examination of those fabrication methods reveals the shortcomings to have been excessive waviness between ribs and stringers, excessive step heights or gap widths at skin joints, and excessive heights of protuberances from certain riveting techniques (e.g., press-countersunk or dimpled rivets). Previous NLF flight experiments (refs. 2 to 26) in which transition location and/or section drag were determined are summarized in table 1. These experiments included both unprepared (production) surfaces, specifically prepared (filled and sanded) surfaces, and airfoil gloves. Because of the fabrication shortcomings noted above, the experiments on the production quality surfaces (refs. 7, 9, 11, 16, 18, 21, 23, and 26) of that period resulted in little or no laminar flow. The single exception was the apparent extensive laminar flow achieved on the filled and smoothed production plywood wings of the Heinkel He.70 reported in reference 13. On the specially prepared surfaces and on gloves (see table 1), transition locations and airfoil performance typically closely matched theoretical predictions and low-turbulence, wind-tunnel-model test results. The successes of the prepared and gloved surface tests provided the initial guidance for development of criteria for allowable waviness as well as for allowable two- and three-dimensional protuberance heights. Development of these criteria was strongly based on wind-tunnel research as well. A summary of these criteria is presented in reference 27 (also see appendix). In general, these criteria provide conservative guidance for the manufacture of NLF surfaces. This conservatism stems from their development origins in wind tunnels where "stream disturbances may exacerbate roughness problems" (ref. 28). In the past, the conservatism may have been partly responsible for the perception that NLF would be very difficult to achieve even on modern production surfaces. This perception was probably heightened by the relatively high unit Reynolds number range, $R_c > 2 \times 10^6$ ft^{-1}, for the World War II high-performance fighters on which early NLF applications were attempted; such free-stream conditions make the laminar boundary layer very sensitive to surface imperfections and insect contamination.

Even when the proper surface quality can be achieved, a concern which remains the subject of much research is the effect of operating environments on NLF maintainability. Past research has increased our understanding of some of the physical transition phenomena resulting from exposure of laminar boundary layers to vibration, atmospheric particles (ice crystals), turbulence, and noise. Reference 28 is a summary of much of this past work. The literature concludes that airframe vibration does not significantly influence boundary-layer transition for many important practical applications (refs. 27 and 28). In flight, there have been no discernible effects observed of atmospheric turbulence on boundary-layer transition (refs. 2 to 4, 8, and 28). Studies on the effects of atmospheric particles (refs. 27 and 28) have identified the potential for significant loss of laminar flow on swept-wing laminar-flow-control airplanes during flight through high-altitude (stratospheric) ice-crystal clouds. At lower altitudes, where liquid-phase cloud particles exist,

little research has been done to determine the influence of such cloud particles on laminar flow of swept or unswept wings. Studies of the influence of noise on boundary-layer transition have shown the potential for loss of laminar flow due to turbine-engine and afterburner noise impingement on laminar surfaces (refs. 27 and 28). Limited evidence exists that engine/propeller noise on piston-driven airplanes may slightly affect transition position on NLF surfaces (ref. 10). The literature is not conclusive on the operational seriousness of insect contamination and propeller slipstream disturbances to laminar flow.

AIRPLANE DESCRIPTIONS AND CORRESPONDING EXPERIMENTS

Airplanes

Eight airplanes were studied in these tests. Seven of the airplanes utilized in the flight experiments were selected because of smooth skin surface conditions existing on all or portions of the airframes. The eighth airplane utilized NLF gloves (as opposed to a production-quality wing surface). The Rutan VariEze, Long-EZ, and Laser Biplane Racer, and the Bellanca Skyrocket airplanes were constructed of composite fiberglass or carbon-fiber skins over full-depth foam core or aluminum honeycomb sandwich structures. The Gates Learjet Model 28/29, Cessna P-210 Centurian, and Beech 24R Sierra airplanes were constructed of aluminum structures with bonded, milled, or flush riveted skins. Waviness measurements were made on some of the surfaces of five of these airplanes. (See appendix.) The eighth airplane was a Beech T-34C airplane fitted with laminar-flow airfoil gloves on the left wing; these gloved sections were used to develop boundary-layer transition measuring techniques and for transition measurements in the propeller slipstream to support related experimental results.

A wind-tunnel investigation was conducted in the Langley 30- by 60-Foot Tunnel to study the aerodynamic characteristics of an advanced canard configuration airplane, the VariEze (see ref. 29). The experiments specifically provided data on the following: (1) Transition locations on the wing, winglet, and canard; and (2) the effect of fixed transition on canard aerodynamics caused by either artificial roughness or by water-spray simulated rain.

Table 2 is a listing of descriptive photographs, drawings, unique airframe features and construction, experiments conducted, and test conditions for each airplane. The flight experiments for all airplanes included, as a minimum, visual observation of transition locations for various airframe components. Other experiments included studies of the effects of fixed boundary-layer transition on the performance and maximum lift of the Bellanca Skyrocket, Rutan VariEze, and Rutan Long-EZ airplanes; fixed-transition effects on stability and control were studied in the VariEze and Long-EZ. Some of the airplanes utilized more extensive flight-test instrumentation than others. For example, chordwise pressure measurements and airfoil wake surveys on the Skyrocket provided section lift and drag data, respectively. Boundary-layer rakes provided measurements of laminar-flow behavior as affected by propeller slipstream on the Skyrocket, and hot-film sensors provided similar information for the Beech T-34C.

Rutan VariEze.- Flight and wind-tunnel experiments were conducted with a pusher-propeller, two-place airplane type with a high-aspect-ratio canard. (See fig. 1.) The airplane physical characteristics and design coordinates are presented in tables 3 and 4. The flight-test airplane is shown in figure 2. The only significant difference between the full-scale wind-tunnel model and the flight article was the

installation of an outboard leading-edge droop on the flight-test airplane. Both airframes were constructed using composite structures of full-depth foam core and fiberglass skins. The airfoil surfaces on the wind-tunnel model were filled and sanded to conform accurately to the airfoil design contours.

Both the wind-tunnel and flight experiments with this configuration included visual determination of transition on the wing, winglet, and canard surfaces, and measurement of the effect of fixed transition (using the method of ref. 30) of wing, winglets, and canard on airplane performance and stability and control. The flight experiments included observation of the effect of flight through clouds on boundary-layer transition (using acoustic transition detection). The calibrated airspeed range of the flight tests was from 65 to 148 knots. Flight transition data using a sublimation technique were taken at a unit Reynolds number of 1.4×10^6 ft^{-1}.

Static-force data and boundary-layer flow visualization data were collected with the wind-tunnel model mounted on an external balance system in the Langley 30- by 60-Foot Tunnel as shown in figure 3. The canard mount was isolated from the model by an internal strain-gage balance, and canard force data were collected simultaneously with model force data. Tests were conducted over a range of angle of attack from -6° to 40° and a range of sideslip from -15° to 15°. The nominal dynamic pressure of the tests was 10.5 psf which corresponds to a unit Reynolds number of 0.625×10^6 ft^{-1}.

Chordwise pressure distribution data were recorded from four spanwise stations on the canard at $\eta = 0.26$, 0.53, 0.79, and 0.95. The effect of rain was simulated in the wind tunnel by water spray from a horizontal airfoil-shaped boom located ahead of the canard as diagrammed in figure 4. Nozzles pointed downstream and located on the boom sprayed water droplets of about 200-μm volume mean diameter at a total flow rate of 1 gal/hr at 60 psi. The boom span of about 6 ft covered the right canard semispan. The height of the boom was varied such that water spray enveloped the canard throughout the angle-of-attack range.

Rutan Long-EZ.- Flight experiments were also conducted on a two-place, pusher-propeller airplane type similar to the VariEze. The airplane configuration utilized a high-aspect-ratio canard with different wings and winglets than the VariEze. Two different Long-EZ airplanes were tested to verify the repeatability of the transition results. The only differences in these airplanes were the size of wheel fairing used to aerodynamically fair the main wheels and the size and shape of the rudder surfaces. Figure 5 contains a sketch of the geometry of these airplanes as designed, and table 5 is a list of the detailed geometric characteristics. Figure 6 is a photograph of one of the two Long-EZ airplanes tested. The design coordinates for the NLF airfoil on the wing and winglets are given in table 6. The canard airfoil is identical to that of the VariEze (coordinates given in table 4). The composite airframe was built using full-depth foam core with fiberglass skins.

The experiments conducted with this airplane included visual observations of transition on the wing, winglet, canard, fuselage nose, and wheel fairings. In addition, the effect of fixed transition on airplane performance and stability and control was determined. The indicated airspeed range for these tests was 65 to 158 knots at density altitudes of 4700 to 7500 ft. The maximum unit Reynolds number during testing was 1.51×10^6 ft^{-1}. When only V_i was available for data reduction purposes, it was assumed that the position error was zero.

Rutan Laser Biplane Racer.- A single-place biplane with large negative-stagger and a tractor-propeller (figs. 7 and 8) was tested in flight. Detailed physical

characteristics of the airplane are shown in table 7. The wing airfoil design coordinates are given in table 8. The composite airframe was built using full-depth foam core with fiberglass skins on the forward wing and graphite skins on the aft wing. Experiments conducted with this airplane included determination of transition locations on portions of the lower (forward) and upper (aft) wings both inside and outside of the propeller slipstream. The indicated airspeed for these tests was 165 knots at a density altitude of 10 000 ft. The corresponding unit Reynolds number during these tests was 1.38×10^6 ft^{-1}.

Gates Learjet Model 28/29 Longhorn.- Higher speed flight experiments were conducted with a twin-engine, turbojet, 10-seat business airplane. (See fig. 9.) The wing was constructed of integrally stiffened milled aluminum skins with leading-edge contour modifications made of sanded filler material. Aircraft physical details are presented in table 9. Experiments conducted with this airplane included visual determination of transition locations on the wing and winglet at high subsonic Mach numbers. The Mach number range for these tests was 0.55 to 0.70 at density altitudes of 15 500 to 16 500 ft. The maximum unit Reynolds number during testing was 3.08×10^6 ft^{-1}.

Cessna P-210 Centurion.- The pressurized six-passenger business airplane shown in figure 10 was utilized for transition measurements on conventional metal surfaces. Physical characteristics of this single-engine, retractable-gear airplane are presented in table 10. The wing incorporates an NACA 64-series airfoil; the horizontal tail uses a symmetric NACA airfoil varying in thickness from 5 to 9 percent. The airframe was constructed of riveted aluminum skins, ribs, and stringers. A limited amount of body-putty filling and sanding was done on half of the region of the left wing, which was painted dark to facilitate sublimating chemical observations. The filling and sanding illustrated in figure 11 were done to reduce surface roughness and waviness in the region of a spanwise row of flush dimpled rivets near the leading edge. Experiments conducted with this airplane included observations of transition locations on the dark portion of the left wing, on the horizontal stabilizer, and on the propeller spinner. The calibrated airspeed range for these tests was 139 to 154 knots. The maximum unit Reynolds number during testing was 1.48×10^6 ft^{-1}.

Beech 24R Sierra.- Flight experiments were conducted with the four-seat, low-wing, single-engine, retractable-gear airplane shown in figure 12. Geometric details are presented in table 11. The wing design incorporates an NACA 63-series airfoil. The propeller uses a Clark Y airfoil. The bonded-aluminum-skin outboard portion of the wing was selected for sublimating chemical transition visualization. In addition, transition observations were made on the vertical tail and on the propeller. The calibrated airspeed for these tests was 133 knots, the propeller was operating at 2700 rpm, and the maximum unit Reynolds number during testing was 1.38×10^6 ft^{-1}.

Bellanca Skyrocket II.- Detailed data on an NACA 63_2-215 NLF airfoil was obtained during flight experiments conducted with the high-performance, single-engine, retractable-gear airplane shown in figure 13. Geometric details are presented in table 12. The airframe was built of fiberglass, aluminum-honeycomb composite sandwich structure. Experiments with the Skyrocket include visual determination of wing transition locations, including the effect of propeller slipstream. A scanning pressure measurement system was utilized to measure airfoil wake profiles for section drag calculations, chordwise static pressures for analysis of section lift and pressure distributions, and boundary-layer velocity profiles inside and outside the propeller slipstream. Figure 14 illustrates the instrumentation installation. A detailed description of these experiments is contained in reference 31. The maximum calibrated airspeed for these tests was 176 knots for a maximum unit

Reynolds number of 1.90×10^6 ft^{-1}. During the observations of propeller slipstream effects on the laminar boundary layer, the propeller was operating at 1800 rpm.

Beech T-34C gloves.- The flight experiments on this two-place, low-wing, single-turbine-engine training airplane were conducted on gloves fabricated with smooth surfaces to support laminar flow. Transition detection experiments were conducted utilizing glue-on, surface-mounted, hot-film transition detectors. The hot films were mounted both inside and outside the propeller slipstream; the high-frequency response of these sensors permitted observation of the time-dependent behavior of the laminar boundary layer with disturbances from each pass of the propeller blade. The propeller was operated over a range from 150 (feathered) to 2000 rpm. In addition, hot films were used to determine the effect on laminar flow of flight through liquid-phase clouds. All these experiments were conducted over a range of airspeeds with a maximum of 166 knots for a unit Reynolds number of 1.5×10^{-6} ft^{-1}.

Testing Procedures

Sublimating chemical detection of boundary-layer transition.- The sublimation method for visually indicating boundary-layer transition involves coating the test surface with a very thin film of volatile chemical solid. During exposure to a free-stream airflow, the chemical film sublimates more rapidly in areas of turbulence than in areas of laminar flow. This difference is due to the higher local shear stress and heat transfer within the turbulent boundary layer. The rate of sublimation is proportional to the chemical vapor pressure - higher vapor pressures produce faster sublimation rates (ref. 32). Chemicals well-suited for testing in subsonic flight include naphthalene, diphenyl, acenaphthene, and fluorene (ref. 33). The relative vapor pressure characteristics of these chemicals at atmospheric temperatures are shown in figure 15. The figure can be used to determine the relative sublimation rates for the various chemicals under a variety of free-stream temperatures. For a given temperature, the various chemicals shown in the figure have different sublimation rates; thus, if operating temperatures can be predicted, the figure allows selection of faster or slower reacting chemicals. Typical sublimation times for transition indication in flight at temperatures from 0°C to 30°C and free-stream velocities less than 250 knots are from 60 to 5 minutes with acenaphthene.

A satisfactory coating application method utilizes "dry spraying" with conventional compressed-air spray-paint equipment. A flat fan nozzle operated at 25 psi produces uniform chemical coatings. A suitable solvent is 1,1,1-trichloroethane mixed in an 8 to 1 solution by volume. The typical rate of chemical solution spraying is 1 quart per 20 to 30 ft^2 of surface. This rate produces a coating thickness of 5 to 10 μm. To avoid formation of turbulent wedges from any unusually large chemical particles which occasionally adhere to the coating, the particles can be removed by gently brushing the surface with a soft bristle brush or cheesecloth prior to testing. In addition, rubbing the chemical coating with a vinyl- or rubber-gloved hand minimizes the occurrence of these particles. Prior to learning the brushing technique, several of the experiments were conducted without brushing the chemical coatings in the manner described. As a result, the chemical transition patterns shown in the photographs in this report frequently contain turbulent wedges caused by chemical roughness particles.

To protect the sublimating chemicals from diffusing prior to reaching the test condition, the surface can be covered with paper with a rip cord running to the cockpit for flight testing. However, using relatively slow sublimating chemicals, it is not necessary to "bag" the surface in this manner. Even at atmospheric temperatures

as high as 30°C, the slower reaction for acenaphthene, for example, permits ample time for takeoff, climb, approach, and landing without affecting the chemical pattern developed at the test condition. Hence, the transition locations can be observed and recorded on the ground. Applied in the manner described, the thin layer of chemical has shown no first-order effects on transition on the variety of NACA 6-series and modern NLF airfoils tested to date. The absence of first-order effects implies that the chemical-coating roughness causes no forward movement of transition. This fact was confirmed by conducting simultaneous transition determination using hot films with and without sublimating chemicals on the T-34C glove. An additional beneficial feature of acenaphthene for either wind-tunnel or flight testing is the durability of the chemical pattern after the test has been run. With thick coatings, the chemical pattern indication of transition lasted up to 48 hours after testing at temperatures near 20°C. Further details on the use of the method are in reference 31.

Acoustic detection of boundary-layer transition.- In order to provide a redundant measure of boundary-layer transition locations, the acoustic technique described in this section was used on the VariEze flight tests. This technique also permitted documentation of the effect of flight through clouds on laminar flow.

The method used for the present tests employed surface total-pressure tubes taped to the wing surface on the VariEze. Figure 16 shows the components used for listening to the boundary layer. The surface pressure tubes were 0.060-in. o.d. stainless steel with one end flattened to an oval shape to attain an outside thickness of 0.015 in. (See fig. 17.) These pressure tubes were then connected by flexible tubing of 0.080 in. o.d. and 0.060 in. i.d. to the airplane cabin. The flexible tubing was terminated in the cabin with an acoustic ear plug for listening. To the human ear, the laminar boundary layer exhibits a quieter sound than the turbulent boundary layer. Ear defenders provided necessary attenuation of background engine noise, propeller noise, and airstream noise.

The locations of the surface pressure tubes during the test are shown in figure 17. These positions were chosen at the visually determined transition locations and within ±5-percent chord forward and aft of transition.

The acoustic transition data were manually recorded in flight. Indicated airspeed was varied from 75 to 150 knots. Testing was conducted at a density altitude of about 4000 ft. At each speed, the three tubes at each spanwise location were listened to one at a time. As each tube was selected, the acoustic signal being heard was checked for validity by means of pulling normal load factors of about 2.0 in banked turns to force transition forward of the selected tube. In this fashion, each tube could be "calibrated" in an absolute fashion for its particular acoustic sound response when passing between laminar and turbulent boundary-layer flow.

Other testing procedures.- For the VariEze, indicated airspeed was calibrated for local flow-field effects (position error) by the pace-airplane technique (ref. 34). Airspeed calibration flights were conducted for both fixed- and free-transition tests.

A chase airplane was utilized during testing of the VariEze to measure elevator deflections and calibrated airspeed for both fixed and free transition. This was accomplished by installing the calibrated elevator deflection pointer and markings shown in figure 18. The elevator deflections were recorded visually from the chase airplane.

Airplane level-flight geometric angle of attack was recorded onboard manually using a calibrated clinometer during testing in both the VariEze and Long-EZ. During all the flight tests, measured pressure altitude and outside air temperature were used to calculate density altitude.

RESULTS

Table 2 is a summary of measured and predicted transition locations for various test conditions in both the wind-tunnel and flight experiments.

Wind-Tunnel VariEze Experiments

Transition locations.- Sublimating chemical transition detection tests were conducted at a test condition of $\alpha = 1.5°$, the angle of attack for cruise lift. Boundary-layer transition is indicated in the photographs of figure 19 by the line of demarcation formed by the chemical coating (white "frosty" area) and the darker area where the chemical has sublimated. This line of demarcation is formed as the chemical coating sublimates rapidly in the turbulent boundary layer, exposing the wing surface. The results indicate that transition was obtained on the canard at $(x/c)_t = 55$ percent and on the wing and winglet at $(x/c)_t = 65$ percent. A limited region of laminar flow was also indicated by the chemical pattern on the highly swept strake.

Measured surface waviness data presented in the appendix show that the largest wave on the wing has an indicated wave height of 0.009 in., and a wavelength of 2.0 in. The amplitude of this wave is only one-fourth of the empirically determined allowable maximum ($h = 0.036$ in. for $\lambda = 2$ in.) for a single wave at the test conditions.

Effect of fixed transition on canard.- As discussed in reference 35, flight in rain or in certain cloud types can result in loss of laminar flow. For conditions with a large amount of laminar flow on the airfoil surfaces, it is of interest to determine if there are significant changes in the stick-fixed or stick-free longitudinal aerodynamic characteristics when there is a loss of laminar flow. The effects of fixed transition were studied by applying a 1/8-in. narrow strip of No. 60 carborundum grit on the full span of the upper and lower surfaces at 5-percent chord of the canard and wing or by spraying water on the canard and wing to simulate the contaminated conditions. Results of this study are presented in figures 20 to 23. The effects of loss of laminar flow on lift and pitching-moment characteristics of the configuration are shown. The data of figure 20 indicate that fixing transition on the canard significantly decreased the airplane pitching moments as a function of angle of attack. The reduction in the pitching-moment curve is related to the loss of lift of the canard. An examination of the chordwise pressure distribution on the canard with artifical transition (fig. 21) indicates that this loss in canard lift is a result of extensive trailing-edge separation. The canard airfoil was designed for attached boundary-layer flow; however, trailing-edge separation is induced on this particular NLF airfoil when the boundary layer becomes turbulent from the leading edge and does not possess sufficient energy to remain attached during pressure recovery. For transition fixed with artificial roughness, the canard lift-curve slope is reduced by about 30 percent as shown in figure 22. Data obtained from the canard balance during the water-spray tests are shown in figure 23. Comparison of these results indicates that the effect of water spray was similar to the effect of fixing transition with artificial roughness; that is, the slope of the lift curve is

reduced. It should be noted that only half of the canard span was enveloped in the water spray; therefore, the results from a fully enveloped canard would be in closer agreement with the fixed-transition canard data shown in figure 23. These data indicate that a nose-down pitch-trim change (with stick fixed) would result from flight through rain or from artificial transition (grit) in this airplane.

Tests were also conducted to determine the effect of fixing transition on the wing with the canard transition already fixed at 5-percent chord. However, loss of laminar flow on the wing has less effect on the configuration pitching moment because of the shorter moment arm from the wing to the aircraft center of gravity and because of the movement of transition of the wing airfoil with angle of attack. That is, the pressure distribution on this airfoil is not favorable for laminar flow above a few degrees angle of attack.

Flight Experiments

Rutan VariEze.- The airspeed calibration data presented in figure 24 show an insignificant effect of fixed versus free transition on position error. At constant α, position error is dominated by bound circulation strength. Therefore, some small effect may be expected because of the effects of fixed transition on lift-curve slope (discussed in this section). The static pressure port for the airplane is located on the side of the fuselage about 1 ft behind and below the trailing edge of the canard.

Transition locations are shown in figure 25 and are listed in table 2 for the wing and winglet at V_c = 135 knots, α = 3°, C_L = 0.35, and $R = 1.40 \times 10^6$ ft^{-1}. Transition on the wing (fig. 25(a)) occurred at $(x/c)_t$ = 60 percent behind the outboard leading-edge drooped strake and at 55 percent elsewhere on the wing. Transition on the winglet occurred at $(x/c)_t$ = 55 percent (fig. 25(b)) on the canard upper surface at $(x/c)_t$ = 55 percent, and on the strake at $(x/c)_t$ = 10 percent. Since the canard airfoils and operating conditions for both the VariEze and Long-EZ are identical, the illustrations of canard transition discussed in this section for the Long-EZ apply to the VariEze as well.

Surface waviness was measured using the dial indicator shown in figure A1. Measured surface waviness data presented in the appendix (table A1 and fig. A2) show the maximum indicated double-wave amplitude on the wing as 0.012 in. in the laminar region. The calculated value (equation in appendix) of maximum allowable amplitude h_a for a single wave at the location of the largest wave is 0.020 in. for λ = 2 in. at the test conditions. Thus, the waviness existing on the airplane airfoil surfaces in the laminar region has not exceeded the empirically determined maximum allowable value.

The effects of total loss of laminar flow (fixed transition) on airplane performance and longitudinal trim characteristics are presented in figure 26. The data show a large increase in the trim elevator deflections required at any airspeed, a 7-knot increase in minimum trim speed (corresponding to a 20-percent decrease in maximum trimmed lift coefficient), and a 10-knot decrease in maximum speed (corresponding to a 23-percent increase in C_D near cruise). The changes in elevator trim deflections and minimum trim speed were caused by large changes in lift-curve slope and in maximum lift caused by leading-edge transition on the canard, wing, and winglet. With transition fixed at the canard leading edge, flow separation was induced near the trailing edge and affected lift, drag, moment, and elevator trim deflections for the canard. The magnitude of these effects was determined during wind-tunnel experiments with the isolated canard and was presented previously in

figures 20 to 23. The reduction in total airplane lift-curve slope due to fixed transition on all lifting surfaces is shown in figure 27. The reduction in canard C_{L_α} is about 30 percent and the reduction in airplane C_{L_α} is about 13 percent. To analyze the stick-free pitch changes due to loss of laminar flow, wind-tunnel-measured elevator hinge moments were compared with fixed and natural transition. These data showed no effect of transition fixed at the leading edge on hinge moments; thus, for the model tested, stick-free flight through rain would not produce elevator deflections due to hinge moment changes and stick-free behavior would be similar to stick-fixed behavior.

The effects of flight through liquid-phase clouds on laminar flow were observed using the acoustic transition detection technique. These tests were conducted at one calibrated airspeed, 130 knots, and one density altitude, 2000 ft. Ambient temperature at the test altitude was 68°F. The surface total-pressure port was located at $x/c = 0.20$ and $\eta = 0.35$. (See fig. 17.) The existence of transition aft of this pressure port was previously determined by sublimating chemicals and by using the maneuvering technique described in the section "Acoustic Detection of Boundary-Layer Transition." The duration of the cloud encounters was less than 1 minute each; there was no visible deposit of mist from the cloud on the wing or windshield. No loss of laminar flow was detected acoustically during flight through these clouds. This observation was reinforced by the absence of any pronounced longitudinal pitch-trim change while in the clouds. Had the cloud particle size and concentration been sufficiently large to cause a significant loss of laminar flow, a nose-down trim change, as discussed previously, would have occurred.

Rutan Long-EZ.- Transition locations are shown in figure 28 and are listed in table 2 for the wing, wing strake, winglet, canard, fuselage nose, and wheel fairing at $V_i = 153$ knots, $\alpha = 1.5°$, $C_L = 0.16$, and $R = 1.42 \times 10^6$ ft^{-1}. As previously noted, two Long-EZ airplanes were tested. Since the test conditions and resulting transition locations of both airplanes were essentially identical, no distinction is made between the results. Transition on the main wing (fig. 28(a)) was $(x/c)_t = 32$ to 34 percent. A small region of turbulent flow about 1 ft in width beginning at the leading edge was observed at the location just outboard of the juncture between the outboard wing strake and the main wing where the canard tip vortex impinged on the wing. Most of the remaining turbulent wedges seen in the figure were caused by chemical particles which adhered to the airfoil surface in the unbrushed chemical coating. Transition on the outboard wing strake (fig. 28(b)) was $(x/c)_t = 10$ to 15 percent. On the inboard portion of the wing strake, the complete sublimation of the chemical coating indicated leading-edge transition. Winglet transition was $(x/c)_t = 32$ to 35 percent (fig. 28(c)). The figure shows the dark leading-edge paint stripe which physically presented a small aft-facing step in the boundary layer. Near the winglet root, this step was well forward on the chord. However, near the winglet tip, the step was farther aft (in percent of local chord) and caused the transition wedges seen in figure 28(c). At the wing-winglet juncture, the local interference effects on transition locations are highlighted by the black lines in figure 28(d). On the suction (inboard) side of the winglet, transition moved slightly forward nearer the wing upper surface. On the wing upper surface, transition appears to have been caused by the vortex which forms at the juncture of two surfaces.

Canard transition, as shown in figure 28(e), was $(x/c)_t = 55$ percent. This transition occurred with an elevator deflection δ_e of 1.8°.

On the fuselage nose (fig. 28(f)), transition occurred at a longitudinal distance of about 16 in., or at a surface length of about 18 in. This extent of laminar flow represents 11 percent of the fuselage length. The figure shows that the laminar boundary layer survived a forward-facing step (h = 0.035 in.) at the leading edge of the removable hatch at a surface length of 14 in. from the nose. Transition occurred at about the same location behind the step as for the surface with no step. The figure also shows that the aft-facing step (h = 0.035 in.) at the hatch-cover countersunk screw caused immediate transition. The existence of the 0.25-in. o.d. pitot tube protruding about 0.50 in. from the tip of the nose had no observable effects on the laminar boundary layer.

Transition on the wheel fairing (fig. 28(g)) occurred at $(x/\ell)_t$ = 33 percent on the upper surface and at $(x/\ell)_t$ = 52 percent on the side surface. Total length of the wheel fairing was 2.75 ft.

The surface waviness data presented in the appendix (table A1 and fig. A3) show that the maximum indicated double-wave amplitude on the wing was 0.006 in. with λ = 2 in. The calculated value of maximum allowable amplitude h_a for a multiple wave (see equation in appendix) is 0.020 in. for $R = 1.42 \times 10^6$ ft^{-1}, λ = 2 in., and c = 3.0 ft. Thus, the waviness existing on the airplane airfoil surfaces has not exceeded the empirically determined maximum allowable value.

The effects of total loss of laminar flow (fixed transition on wings, winglets, nose, and canard) on airplane performance and longitudinal trim characteristics are presented in figure 29. This configuration experienced an 11-knot increase in minimum trim speed, corresponding to a 27-percent decrease in trimmed maximum lift coefficient. Maximum speed for the airplane was reduced with fixed transition by 11 knots, corresponding to a 24-percent increase in C_D in cruise. As with the VariEze, large changes in elevator trim deflections and minimum trim speed were caused by the significant effects of fixed transition on canard airfoil aerodynamics. The reduction in total airplane lift-curve slope caused by fixed transition on all lifting surfaces as presented in figure 30 is about 7 percent. The previously discussed change in canard lift-curve slope was manifested in a slight reduction in short-period damping at cruise speed.

Rutan Laser Biplane Racer.- Transition locations are shown in figure 31 and listed in table 2 for the lower (hereinafter referred to as forward) wing and the upper (aft) wing at V_i = 165 knots, C_L = 0.13, and $R = 1.38 \times 10^6$ ft^{-1}. Transition on both the forward and aft wings was $(x/c)_t$ = 61 percent outside the propeller wake. The turbulent wedges seen in the figure for both wings were caused by chemical particles which adhered to the wing surface without brushing during application of the coating.

On the inboard portion of the aft wing immersed in the propeller slipstream (fig. 31(b)), the chemical pattern in the propeller wake was similar to that outside the propeller wake showing transition at $(x/c)_t$ = 61 percent. A dissimilar feature of the chemical patterns inside the propeller wake was a thin chemical film remaining in the propeller wake aft of the observed transition location on the aft wing. The existence of this thin film aft of transition in the propeller wake (and not outside the propeller wake) could be caused by a transient loss of laminar flow due to the impingement of the propeller vortex sheet in the boundary layer. Such a transient loss of laminar flow could thicken the turbulent boundary layer. This thickening decreases shear stresses sufficiently to significantly slow the sublimation process, thereby leaving the thin chemical film observed in the turbulent pressure recovery

region of the airfoil. Further observations of propeller slipstreams are made subsequently for the Skyrocket II and T-34C airplanes.

Gates Learjet Model 28/29 Longhorn.- Transition locations are shown in figure 32 and are listed in table 2 for the wing and winglet at $M = 0.7$, $h_d = 16\ 500$ ft, $C_L = 0.12$, and $R = 3.08 \times 10^6$ ft^{-1}. This test altitude was chosen to provide a static temperature conducive to rapid sublimation of the chemicals. It is not representative of cruise conditions. The resulting Reynolds number was about 400 percent higher than typical cruise values; in this sense, the results of these experiments are conservative.

Transition on the wing (fig. 32(a)) was $(x/c)_t = 40$ to 45 percent. In the figure, several turbulent wedges are seen which terminate in the natural transition location noted. Most of the turbulent wedges were attributed to large chemical particles which adhered to the wing surface during application.

The most rearward natural transition on the winglet (fig. 32(b)) was $(x/c)_t = 55$ percent. Many turbulent wedges were observed emanating from chemical particles adhering to the surface as well as from surface irregularities at the juncture between the winglet leading edge and the surface skin on the suction (inner) side. Spanwise and chordwise rows of flush-countersunk structural screwheads initiated the transition.

The largest wave measured on the wing in the laminar region was $h \approx 0.002$ in. with $\lambda = 2.0$ in. (See appendix.) For the test condition with $c = 6.58$ ft, the maximum allowable single wave height, as determined by using the equation in the appendix, is 0.008 in. for $\lambda = 2.0$ in. Thus, the empirically determined maximum allowable wave height was not exceeded by waviness existing on the wing in the laminar region. On the lower span of the winglet, the measured height of an aft-facing step near the leading edge exceeded the allowable height, and the premature transition observed on that portion of the winglet can be attributed to this step. (See fig. 32(b).)

No spanwise contamination due to the leading-edge wing sweep Λ_{le} of 17° was observed. The maximum value of attachment-line momentum thickness Reynolds number R_θ at the test condition was 74.

Cessna P-210 Centurion.- Transition locations are shown in figure 33 and are listed in table 2 for the wing upper and lower surfaces and the horizontal stabilizer for $V_c = 139$ to 154 knots, $R = 1.34 \times 10^6$ to 1.48×10^6 ft^{-1}, and $C_L = 0.36$ to 0.32. Observations on the variation of the upper surface transition locations with angle of attack are given in the following table:

V_c, knots	C_L	R, ft^{-1}	$(x/c)_t$, percent
139	0.35	1.34×10^6	5
149	.28	1.43×10^6	29
154	.26	1.48×10^6	44

Figure 33(a) shows $(x/c)_t = 29$ percent at $V_c = 149$ knots. On the lower part of this figure, transition of $(x/c)_t = 44$ percent at $V_c = 154$ knots is faintly

visible on the white portion of the wing adjacent to the dark painted area. The reduced skin-surface temperatures on the white area (relative to the hotter dark skin) reduced the chemical sublimation rate sufficiently for the successful measurement of free transition in the white region. It is noteworthy that there exists little significant difference in transition locations on the prepared (filled and sanded) and production wing surfaces. (See fig. A4.) The stiffness of the 0.020-in-thick skin was sufficient at the unprepared surface location tested to preclude detrimental waviness under flight loads. Most of the turbulent wedges seen in the figure were initiated by chemical particles adhering in the unbrushed chemical coating.

Figure 33(b) shows lower surface transition of $(x/c)_t = 40$ percent at $V_c = 149$ knots. Transition was initiated in this case by the 0.035-in. aft-facing step at a skin joint at that location. Figure 33(c) shows the horizontal-tail free transition location of $(x/c)_t = 27$ percent. The local chord length at this measurement location was $c = 3.67$ ft. Figure 33(d) shows the propeller-spinner transition location of $s_t = 12$ in. The length of the propeller spinner length was 22 in. and the rotation rate was 1900 rpm.

Measured surface waviness data presented in the appendix show the maximum indicated double-wave amplitude was 0.010 in. for $R = 1.48 \times 10^6$ ft^{-1}, $\lambda = 2$ in., and $c = 4.83$ ft. For a single wave under the same conditions, the criterion is $h_a = 0.020$ in. Thus, the surface waviness criteria were not exceeded on either the prepared or production wing surface regions tested.

Beech 24R Sierra.- Transition locations are shown in figure 34 and are listed in table 2 for the wing upper surface, propeller, and vertical stabilizer for $V_c = 133$ knots, $R = 1.38 \times 10^6$ ft^{-1}, and $C_L = 0.30$. Natural transition on the wing upper surface shown in figure 34(a) was $(x/c)_t = 45$ percent. Over much of the area tested, free transition was obliterated by convergence of turbulent wedges caused by chemical particles stuck in the unbrushed chemical coating. Figure 34(b) shows several turbulent wedges caused by insect remains and by paint surface imperfections. The spanwise sloping dark paint stripes had no effect on the laminar boundary layer. Though not measured, the roughness heights of these paint stripes are less than critical. On the lower surface of the wing, free transition was $(x/c)_t = 42$ percent. Transition on the vertical tail (fig. 34(c)) was triggered by the aft-facing 0.0020-in. skin lap joint step about 6 to 8 in. aft of the leading edge, or about 10-percent chord.

Transition locations on the suction (forward) and pressure (aft) faces of the propeller are shown in figures 34(d) and 34(e), respectively. Transition was $(x/c)_t = 38$ percent on the forward face and $(x/c)_t = 80$ percent on the aft face. The local chord at these measurement locations was about 6.5 in.; the radial location was between 25 and 75 percent of the blade length. The propeller was operating at 2700 rpm or $J = 0.84$. At these conditions, the local blade unit Reynolds number at 50 percent of the blade radius was 2.89×10^6 ft^{-1}, and the local Mach number was 0.46. Additional observations of laminar flow on propellers in flight are discussed in reference 31.

Bellanca Skyrocket II.- Figure 35 illustrates the transition locations on the upper and lower wing surfaces at a unit Reynolds number of 1.88×10^6 ft^{-1}. Transition occurred at $(x/c)_t = 45$ to 46 percent on the lower surface. Airplane trimmed lift coefficient was 0.22 and Mach number was 0.31. At these flight conditions, the chord Reynolds number R_c at the inboard wake probe station was 9.7×10^6 and

9.0×10^6 at the outboard station. The turbulent wedges seen in figure 35(a) were caused by large chemical particles which adhered to the surface during application of the coating. In figure 35(b), turbulent wedges which were caused by insects are marked with an asterisk. The unmarked wedges were caused by artificial roughness (1/4-in-square patch of No. 80 grit). Note the absence of any chemical particle-induced wedges in this pattern; this resulted from mechanically loosening the particles by brushing the chemical coating prior to flight. Figure 35(c) is a summary of the transition locations across the wing semispan. It shows the effects of twist and propeller slipstream. Airfoil contour accuracy and surface-waviness measurements were made at several wing stations on the Skyrocket. Deviations between the actual and theoretical contours as large as 0.117 in. (of excess thickness near the mid-chord) were measured. Detailed waviness data for the Skyrocket are presented in the appendix (fig. A5 and table A1). The largest indicated wave height appeared near the leading edge of the lower surface at the inboard wake probe station where $h \approx 0.015$ in. This particular wave occurred at the bonded leading-edge attachment joint. More typical wave heights on the Skyrocket wings were about $h = 0.002$. Using the free-stream conditions of the flight test, and the empirical criterion of reference 27, the allowable wave height for a single wave ($\lambda = 2$ in.) on the Skyrocket varies between 0.017 and 0.015 from the wing tip to the root. However, since the testing was conducted at low altitudes and high speeds, the allowable waviness at more typical cruise conditions is larger. Thus, the waviness existing on the Skyrocket wing was less than that allowable for NLF.

From reference 31, an example of the location of measured transition relative to the predicted chordwise pressure distribution is shown in figure 36. Predicted transition (ref. 36) using an integral boundary-layer method with the Granville transition criterion is also shown. Both measured and predicted transition locations occur well downstream of the location of minimum pressure (pressure peak) on both upper and lower surfaces.

Figure 37, from reference 31, presents flight-measured airfoil drag polars, which illustrate the effects of fixed transition and comparisons with low-turbulence wind-tunnel measurements (ref. 37) and predicted airfoil performance (ref. 36) on the same airfoil. Excellent agreement exists between analytically predicted and flight-measured airfoil section drag polars at lower lift coefficients. At higher values of C_ℓ, lower to upper surface air leakage was apparently responsible for increased drag in flight. The predictions were based on template-measured Skyrocket airfoil coordinates. The effect of fixed transition appears as an 80-percent increase in wing-section profile drag for cruise lift coefficients ($C_\ell \leq 0.3$). Based on speed-power measurements with natural and fixed transition, the Skyrocket gained 25 percent in cruise range as the result of laminar flow (ref. 31). No significant effect of fixed transition on Skyrocket lift-curve slope or on high-angle-of-attack handling qualities was observed; the maximum lift coefficient increased only by about 4 percent with fixed transition. (See details in ref. 31.)

During the Skyrocket tests, a 2.2-hr flight was conducted at less than 500 ft above ground level at $V_c = 178$ knots to collect a sample of insect debris patterns and to determine which insect strikes caused transition (supercritical) and which did not (subcritical). This flight was conducted in late March after several weeks of warm weather in the Tidewater region of Virginia between 1430 and 1630 eastern standard time. Figure 38 depicts the heights and positions of the insects collected along the span of the right wing, and figure 35(b) shows the lower surface insect debris contamination wedges for this flight.

As illustrated in figure 38, only about 25 percent of the insects collected were of supercritical height and caused transition. In the figure, supercritical insects protrude out from the airfoil surface and subcritical ones protrude inward. Very near the stagnation point, rather large insect remains were recorded which did not cause transition. The long duration of the flight and the relatively rapid response of the chemicals to boundary-layer turbulence - especially on the forward part of the airfoil - make it unlikely that supercritical insect strikes occurred which did not record a transition wedge in the chemical pattern. For the 3° wing washout, the stagnation line on this leading edge varied approximately between $x/c = 0$ and 0.002 at the test conditions.

During the Skyrocket experiments, detailed boundary-layer measurements were made in the propeller slipstream. Figures 35(b) and 35(c) show that transition, as indicated by the chemical pattern, moved forward on the upper surface from $(x/c)_t = 42$ percent outside the slipstream to $(x/c)_t = 36$ percent inside. On the lower surface, transition moved forward by a similar increment. An interesting detail was the lack of any apparent effect of the propeller tip vortices on transition where they impinged on the wing. One possible explanation for the forward motion of chemical-indicated transition in the propeller wake is the effect of an increased disturbance environment in the propeller slipstream. These large disturbances might amplify to transition earlier along the chord than the smaller disturbances outside the slipstream.

Time-averaged boundary-layer profiles were measured by rakes inside and outside the propeller slipstream with both free and fixed transition on the Skyrocket. (See fig. 39.) These measurements were made at $s/c = 28.7$ percent, $R = 1.715 \times 10^6$ ft^{-1}, $M = 0.31$, and $n = 1800$ rpm. Inside the slipstream, the estimated mean unit Reynolds number was 1.778×10^6 ft^{-1} (using propeller momentum theory).

With free transition, figure 39 shows the thin laminar boundary layer outside the propeller slipstream where $\delta \approx 0.06$ in. Inside the slipstream, the profile has thickened to $\delta \approx 0.24$ in., and the profile has changed, appearing more turbulent in shape. The inside rake was positioned in the slipstream at a chordwise position which was laminar as shown by sublimating chemical patterns. Thus, this thickened profile was not a turbulent one in the normal sense. To verify the shape and thickness of an actual turbulent profile at this position, transition was fixed in front of the rakes inside and outside the propeller slipstream. The resulting turbulent profiles are seen in figure 39 as the solid symbols. It is apparent that the effect of the propeller slipstream on time-averaged boundary-layer profile measurements is to create a shape which is turbulent in appearance and which is increased in thickness to near the actual turbulent boundary-layer thickness ($\delta \approx 0.28$ in. for the solid symbols in the high-speed case).

Beech T-34C gloves.- Since the Skyrocket boundary-layer measurements in the propeller slipstream discussed in the preceding section were time averaged, and since the phenomena in the propeller slipstream environment are time dependent and of high frequency, experiments were conducted using hot films on the T-34C to gain a better understanding of the laminar boundary-layer behavior in this environment. The results of this experiment are illustrated in figure 40. The hot-film signals shown are oscilloscope traces of the voltage fluctuations which occur due to local velocity fluctuations (and therefore heat-transfer fluctuations) in the boundary layer.

A cyclic behavior, at the propeller blade-passing frequency, is seen in the laminar boundary layer. The sensor on the miniglove at the leading edge records an

apparent small velocity rise at the propeller blade-passing frequency. When this disturbance reaches the second, third, and fourth sensors, it has progressively grown in amplitude and in duration. The sensors on the NLF glove outside the propeller slipstream show the relative magnitudes of laminar and turbulent signals. Although the data presented are for a relatively low propeller rpm, the same general behavior of the boundary layer was observed at conditions of 2000 rpm.

The hot-film signals were observed using an onboard oscilloscope. During flight inside clouds for which no deposit of mist on the windscreen or laminar glove occurred, the boundary layer remained laminar to near the 40-percent-chord station (the same transition location as for flight in clear air). When mist accumulated on the canopy windscreen and on the glove leading edge in clouds, the hot films indicated turbulent boundary-layer conditions at all chordwise stations from the leading edge to the 40-percent-chord hot-film locations. Upon exiting the cloud, the boundary layer very quickly reverted to the laminar state.

DISCUSSION

When viewed as a whole, the results of these flight and wind-tunnel experiments on modern production-quality airframes provide a new appreciation for the achievability and maintainability of NLF for chord Reynolds numbers up to about 30×10^6 and speeds up to about $M = 0.7$. The discussion which follows summarizes these experimental results and their implications.

Transition Locations

In studying the transition locations, it was of interest to determine the influence of background disturbances including such things as engine/propeller noise, airframe vibration, and surface roughness and waviness. Any first-order effects (or bypasses) of such disturbances become apparent by comparing the measured transition location with the location of minimum pressure on the airfoil. For the Reynolds numbers of the present tests, transition forward of minimum pressure provides evidence of the existence of disturbances other than normal amplification of T-S waves. Two-dimensional empirical predictions of boundary-layer transition locations were made using the method of reference 36, 38, or 39 for comparison with measured transition locations from the wind-tunnel and flight experiments. These empirical methods use integral boundary-layer parameters and shape factors to predict transition. Because the flight experiments did not provide a direct measure of local angle of attack at the locations where transition observations were made, the angle of attack used for the transition predictions was estimated using the flight value of airplane trimmed lift coefficient. For the moderate-aspect-ratio wings tested, this procedure produces meaningful comparisons of predicted and measured transition locations.

In the present experiments, where analysis of pressure distributions was possible, all the transition locations occurred downstream of the point of minimum pressure (e.g., fig. 36). This observation is consistent with other similar comparative analyses reported in the literature (e.g., refs. 3, 4, 7 to 12, 14 to 20, 22, and 23). The comparisons for the present experiments of measured and predicted transition are summarized in table 2. Generally, for the surfaces with little sweep where three-dimensional effects should be minimal, measured transition occurred downstream of the transition location predicted using two-dimensional analysis (refs. 36, 38, and 39). Typically, the measured transition locations reported in table 2 for these surfaces occurred downstream of the point of minimum pressure; in fact, for the

Skyrocket, transition occurred at the predicted location of laminar separation in the adverse pressure gradient. The implication of this comparison is that in flight at higher Reynolds numbers than previously thought, the transition process is not dominated by background disturbances such as acoustic, surface, or turbulent free-stream disturbances in the boundary layer. Rather, transition appears to be dominated by amplification of two-dimensional T-S instabilities in the adverse pressure gradient or by instabilities in the free-shear layer (laminar separation). Transition of this type occurred on the Gates Learjet Model 28/29 wing, where flight-measured transition occurred at 40-percent chord at a chord Reynolds number (near the wing root) of about 30×10^6. The predicted point of minimum pressure was at 35-percent chord. This extent of laminar flow occurred in spite of the proximity of the turbojet engine inlet to the wing upper surfaces. This indicates a lack of influence of the engine inlet noise on the laminar boundary layer, which is perhaps aided by some noise attenuation by an upper surface shock at about 70-percent chord under the test conditions flown. These data suggest that since laminar boundary layers in the flight environment possess sufficient stability as the result of favorable pressure gradients, transition can be expected downstream of the point of minimum pressure, even at relatively large chord Reynolds numbers in two-dimensional flows.

Effects of Precipitation and Cloud Particles

Under certain conditions, the operation of a laminar-flow wing can be affected by either precipitation onto the laminar-flow surface or by the flux of free-stream cloud particles through the laminar boundary layer. Precipitation can cause loss of laminar flow by creating three-dimensional roughness elements on the airfoil surface which, in sufficient quantity and size, act as a boundary-layer trip near the leading edge. Cloud particles can cause loss of laminar flow by the shedding of turbulent wakes from the particles as they traverse the laminar boundary layer. At sufficient flux (particles per unit area per unit time) and sufficient particle Reynolds number, partial or total loss of laminar flow can occur. The present experiments provide limited data on the effects of precipitation and cloud particles on NLF.

The VariEze wind-tunnel tests demonstrated that rain impinging on the canard surfaces caused a loss of laminar flow. Comparison of the aerodynamic characteristics of the canard in a heavy water spray and with transition fixed by artificial roughness (fig. 23) shows that the effect of water drops on the airfoil is to move transition to near the leading edge.

Results of early flight experiments on the Hawcon (ref. 13) showed that when a mist deposit occurred on the laminar-flow surface during flight through clouds, the boundary layer became turbulent. During the Hawcon flights (see table 1), wake-rake drag measurements were made with a mist deposit from flight through clouds on the wing. The Hawcon measurements showed a 42-percent increase in section drag due to the mist deposit on the wing (at $6.5 < R_c < 8.5 \times 10^6$). It is possible that the mist deposit creates a supercritical roughness. These results suggest the mechanism for loss of laminar flow during flight through clouds at low altitudes (above freezing temperatures), where a mist deposit on the wing occurs.

The VariEze flight experiments demonstrated the effects of flight through liquid-phase clouds on laminar flow when no mist deposit occurs on the wing. Previous research on the effects of cloud particles on NLF (refs. 40 to 42) has dealt principally with ice crystals occurring at high altitudes (in the stratosphere). In the X-21 flight experiments (ref. 40) laminar flow was lost as a result of flight through ice-crystal clouds. In the present flight experiments, when no mist deposit

occurred on the laminar surface, the laminar boundary layer was unaffected by the cloud particles in the free stream. Using Hall's criterion (refs. 40 and 41) for a critical spherical particle Reynolds number of 400 (based on a particle diameter), the calculated critical particle size for the VariEze flight condition is 88 μm. Since liquid-phase cloud particles in the free stream are considerably smaller than this, no loss of laminar flow would be expected at the VariEze flight condition. However, if the average cloud particle size had been 20 μm, an airspeed of 587 knots would have been required (at the VariEze test altitude and temperature) to cause a loss of laminar flow. These results illustrate an insensitivity of the laminar boundary layer to flight through clouds at low altitudes where the particles do not deposit on the surface.

Effects of Fixed Transition

For several of the airplanes tested, transition was fixed near the leading edge to determine the effects of a complete loss of laminar flow on aerodynamic performance. These airplanes included the VariEze (wind tunnel and flight), the Long-EZ, and the Skyrocket II. As discussed in the preceding section, a loss of laminar flow could occur due to atmospheric effects. Additionally, insect debris, leading-edge erosion, or ice accretion could produce losses in laminar flow. Whatever the cause, the changes in performance and handling qualities with and without laminar flow are important to understand.

Increases of 25 percent in the cruise drag due to fixed transition were measured on the VariEze, Long-EZ, and Skyrocket II airplanes. (See figs. 26 and 29.) These large drag changes result from the relatively large proportion of the airplane wetted area which had been laminar and then became either turbulent or separated. Airplanes with less lifting surface relative to total wetted area, or with larger values of profile drag, experience smaller benefits due to NLF.

These three airplanes also provided data on the effect of fixed transition on airplane lift-curve slope. For both the VariEze and Long-EZ airplanes, where fixed transition induced significant flow separation on the canard, airplane total lift-curve slope was reduced from 7 to 13 percent (see figs. 27 and 30). This canard flow separation produced a nose-down longitudinal pitch-trim change (stick fixed). This result, first observed in the wind-tunnel experiments on the VariEze, was also reproduced in flight on the VariEze and Long-EZ using artificial roughness to trip the boundary layer near the leading edge. Although this effect of fixed transition was observed on the two canard configurations tested, the effect is predominantly airfoil-related rather than configuration-related. That is, the canard airfoil (which was the same for both airplanes) was designed in such a fashion that the boundary layer separated if no laminar flow existed from the leading edge. This design feature is not typical of NLF airfoils. Canard airfoils can be designed with no separation under turbulent boundary-layer conditions such that pitch-down during flight through rain should not occur. On canard configurations with highly loaded trimming surfaces (i.e., the canard), NLF airfoils should be selected which do not experience flow separation and lift loss upon loss of laminar flow. For the Skyrocket II, fixed transition on wing and tail surfaces induced no separation and had no measurable effect on lift-curve slope (ref. 31).

Both the VariEze and Long-EZ experienced large reductions in maximum trimmed lift coefficient due to fixed transition; the reductions range from 20 to 27 percent (see figs. 27 and 30). As with lift-curve slope, these large changes are attributable to the significant flow separation induced by fixed transition on the particular

canard airfoil incorporated on those two airplanes. On the Skyrocket, where fixed transition does not induce significant flow separation, no reduction in maximum lift coefficient occurred. In fact, as discussed in reference 31, maximum lift coefficient actually increased as the result of fixed transition.

The significant changes which occur in performance or handling qualities as the result of loss of laminar flow indicate the importance of fixed-transition flight tests as a standard procedure for any airplane with surfaces smooth enough to support NLF.

Propeller Slipstream Effects

Past observations of the effect of the propeller slipstream on boundary-layer transition (refs. 5, 6, 16, 17, and 43 to 45) produced varying conclusions. The research reported by Young (refs. 5 and 6) and Hood (ref. 44) indicates that the effect of the slipstream was to effectively move transition to the wing leading edge behind the propeller. In the case of Young's flight experiments, boundary-layer thickness, measured by a total-pressure survey probe, was used to judge transition location. Where the measured boundary-layer thickness exceeded the calculated laminar thickness, transition was assumed to have occurred. Young thus reported transition near the leading edge on two different airplanes. Hood, using similar methods, reported similar results in wind-tunnel tests for a propeller mounted at a 20-percent-chord position in front of the wing leading edge. Concerns about the validity of these conclusions are discussed in the following paragraphs.

Experiments reported by Zalovcik (refs. 16 and 17) and Wenzinger (ref. 45) gave evidence that the effect of the propeller slipstream might not be as detrimental as indicated by Young and Hood. Wenzinger's tunnel experiments showed moderate effects of propeller slipstream on the wake-probe-measured section drag for an NACA 66-series NLF airfoil. Zalovcik reported extensive laminar flow in the propeller slipstream during his flight experiments on the P-47 and P-51 airplanes. These latter flight experiments were the first to rely on detailed boundary-layer rake measurements to determine transition locations as indicated by large profile changes at transition.

Three of the present flight experiments (the Skyrocket, the Biplane Racer, and the T-34C) included observations and measurements of the laminar boundary layer in the slipstream on the configurations illustrated in figures 7, 14, and 40. On the Rutan Biplane Racer, the chemical pattern on the inboard portion of the aft wing immersed in the propeller slipstream showed little if any apparent effect of the slipstream (see fig. 31(b)). During the Skyrocket experiment, measurements (see figs. 35(b) and 35(c)) showed that transition as indicated by the chemical pattern moved slightly forward inside the slipstream. The flight experiments conducted using surface hot films in a laminar boundary layer in the propeller slipstream on the T-34C airplane (fig. 40) illustrate the cyclic nature of time-dependent laminar boundary-layer behavior in propeller slipstreams. Such cyclic laminar behavior raises the question of the possibility of laminar-flow drag-reduction benefits on surfaces immersed in propeller slipstreams (i.e., wings, nacelles, and empennages). Analysis of the Wenzinger data (ref. 45) presented in reference 31 indicates that the drag increase of laminar airfoils in propeller slipstreams is significantly less than that due to total loss of laminar flow.

These recent observations suggest that previous conclusions about the loss of laminar flow in propeller slipstreams may be incorrect, since some of the early experiments mistakenly depended on time-average-measured boundary-layer thickness or

shape as an indication of transition. The implication of the present observations is that the section drag increase associated with the transition changes in propeller slipstreams may not be as large as that for fixed leading-edge transition. Thus, NLF airfoils may provide drag reduction benefits, even on multiengine configurations with wing-mounted tractor engines.

Waviness

No premature transition was observed in any of the experiments which could be attributed to surface waviness even though the surfaces tested were not perfectly smooth and wave free. These results occurred on surfaces which received no special contour preparation; the surfaces tested represented modern production-quality smoothness achieved in either metal or composites.

As a historical comparison, the waviness from the 1950 King Cobra test (ref. 21) and the waviness from the Skyrocket tests are shown in figure 41. This waviness for the King Cobra produced the minimum level of profile drag measured in those flight experiments at $R_c = 17 \times 10^6$. A qualitative comparison of the waviness measurements confirms the fact that the modern composite surface on the Skyrocket with no special contour preparation provides a lower level of waviness than the King Cobra metal surface, which required extensive filling and sanding to achieve the waviness shown. This comparison illustrates the achievability, with modern fabrication methods, of surface waviness compatible with laminar flow at medium to relatively high Reynolds numbers. Conversely, the results illustrate the point that some significant amount of surface waviness is acceptable on laminar-flow surfaces in favorable pressure gradients of moderate strength.

Sweep Effects

The two significant wing-geometry-related phenomena which can adversely affect laminar boundary layers on swept surfaces are crossflow instability and turbulent contamination of the leading-edge attachment line flow (or leading-edge contamination). Since no obvious crossflow instability was observed on the swept wings and winglets in these flight experiments, this discussion centers on leading-edge contamination. Crossflow instability can be recognized by the existence of closely spaced streamwise streaks preceding transition in the sublimating chemical coating.

A comparison betweeen the flight data and the spanwise contamination criterion is presented in figure 42 for the VariEze and the Long-EZ. The spanwise contamination criterion is summarized in reference 46 as

$$R_\theta = 0.404 \frac{\sin \Lambda}{\sqrt{\cos \Lambda}} \sqrt{R \frac{r_{le}}{1 + (t/c)}} \qquad (1)$$

where no spanwise contamination occurs for $R_\theta < 100$. For various roughness conditions, there may be no spanwise contamination for $R_\theta < 240$. For $R_\theta > 240$, turbulent contamination from any source freely propagates spanwise along the attachment line. On the swept VariEze ($\Lambda = 27°$) and the Long-EZ ($\Lambda = 23°$) wings, the data in figure 42 show that R_θ did not exceed 100. The same was true for the winglets on both airplanes; R_θ at the root was 51 for the VariEze and 36 for the Long-EZ. On

the swept strakes of both the VariEze ($\Lambda = 61°$) and the Long-EZ ($\Lambda = 51°$), R_θ exceeded 100. However, small regions of laminar flow were still observed near the leading edges of both strakes. Relaminarization by rapid flow acceleration might have been responsible for the short laminar runs observed on the strakes. Calculations, by the method of reference 46, of conditions necessary for relaminarization to occur show that the necessary flow acceleration may have been present on the upper surface of the VariEze and Long-EZ strakes within about 1-percent chord of the leading edge. On the Long-EZ, on the very short inboard strake ($\Lambda = 64°$) where $R_\theta \approx 240$, no laminar flow was recorded by the chemical pattern. At the leading-edge break between $\Lambda = 64°$ and $\Lambda = 51°$, the leading-edge contamination from the 64° swept region did not propagate onto the 51° swept region in spite of the fact that R_θ varied from 127 to 148 for this region. (See fig. 42(b).)

On the Learjet wing ($\Lambda = 17°$), R_θ did not exceed 100 in spite of the extremely high unit Reynolds number during the test. On the Learjet winglet, where R_θ varied from 151 at the root to 75 at the tip during the tests, it could not be ascertained whether spanwise contamination was present on the portions of the winglet which were turbulent. This uncertainty was caused by excessive roughness in the form of screw heads and a step which caused transition in some regions of the leading edge.

Even if spanwise contamination were present at the test condition where $R = 3.08 \times 10^6$ ft^{-1}, at typical cruise ($R = 0.87 \times 10^6$ ft^{-1}), the values of R_θ would drop to 80 at the winglet root and 40 at the tip, thus ensuring no spanwise contamination. In fact, at the aforementioned Learjet cruise unit Reynolds number on a surface swept 40°, the leading-edge radius could be as large as 1.5 in. and still keep $R_\theta < 100$ for no spanwise contamination.

This observation implies that, in general, on certain relatively large lifting surfaces, spanwise contamination at high-altitude cruise may not be a serious concern. As an example, on the Gulfstream Aerospace GIII airplane (chosen for its large size in the business jet class), at an altitude of 45 000 ft and at $M = 0.85$, R_θ varies from 80 at the wing root to 68 at the tip, precluding spanwise contamination. As a final example of operations below the spanwise contamination criterion, R_θ for the DC-10 winglet (ref. 47) varies from 64 at the root to 40 at the tip for $M = 0.82$, at a cruise altitude of 35 000 ft, and at a cruise unit Reynolds number of about 1.9×10^6 ft^{-1}. Based on these observations, it appears that for certain important potential applications, spanwise contamination need not be a concern for relatively large lifting surfaces.

Insect Debris Contamination

The effect of contamination on NLF wings by insect debris is an important consideration in NLF airfoil design as well as in the operation of airplanes with laminar-flow wings. These considerations, as well as insect population characteristics, are discussed in some detail in the literature (refs. 48 to 54). In practice, the seriousness of insect debris contamination will likely be dependent on airplane characteristics and mission. If needed, active methods of insect protection such as porous, fluid-exuding leading edges may serve the purposes of both insect and ice protection. The ice-protection performance features of such systems are discussed in reference 55, and the ability of wetted leading edges to protect against insect debris contamination is discussed in references 56 and 57.

For a representative insect debris contamination pattern accumulated in flight on the Bellanca Skyrocket, only 25 percent of the insects caused transition at sea

level. Analysis shows that at a more typical cruise altitude of 25 000 ft and with a thicker boundary layer, caused by a lower unit Reynolds number, only about 9 percent of the insects would have caused transition (fig. 35(b)). Thus, even though large numbers of insects might be collected on a wing leading edge, relatively few of them can be expected to cause transition at high cruise altitudes.

The sample insect contamination data presented here serve to illustrate a certain inherent level of insensitivity of this particular combination of airfoil geometry and operating conditions to insect contamination. Examples of varying sensitivity of different airfoil geometries to insect contamination effects are presented in reference 54. It is important to recognize that although sufficient insect contamination can seriously degrade airplane performance, the occurrence of serious contamination levels is infrequent for many combinations of place, time of day, time of year, airfoil geometry, and mission profile.

CONCLUSIONS

Flight and wind-tunnel natural laminar flow (NLF) experiments have been conducted on various lifting and nonlifting surfaces of several airplanes at chord Reynolds numbers representative of business and commuter transport airplanes. The airplanes tested were constructed using either composite or aluminum structures. The surfaces tested were selected to provide relatively stiff skin conditions, free from significant roughness and waviness, and were representative of typical smooth, modern production airframes. The following conclusions relate to the most significant findings of the investigation.

1. Taken as a whole, the results of these investigations suggest that significant regions of NLF exist and that this boundary-layer behavior is more persistent and durable on certain practical production airplane surfaces than previously expected. Where comparisons could be made, the transition locations observed occurred downstream of the calculated minimum pressure locations for the design contours of the surface shapes tested. Thus, evidence is provided that flight environment disturbances to the laminar boundary layer are sufficiently small that typical favorable pressure gradients provide enough stability for this to occur even at relatively large chord Reynolds numbers in two-dimensional flows.

2. Significant effects on performance and stability and control resulting from total loss of laminar flow were measured in flight using artificial roughness to trigger transition. Measurements were made of increases in cruise drag as large as 24 percent, decreases in maximum trimmed lift coefficient as large as 27 percent, and decreases in airplane lift-curve slope as large as 13 percent. These observations indicate the importance of fixed-transition tests as a standard flight-test procedure for any airplane with smooth aerodynamic surfaces. Heavy water spray to simulate rain causes the same airfoil aerodynamic changes as fixing the transition near the leading edge.

3. No discernible effects on transition due to surface waviness were observed on any of the surfaces tested. Measured surface wave amplitudes were generally smaller than the allowable maximum wave heights determined by an empirical criterion.

4. In all cases tested, the agreement between the empirical spanwise contamination criteria and the observed laminar-flow results was consistent with previous research.

5. The effect of flight through clouds on transition was observed for flight through low-altitude, liquid-phase clouds. With no mist deposit occurring on the windscreen (or wing), laminar flow is unaffected for subsonic flight at low altitudes.

Langley Research Center
National Aeronautics and Space Administration
Hampton, VA 23665
May 3, 1984

APPENDIX

SURFACE WAVINESS ON RESEARCH MODELS

The accurate measurement of airfoil surface waviness is important for both laminar boundary-layer research and production of laminar-flow wings. The physical presence of waves on a laminar airfoil surface can create macroscopic changes in the local pressure gradient which can in turn trigger transition to turbulence. The critical amplitudes and wavelengths which can trigger transition have been empirically related to Reynolds number for a single wave in reference 27 by the equation

$$\frac{h}{\lambda} = \left(\frac{59\ 000c\ \cos^2 \Lambda}{\lambda R_c^{1.5}} \right)^{1/2}$$

where h is the double-amplitude wave height in inches, λ is the wavelength in inches, c is the wing chord in inches, and Λ is the wing leading-edge sweep. For multiple waves, h/λ is one-third the value of a single wave.

The dial indicator (fig. A1) used for measuring surface waviness during this investigation is mounted on a solid base with three fixed legs. A single leg is spaced 2 in. from the paired legs, which are 0.6 in. apart for stability. The dial indicator leg is placed at the center. This method was selected simply to permit comparison of modern waviness data with data from early natural laminar flow (NLF) research, for which this waviness gauge design was originally used.

The procedure for making waviness measurements using a dial indicator is as follows. For convenience in reference marking, transparent tape was placed chordwise over the line on which waviness was to be measured. Beginning at the chord leading edge, 1/4-in. intervals were marked on the tape, and gauge deflections were recorded at each interval. The gauge reading was then plotted versus the distance around the surface from the leading edge. A nine-point running average (for 1/4-in. intervals) was plotted over the raw data, because the actual airfoil surface curvature was not accurately known. The difference between the two plots is representative of the actual waviness. Nine points were chosen for the calculations to provide artificial smoothing over the 2-in. length of the dial indicator base.

There are several shortcomings which arise with this type of measurement device and procedure used to calculate waviness. Foremost is the fact that the waviness measured is without flight loads on the surface. With certain structures (e.g., those with lightly stressed thin metal wing skins), waviness in addition to that measured on the ground probably exists under flight loads. Additionally, difficulty arises from the fact that the center leg is deflected successively as each of the base legs passes through a wave. This deflection yields a distorted wave with more cycles and with both larger and smaller amplitudes than the surface being measured. The dial resolution is one-half of 1×10^{-3} in., and the 1/4-in. intervals on the wing were accurate to within 1/32 in. Swept or tapered wings can also affect interpretation or meaning of the gauge readings. If the gauge is skewed slightly from the chord line being measured, the legs will rest at a different level and will produce an added deflection. During the measurements on the airplanes discussed herein, this source of error was minimized by care in streamwise alignment of the dial indicator

base. Because of these shortcomings in the dial indicator method of waviness measurement, the data are defined as "indicated" waviness.

The indicated waviness data measured on the airplanes tested are presented in figures A2 through A7. Table A1 is a summary of the waviness data in terms of the number of waves at each location and the chordwise position, double amplitude, and wavelengths of the largest wave in the laminar region and over the total chord at each spanwise measurement location. Only waves that were 2 in. or shorter were counted; most waves fell in this category. Waves which occurred in the turbulent region of the chord were included in the table as an indication of overall surface quality. The maximum allowable multiple wave heights are also given in table A1. A comparison between the maximum measured and maximum allowable wave heights shows that the waves existing in the laminar region of all but one of the test airplanes were smaller than allowable for premature transition.

APPENDIX

TABLE A1.- SUMMARY OF INDICATED WAVINESS MEASURED ON TEST AIRPLANES

Airplane	Surface	η	Largest wave measured			Largest wave measured in laminar region			h_a/λ (λ = 2 in.)
			Position, s/c	λ, in.	h/λ	Position, s/c	λ, in.	h/λ	
VariEze in flight	Right wing	0.25 .40 .55 .85 .95	0.736 .309 .578 .704 .535	2.0 2.0 2.0 2.0 2.0	0.0035 .0060 .0030 .0075 .0030	0.194 .309 .316 .477 .347	3.0 2.0 3.0 4.0 2.0	0.0030 .0060 .0020 .0015 .0020	0.0100 .0100 .0105 .0115 .0120
	Right winglet	0.55	0.678	2.0	0.0070	0.465	3.5	0.0017	0.0125
Long-Ez	Right wing	0.55 .85	0.189 .208	2.0 2.0	0.0030 .0020	.189 .208	2.0 2.0	0.0030 .0020	0.0100 .0110
	Right winglet	0.55	0.270	3.0	0.0020	0.270	3.0	0.0020	0.0115
	Right canard	0.45	0.356	1.75	0.0046	0.356	1.75	0.0046	0.0135
VariEze in tunnel	Right wing	0.25 .55 .75	0.333 .433 .511	2.0 2.5 2.0	0.0045 .0024 .0030	0.333 .433 .511	2.0 2.5 2.0	0.0045 .0024 .0030	0.0180 .0193 .0205
	Right winglet	0.25 .80	0.223 .533	2.0 3.25	0.0045 .0018	0.223 .533	2.0 3.25	0.0045 .0018	0.0215 .0248
Cessna P-210	U.S. - production U.S. - filled and sanded L.S. - filled and sanded		0.228 .095 .125	3.5 2.0 3.5	0.0020 .0050 .0011	0.228 .095 .125	3.5 2.0 3.5	0.0020 .0050 .0011	0.0100 .0100 .0100
Bellanca Skyrocket II	Inboard wake probe	Upper Lower	0.312 .065	2.0 2.0	0.0015 .0075	0.312 .065	2.0 2.0	0.0015 .0075	0.0078 .0078
	Outboard wake probe	Upper Lower	0.065 .065	2.0 2.0	0.0045 .0070	0.065 .065	2.0 2.0	0.0045 .0070	0.0079 .0079
Gates Learjet Model 28/29 Longhorn	Right wing	0.48 .72	0.430 .450	2.0 3.0	0.0020 .0030	0.10	2.0	0.0010	0.0040 .0041
	Right winglet	0.10 .63	0.17 .69	2.0 2.0	0.0135 .0010	0.17	2.0	0.0135	0.0050 .0070

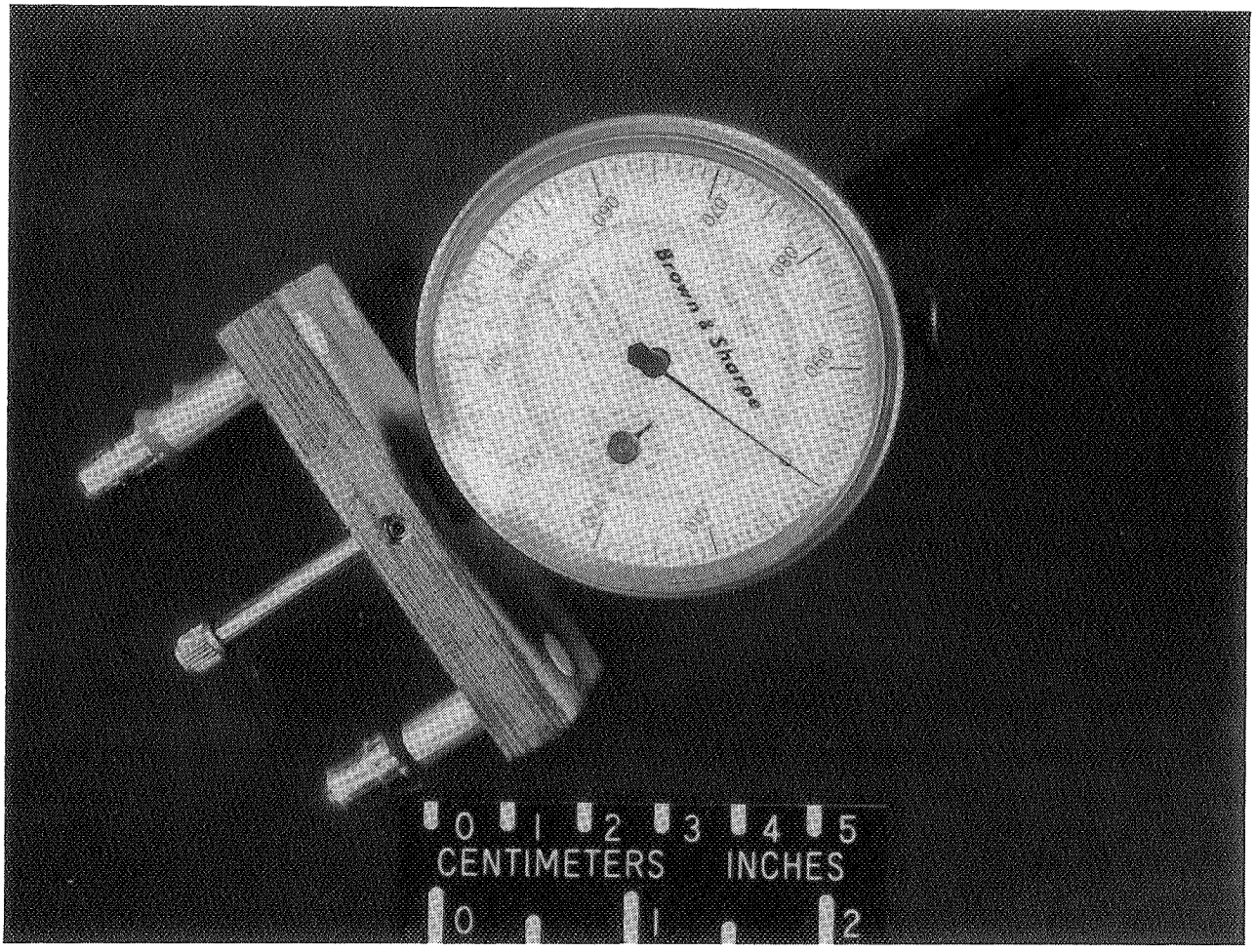

L-81-9530

Figure A1.- Airfoil surface waviness gauge with 2-in. base.

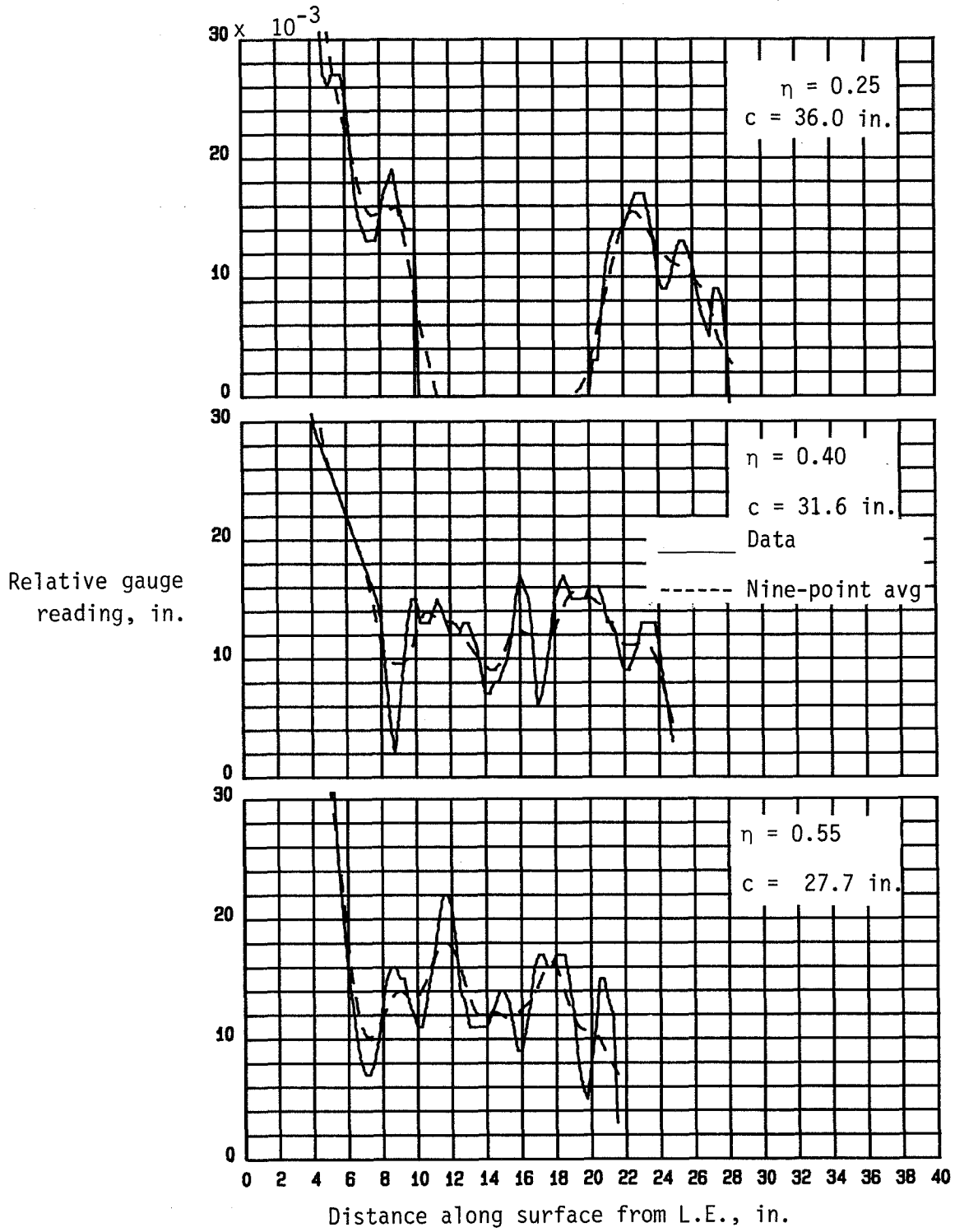

(a) Upper surface of right wing.

Figure A2.- Indicated waviness data on flight-test airfoil surface of VariEze airplane.

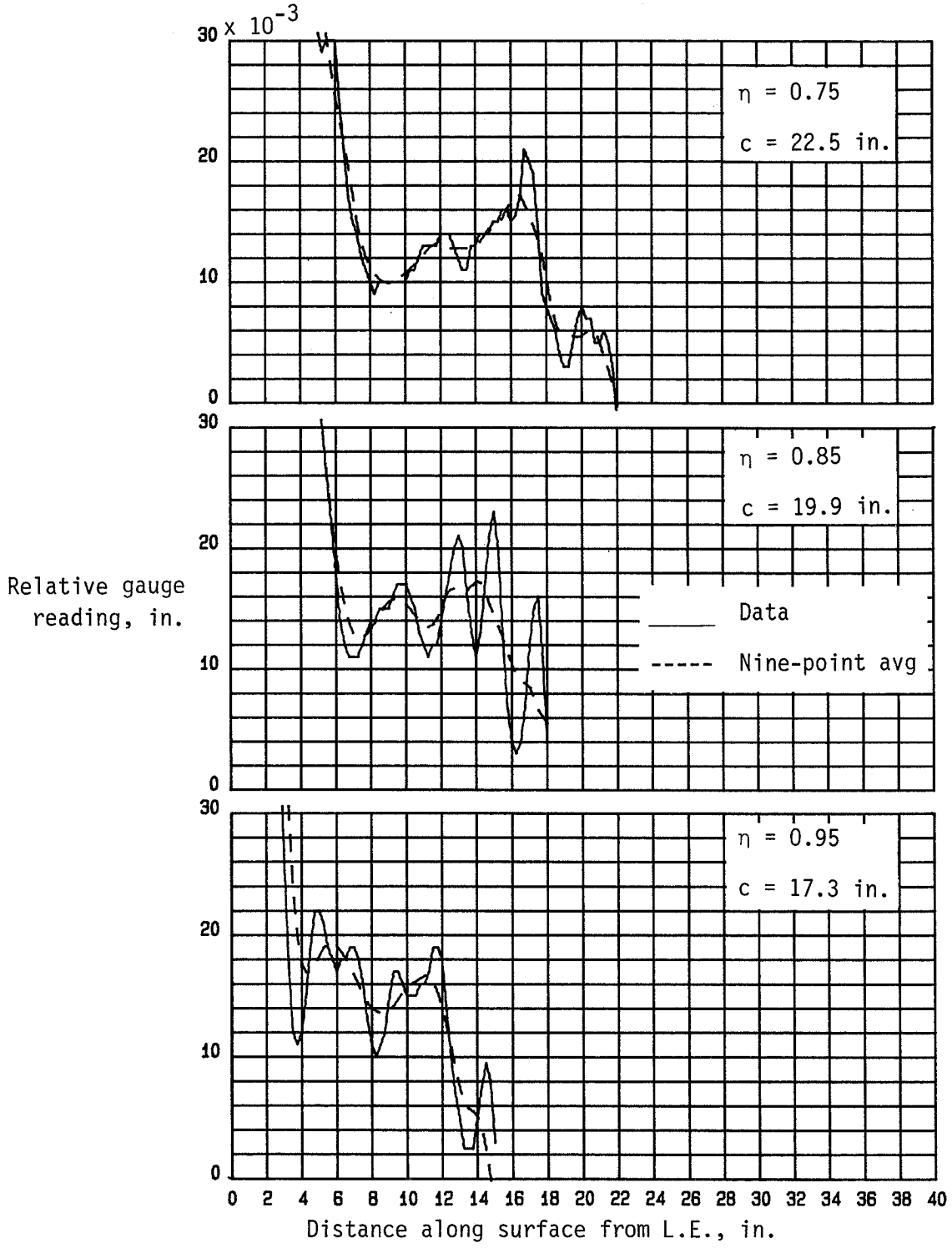

(a) Concluded.

Figure A2.- Continued.

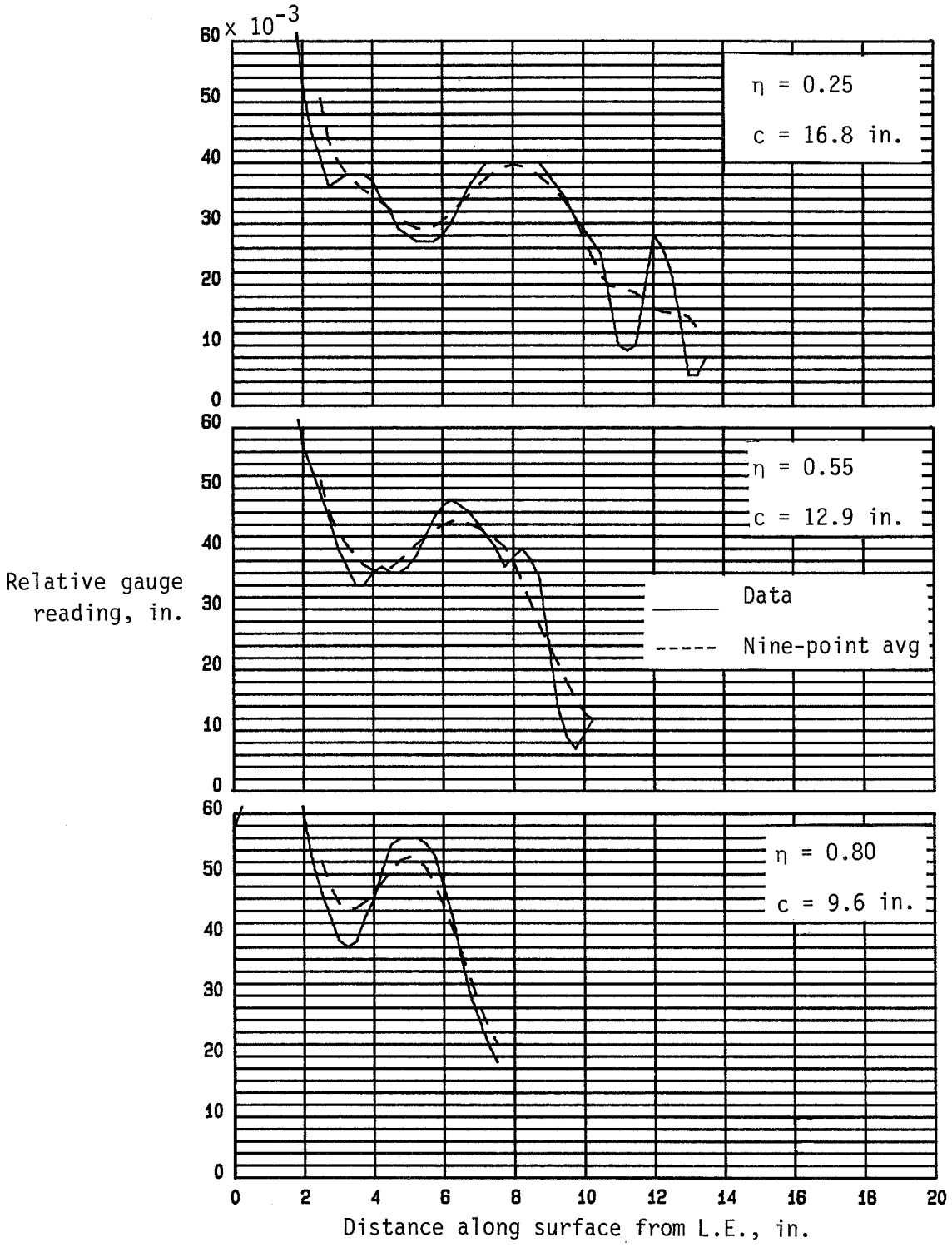

(b) Upper surface of right winglet.

Figure A2.- Continued.

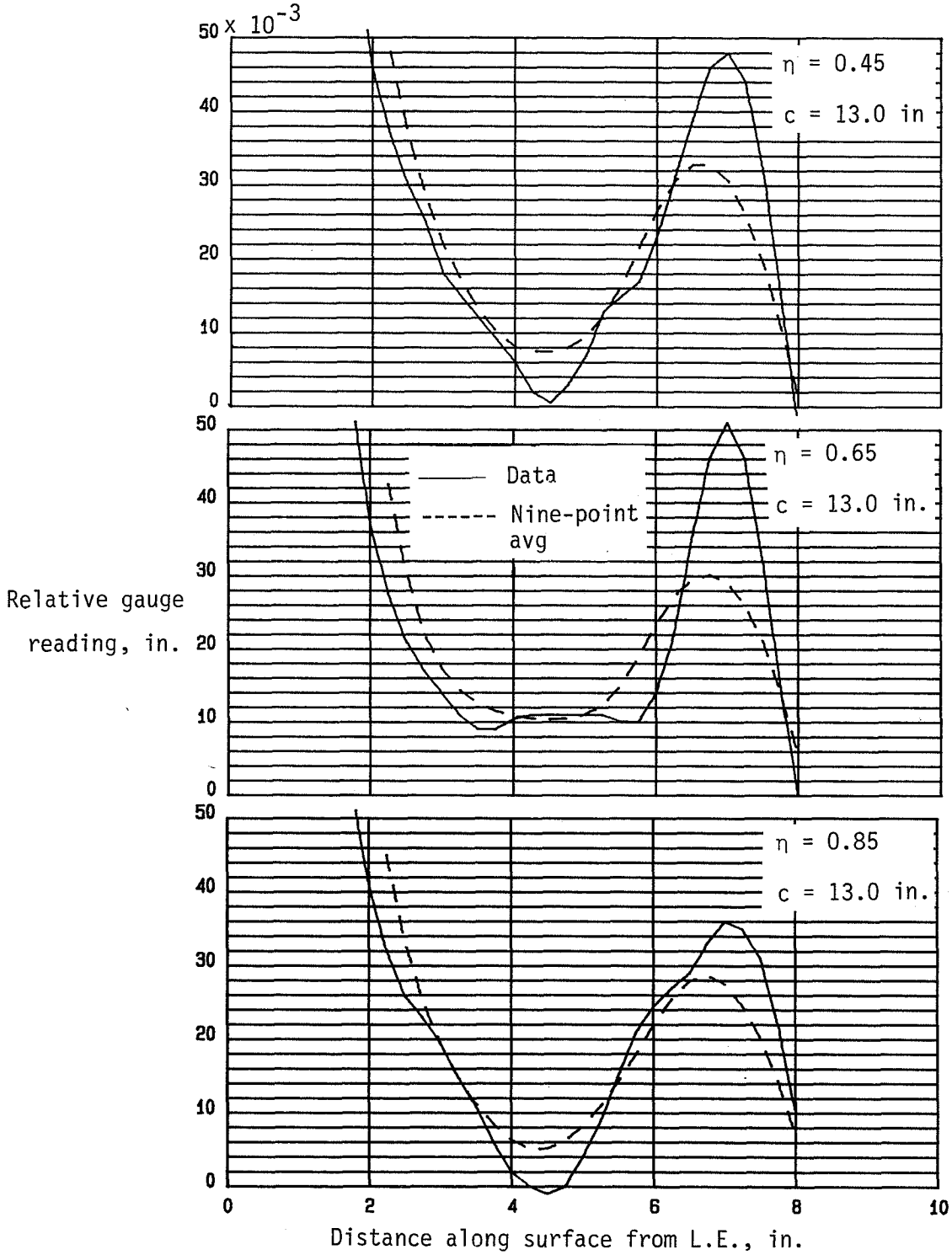

(c) Upper surface of right canard.

Figure A2.- Concluded.

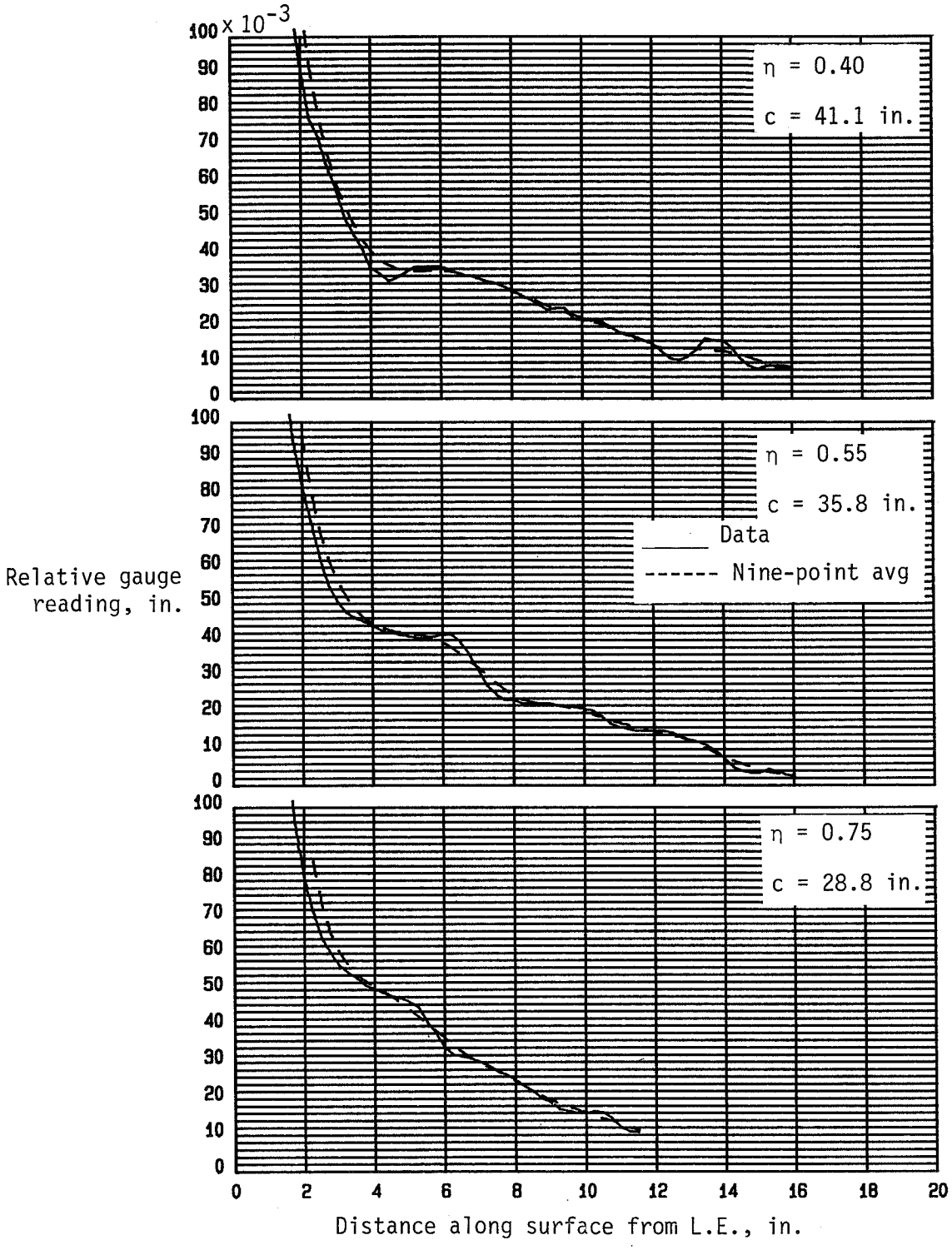

(a) Upper surface of right wing.

Figure A3.- Indicated waviness data on airfoil surface of Long-EZ airplane.

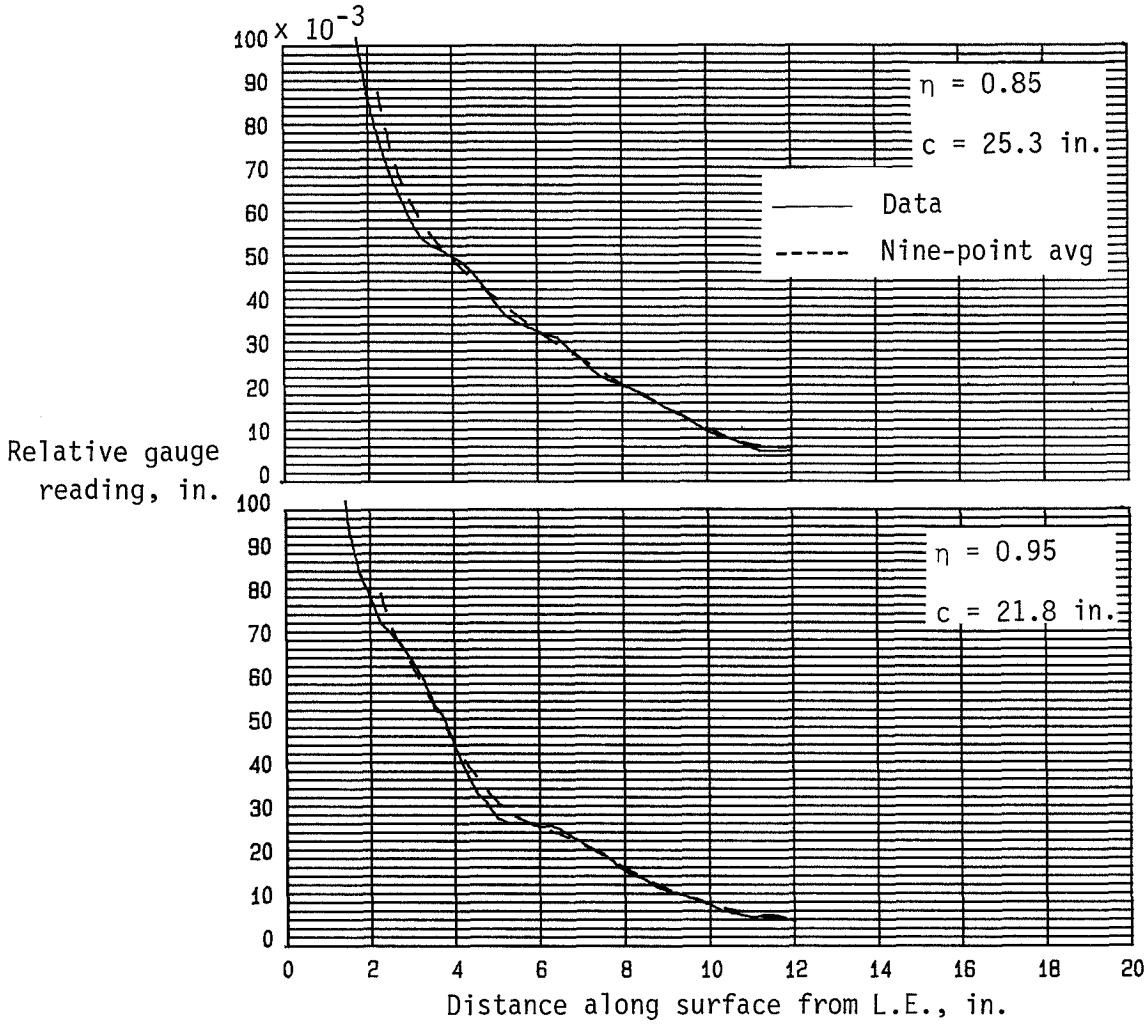

(a) Concluded.

Figure A3.- Continued.

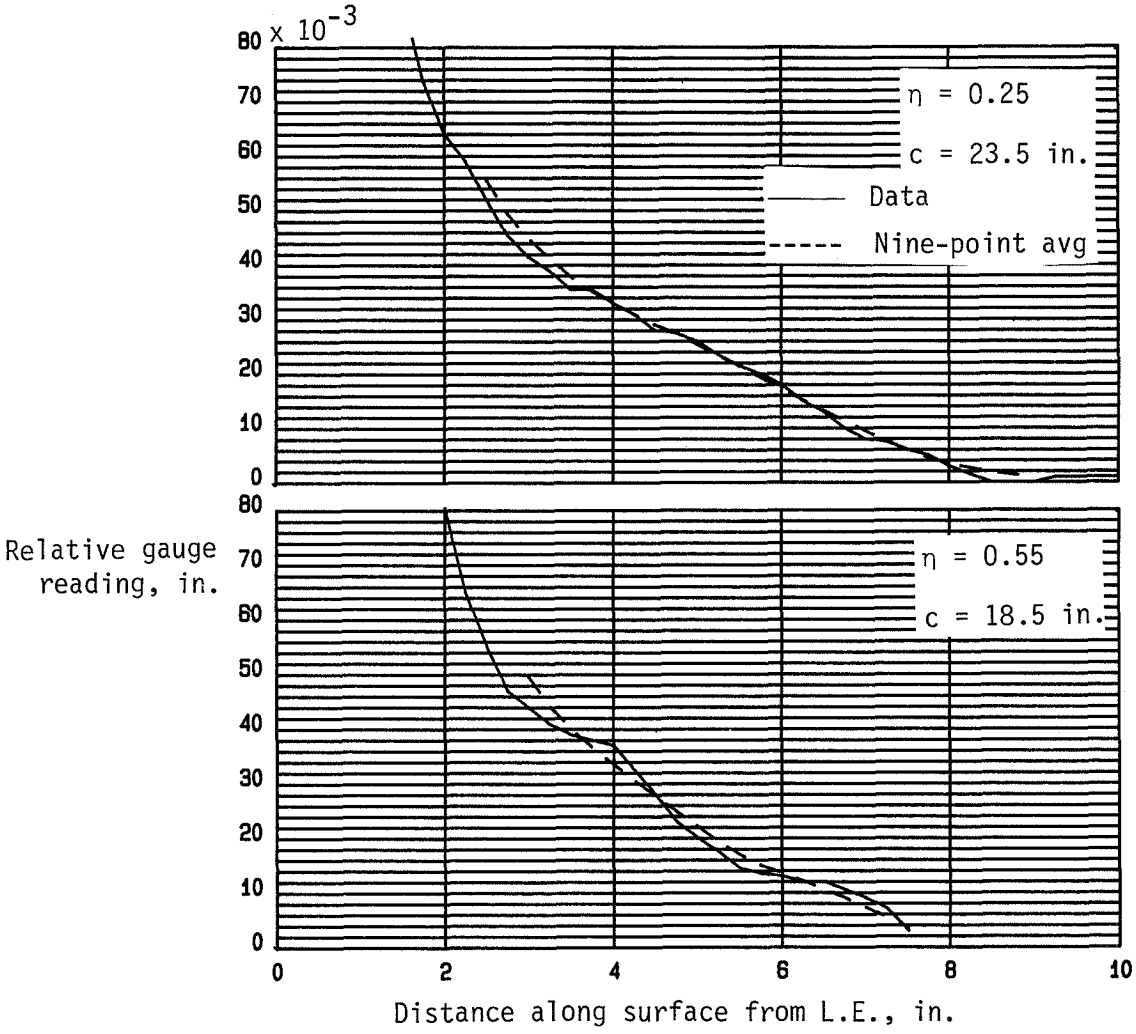

(b) Upper surface of right winglet.

Figure A3.- Continued.

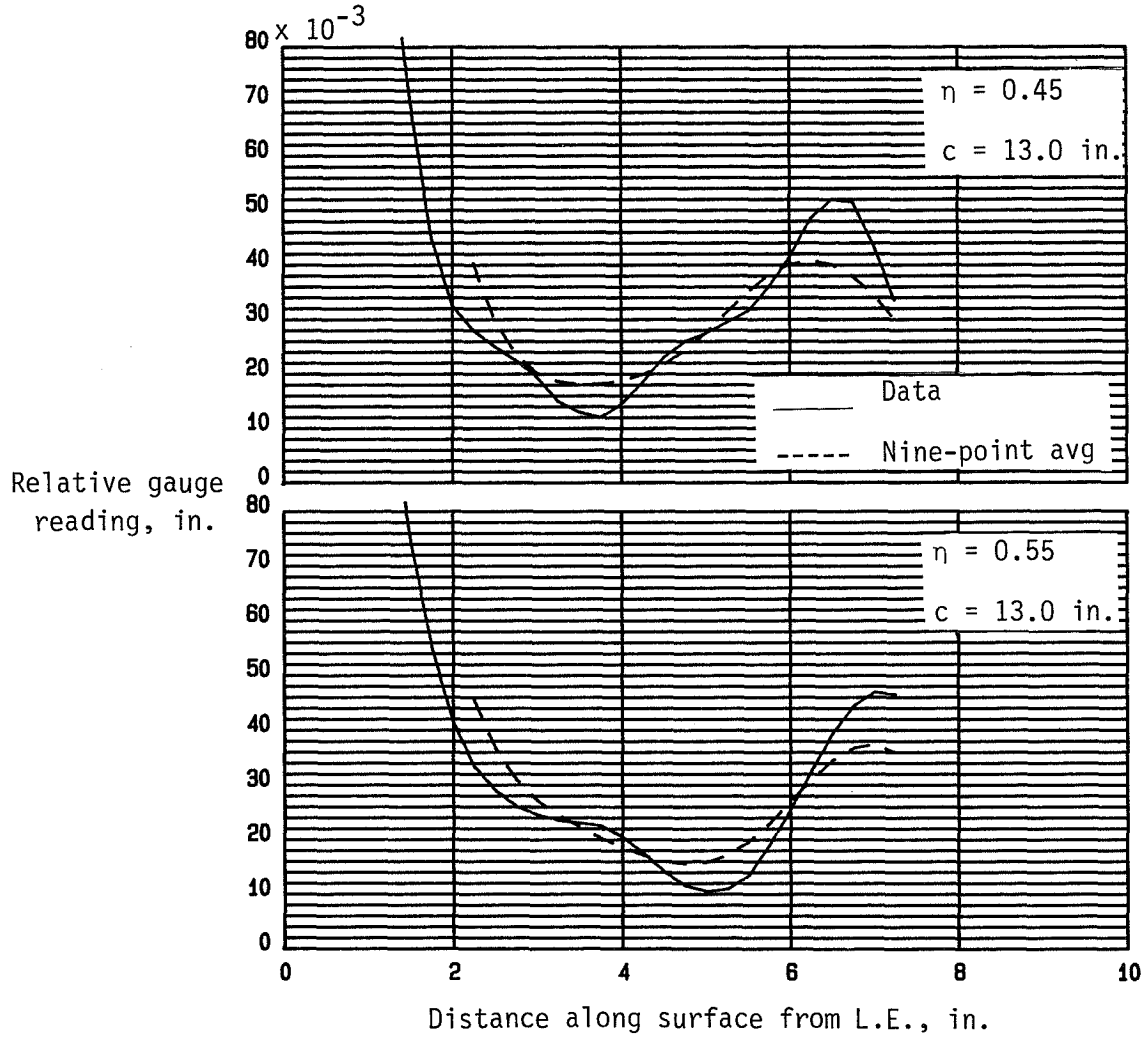

(c) Upper surface of right canard.

Figure A3.- Concluded.

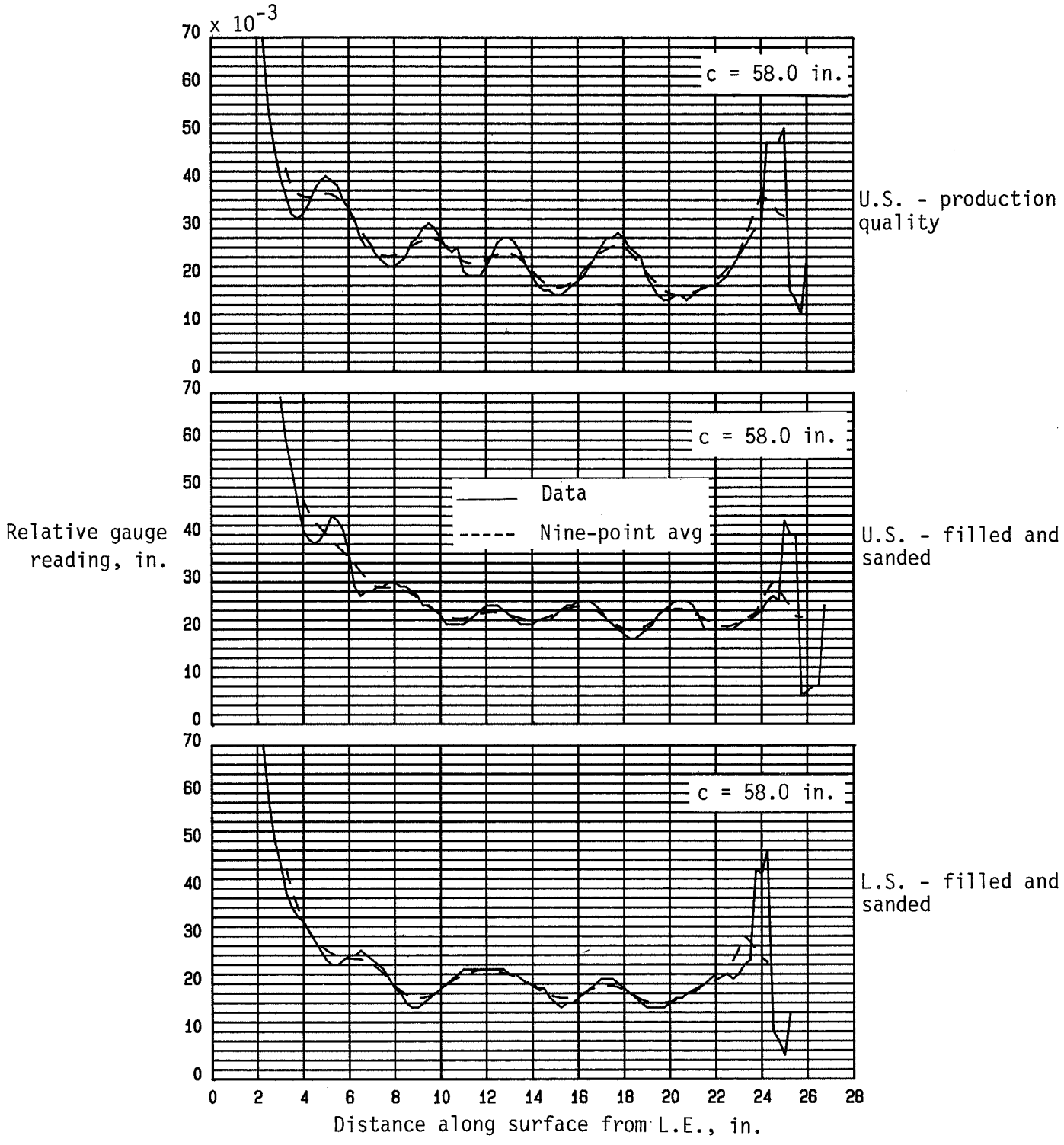

Figure A4.- Indicated waviness data on airfoil surface of Cessna P-210 airplane.

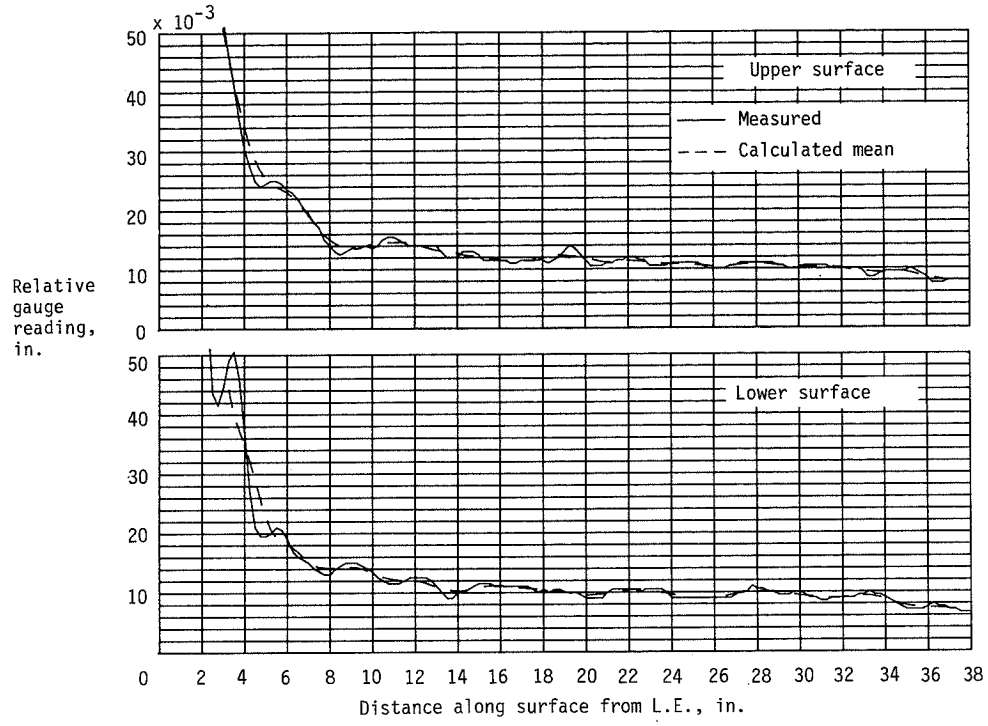

(a) Inboard wake-probe station.

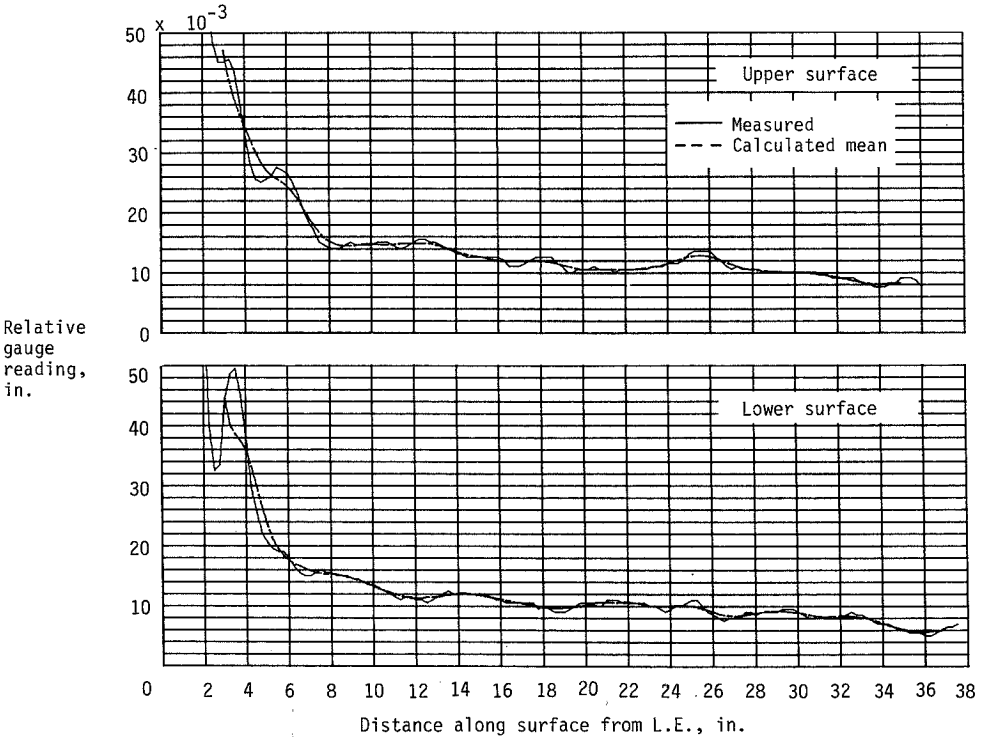

(b) Outboard wake-probe station.

Figure A5.- Indicated waviness data on airfoil surface of Bellanca Skyrocket II airplane.

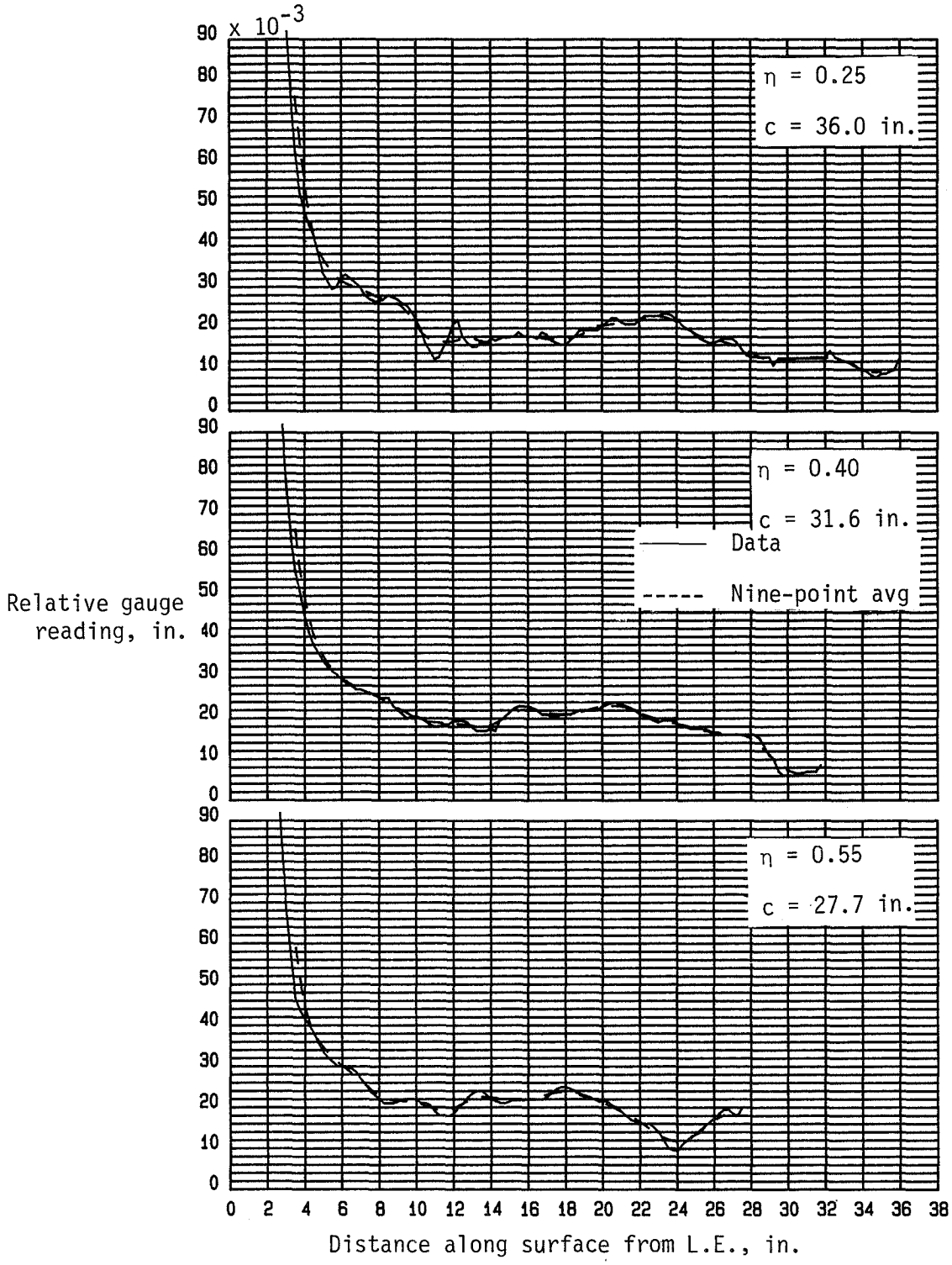

(a) Upper surface of right wing.

Figure A6.- Indicated waviness data on wind-tunnel airfoil surface of VariEze airplane.

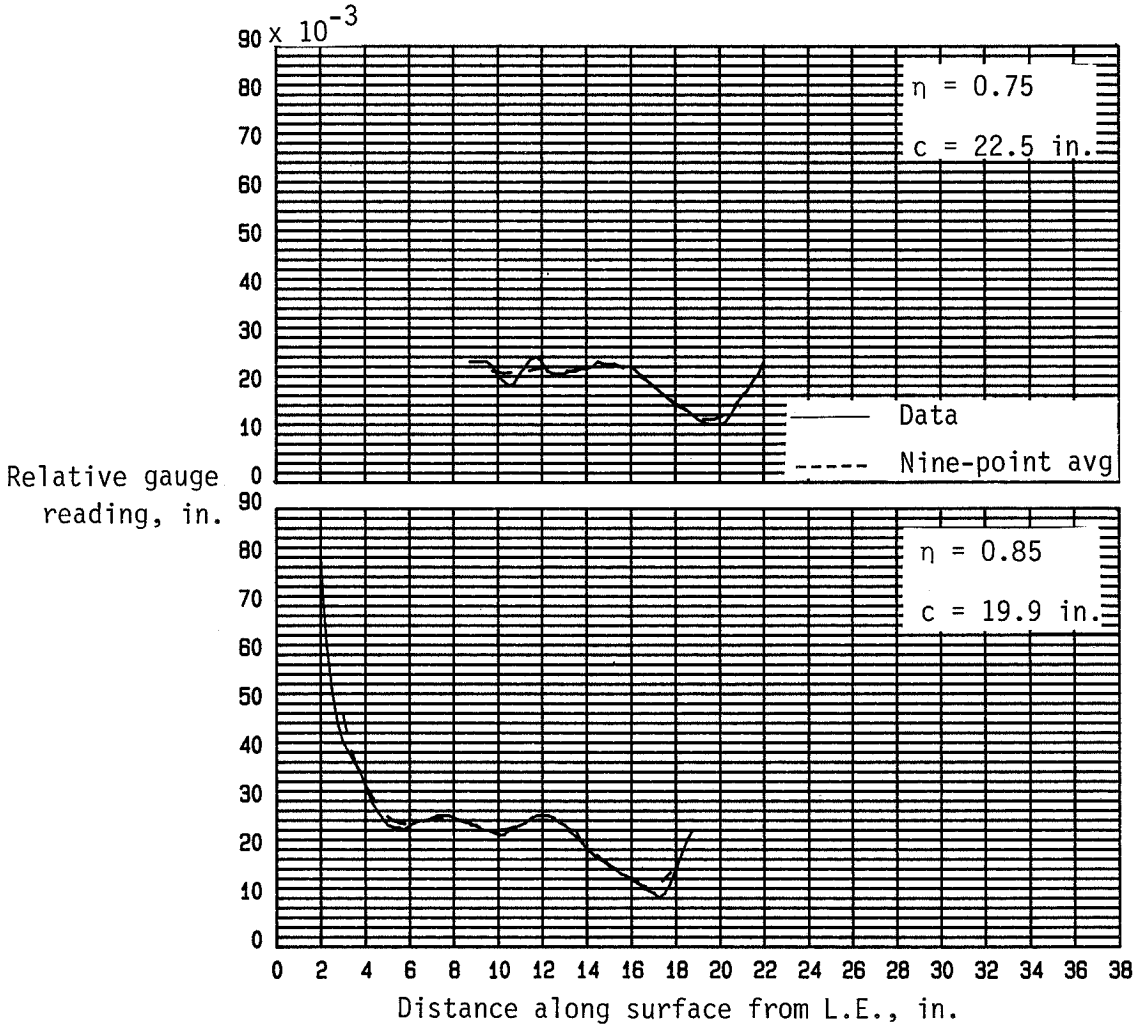

(a) Concluded.

Figure A6.- Continued.

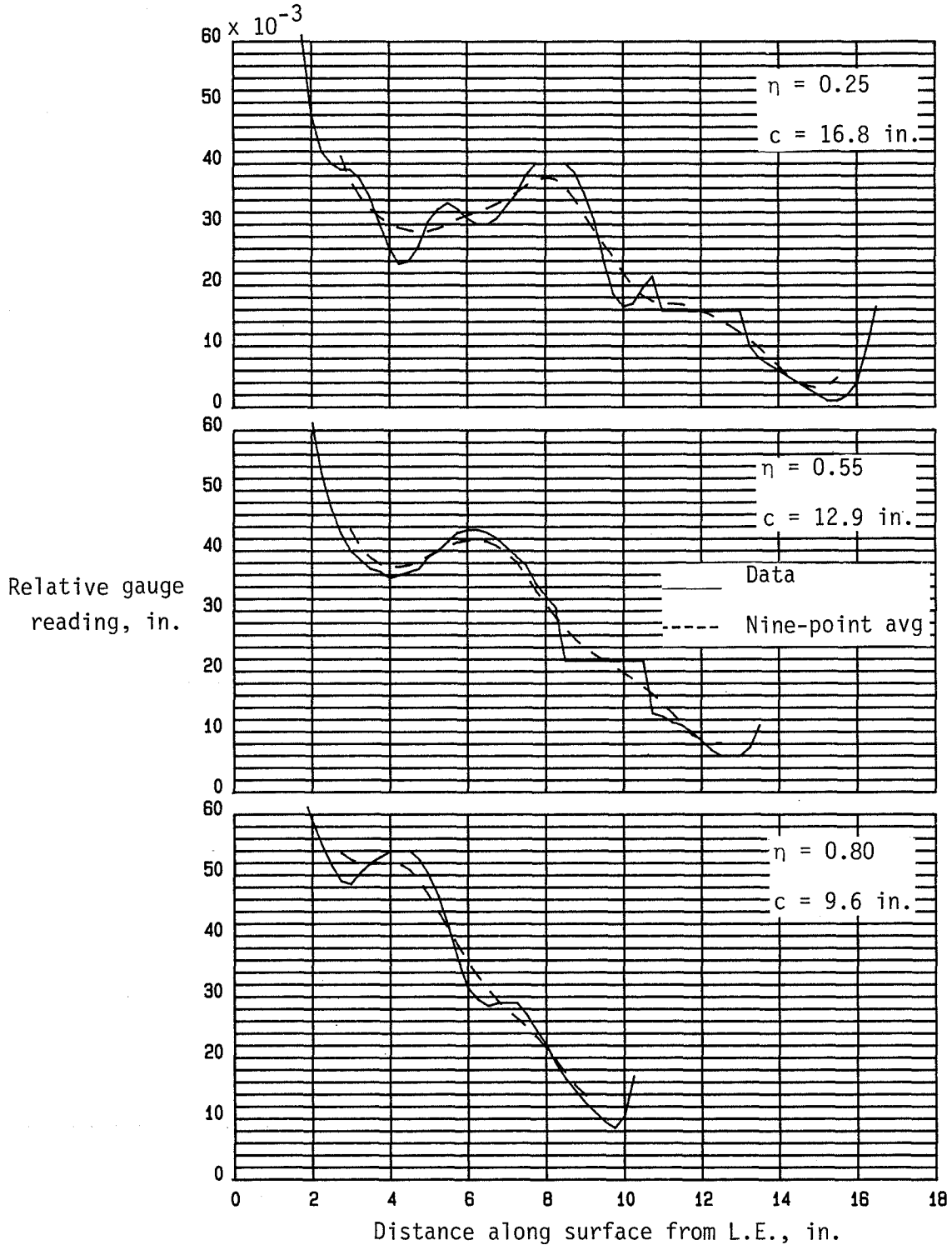

(b) Upper surface of right winglet.

Figure A6.- Continued.

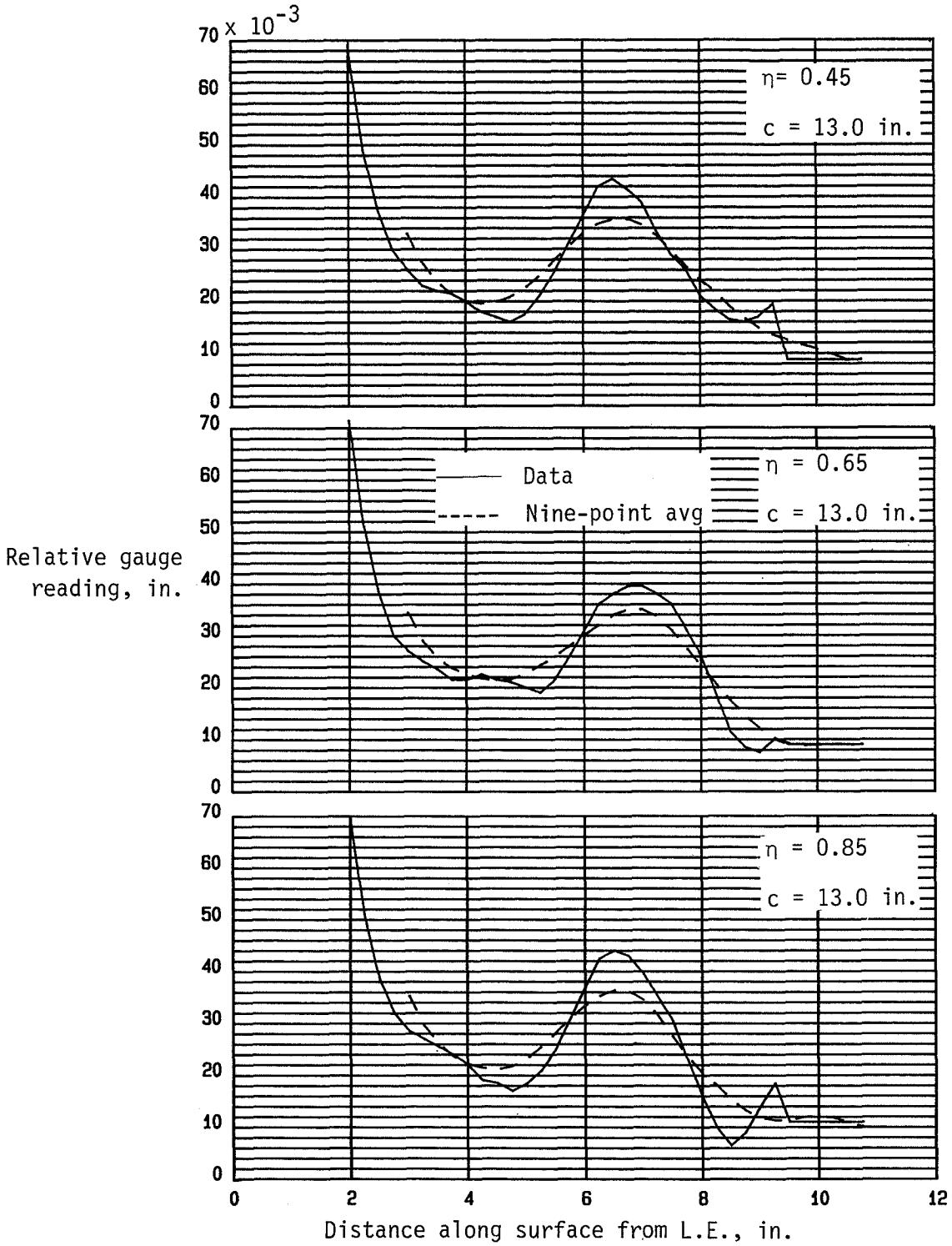

(c) Upper surface of right canard.

Figure A6.- Concluded.

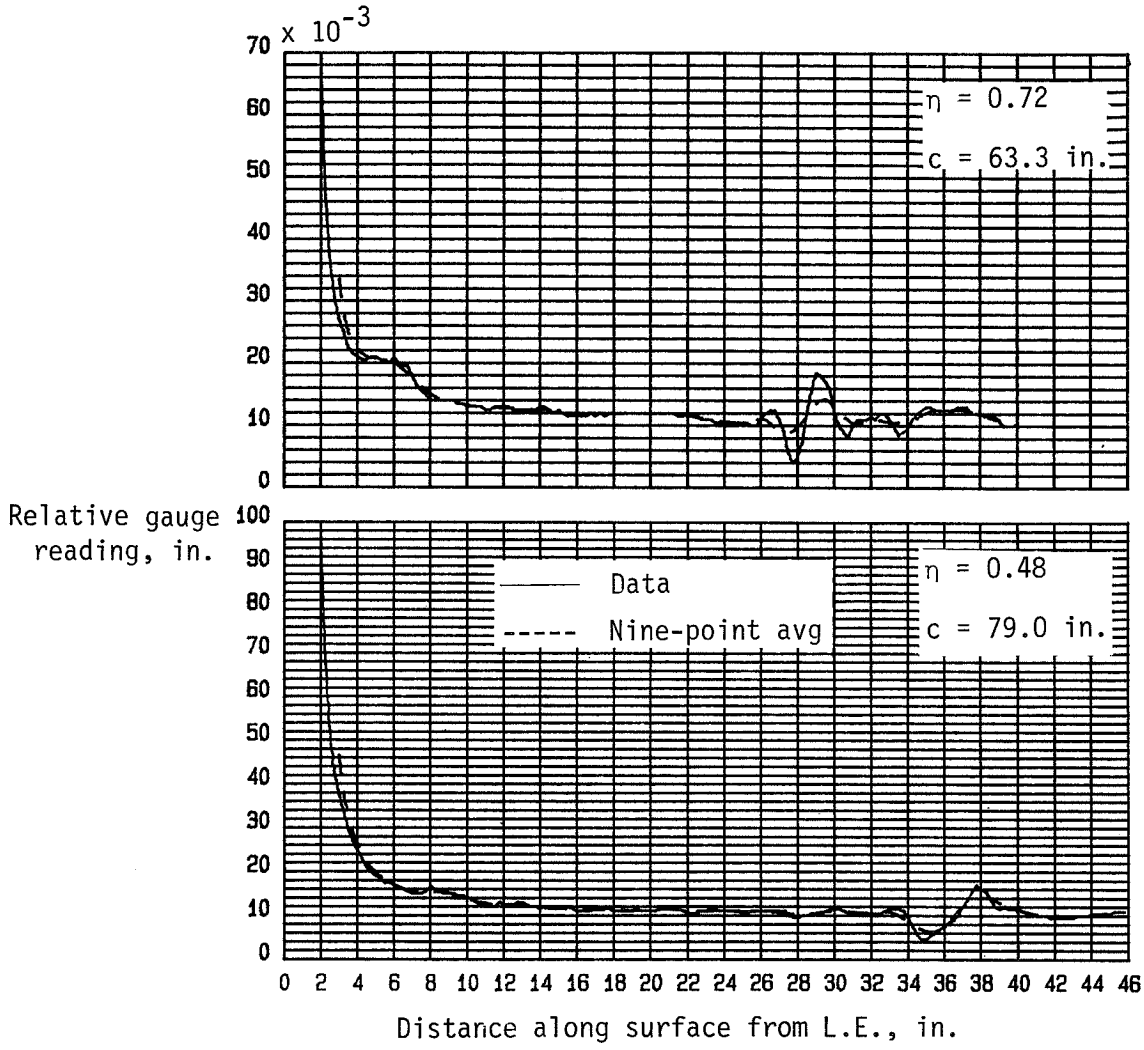

(a) Upper surface of right wing.

Figure A7.- Indicated waviness data on airfoil surface of Gates Learjet Model 28/29 airplane.

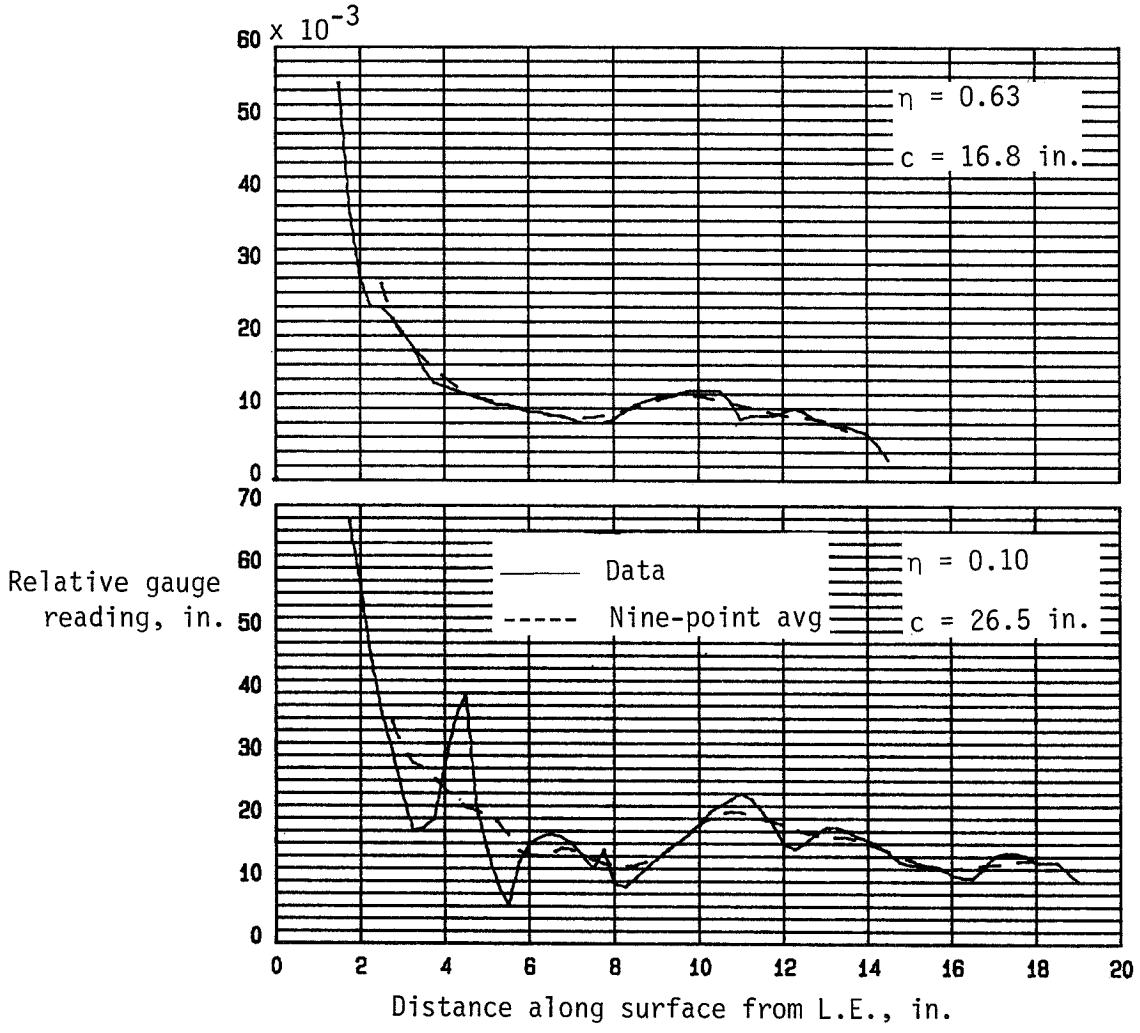

(b) Upper surface of right winglet.

Figure A7.- Concluded.

REFERENCES

1. Loftin, Laurence K., Jr.: Subsonic Aircraft: Evolution and the Matching of Size to Performance. NASA RP-1060, 1980.

2. Stüper, J.: Investigation of Boundary Layers on an Airplane Wing in Free Flight. NACA TM 751, 1934.

3. Jones, Melvill: Flight Experiments on the Boundary Layer. J. Aeronaut. Sci., vol. 5, no. 3, Jan. 1938, pp. 81-94.

4. Stephens, A. V.; and Haslam, J. A. G.: Flight Experiments on Boundary Layer Transition in Relation to Profile Drag. R. & M. No. 1800, British A.R.C., 1938.

5. Young, A. D.; and Morris, D. E.: Note on Flight Tests on the Effect of Slipstream on Boundary Layer Flow. R. & M. No. 1957, British A.R.C., 1939.

6. Young, A. D.; and Morris, D. E.: Further Note on Flight Tests on the Effect of Slipstream on Boundary Layer Flow. Rep. No. B.A. 1404b, British R.A.E., Sept. 1939.

7. Young, A. D.; Serby, J. E.; and Morris, D. E.: Flight Tests on the Effect of Surface Finish on Wing Drag. R. & M. No. 2258, British A.R.C., 1939.

8. Goett, Harry J.; and Bicknell, Joseph: Comparison of Profile-Drag and Boundary-Layer Measurements Obtained in Flight and in the Full-Scale Wind Tunnel. NACA TN 693, 1939.

9. Bicknell, Joseph: Determination of the Profile Drag of an Airplane Wing in Flight at High Reynolds Numbers. NACA Rep. 667, 1939.

10. Wetmore, J. W.; Zalovcik, J. A.; and Platt, Robert C.: A Flight Investigation of the Boundary-Layer Characteristics and Profile Drag of the NACA 35-215 Laminar-Flow Airfoil at High Reynolds Numbers. NASA WR L-532, 1941. (Formerly NACA MR.)

11. Zalovcik, John A.: A Profile-Drag Investigation in Flight on an Experimental Fighter-Type Airplane - The North American XP-15 (Air Corps Serial No. 41-38). NACA ACR, Nov. 1942.

12. Serby, J. E.; Morgan, M. B.; and Cooper, E. R.: Flight Tests on the Profile Drag of 14% and 25% Thick Wings. R. & M. No. 1826, British A.R.C., 1937.

13. Serby, J. E.; and Morgan, M. B.: Note on the Progress of Flight Experiments on Wing Drag. Rep. No. B.A. 1360, British R.A.E., Dec. 1936.

14. Tani, Itiro: On the Design of Airfoils in Which the Transition of the Boundary Layer is Delayed. NACA TM 1351, 1952.

15. Zalovcik, John A.: Profile-Drag Coefficients of Conventional and Low-Drag Airfoils as Obtained in Flight. NACA WR L-139, 1944. (Formerly NACA ACR L4E31.)

16. Zalovcik, John A.; and Skoog, Richard B.: Flight Investigation of Boundary-Layer Transition and Profile Drag of an Experimental Low-Drag Wing Installed on a Fighter-Type Airplane. NACA WR L-94, 1945. (Formerly NACA ACR L5C08a.)

17. Zalovcik, John A.: Flight Investigation of Boundary-Layer and Profile-Drag Characteristics of Smooth Wing Sections of a P-47D Airplane. NACA WR L-86, 1945. (Formerly ACR L5H11a.)

18. Zalovcik, John A.; and Daum, Fred L.: Flight Investigation at High Speeds of Profile Drag of Wing of a P-47D Airplane Having Production Surfaces Covered With Camouflage Paint. NACA WR L-98, 1946. (Formerly NACA ACR L6B21.)

19. Plascott, R. H.: Profile Drag Measurements on Hurricane II Z.3687 Fitted With "Low Drag" Section Wings. Rep. No. Aero. 2153, British R.A.E., Sept. 1946.

20. Plascott, R. H.; Higton, D. J.; Smith, F.; and Bramwell, A. R.: Flight Tests on Hurricane II, Z.3687 Fitted With Special Wings of "Low-Drag" Design. R. & M. No. 2546, British A.R.C., Sept. 1946.

21. Smith, F.; and Higton, D. J.: Flight Tests on "King Cobra" FZ.440 To Investigate the Practical Requirements for the Achievement of Low Profile Drag Coefficients on a "Low Drag" Aerofoil. R. & M. No. 2375, British A.R.C., Aug. 1945.

22. Britland, C. M.: Determination of the Position of Boundary Layer Transition on a Specially-Prepared Section of Wing in Flight at Moderate Reynolds Number and Mach Number. Tech. Memo. No. Aero 193, British R.A.E., Sept. 1951.

23. Davies, Handel: Some Aspects of Flight Research. J. R. Aeronaut. Soc., vol. 55, June 1951, pp. 325-361.

24. Gray, W. E.; and Davies, H.: Note on the Maintenance of Laminar-Flow Wings. R. & M. No. 2485, British A.R.C., 1952.

25. Montoya, Lawrence C.; Steers, Louis L.; Christopher, David; and Trujillo, Bianca: F-111 TACT Natural Laminar Flow Glove Flight Results. Advanced Aerodynamics - Selected NASA Research, NASA CP-2208, 1981, pp. 11-20.

26. Banner, Richard D.; McTigue, John G.; and Petty, Gilbert, Jr.: Boundary-Layer-Transition Measurements in Full-Scale Flight. NACA RM H58E28, 1958.

27. Final Report on LFC Aircraft Design Data Laminar Flow Control Demonstration Program. NOR 67-136 (Contract AF 33(657)-13930), Northrop Corp., June 1967. (Available from DTIC as AD 819 317.)

28. Bushnell, Dennis M.; and Tuttle, Marie H.: Survey and Bibliography on Attainment of Laminar Flow Control in Air Using Pressure Gradient and Suction. Volume I. NASA RP-1035, 1979.

29. Yip, Long P.; and Coy, Paul F.: Wind-Tunnel Investigation of a Full-Scale Canard-Configured General Aviation Aircraft. Proceedings of the 13th Congress of the International Council of the Aeronautical Sciences and AIAA Aircraft Systems and Technology Conference, Volume 2, B. Laschka and R. Staufenbiel, eds., Aug. 1982, pp. 1470-1488. (Available as ICAS-82-6.8.2.)

30. Braslow, Albert L.; and Knox, Eugene C.: Simplified Method for Determination of Critical Height of Distributed Roughness Particles for Boundary-Layer Transition at Mach Numbers From 0 to 5. NACA TN 4363, 1958.

31. Holmes, Bruce J.; Obara, Clifford J.; Gregorek, Gerald M.; Hoffman, Michael J.; and Freuhler, Rick J.: Flight Investigation of Natural Laminar Flow on the Bellanca Skyrocket II. SAE Paper 830717, Apr. 1983.

32. Owen, P. R.; and Ormerod, A. O.: Evaporation From the Surface of a Body in an Airstream (With Particular Reference to the Chemical Method of Indicating Boundary-Layer Transition). R. & M. No. 2875, British A.R.C., 1954.

33. Main-Smith, J. D.: Chemical Solids as Diffusible Coating Films for Visual Indications of Boundary-Layer Transition in Air and Water. R. & M. No. 2755, British A.R.C., 1950.

34. Holmes, Bruce J.: Low-Speed Airspeed Calibration Data for a Single-Engine Research-Support Airplane. NASA TM-81832, 1980.

35. Carmichael, Bruce H.: Summary of Past Experience in Natural Laminar Flow and Experimental Program for Resilient Leading Edge. NASA CR-152276, 1979.

36. Stevens, W. A.; Goradia, S. H.; and Braden, J. A.: Mathematical Model for Two-Dimensional Multi-Component Airfoils in Viscous Flow. NASA CR-1843, 1971.

37. Abbott, Ira H.; Von Doenhoff, Albert E.; and Stivers, Louis S., Jr.: Summary of Airfoil Data. NACA Rep. 824, 1945. (Supersedes NACA WR L-560.)

38. Eppler, Richard; and Somers, Dan M.: A Computer Program for the Design and Analysis of Low-Speed Airfoils. NASA TM-80210, 1980.

39. Melnik, R. E.; Mead, H. R.; and Jameson, A.: A Multi-Grid Method for the Computation of Viscid/Inviscid Interactions on Airfoils. AIAA-83-0234, Jan. 1983.

40. Hall, G. R.: On the Mechanics of Transition Produced by Particles Passing Through an Initially Laminar Boundary Layer and the Estimated Effect on the LFC Performance of the X-21 Aircraft. Northrop Corp., Oct. 1964.

41. Hall, G. R.: Interaction of the Wake From Bluff Bodies With an Initially Laminar Boundary Layer. AIAA J., vol. 5, no. 8, Aug. 1967, pp. 1386-1392.

42. Nastrom, Gregory D.; Holdeman, James D.; and Davis, Richard E.: Cloud-Encounter and Particle-Concentration Variabilities From GASP Data. NASA TP-1886, 1981.

43. Holmes, B. J.; and Obara, C. J.: Observations and Implications of Natural Laminar Flow on Practical Airplane Surfaces. ICAS Paper No. 82-5.1.1, Aug. 1982.

44. Hood, Manley J.; and Gaydos, M. Edward: Effects of Propellers and of Vibration on the Extent of Laminar Flow on the N.A.C.A. 27-212 Airfoil. NACA WR L-784, Oct. 1939. (Formerly NACA ACR.)

45. Wenzinger, Carl J.: Wind-Tunnel Investigation of Several Factors Affecting the Performance of a High-Speed Pursuit Airplane With Air-Cooled Radial Engine. NACA ACR, Nov. 1941.

46. Beasley, J. A.: Calculation of the Laminar Boundary Layer and Prediction of Transition on a Sheared Wing. R. & M. No. 3787, British A.R.C., 1976.

47. Gilkey, R. D.: Design and Wind Tunnel Tests of Winglets on a DC-10 Wing. NASA CR-3119, 1979.

48. Glick, P. A.: The Distribution of Insects, Spiders, and Mites in the Air. Tech. Bull. No. 673, U.S. Dep. Agriculture, May 1939.

49. Freeman, J. A.: Studies in the Distribution of Insects by Aerial Currents - The Insect Population of the Air From Ground Level to 300 Feet. J. Anim. Ecol., vol. 14, 1945, pp. 128-154.

50. Atkins, P. B.: Wing Leading Edge Contamination by Insects. Flight Note 17, Aeronaut. Res. Labs. (Melbourne), Oct. 1951.

51. Johnson, D.: Brief Measurements of Insect Contamination on Aircraft Wings. Tech. Note No. Aero. 2164, British R.A.E., May 1952.

52. Lachmann, G. V.: Aspects of Insect Contamination in Relation to Laminar Flow Aircraft. C.P. No. 484, British A.R.C., 1960.

53. Coleman, W. S.: Roughness Due to Insects. Boundary Layer and Flow Control, Volume 2, G. V. Lachmann, ed., Pergamon Press, 1961, pp. 682-747.

54. Boermans, L. M. M.; and Selen, J. J. W.: On the Design of Some Airfoils for Sailplane Application. VTH-LR-326, Dep. Aerospace Eng., Delft Univ. of Technol., Apr. 1981.

55. Kohlman, David L.; Schweikhard, William G.; and Albright, Alan E.: Icing Tunnel Tests of a Glycol-Exuding Porous Leading Edge Ice Protection System on a General Aviation Airfoil. NASA CR-165444, 1981.

56. Lockheed-Georgia Co.: Evaluation of Laminar Flow Control System Concepts for Subsonic Commercial Transport Aircraft. NASA CR-159253, 1980.

57. Peterson, John B., Jr.; and Fisher, David F.: Flight Investigation of Insect Contamination and Its Alleviation. CTOL Transport Technology - 1978, NASA CP-2036, Part I, 1978, pp. 357-373.

TABLE 1.- NATURAL LAMINAR FLOW FLIGHT EXPERIMENTS

Principal investigators	References	Airplane	Airfoil	Type surface	Speed or chord Reynolds number	Measurements	Results	Comments
Stüper	2	Klenm L26Va		Sanded plywood glove	4.88×10^6	C_p; u/u_e	$(x/c)_t > 30\%$	First in-flight transition measurements
Jones, Stephens, Haslam	3, 4	Snark L6103	t/c = 17.5%	Sanded plywood glove	2.8 to 10.8×10^6	C_d; C_p; u/u_e	$16\% < (x/c)_t < 30\%$	Waviness measured
		Hart K1442	t/c = 10%	Metal glove				Effects of steps on transition measured
Young, Morris	5, 6	Anson	NACA 2218	Metal glove	139 knots	u/u_e	$(x/c)_t = 17\%$	Measurements inside and outside propeller slipstream
		Courier	NACA 2219	Metal glove	122 knots	u/u_e	$(x/c)_t = 25\%$, outside propeller slipstream	
Young, Serby, Morris	7	Battle	NACA 2417	Metal glove; production-metal wing surface; camouflage	12 to 18×10^6	C_d; C_p; u/u_e	$(x/c)_t = 18\%$, on glove	Drag of rivets and lap joints measured No effect of camouflage paint on transition No appreciable NLF on production surface
Goett, Bicknell	8	Fairchild 22	N-22	Stiffened metal test panel	3.9 to 4.6×10^6	C_d; C_p; u/u_e	$(x/c)_t = 37\%$, downstream of predicted laminar separation	Proximate transition locations for flight and Langley 30- by 60-Foot Tunnel
Bicknell	9	Northrup A-17A	NACA 2414.5	Production metal wing (flush rivets, aft-facing lap joint at x/c = 8%); metal glove	15×10^6	C_d; C_p; u/u_e	$(x/c)_t = 17.5\%$, glove	No appreciable NLF on production surface

TABLE 1.- Continued

Principal investigators	References	Airplane	Airfoil	Type surface	Speed or chord Reynolds number	Measurements	Results	Comments
Wetmore, Zalovcik, Platt	10	Douglas B-18	NACA 35-215	Wood glove	30×10^6	C_d; C_p; u/u_e	$(x/c)_t = 42.4\%$	Waviness measured Engine operation effects measured
Zalovcik	11	XP-51	NACA $64_1$2-(1.4), (13.5)	Production metal surface; various surface conditions	16×10^6	C_d; C_p; u/u_e		Waviness measured No appreciable NLF on production surface
Serby, Morgan, Cooper	12	Hawcon	t/c = 14% t/c = 25%	Wood glove Metal glove	5.7 to 8×10^6	C_d; C_p; u/u_e	$30\% < (x/c)_t < 40\%$	
Serby, Morgan	13	Hawcon	t/c = 14%	Metal glove	5 to 9×10^6	C_d		
		Heinkel He.70	t/c = 12.5%	Production wood surface	17×10^6	C_d	$C_{d,min} = 0.0065$	Drag increases with mist deposit on laminar wing measured Low drag of production wood wing suggested extensive NLF
Tani	14	Japanese biplane		Wood glove	5 to 10×10^6	C_d; C_p; u/u_e	$40\% < (x/c)_t < 51\%$	
Zalovcik	15	Several aircraft	8 airfoils	Smoothed and gloved surfaces	4 to 32×10^6	C_d; C_p; u/u_e	Extensive NLF runs measured	Waviness measured

TABLE 1.- Continued

Principal investigators	References	Airplane	Airfoil	Type surface	Speed or chord Reynolds number	Measurements	Results	Comments
Zalovcik, Skoog	16	XP-47F	NACA 66(215)-1 (16.5), a = 1.0 NACA 67(115)-213, a = 0.7	Production metal surface Smoothed surface	9 to 18 × 10^6	C_d; C_p; u/u_e	$(x/c)_t$ = 50%	No appreciable NLF on production surface Propeller slipstream effects measured
Zalovcik	17	P-47D	Republic S-3 t/c = 11%, t/c = 14.6%	Smoothed surface	7.7 to 19.7 × 10^6	C_d; C_p; u/u_e	$(x/c)_t$ = 20%, $C_{d,min}$ = 0.0062	Waviness measured
Zalovcik, Daum	18	P-47D	Republic S-3	Production metal surface with camouflage paint	0.25 < M < 0.78 8.4 to 23.1 × 10^6	C_d; C_p	$C_{d,min}$ = 0.0097, compare with reference 17	No appreciable NLF on production surface Waviness and roughness measured
Plascott, Higton, Smith, Bramwell	19, 20	Hurricane II	NPL t/c = 14.8 to 17.9%	Smoothed surface	20 × 10^6	C_d; C_p	$(x/c)_t$ = 60%	Waviness measured
Smith, Higton	21	King Cobra	NACA 662x-116 NACA 662x-216	Production metal surface Smoothed surface	17 × 10^6	C_d; sublimating chemicals	$(x/c)_t$ = 65%	Waviness measured No appreciable NLF on production surface

TABLE 1.- Concluded

Principal investigators	References	Airplane	Airfoil	Type surface	Speed or chord Reynolds number	Measurements	Results	Comments
Britland	22	Vampire	NACA 67,1-314, a = 1.0	Metal glove	M = 0.7; 30.4×10^6	C_p; sublimating chemicals	$(x/c)_t > 50\%$	Waviness measured
Davies	23	Several aircraft		Production surface; smoothed surface		C_d; sublimating and oxidizing chemicals; C_p, u/u_e		Waviness measured No appreciable NLF on production surface
Gray, Davies	24	King Cobra	NACA 662x-116 NACA 662x-216	Smoothed surface	17×10^6	C_d; sublimating chemicals	Skin-joint filler cracks most serious surface maintenance problem	Insect contamination discussed Laminar flow maintainability studied
Montoya, Steers, Christopher, Trujillo	25	F-111 TACT	Supercritical NLF	Glove	Up to 30×10^6	u/u_e	$(x/c)_t = 56\%$ at $\Lambda = 10\%$	Sweep effects studied
Banner, McTigue, Petty	26	F-104	Biconvex t/c = 3.4%	Production metal; fiberglass gloved surface	$1.2 < M < 2$	Hot films; sublimating chemicals	$1.2 < R_t < 8 \times 10^6$	Less laminar flow on production than on gloved surface

TABLE 2.- SUMMARY OF MEASURED AND PREDICTED TRANSITION LOCATIONS

Airplane (construction)	Component	Airspeed, V_c, knots	C_L	R_c	R, ft^{-1}	Leading edge		Transition location, x/c		Transition prediction		Comments	Data figures		Geometry figures		Geometry tables	
						Λ_{le}, deg	R_θ	Measured	Predicted	α, deg	Method, ref.		Number	Page	Number	Page	Number	Page
VariEze in tunnel (composite)	Wing Winglet Canard Strake	56	0.27	1.61×10^6 $.76 \times 10^6$ $.68 \times 10^6$	0.625×10^6	27 29 0 61	23-47 <45 123	0.65 0.65 0.55 >0.05	0.59 .52 .57	-2.0 0 -1.25	38 38 38	Effects of fixed transition and simulated rain measured; waviness measured	19(a), (c) 19(d) 19(b)	92,94 95 93	1	73	3,4	57, 58
VariEze in flight (fiberglass composite)	Wing, root Wing, tip Winglet Canard Strake	135	0.35	4.17×10^6 1.87×10^6 1.69×10^6 1.52×10^6	1.40×10^6	27 27 29 0 61	66 37 51 175	0.30 0.55 0.55 0.55 >0.05	0.58 .61 .52 .57	-1.60 -5.70 0 -1.70	38 38 38 38	Effects of fixed transition measured; waviness measured; effect of flight through clouds observed	25(a) 25(a) 25(b)	101 101 102	1	73	3,4	57, 58
Long-EZ (fiberglass composite)	Wing Outboard strake Inboard strake Winglet Canard Fuselage nose Wheel fairing	153	0.16	4.45×10^6 2.43×10^6 1.54×10^6	1.42×10^6	23 51 64 28 0	47-51 123-144 >240 33-36	0.32-0.34 0.10-0.15 0 0.32-0.35 0.55 (a) (b)	0.26 .30 .57	-0.77 0 -1.70	38 38 38	Effects of fixed transition measured; waviness measured	28(a) 28(b) 28(b) 28(c), (d) 28(e) 28(f) 28(g)	105 106 106 107, 108 109 110 111	5	77	4,5, 6	58,62 63
Biplane Racer (composite)	Forward wing Aft wing	165	0.13	3.68×10^6 2.65×10^6	1.38×10^6	3.2 6.3		0.61 0.61	0.56 .60	-0.80 0	38 38	Propeller wake effects observed; n = 3100 rpm	31(a) 31(b)	114 115	7	80	7,8	66,67
Gates Learjet Model 28/29 (milled Al skins; integrally stiffened)	Wing Winglet	357 M = 0.7	0.12	21.3×10^6 6.61×10^6	3.08×10^6	17 40	47-74 75-151	0.40-0.45 0.55	0.24	-0.15	39	Waviness measured	32(a) 32(b)	116 117			9	69
Cessna P-210 (flush-riveted aluminum)	Wing, U.S. Wing, U.S. Wing, U.S. Wing, L.S. Horizontal tail, pressure side Propeller spinner	139 149 154 149 139-154 139-154	0.32 0.28 0.26 0.28 0.28-0.32 0.28-0.32	6.81×10^6 7.27×10^6 7.52×10^6 7.27×10^6	1.34×10^6 1.43×10^6 1.48×10^6 1.43×10^6 $1.34\text{-}1.43 \times 10^6$	0		<0.05 0.29 0.44 0.40 0.27 (c)	0.44 .44 .44 .43 .26	1.30 1.00 .80 1.00 .60	38 38 38 38 38	Waviness measured; transition at skin lap joint on wing L.S.; n = 1900 rpm	33(a) 33(a) 33(a) 33(b) 33(c) 33(d)	118 118 118 119 120 121			10	70
Beech 24R (bonded aluminum)	Wing, U.S. Wing, L.S. Vertical tail Propeller, suction side Propeller, pressure side	133	0.30	6.07×10^6 6.07×10^6	1.38×10^6 1.38×10^6 1.38×10^6 2.89×10^6 2.89×10^6	0 0 0 <10.0		0.45 0.42 (d) 0.38 0.80	0.38 .38	0 0	38 38	Transition at skin lap joint on vertical fin; n = 2700 rpm; J = 0.84	34(a), (b) 34(c) 34(d) 34(e)	122, 123 124 125 126			11	71
Bellanca Skyrocket II (fiberglass/ aluminum honeycomb)	Wing, U.S., η = 0.53 Wing, U.S., η = 0.66 Wing, L.S., η = 0.53 Wing, L.S., η = 0.66 Propeller, suction side Propeller, pressure side Horizontal tail, U.S. Horizontal tail, L.S.	175.5	0.22	9.7×10^6 9.0×10^6 9.7×10^6 9.0×10^6	1.88×10^6 1.88×10^6 1.88×10^6 1.88×10^6 2.77×10^6 2.77×10^6 1.88×10^6 1.88×10^6	2.8 2.8 2.8 2.8		0.46 0.48 0.46 0.45 0.50-0.75 0.83 0.44 0.25	0.41 .44 .44 .39	0.66 .14 .66 .14	36 36 36 36	Measured at outboard and inboard wake-probe stations; n = 1800 rpm; J = 1.45; waviness measured on wing; effect of fixed transition measured; effect of propeller slipstream on boundary layer measured	35(c) 35(a) 35(c) 35(b)	129 127 129 128	14	87	12	72
Beech T-34C	Main glove Mini glove	165			1.50×10^6	0 38.4						Effect of flight through clouds; effect of propeller slipstream; n = 150-2200 rpm; used hot films	40	136				

[a] s = 18 in.
[b] s = 17 in.
[c] s = 12 in.
[d] s = 6 to 8 in.

TABLE 3.- PHYSICAL CHARACTERISTICS OF VARIEZE

Gross weight, lb	1050
Wing:	
Area, ft^2	53.6
Span, in.	267.6
Aspect ratio	9.28
Taper ratio (main wing)	0.44
Airfoil section (main wing)	LS(1)-0417 (Modified)
Root chord (main wing), in.	35.75
Tip chord (main wing), in.	16
Mean aerodynamic chord, in.	31
Root chord (strake), in.	88
Tip chord (strake), in.	35.75
Twist (washout), deg	3.0
Dihedral, deg	-4.0
Incidence at root, deg	1.2
Sweep at leading edge (main wing), deg	27
Sweep at leading edge (strake), deg	61
Canard:	
Area, ft^2	12.3
Span, in.	141.6
Aspect ratio	11.32
Taper ratio	1.0
Airfoil section (see table 4)	GU25-5(11)
Mean aerodynamic chord, in.	13
Twist, deg	0
Dihedral, deg	0
Incidence at root, deg	0
Sweep at leading edge, deg	0
Winglet (upper):	
Length, in.	36
Root chord, in.	20
Tip chord, in.	7
Mean aerodynamic chord, in.	14.5
Area (projected vertically), ft^2	3.35
Aspect ratio (based on vertically projected geometry)	2.6
Taper ratio	0.35
Sweep at leading edge, deg	29
Twist, deg	0
Incidence at root, deg	0
Cant angle, deg	5
Airfoil section	See table 2
Powerplant:	
Manufacturer	Teledyne Continental Motors Corp.
Model	O-200A
Takeoff and maximum continuous power, hp	100
Revolutions per minute, maximum	2750
Propeller (fixed pitch):	
Manufacturer	Ted Hendrickson, Snohomish, Washington
Number of blades	2
Pitch, in.	70
Diameter, in.	56

TABLE 4.- AIRFOIL DESIGN COORDINATES FOR WING AND WINGLET OF VARIEZE AND CANARD OF VARIEZE AND LONG-EZ

(a) VariEze wing at BL32

$(x/c)_U$	$(z/c)_U$	$(x/c)_L$	$(z/c)_L$
0.00000	0.00000	0.00000	0.00000
.00500	.02090	.00500	-.01120
.01000	.03070	.01000	-.01760
.02000	.03910	.02000	-.02370
.03000	.04750	.03000	-.02790
.04000	.05310	.04000	-.03210
.05000	.05870	.05000	-.03600
.06000	.06280	.06000	-.03910
.07000	.06620	.07000	-.04230
.08000	.06980	.08000	-.04470
.09000	.07320	.09000	-.04610
.10000	.07630	.10000	-.04830
.15000	.08770	.15000	-.05680
.20000	.09690	.20000	-.06150
.25000	.10340	.25000	-.06540
.30000	.10700	.30000	-.06790
.35000	.11000	.35000	-.06955
.40000	.11060	.40000	-.06899
.45000	.11030	.45000	-.06676
.50000	.10950	.50000	-.06310
.55000	.10590	.55000	-.05720
.60000	.10000	.60000	-.05110
.65000	.09100	.65000	-.04190
.70000	.08000	.70000	-.03320
.75000	.06980	.75000	-.02680
.80000	.05730	.80000	-.01930
.85000	.04190	.85000	-.01120
.90000	.03040	.90000	-.00590
.95000	.01680	.95000	-.00170
1.00000	.00000	1.00000	.00000

TABLE 4.- Continued

(b) VariEze winglet root

$(x/c)_U$	$(z/c)_U$	$(x/c)_L$	$(z/c)_L$
0.00000	0.00000	0.00000	0.00000
.00250	.01150	.00250	-.00700
.00500	.01550	.00500	-.01150
.01000	.02150	.01000	-.01700
.01500	.02600	.01500	-.02050
.02000	.02900	.02000	-.02300
.03000	.03500	.03000	-.02700
.04000	.04000	.04000	-.02950
.06000	.04950	.06000	-.03200
.08000	.05700	.08000	-.03400
.10000	.06500	.10000	-.03500
.12500	.07300	.12500	-.03650
.15000	.08050	.15000	-.03750
.17500	.08700	.17500	-.03800
.20000	.09250	.20000	-.03800
.22500	.09800	.22500	-.03800
.25000	.10300	.25000	-.03750
.27500	.10750	.27500	-.03700
.30000	.11150	.30000	-.03650
.32500	.11500	.32500	-.03600
.35000	.11700	.35000	-.03550
.37500	.11900	.37500	-.03500
.40000	.12000	.40000	-.03450
.42500	.12050	.42500	-.03300
.45000	.12000	.45000	-.03150
.47500	.11900	.47500	-.03050
.50000	.11700	.50000	-.02950
.52500	.11400	.52500	-.02800
.55000	.11000	.55000	-.02650
.57500	.10650	.57500	-.02450
.60000	.10200	.60000	-.02200
.62500	.09700	.62500	-.02000
.65000	.09150	.65000	-.01750
.67500	.08550	.67500	-.01500
.70000	.08000	.70000	-.01300
.72500	.07350	.72500	-.01100
.75000	.06700	.75000	-.00950
.77500	.06000	.77500	-.00750
.80000	.05250	.80000	-.00550
.82500	.04550	.82500	-.00400
.85000	.03850	.85000	-.00300
.87500	.03100	.87500	-.00200
.90000	.02400	.90000	-.00250
.92500	.01650	.92500	-.00350
.95000	.00850	.95000	-.00550
.97500	.00000	.97500	-.00800
1.00000	-.00900	1.00000	-.01000

TABLE 4.- Continued

(c) VariEze winglet tip

$(x/c)_U$	$(z/c)_U$	$(x/c)_L$	$(z/c)_L$
0.00000	0.00000	0.00000	0.00000
.00430	.01570	.00430	-.01570
.00710	.02140	.00710	-.02140
.01430	.02860	.01430	-.03000
.02860	.03710	.02860	-.03710
.04290	.04430	.04290	-.04140
.05710	.05000	.05710	-.04290
.08570	.06140	.08570	-.04570
.11430	.07140	.11430	-.04860
.17140	.08570	.17140	-.05000
.22860	.09860	.22860	-.05290
.28570	.10710	.28570	-.05140
.34290	.11290	.34290	-.04860
.40000	.11930	.40000	-.04570
.45710	.11930	.45710	-.04290
.51430	.11930	.51430	-.03570
.57140	.11000	.57140	-.02860
.62860	.10140	.62860	-.02290
.68570	.09140	.68570	-.01860
.74290	.07710	.74290	-.01570
.80000	.05860	.80000	-.01430
.85710	.04000	.85710	-.01290
.91430	.01860	.91430	-.01140
.97140	-.00430	.97140	-.01290
1.00000	-.01430	1.00000	-.01430

TABLE 4.- Concluded

(d) VariEze and Long-EZ canard

$(x/c)_U$	$(z/c)_U$	$(x/c)_L$	$(z/c)_L$
0.00000	0.00000	0.00000	0.00000
.00130	.00583	.00076	-.00273
.00492	.01387	.00203	-.00438
.01057	.02288	.00406	-.00651
.01777	.03154	.00814	-.00955
.02676	.04068	.01707	-.01412
.03907	.05166	.02678	-.01749
.05088	.06099	.03827	-.02030
.07473	.07725	.05079	-.02256
.10035	.09211	.07482	-.02558
.12444	.10402	.10063	-.02752
.15030	.11494	.12747	-.02872
.17745	.12488	.15074	-.02946
.20049	.13280	.17784	-.03013
.22661	.14103	.20034	-.03046
.25016	.14713	.22668	-.03089
.27677	.15294	.25019	-.03143
.30006	.15771	.27550	-.03178
.32718	.16248	.30056	-.03145
.34970	.16539	.32512	-.03076
.37502	.16757	.35043	-.03017
.39932	.16914	.37600	-.02990
.42566	.17041	.39978	-.02925
.44662	.17077	.42536	-.02815
.47449	.16972	.45041	-.02700
.49954	.16686	.50003	-.02472
.52330	.16275	.55066	-.02253
.54655	.15758	.59977	-.02057
.57413	.15045	.65015	-.01850
.59865	.14332	.69951	-.01639
.62444	.13530	.74937	-.01417
.64946	.12720	.79976	-.01183
.69951	.10997	.84937	-.00924
.74980	.09171	.89949	-.00617
.79934	.07345	.94477	-.00312
.84963	.05496	1.00000	-.00025
.89993	.03638		
.94869	.01843		
1.00000	.00025		

TABLE 5.- PHYSICAL CHARACTERISTICS OF LONG-EZ

Gross weight, lb	1325
Wing:	
Area, ft^2	81.99
Span, in.	313.2
Aspect ratio	8.3
Taper ratio (main wing)	0.48
Airfoil section (main wing)	See table 4
Root chord (main wing), in.	41.4
Tip chord (main wing), in.	20
Mean aerodynamic chord, in.	37.6
Root chord (outboard strake), in.	76
Tip chord (outboard strake), in.	41.4
Twist (washout), deg	BL157:-2.7 BL106.25:-0.46 BL55.5:-0.6
Dihedral, deg	0
Incidence at root, deg	0
Sweep at leading edge (main wing), deg	23
Sweep at leading edge (outboard strake), deg	51
Sweep at leading edge (inboard strake), deg	64
Canard:	
Area, ft^2	12.8
Span, in.	141.6
Aspect ratio	10.88
Taper ratio	1.0
Airfoil section (see table 2)	GU25-5(11)8
Mean aerodynamic chord, in.	13
Twist, deg	0
Dihedral, deg	0
Incidence at root, deg	0.6
Sweep at leading edge, deg	0
Winglet (upper):	
Length, in.	49
Root chord, in.	27.1
Tip chord, in.	11
Mean aerodynamic chord, in.	20.5
Area (projected vertically), ft^2	6.57
Aspect ratio (based on vertically projected geometry)	2.54
Taper ratio	0.40
Sweep at leading edge, deg	28
Twist, deg	0
Incidence at root, deg	0.5
Cant angle, deg	0
Airfoil section	See table 4
Powerplant:	
Manufacturer	Avco Lycoming Corp.
Model	0.235
Takeoff and maximum continuous power, hp	118
Revolutions per minute, maximum	2800
Propeller (fixed pitch):	
Manufacturer	Ted Hendrickson, Snohomish, Washington
Number of blades	2
Pitch, in.	70
Diameter, in.	58

TABLE 6.- AIRFOIL DESIGN COORDINATES FOR WING AND WINGLET OF LONG-EZ

(a) Wing

$(x/c)_U$	$(z/c)_U$	$(x/c)_L$	$(z/c)_L$
0.00066	0.00581	0.00002	-0.00103
.00296	.01331	.00126	-.00675
.00688	.02129	.00507	-.01165
.01236	.02958	.01154	-.01641
.01937	.03807	.02015	-.02102
.02789	.04665	.03077	-.02538
.03787	.05521	.04334	-.02937
.04928	.06366	.05789	-.03294
.06206	.07191	.07441	-.03613
.07618	.07987	.09284	-.03898
.09157	.08744	.11309	-.04152
.10817	.09454	.13505	-.04378
.12591	.10105	.15860	-.04575
.14478	.10683	.18361	-.04745
.16479	.11180	.20997	-.04887
.18594	.11591	.23753	-.05000
.20823	.11911	.26617	-.05084
.23166	.12138	.29574	-.05139
.25623	.12274	.32610	-.05162
.28190	.12325	.35711	-.05153
.30860	.12294	.38861	-.05110
.33627	.12186	.42045	-.05031
.36482	.12005	.45249	-.04910
.39414	.11758	.48460	-.04739
.42415	.11449	.51674	-.04516
.45472	.11085	.54884	-.04239
.48574	.10671	.58083	-.03912
.51708	.10214	.61264	-.03537
.54861	.09722	.64419	-.03116
.58019	.09200	.67547	-.02648
.61167	.08655	.70000	-.02400
.64290	.08094	.72000	-.02200
.67373	.07524	.74000	-.02000
.70399	.06950	.76800	-.01800
.73353	.06378	.79400	-.01600
.76219	.05812	.82200	-.01400
.78980	.05258	.85000	-.01200
.81622	.04720	.88000	-.01000
.84128	.04199	.89800	-.00800
.86484	.03699	.92800	-.00600
.88676	.03221	.95200	-.00400
.90691	.02765	.98000	-.00200
.92517	.02331	1.00000	-.00010
.94141	.01915		
.95562	.01503		
.96797	.01095		
.97859	.00715		
.98742	.00396		
.99418	.00167		
.99850	.00089		
1.00000	.00010		

TABLE 6.- Continued

(b) Winglet root

$(x/c)_U$	$(z/c)_U$	$(x/c)_L$	$(z/c)_L$
0.00000	0.00000	0.00000	0.00000
.00000	.00009	.00000	-.00009
.00196	.00846	.00140	-.00783
.00644	.01516	.00280	-.01116
.01175	.02010	.00866	-.01798
.02265	.02727	.02012	-.02324
.03607	.03461	.03018	-.02597
.05621	.04392	.04696	-.02906
.07858	.05205	.07128	-.03141
.10653	.06002	.09840	-.03289
.12891	.06538	.14005	-.03528
.15435	.07007	.16884	-.03737
.18314	.07295	.20266	-.03961
.21977	.07499	.23342	-.04081
.25415	.07656	.27451	-.04211
.29944	.07731	.31812	-.04301
.33970	.07625	.34943	-.04276
.38331	.07377	.38354	-.04154
.41798	.07154	.42016	-.04021
.45991	.06848	.46154	-.03892
.49122	.06576	.50767	-.03753
.53120	.06235	.55129	-.03580
.56251	.05974	.60217	-.03289
.60639	.05562	.64858	-.03006
.64525	.05116	.69862	-.02713
.68272	.04599	.73608	-.02466
.72102	.04060	.79060	-.02080
.77748	.03310	.84288	-.01721
.82528	.02686	.89124	-.01397
.87588	.01996	.95052	-.00946
.91838	.01406	.99972	-.00292
.96366	.00774		
1.00000	.00296		

TABLE 6.- Concluded

(c) Winglet tip

$(x/c)_U$	$(z/c)_U$	$(x/c)_L$	$(z/c)_L$
0.00000	0.00000	0.00000	0.00000
.00000	.00018	.00000	-.00018
.00026	.00283	.00053	-.00370
.00212	.00809	.00210	-.00727
.00503	.01365	.00394	-.00951
.00793	.01814	.00841	-.01251
.01215	.02315	.01369	-.01496
.01665	.02754	.02107	-.01757
.02244	.03245	.02923	-.01968
.02852	.03695	.03977	-.02189
.03617	.04213	.07508	-.02793
.05120	.05134	.11172	-.03275
.06966	.06052	.14940	-.03597
.08944	.06838	.18656	-.03770
.11106	.07551	.22346	-.03885
.13216	.08167	.26010	-.03957
.15114	.08619	.29489	-.04012
.16828	.08940	.33311	-.04061
.18647	.09211	.37185	-.04052
.20492	.09431	.40744	-.03976
.22311	.09609	.44302	-.03876
.26054	.09815	.48097	-.03743
.30034	.09816	.52024	-.03527
.33566	.09663	.55821	-.03239
.37308	.09418	.59037	-.02998
.41103	.09132	.62938	-.02710
.44872	.08802	.66549	-.02459
.48377	.08452	.70371	-.02183
.52225	.08048	.73930	-.01933
.55967	.07621	.78200	-.01632
.59550	.07147	.82734	-.01332
.63346	.06575	.86768	-.01072
.67035	.05958	.91196	-.00779
.70513	.05382	.94306	-.00559
.74518	.04719	.97628	-.00323
.78129	.04109	.99947	-.00184
.82003	.03436		
.85191	.02869		
.88959	.02194		
.93386	.01408		
.97392	.00695		
1.00000	.00185		

TABLE 7.- PHYSICAL CHARACTERISTICS OF BIPLANE RACER

Gross weight, lb	1200
Wing (forward):	
Area, ft^2	47.6
Span, in.	213.6
Aspect ratio	6.68
Taper ratio (main wing)	0.68
Airfoil section (main wing)	See table 6
Root chord (main wing), in.	37
Tip chord (main wing), in.	26
Mean aerodynamic chord, in.	32
Twist (washout), deg	0
Anhedral, deg	6.5
Incidence at root, deg	0
Sweep at leading edge, deg	6
Wing (aft):	
Area, ft^2	44.1
Span, in.	270
Aspect ratio	11.48
Taper ratio	0.52
Airfoil section	See table 6
Mean aerodynamic chord, in.	23
Root chord, in.	29
Tip chord, in.	16
Twist, deg	0
Dihedral, deg	4
Incidence at root, deg	0
Sweep at leading edge, deg	3.2
Powerplant:	
Manufacturer	Avco Lycoming Corp.
Model	IO-320
Takeoff and maximum continuous power, hp	160
Revolutions per minute, maximum	2800
Propeller (fixed pitch):	
Number of blades	2
Diameter, in.	60

TABLE 8.- AIRFOIL DESIGN COORDINATES FOR FORWARD AND AFT WINGS OF BIPLANE RACER

(a) Forward wing

$(x/c)_U$	$(z/c)_U$	$(x/c)_L$	$(z/c)_L$
0.00000	0.00000	0.00000	0.00000
.00194	.00977	.00194	-.00934
.00388	.01353	.00388	-.01267
.00775	.01857	.00775	-.01690
.03000	.03318	.03000	-.02698
.06000	.04349	.06000	-.03167
.09000	.05054	.09000	-.03364
.12000	.05609	.12000	-.03465
.15000	.06070	.15000	-.03523
.18000	.06465	.18000	-.03566
.21000	.06810	.21000	-.03605
.24000	.07109	.24000	-.03640
.27000	.07357	.27000	-.03674
.30000	.07562	.30000	-.03705
.33000	.07717	.33000	-.03729
.36000	.07822	.36000	-.03740
.39000	.07880	.39000	-.03744
.42000	.07884	.42000	-.03725
.45000	.07833	.45000	-.03690
.48000	.07733	.48000	-.03632
.51000	.07574	.51000	-.03550
.54000	.07364	.54000	-.03446
.57000	.07101	.57000	-.03314
.60000	.06787	.60000	-.03159
.63000	.06426	.63000	-.02977
.66000	.06023	.66000	-.02775
.69000	.05578	.69000	-.02550
.72000	.05097	.72000	-.02310
.75000	.04585	.75000	-.02054
.78000	.04054	.78000	-.01791
.81000	.03504	.81000	-.01523
.84000	.02942	.84000	-.01260
.87000	.02384	.87000	-.01004
.90000	.01837	.90000	-.00767
.93000	.01310	.93000	-.00558
.96000	.00814	.96000	-.00380
.99000	.00360	.99000	-.00252
1.00000	.00221	1.00000	-.00221

TABLE 8.- Concluded

(b) Aft wing

$(x/c)_U$	$(z/c)_U$	$(x/c)_L$	$(z/c)_L$
0.00000	0.00000	0.00000	0.00000
.00288	.01168	.00288	-.01145
.00575	.01600	.00575	-.01554
.01151	.02158	.01151	-.02072
.02998	.03159	.02998	-.02929
.05996	.04022	.05996	-.03585
.08994	.04581	.08994	-.03942
.11992	.05001	.11992	-.04183
.14990	.05346	.14990	-.04362
.17988	.05645	.17988	-.04506
.20986	.05910	.20986	-.04627
.23984	.06146	.23984	-.04730
.26982	.06347	.26982	-.04816
.29980	.06514	.29980	-.04885
.32978	.06646	.32978	-.04932
.35977	.06744	.35977	-.04960
.38975	.06802	.38975	-.04960
.41973	.06819	.41973	-.04932
.44971	.06790	.44971	-.04874
.47969	.06721	.47969	-.04782
.50967	.06600	.50967	-.04661
.53965	.06433	.53965	-.04511
.56963	.06226	.56963	-.04322
.59961	.05967	.59961	-.04109
.62959	.05668	.62959	-.03861
.65957	.05329	.65957	-.03585
.68955	.04949	.68955	-.03286
.71953	.04534	.71953	-.02969
.74951	.04097	.74951	-.02641
.77949	.03631	.77949	-.02296
.80947	.03148	.80947	-.01951
.83945	.02659	.83945	-.01611
.86943	.02164	.86943	-.01283
.89941	.01675	.89941	-.00972
.92939	.01203	.92939	-.00696
.95937	.00760	.95937	-.00460
.98935	.00357	.98935	-.00276
1.00000	.00224	1.00000	-.00224

TABLE 9.- PHYSICAL CHARACTERISTICS OF GATES LEARJET MODEL 28/29

Gross weight, lb	15 000
Wing:	
Area, ft^2	274.3
Span, in.	506.4
Aspect ratio	6.48
Taper ratio (main wing)	0.39
Root chord (main wing), in.	112
Tip chord (main wing), in.	43.8
Mean aerodynamic chord, in.	83
Twist (washout), deg	0
Dihedral, deg	2.5
Incidence at root, deg	1
Sweep at leading edge, deg	17
Winglet (upper):	
Length, in.	44.9
Root chord, in.	28.53
Tip chord, in.	9.99
Mean aerodynamic chord, in.	20.76
Area (projected vertically), ft^2	6
Aspect ratio (based on vertically projected geometry)	2.33
Taper ratio	0.35
Sweep at leading edge, deg	40
Twist (leading edge outward within lower 40-percent span), deg	1
Incidence at root (leading edge toed out), deg	-2
Cant angle (winglet tip canted out)	15
Airfoil section	LS(1)-0413 thinned to t/c = 0.08
Powerplant:	
Manufacturer	General Electric
Model	CJ610-8A
Rated thrust, lb	2950

TABLE 10.- PHYSICAL CHARACTERISTICS OF CESSNA P-210 CENTURION

Gross weight, lb	4000
Wing:	
Area, ft^2	175
Span, ft	441
Aspect ratio	7.72
Taper ratio (main wing)	0.70
Airfoil section:	
Root	NACA 64_2A215 (a = 0.5)
Tip	NACA 64_1A412 (a = 0.5)
Root chord, in.	70.8
Tip chord, in.	50
Mean aerodynamic chord, in.	61
Twist (washout), deg	3.0
Dihedral, deg	2.6
Incidence at root, deg	1.5
Sweep at leading edge, deg	0
Powerplant:	
Manufacturer	Teledyne Continental Motors Corp.
Model	TSIO-540-P
Takeoff and maximum continuous power, hp	310
Revolutions per minute, maximum	2700
Propeller (constant speed):	
Manufacturer	McCauley Accessories Div., Cessna Aircraft Co.
Number of blades	3
Diameter, in.	80
Horizontal tail:	
Area, ft^2	48
Span, in.	156
Aspect ratio	3.5
Taper ratio (main wing)	0.58
Airfoil section:	
Root	NACA 0009
Tip	NACA 0005
Root chord, in.	56
Tip chord, in.	33
Mean aerodynamic chord, in.	45.5
Twist, deg	0
Incidence at root, deg	-3.6
Sweep at leading edge, deg	8

TABLE 11.- PHYSICAL CHARACTERISTICS OF BEECH 24R SIERRA

Gross weight, lb	2750
Wing:	
Area, ft^2	146
Span, in.	393
Aspect ratio	7.34
Taper ratio	1.0
Airfoil section	NACA 63_2A415
Mean aerodynamic chord, in.	52.8
Twist (washout), deg	-2.0
Dihedral, deg	6.5
Incidence at root, deg	3.0
Sweep at leading edge, deg	0
Powerplant:	
Manufacturer	Avco Lycoming Corp.
Model	IO-360-A1B6
Takeoff and maximum continuous power, hp	200
Revolutions per minute, maximum	2700
Propeller (constant speed):	
Manufacturer	Hartzell Propeller Co.
Number of blades	2
Diameter, in.	76
Airfoil section	Clark Y
Chord at 0.25d, in.	6.5

TABLE 12.- PHYSICAL CHARACTERISTICS OF BELLANCA SKYROCKET II

Gross weight, lb	4100
Wing:	
Airfoil	NACA 63_2-215
Area, ft^2	182.6
Span, ft	35.0
Aspect ratio	6.7
Taper ratio	0.57
Root chord, in.	80.2
Tip chord, in.	45.9
Mean aerodynamic chord, in.	64.6
Incidence, deg	2
Dihedral, deg	2
Twist, deg	3
Sweep at leading edge, deg	2.8
Powerplant:	
Manufacturer	Teledyne Continental Motors Corp.
Model	GTS10-520F
Maximum continuous power, hp	435
Revolutions per minute, maximum	3400
Propeller (constant speed):	
Manufacturer	Hartzell Propeller Co.
Model	HC-H3YN-1RF/F8475-4
Number of blades	3
Diameter, in.	82
Revolutions per minute, maximum	2270

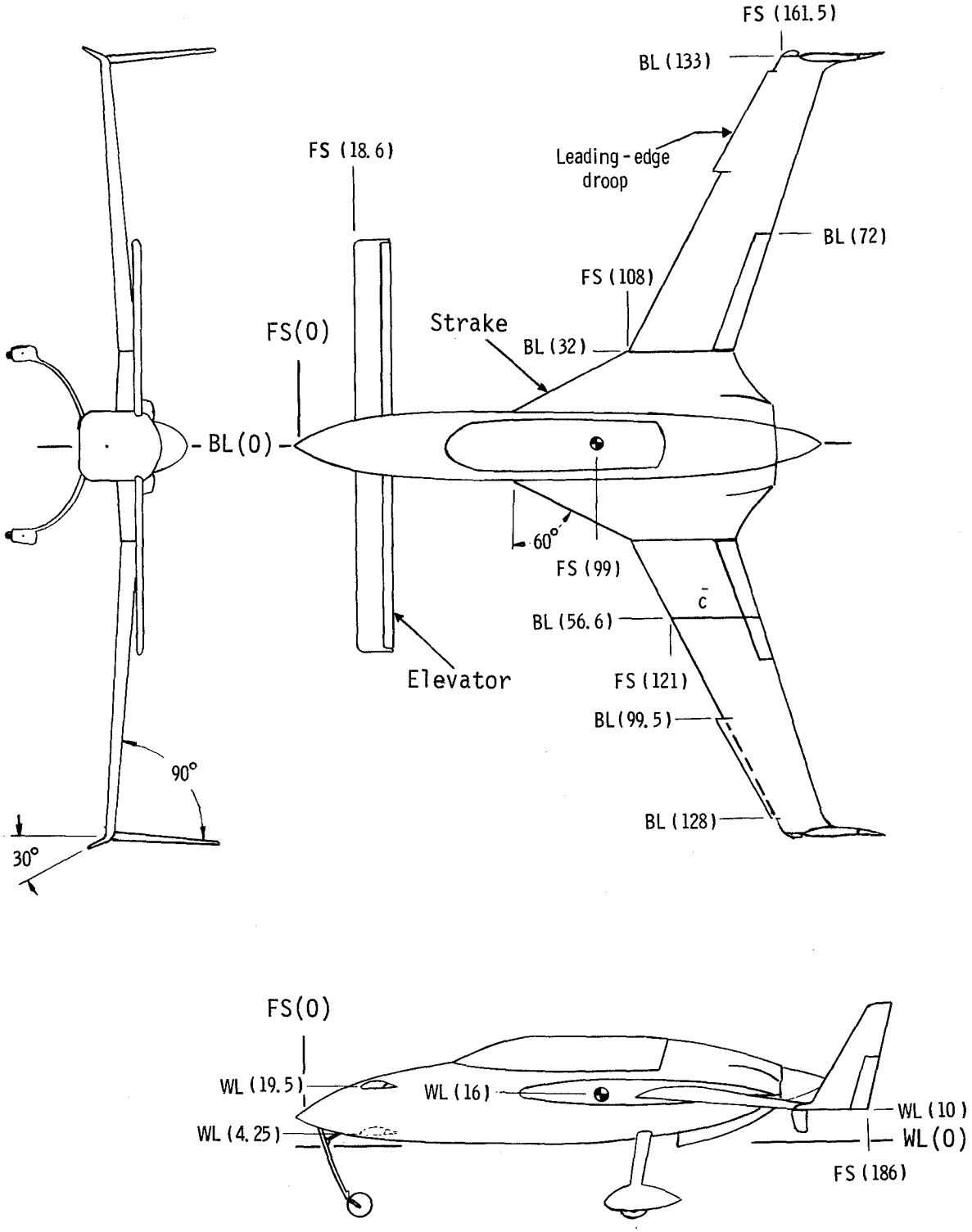

Figure 1.- Geometric characteristics of VariEze airplane. Dimensions are in inches.

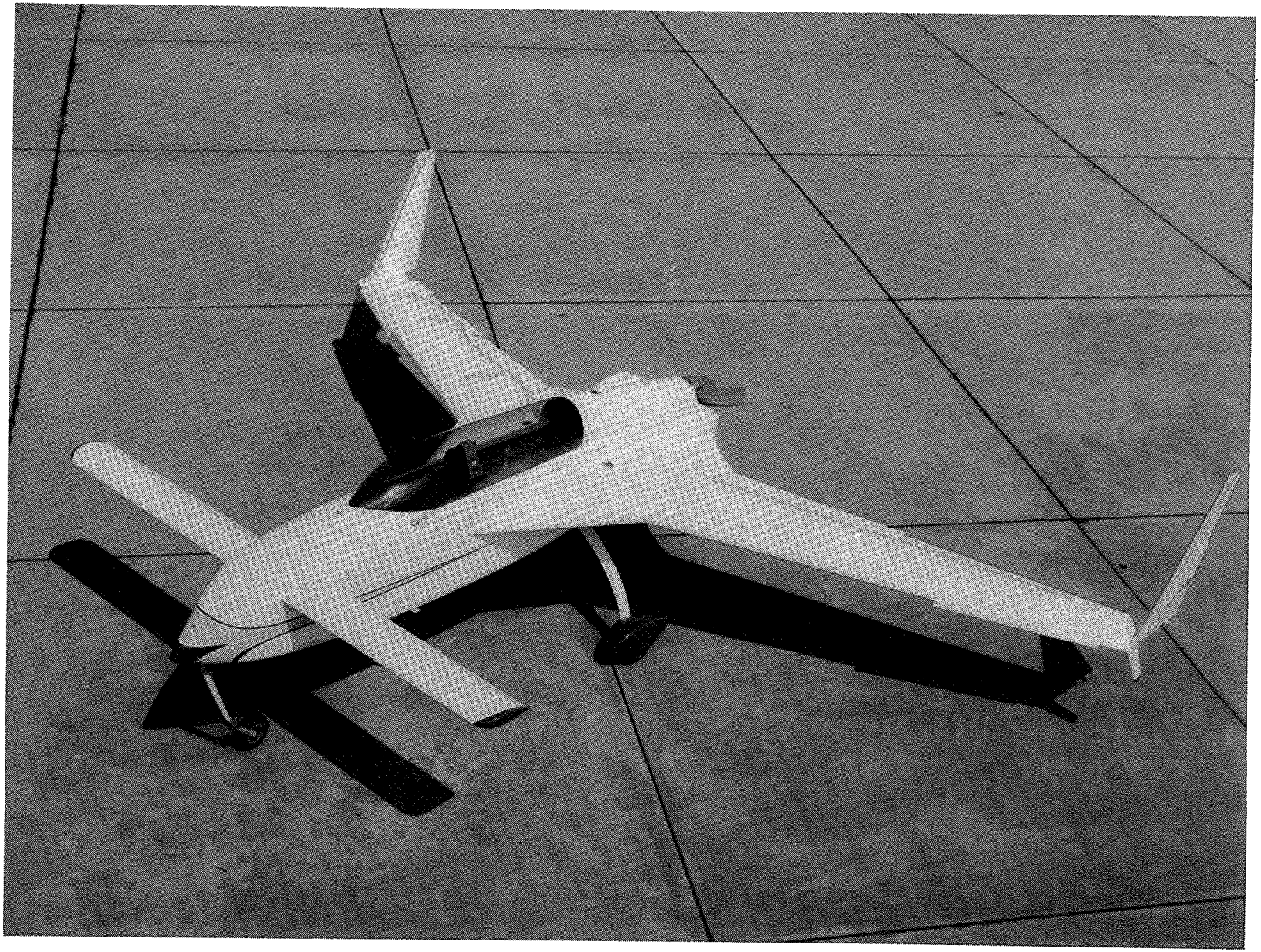

L-81-9255

Figure 2.- VariEze airplane used for natural laminar flow flight experiments.

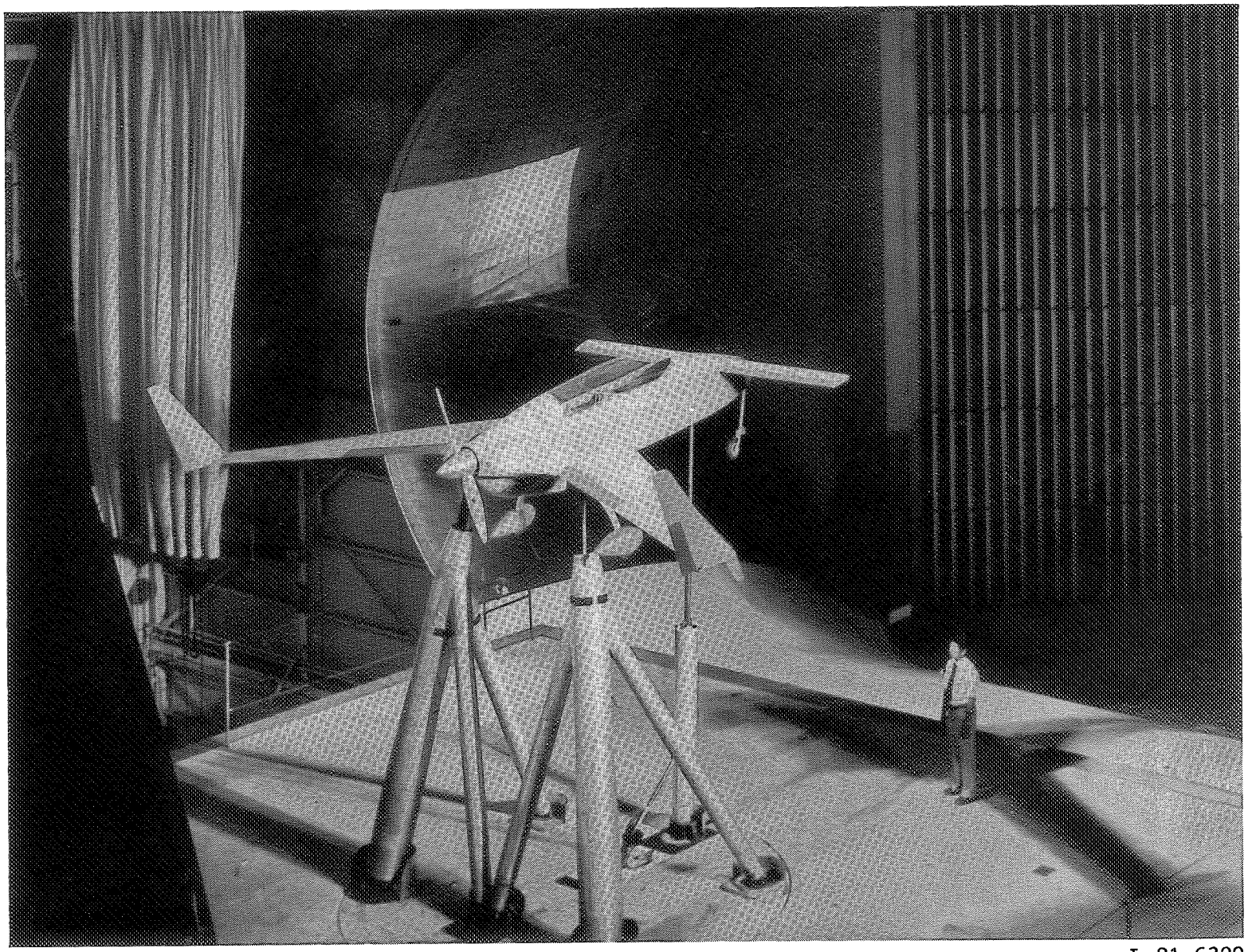

L-81-6300

Figure 3.- VariEze model installed in Langley 30- by 60-Foot Tunnel.

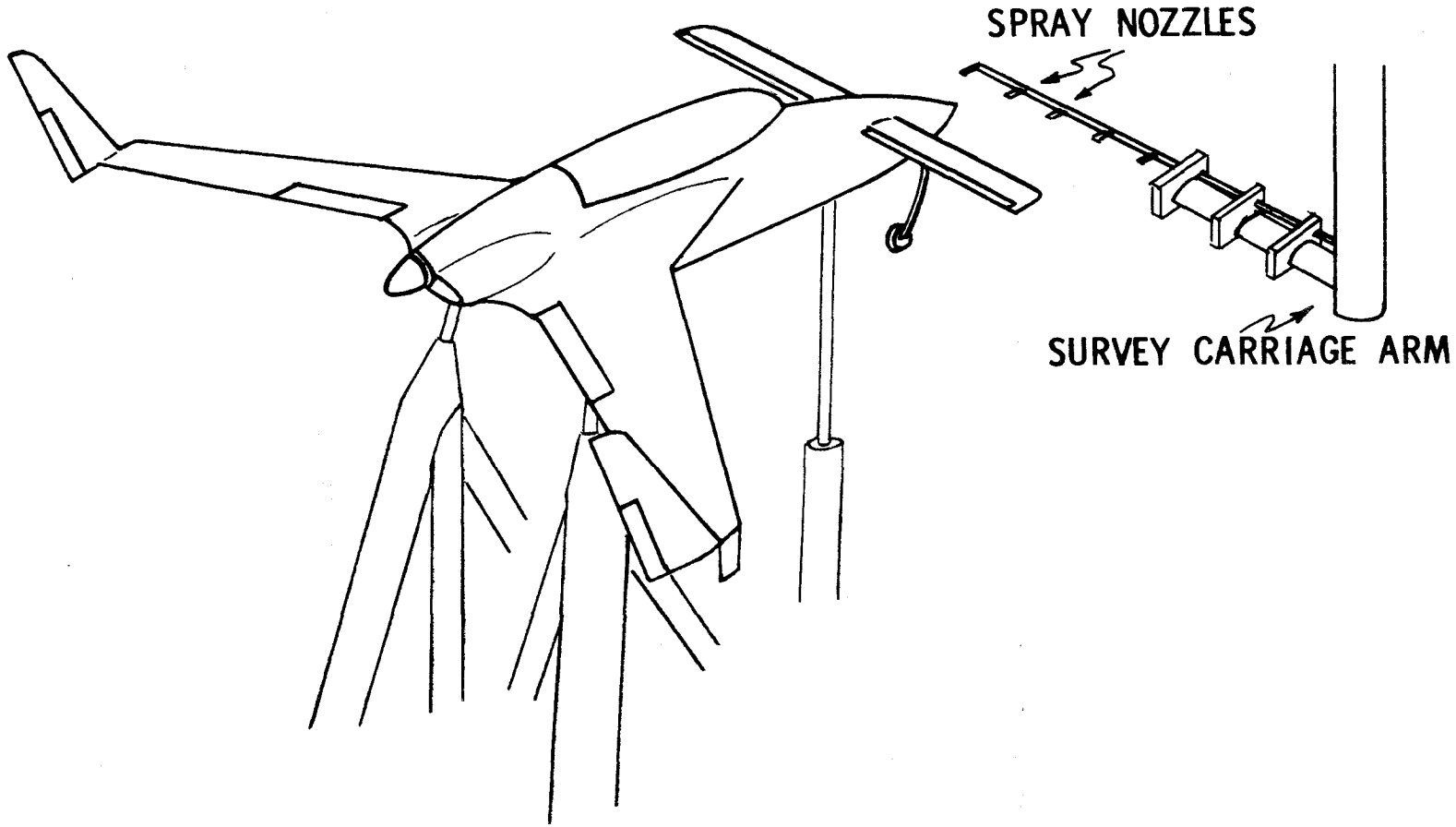

Figure 4.- Sketch of rain simulation apparatus.

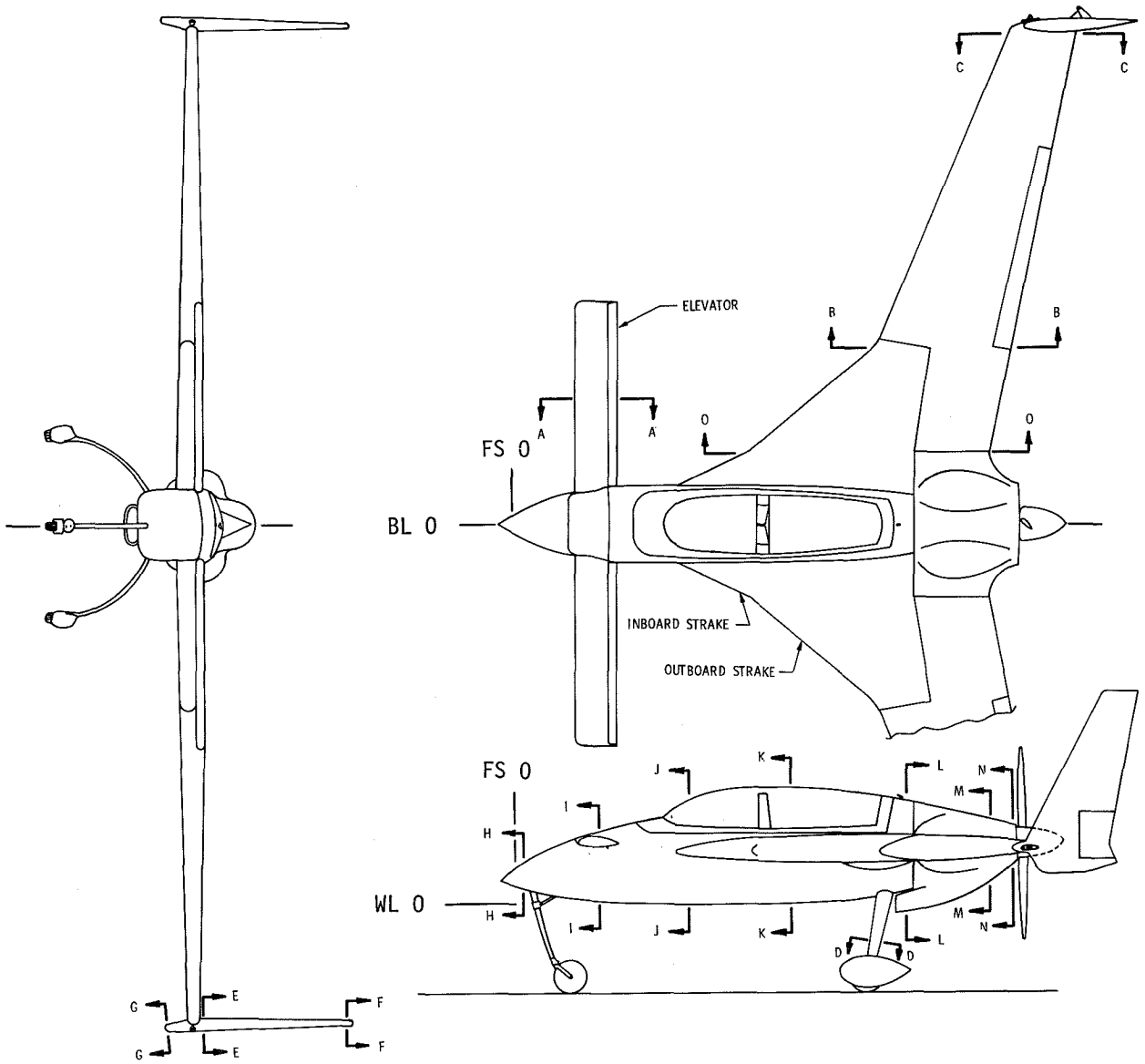

(a) Planforms.

Figure 5.- Geometry of Long-EZ airplane used for natural laminar flow flight experiments.

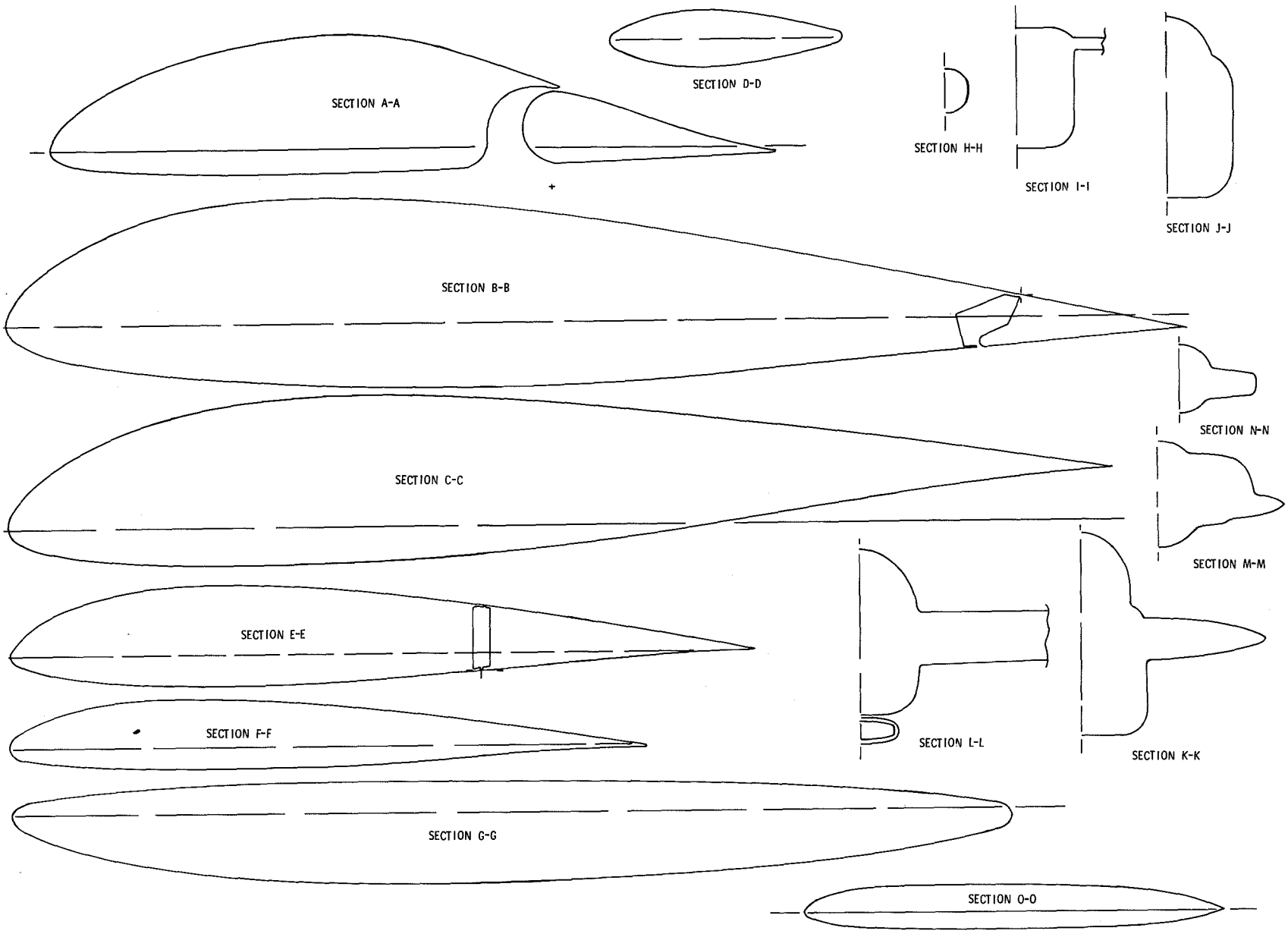

(b) Cross sections.

Figure 5.- Concluded.

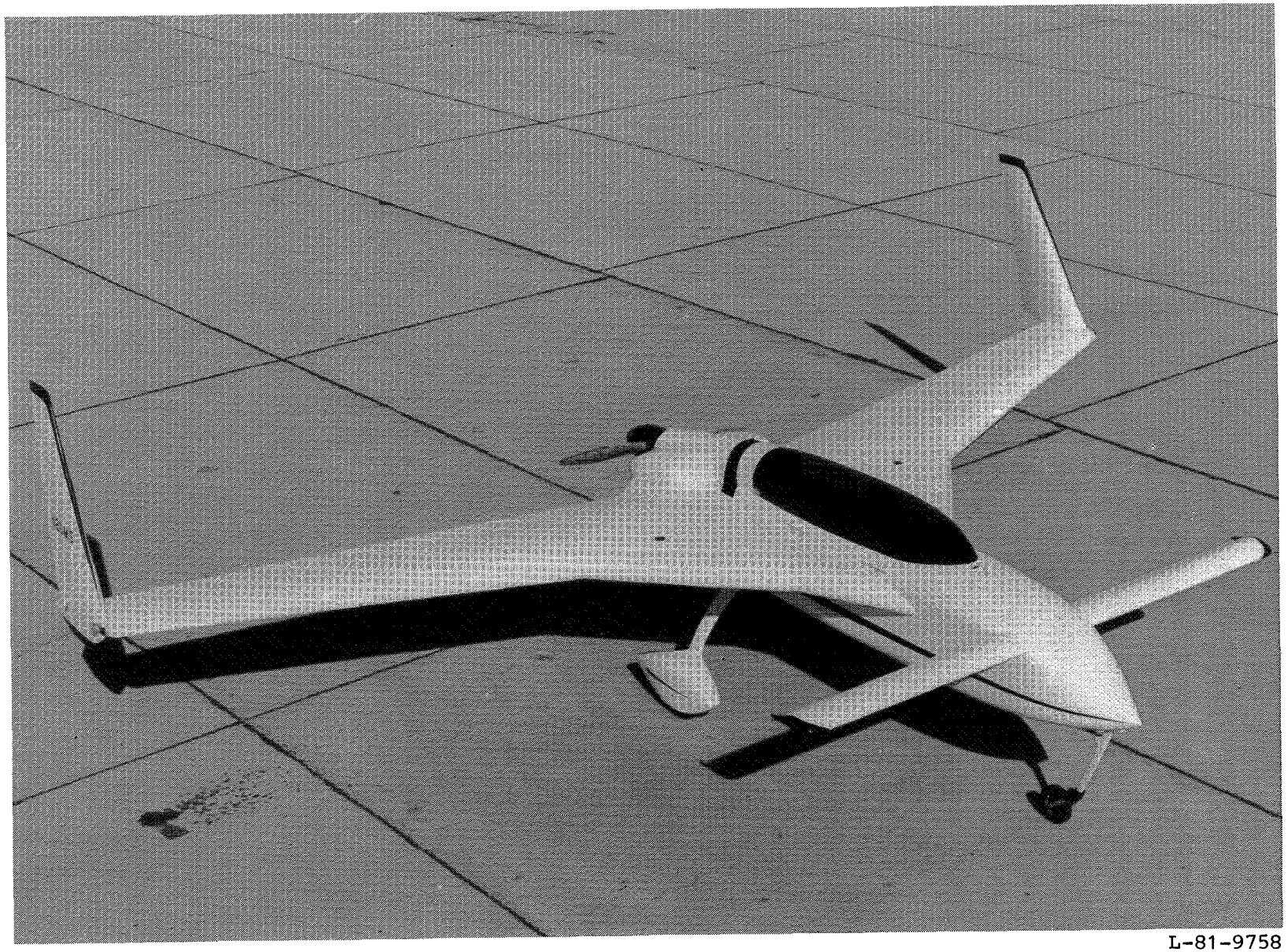

L-81-9758

Figure 6.- Long-EZ airplane used for natural laminar flow flight experiments.

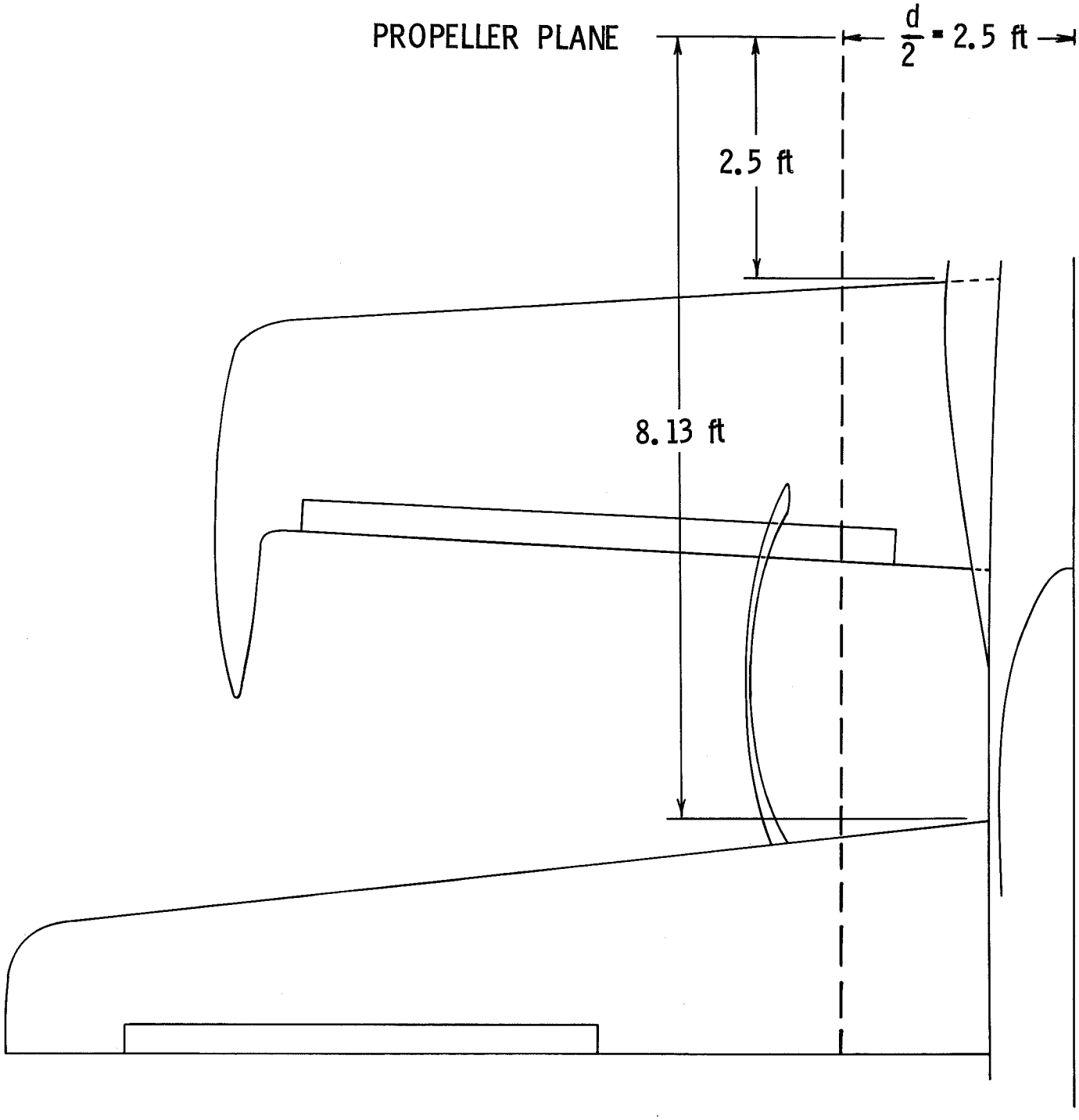

Figure 7.- Planview of Biplane Racer used in natural laminar flow flight experiments.

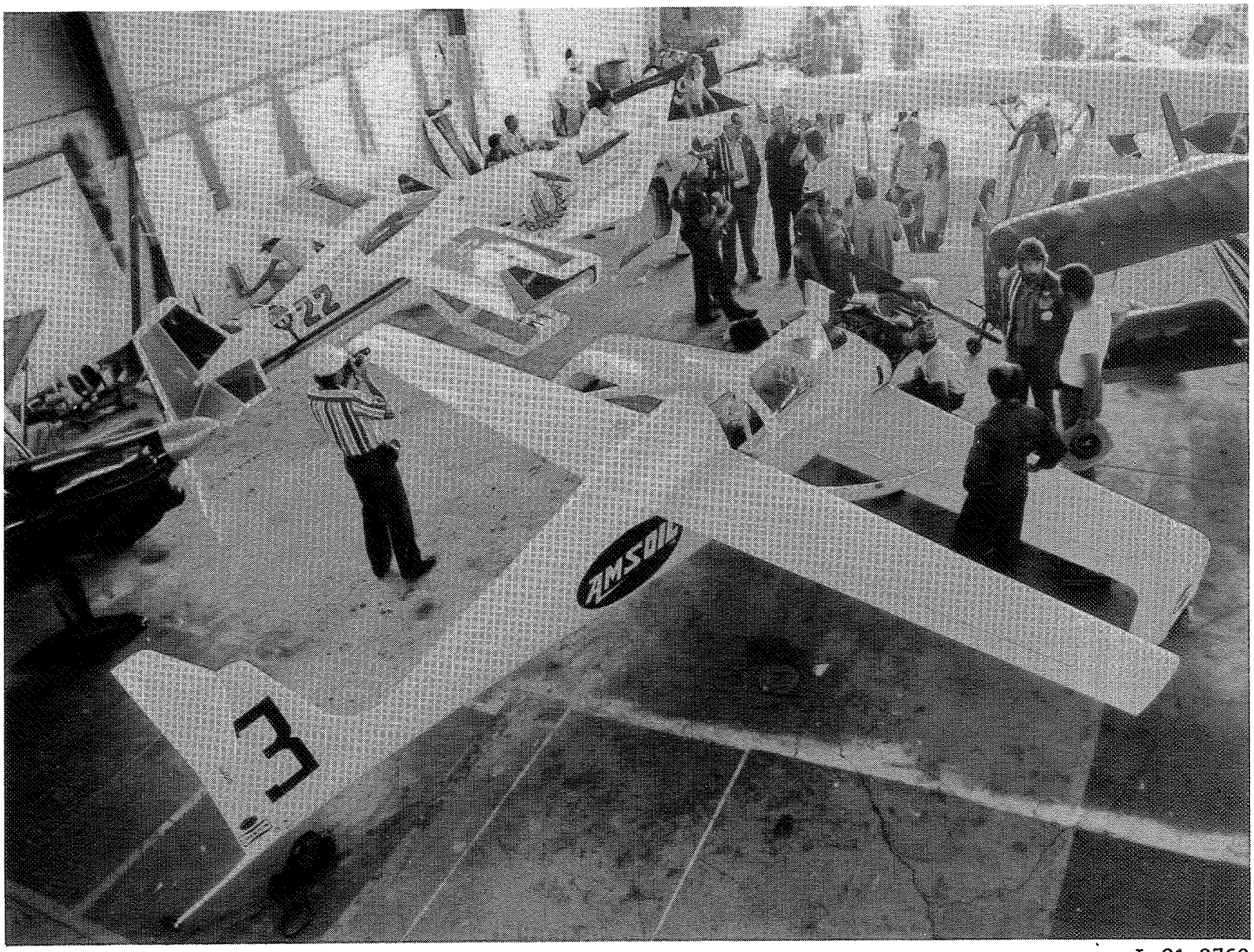

L-81-9760

Figure 8.- Biplane Racer used in natural laminar flow flight experiments.

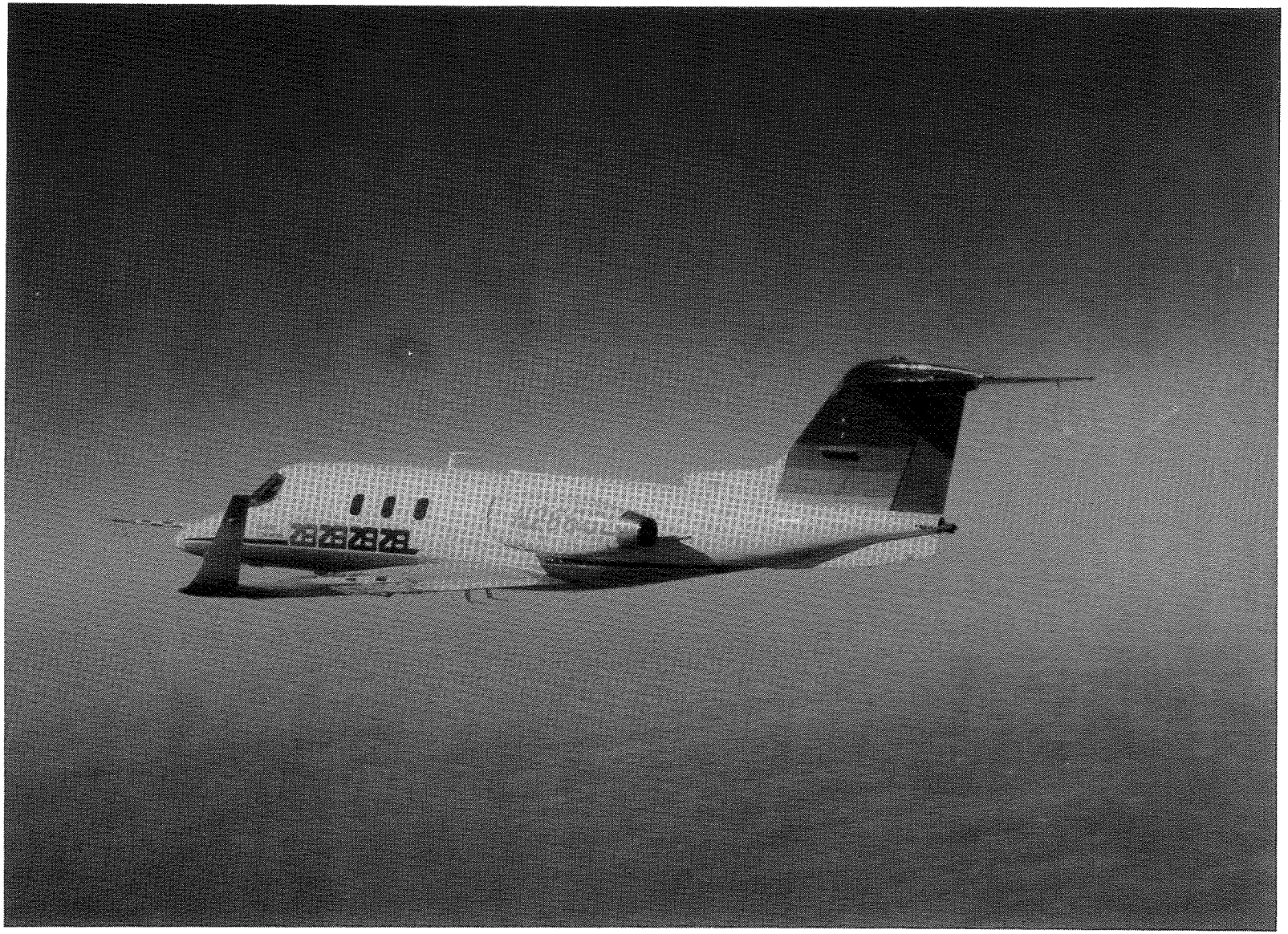

L-82-1220

Figure 9.- Gates Learjet Model 28/29 used in natural laminar flow flight experiments.

L-82-1195

Figure 10.- Cessna P-210 Centurion used in natural laminar flow flight experiments.

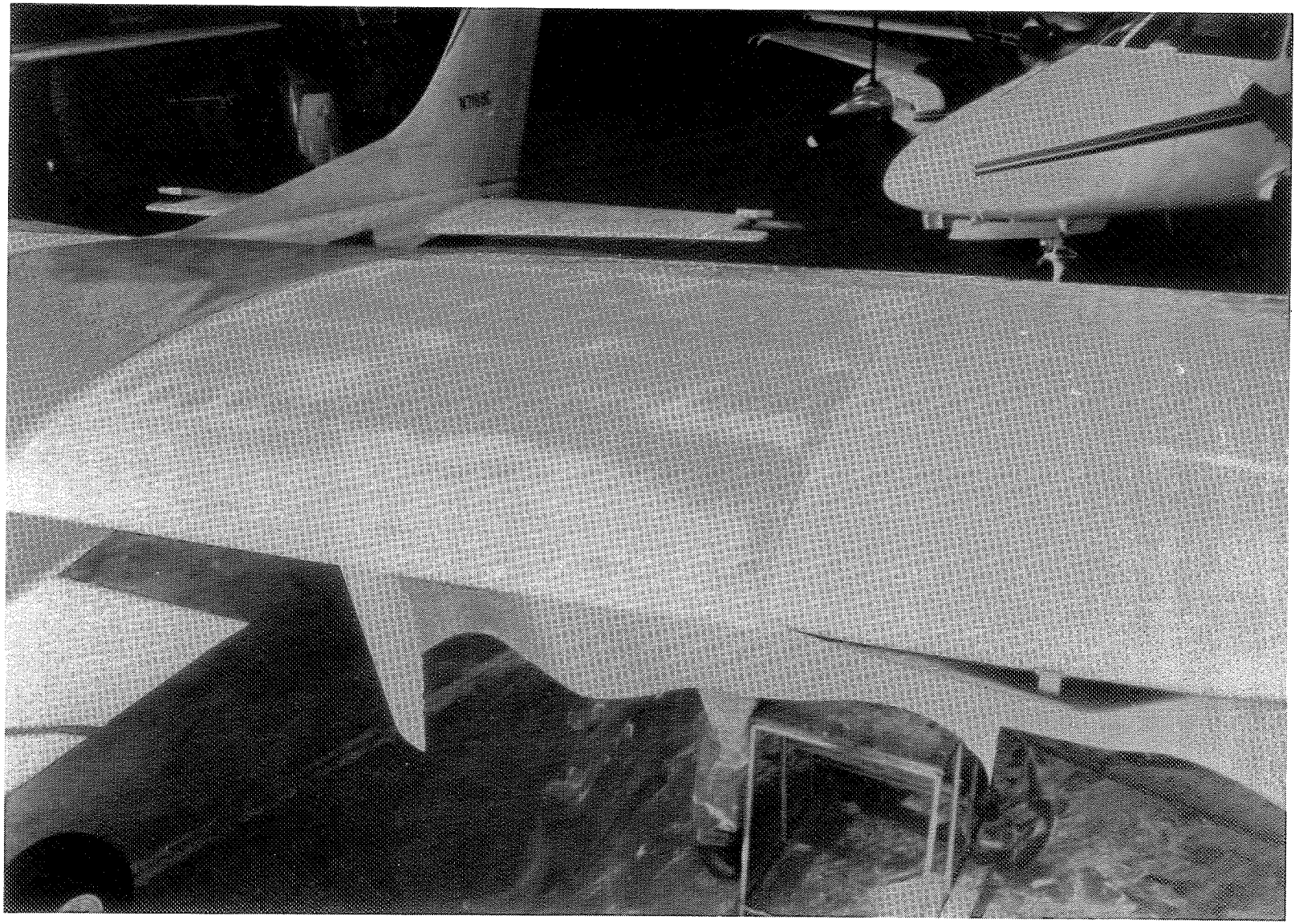

L-82-1205

Figure 11.- Filled and sanded region on left wing of Cessna P-210 Centurion (before painting).

L-82-1218

Figure 12.- Beech 24R Sierra used in natural laminar flow flight experiments.

L-82-3004

Figure 13.- Bellanca Skyrocket II used in natural laminar flow flight experiments.

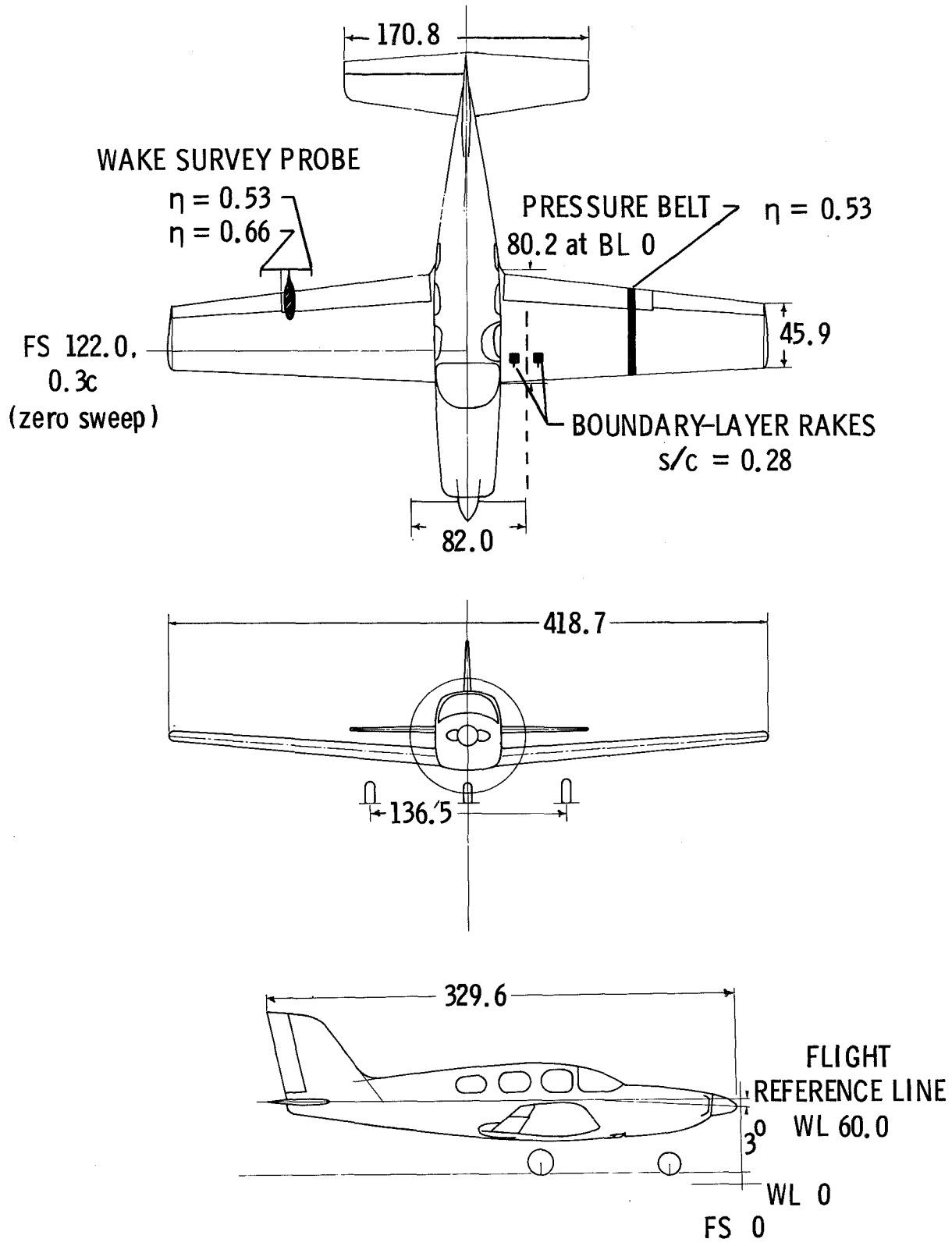

Figure 14.- Three-view drawing of Bellanca Skyrocket II with instrument locations. Linear dimensions are in inches.

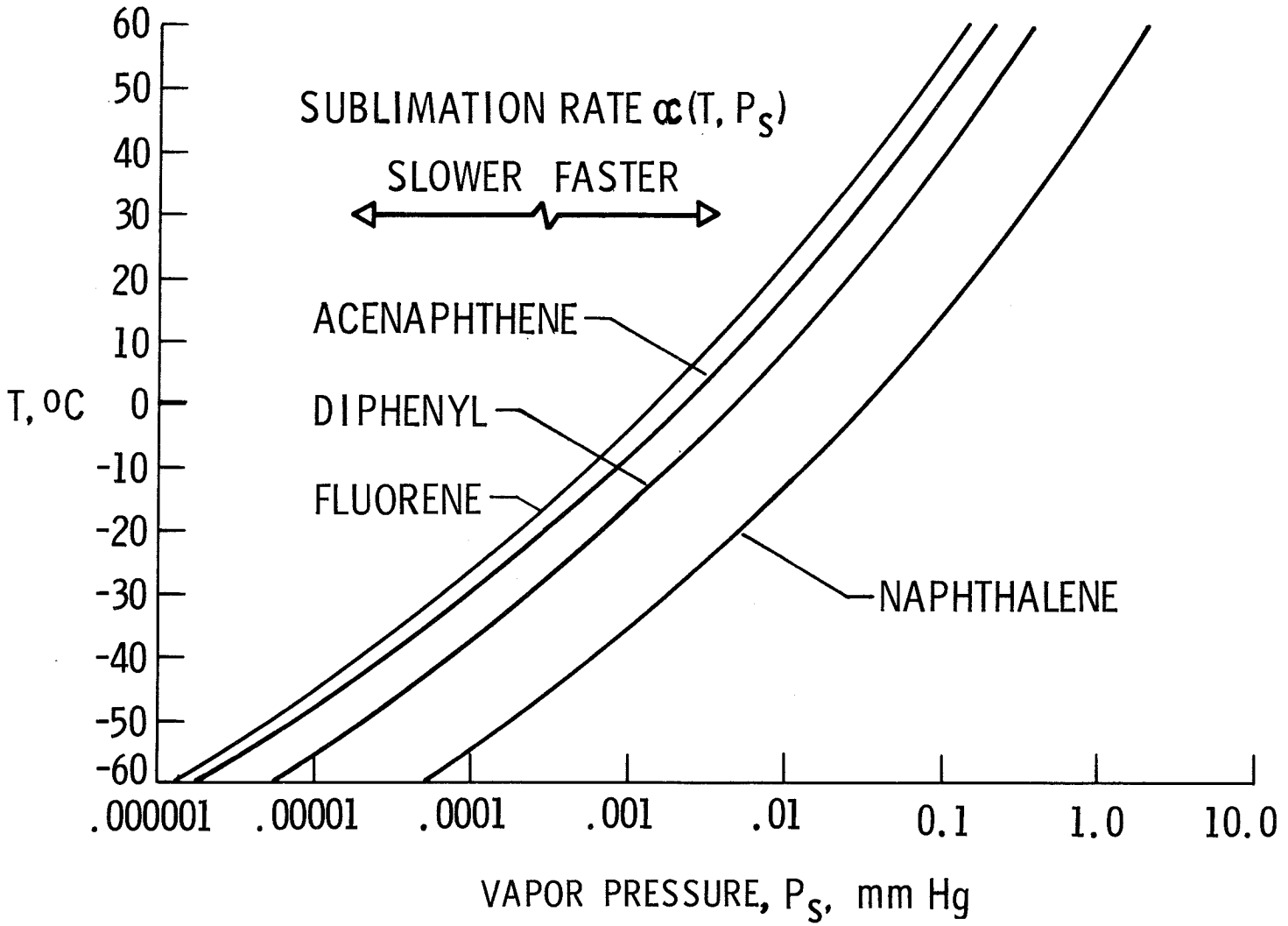

Figure 15.- Vapor pressure of sublimable solids.

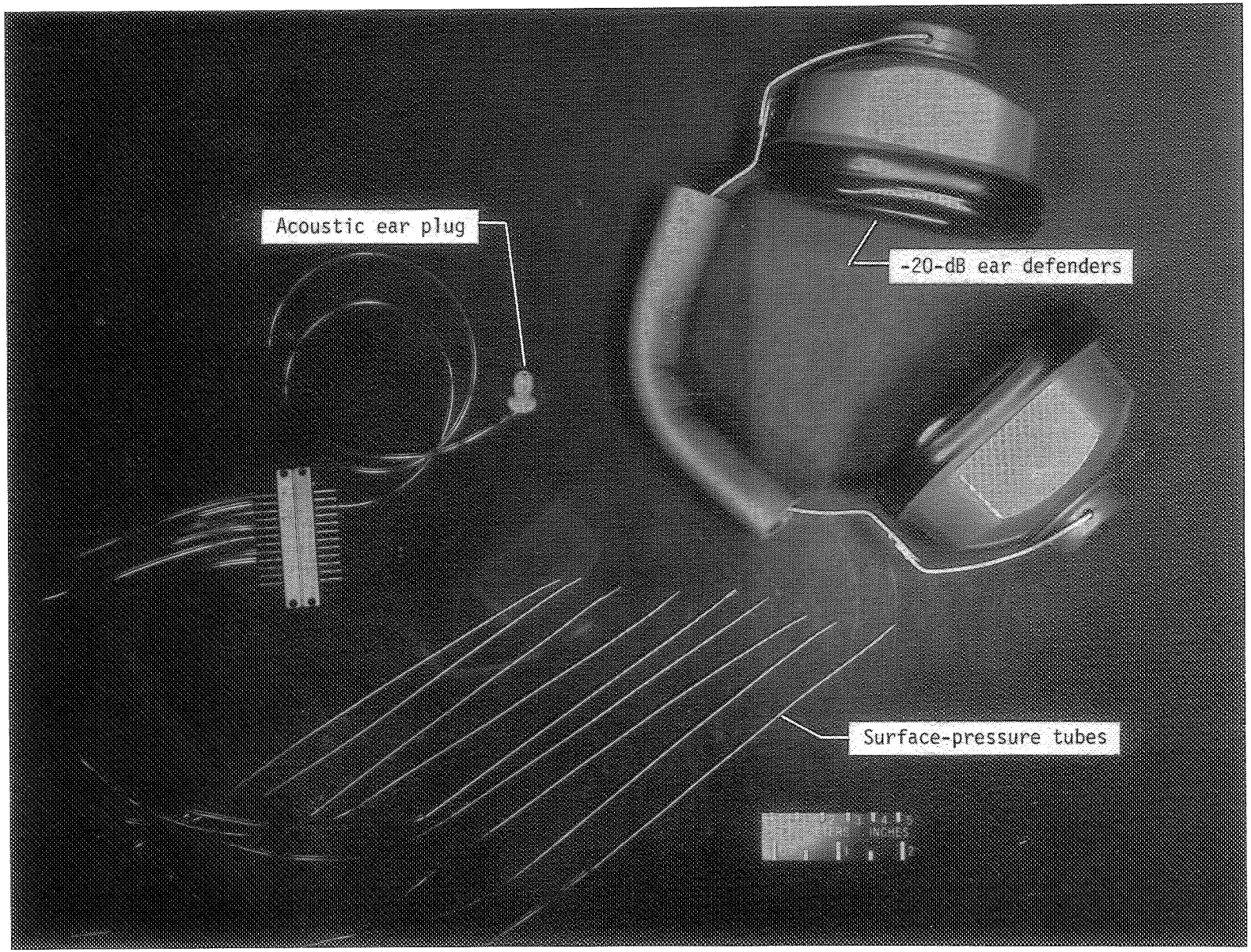

L-81-9092

Figure 16.- Equipment for acoustic detection of boundary-layer transition.

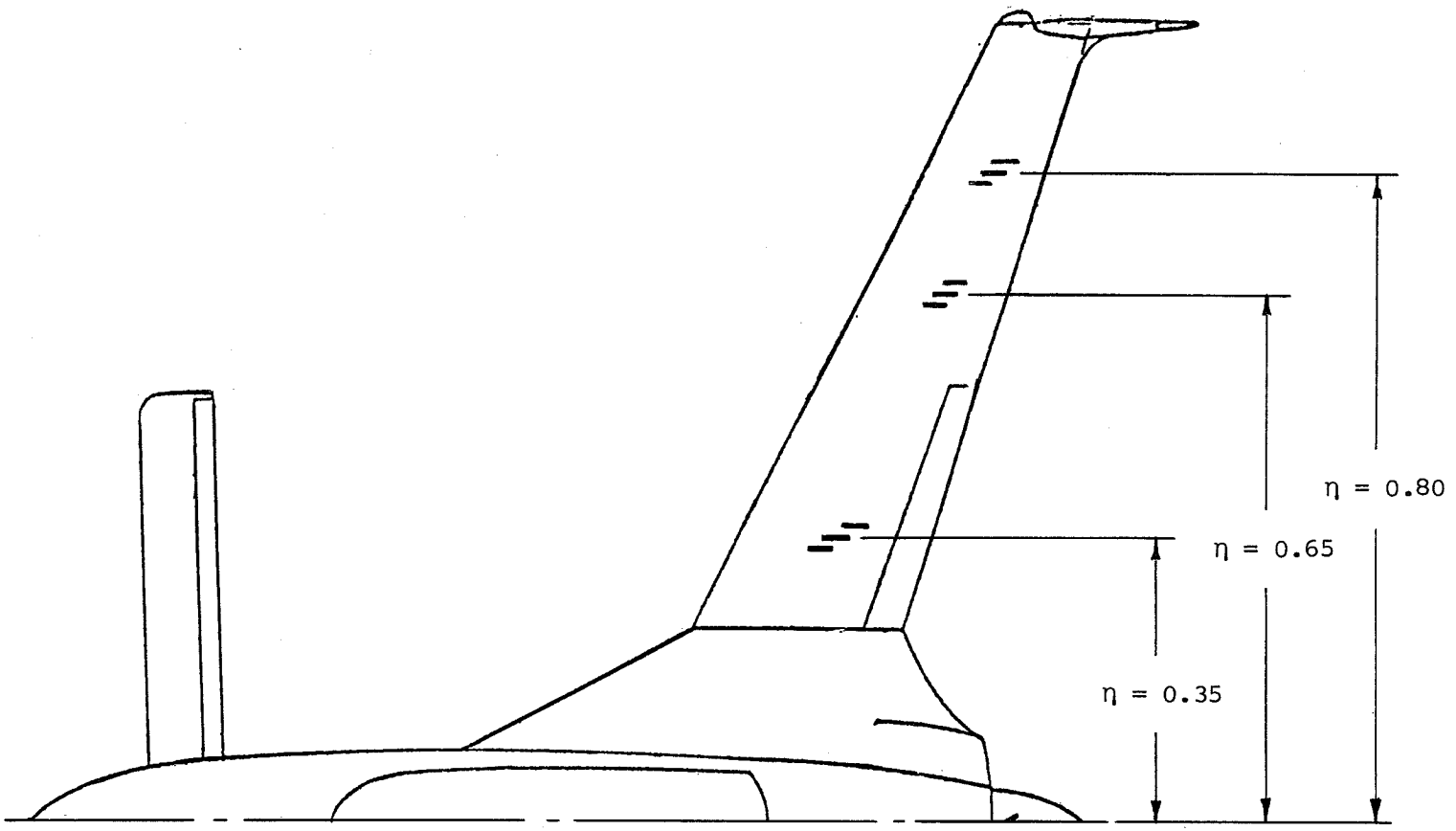

(a) Port locations on wing planform.

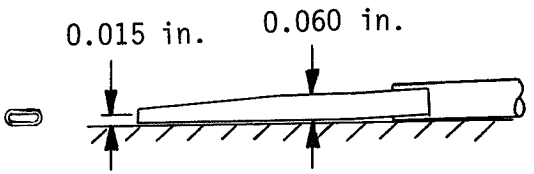

(b) Details of surface total-pressure tube.

Figure 17.- Detail of surface-mounted total-pressure-tube installation used for acoustic detection of transition of VariEze airplane.

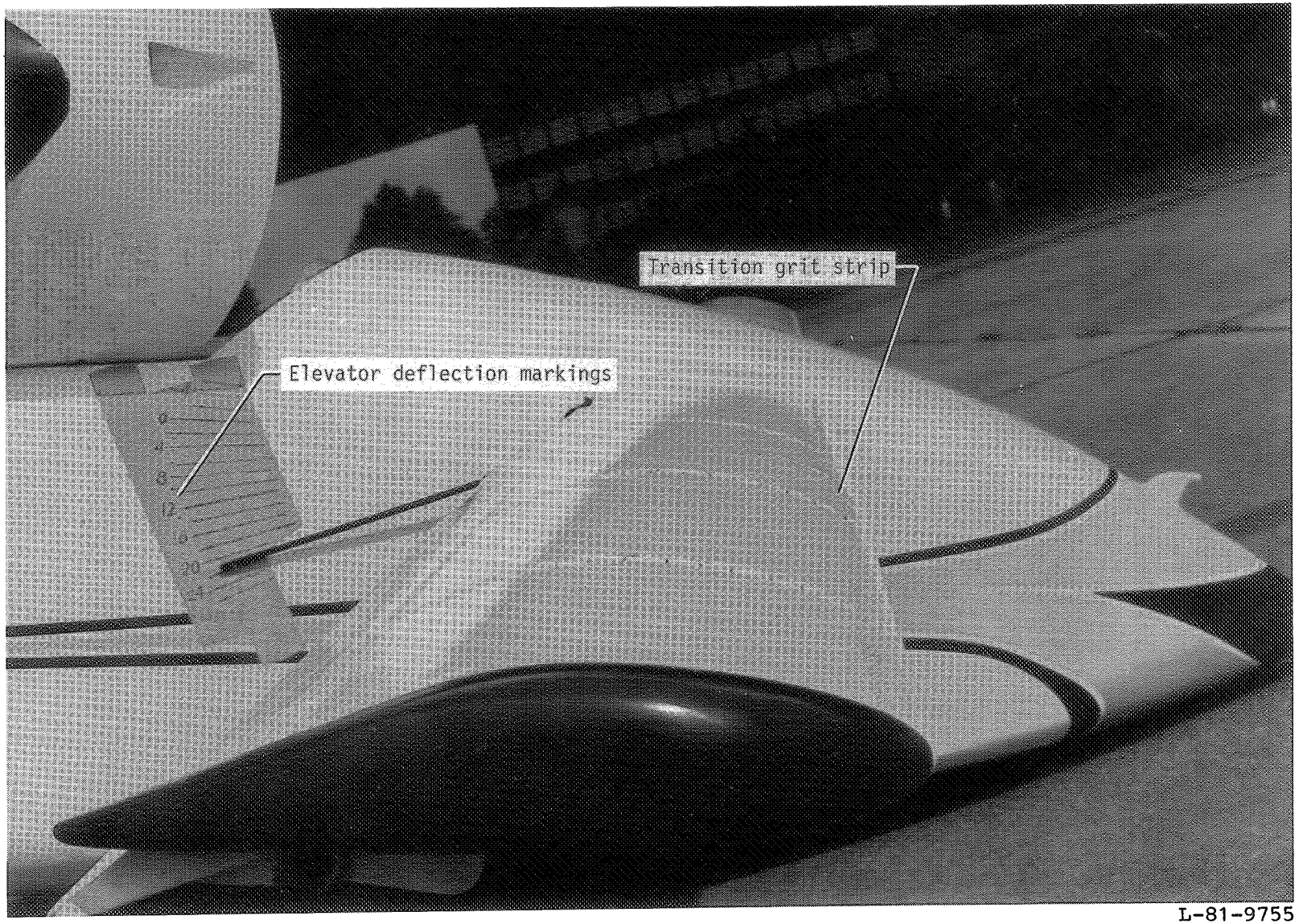

Figure 18.- Elevator deflection indicator utilized on VariEze airplane.

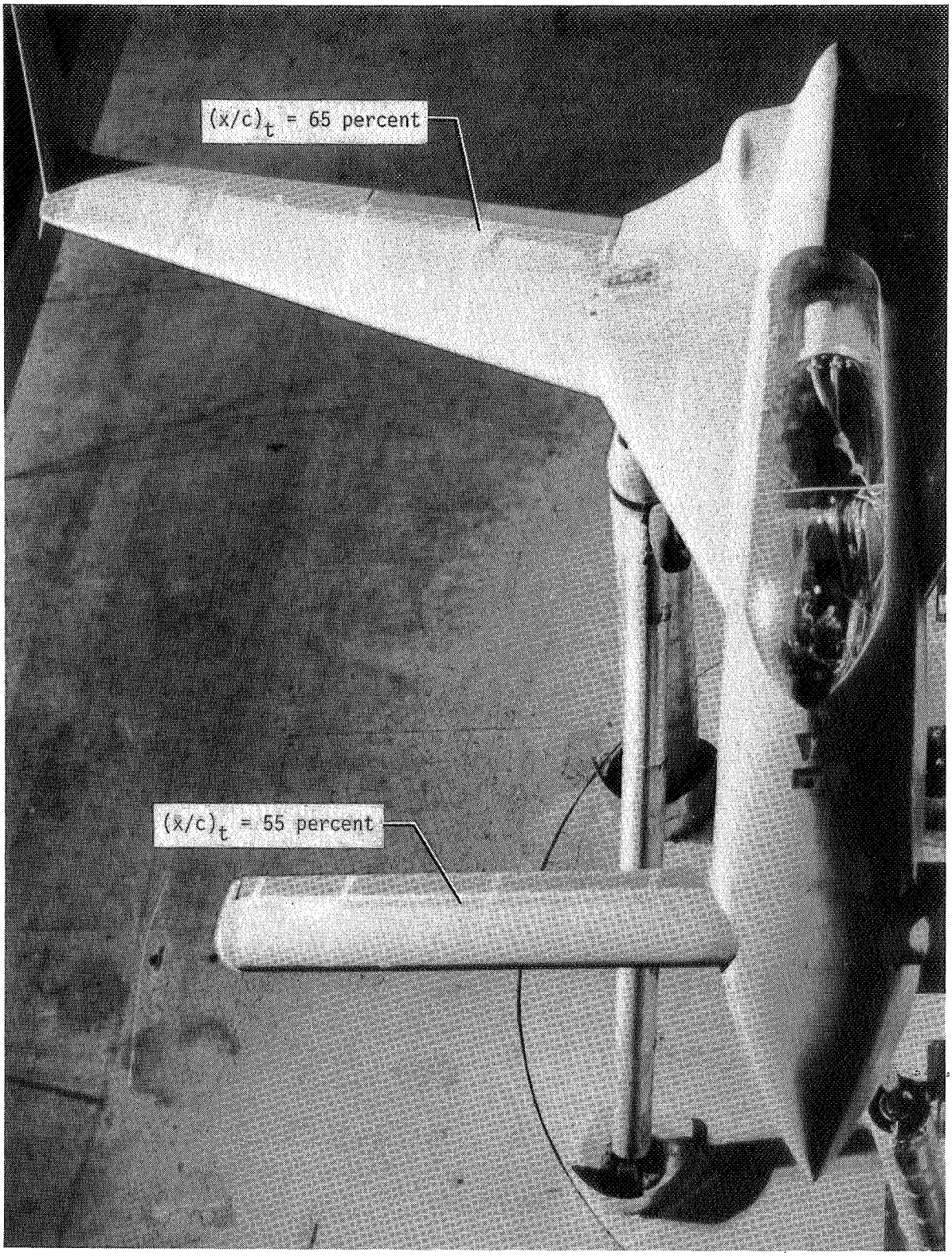

L-81-8426

(a) Top view.

Figure 19.- Visualization of boundary-layer transition on VariEze airplane. $R = 0.625 \times 10^6$ ft^{-1}; $C_L = 0.20$.

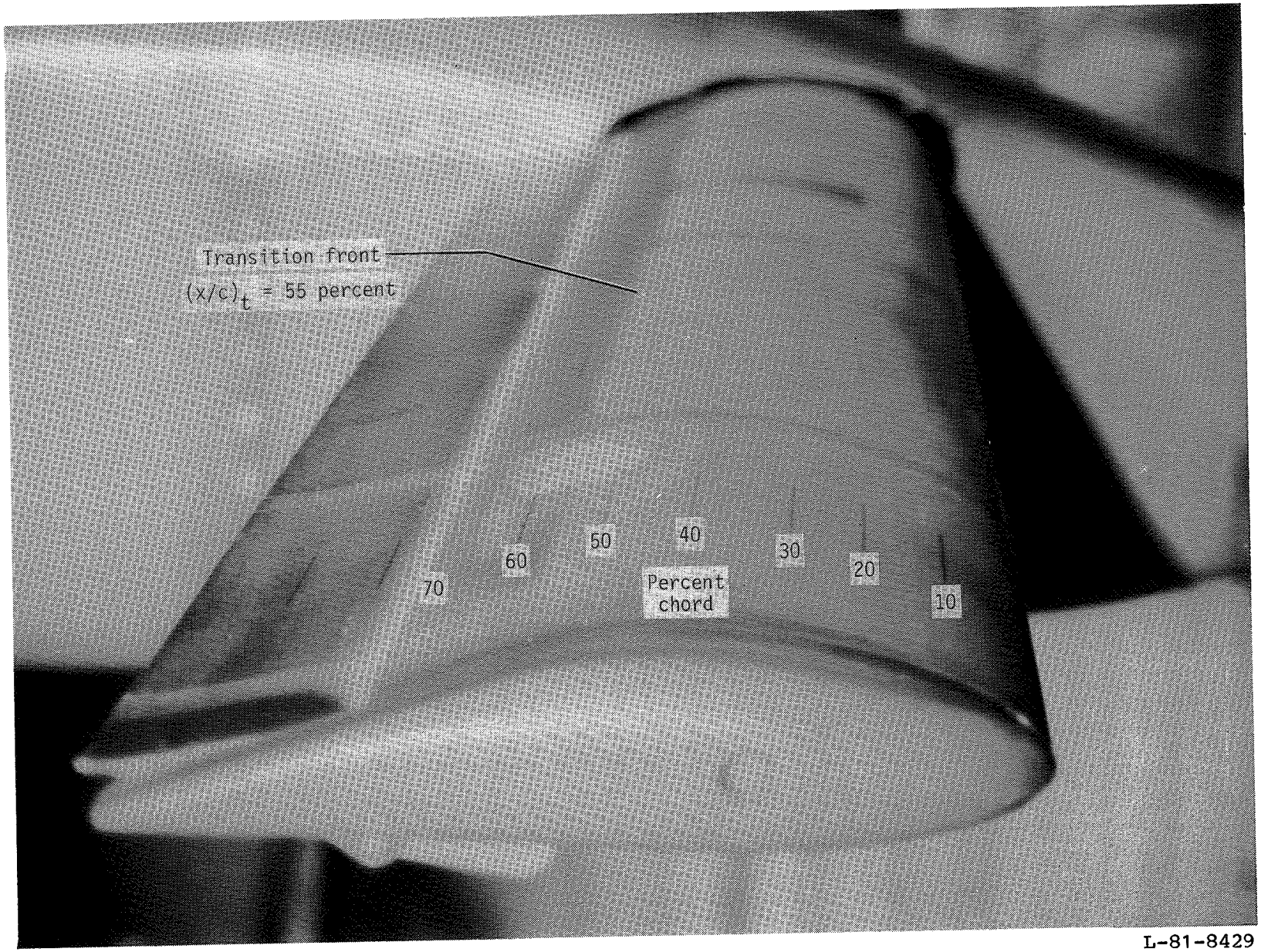

(b) Canard side view.

Figure 19.- Continued.

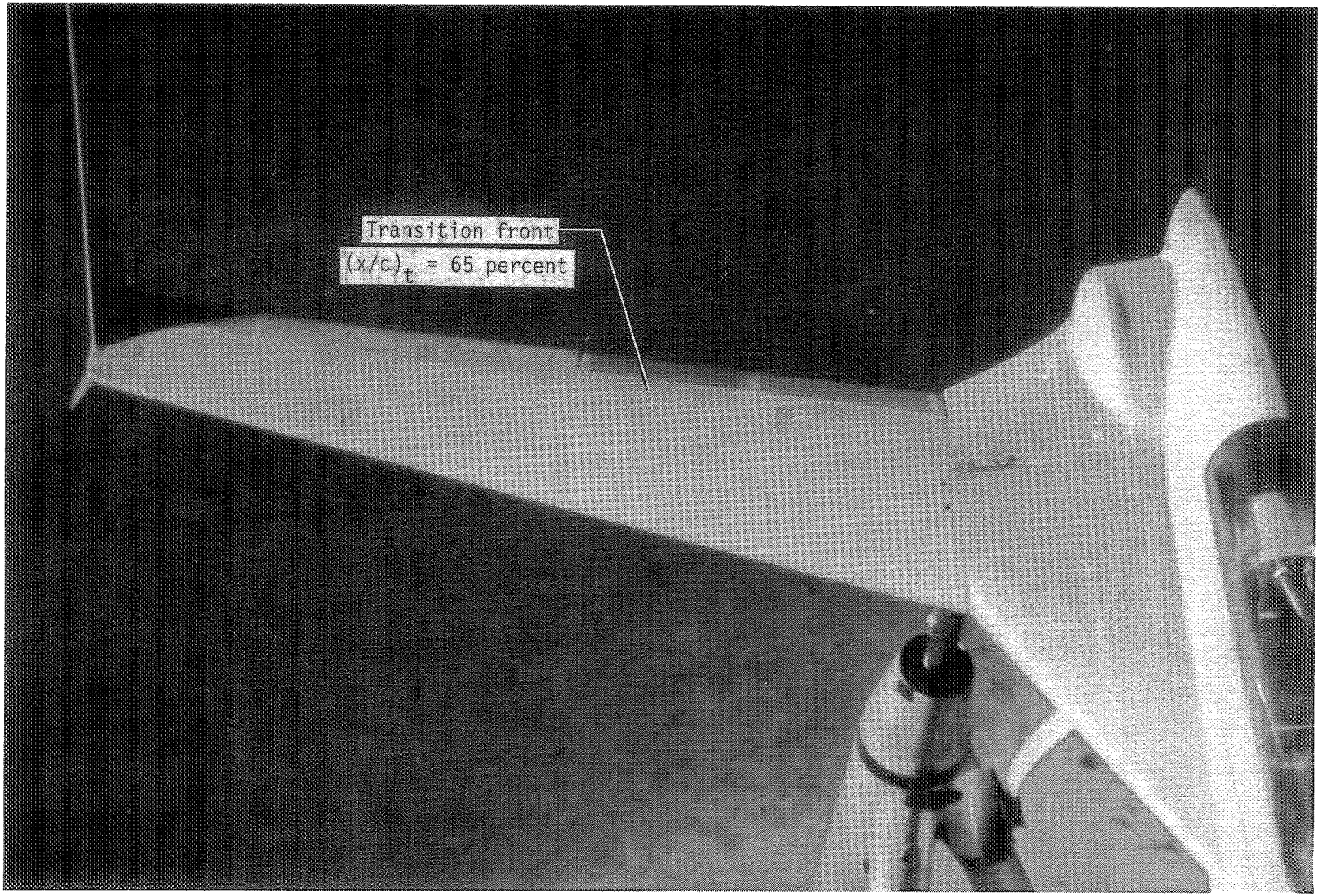

L-81-8431

(c) Wing.

Figure 19.- Continued.

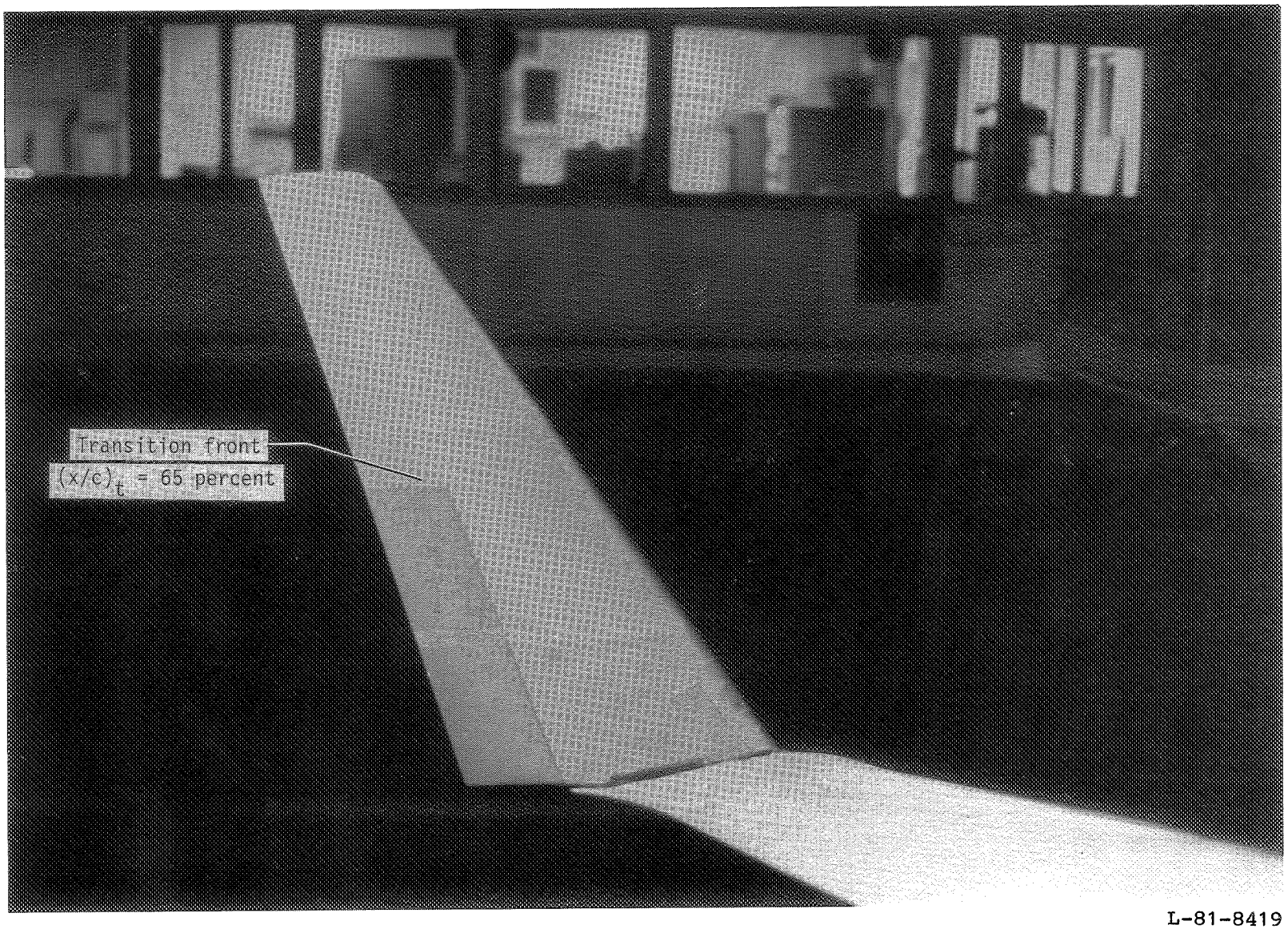

L-81-8419

(d) Winglet.

Figure 19.- Concluded.

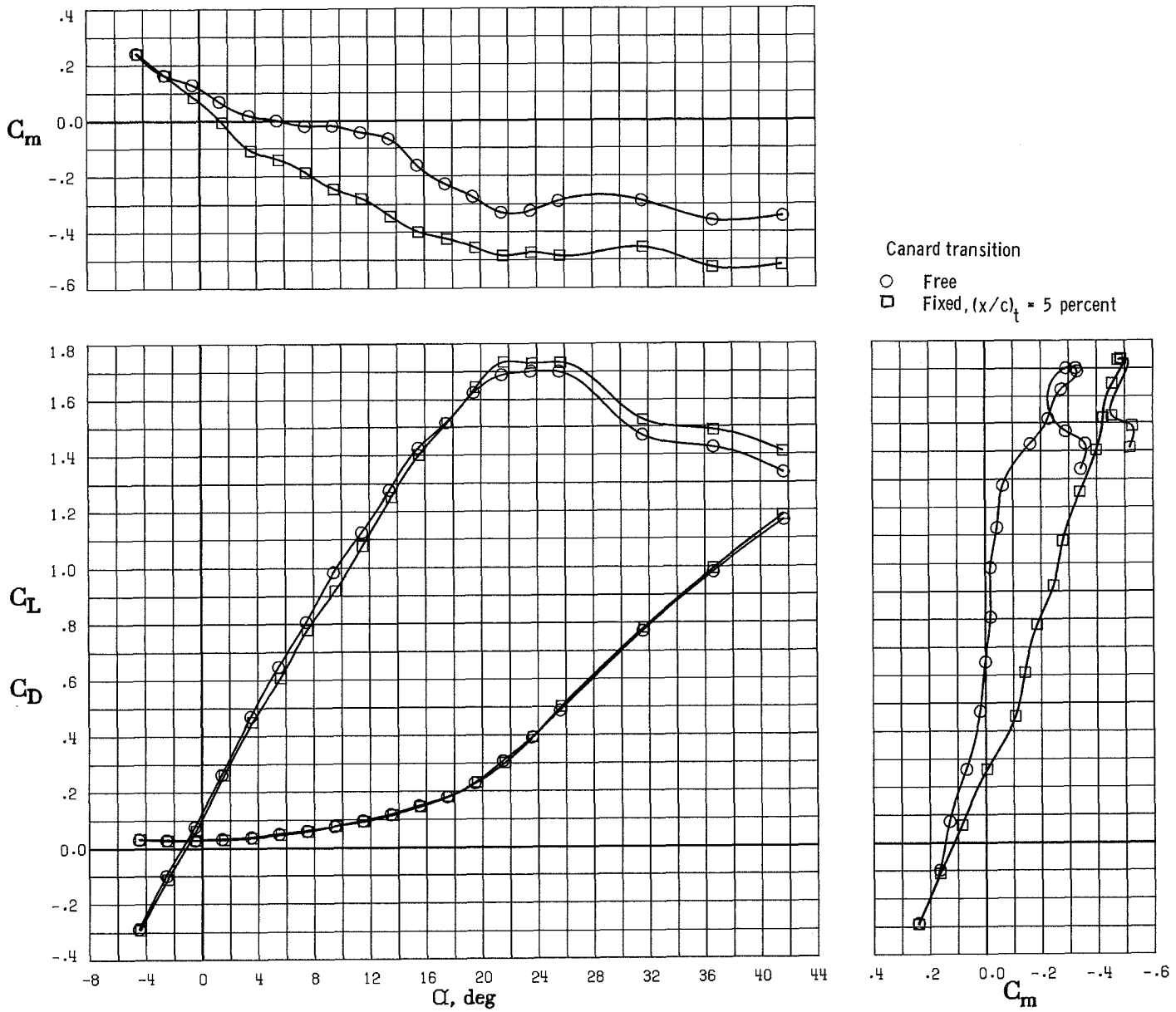

Figure 20.- Effect of fixing canard transition on longitudinal aerodynamic characteristics of VariEze model in Langley 30- by 60-Foot Tunnel.

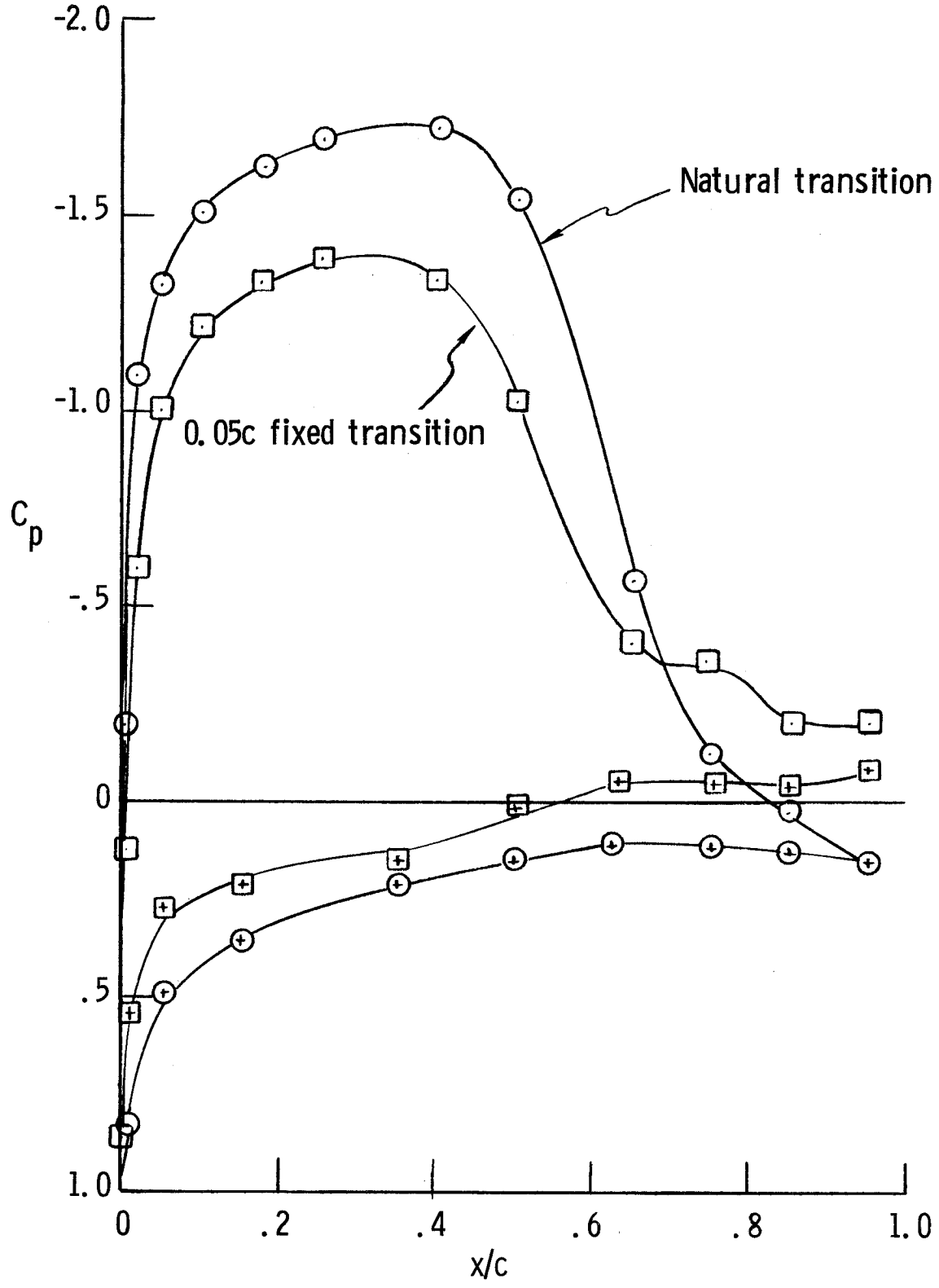

Figure 21.- Effect of fixed transition on chordwise pressure distribution. $\alpha = 8$; $\eta = 0.25$.

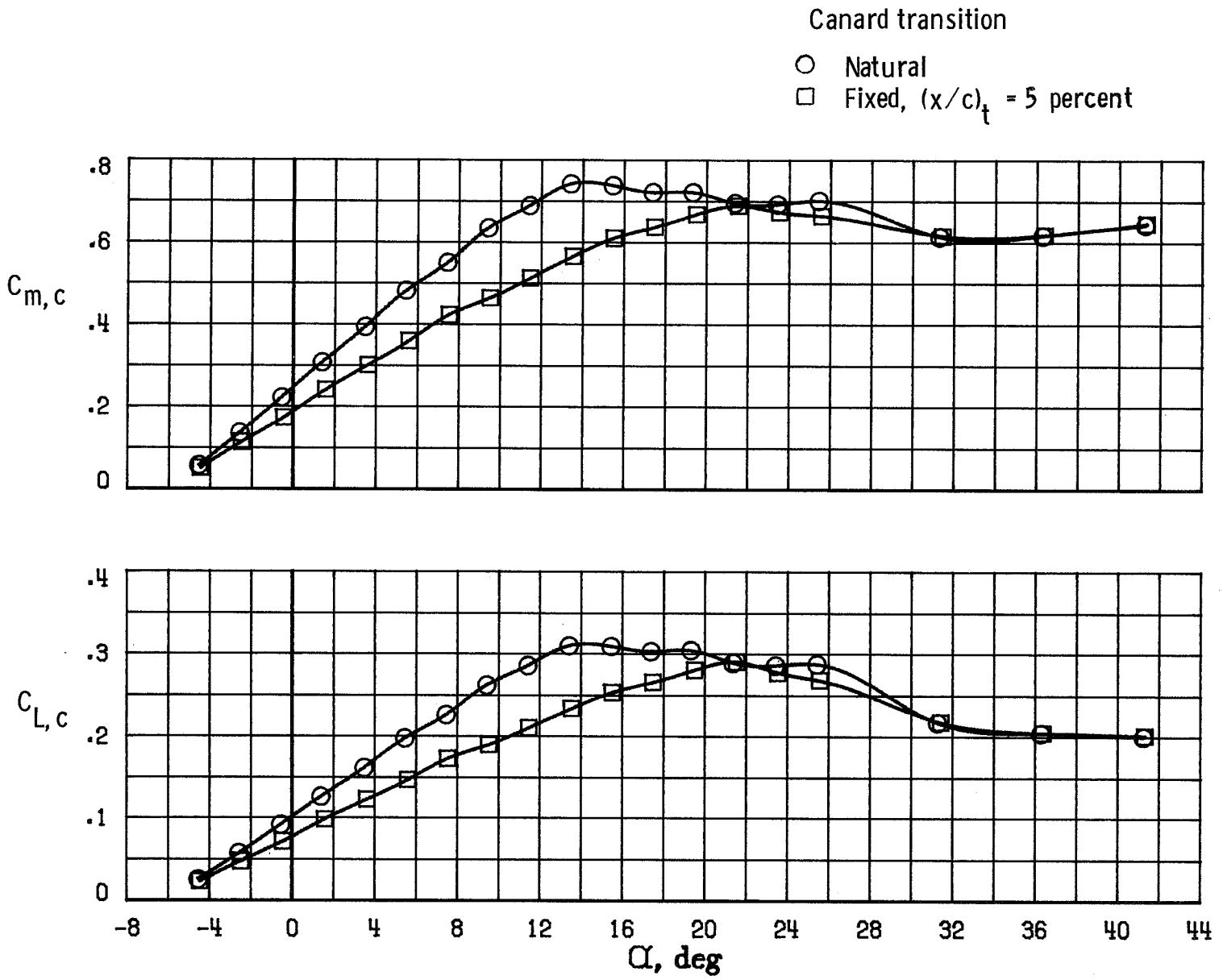

Figure 22.- Effect of fixing canard transition on the canard lift characteristics.

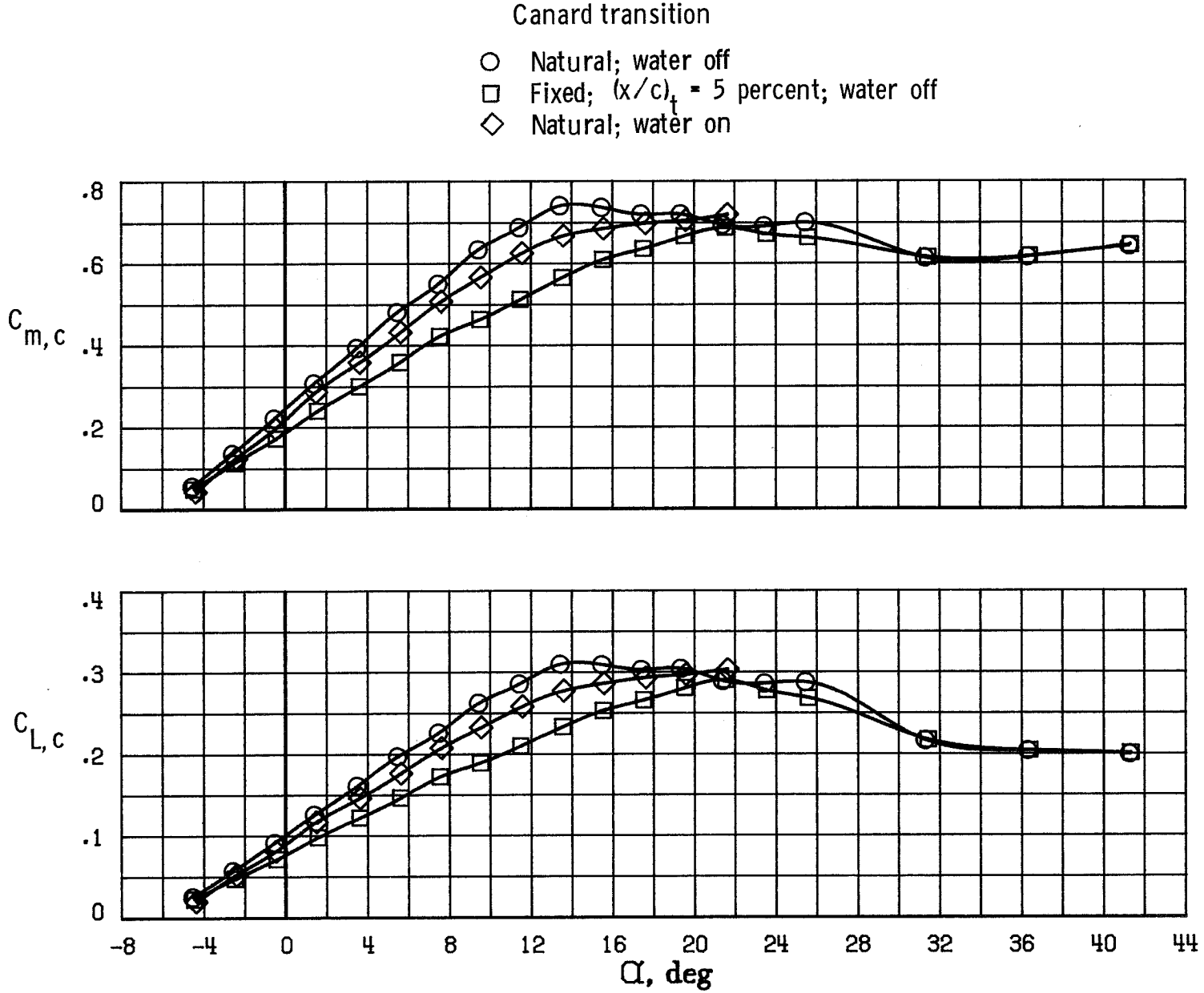

Figure 23.- Effect of water spray on canard lift.

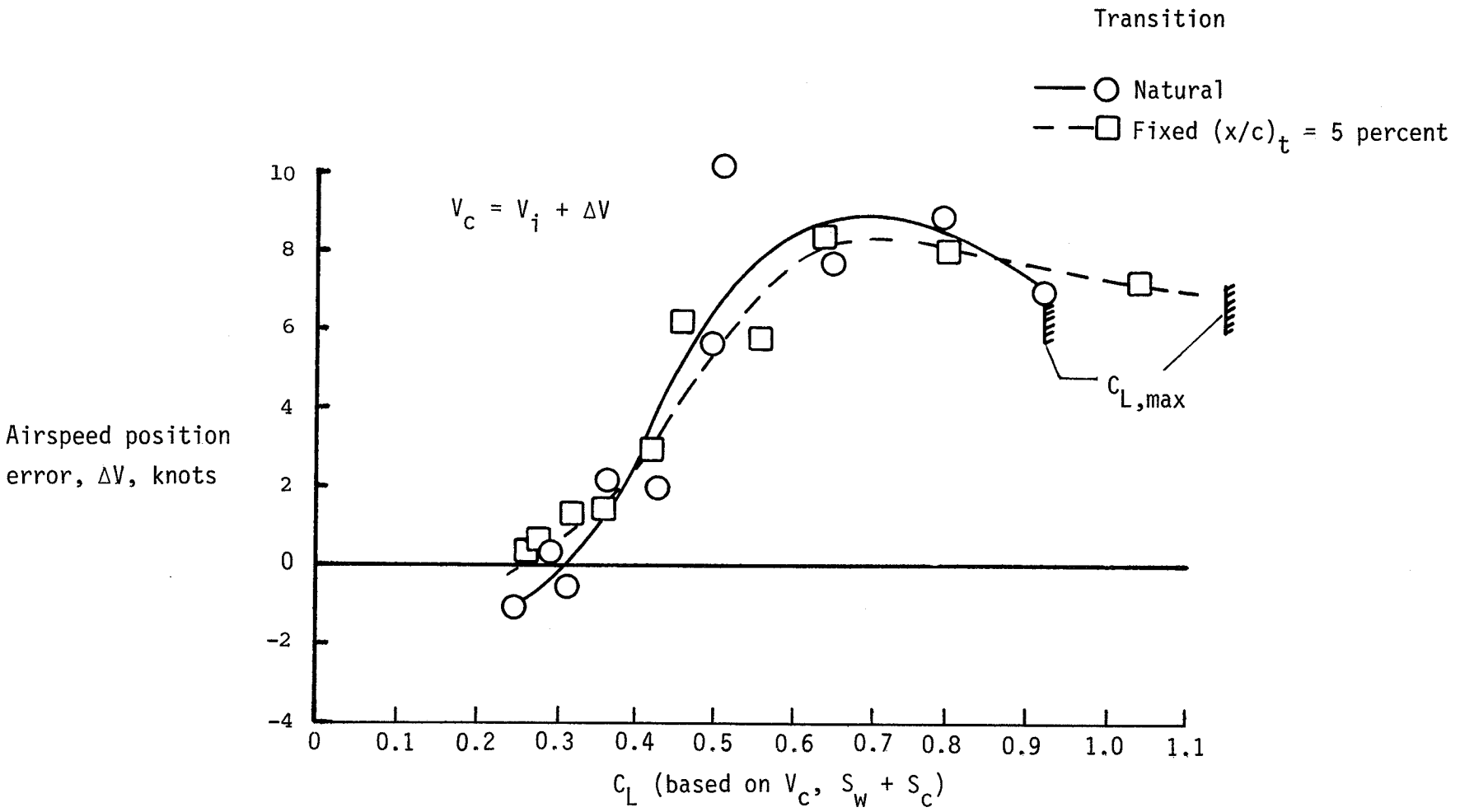

Figure 24.- Airspeed calibration for VariEze airplane from pace-airplane method.

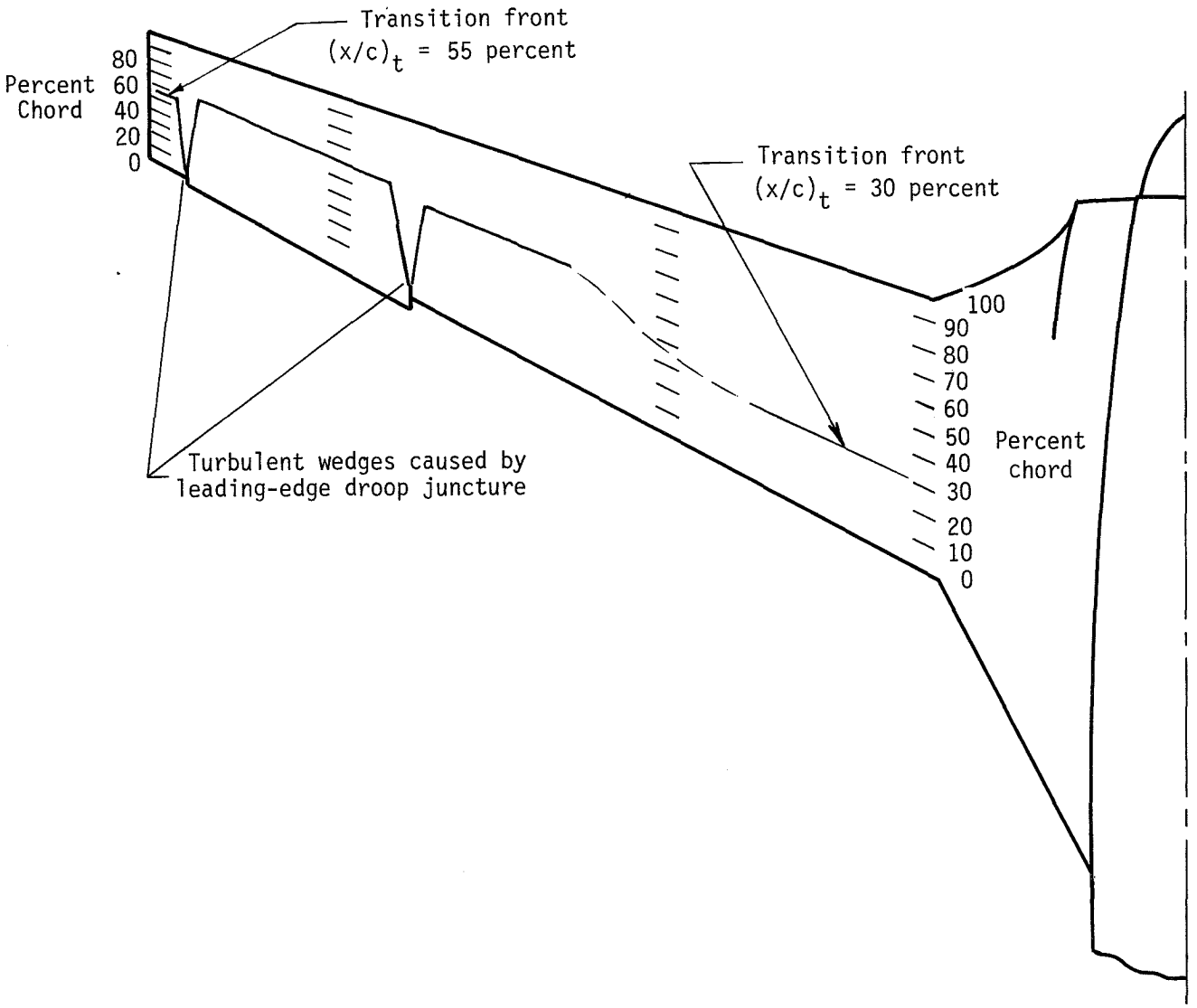

(a) Wing.

Figure 25.- Transition on VariEze measured during flight by sublimating chemical. $R = 1.40 \times 10^6$ ft^{-1}; $C_L = 0.35$.

(b) Winglet.

Figure 25.- Concluded.

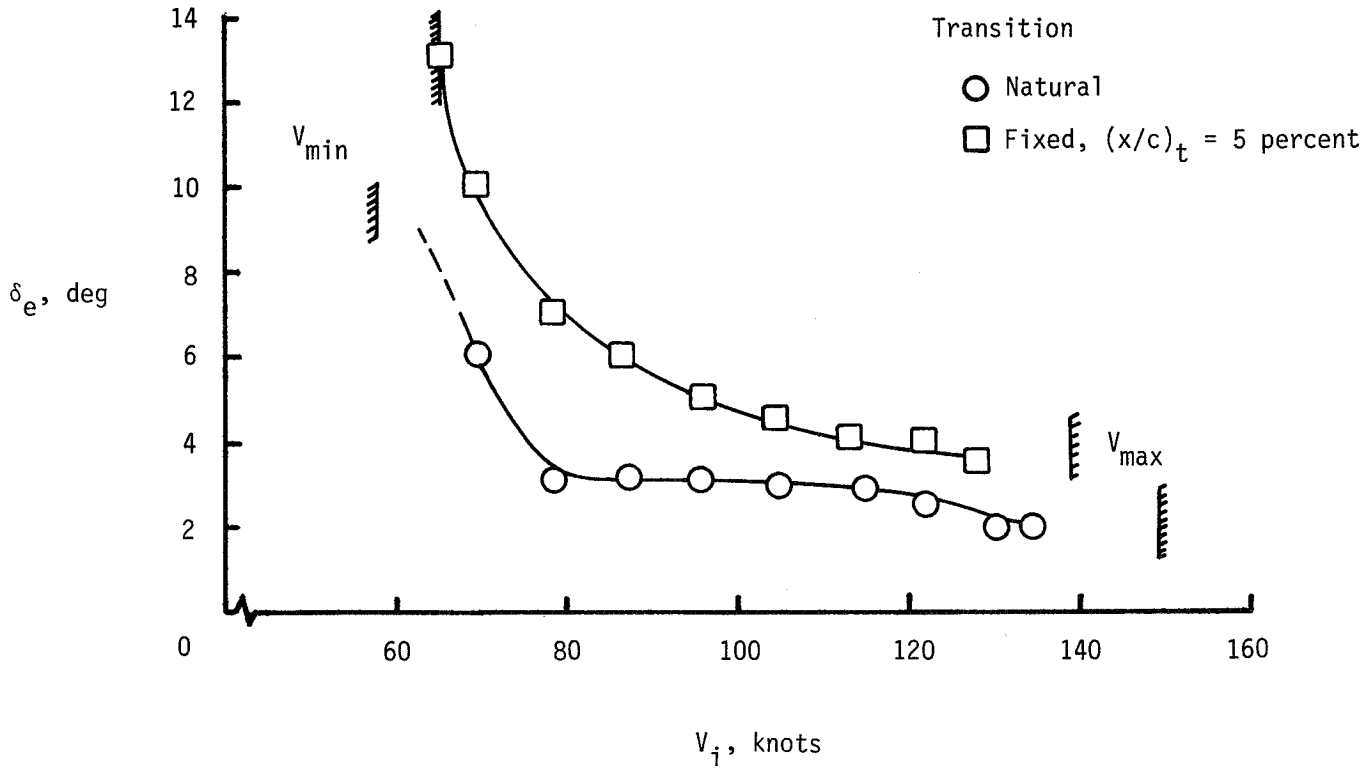

Figure 26.- Comparison of fixed- versus free-transition performance and longitudinal control characteristics for VariEze airplane during flight.

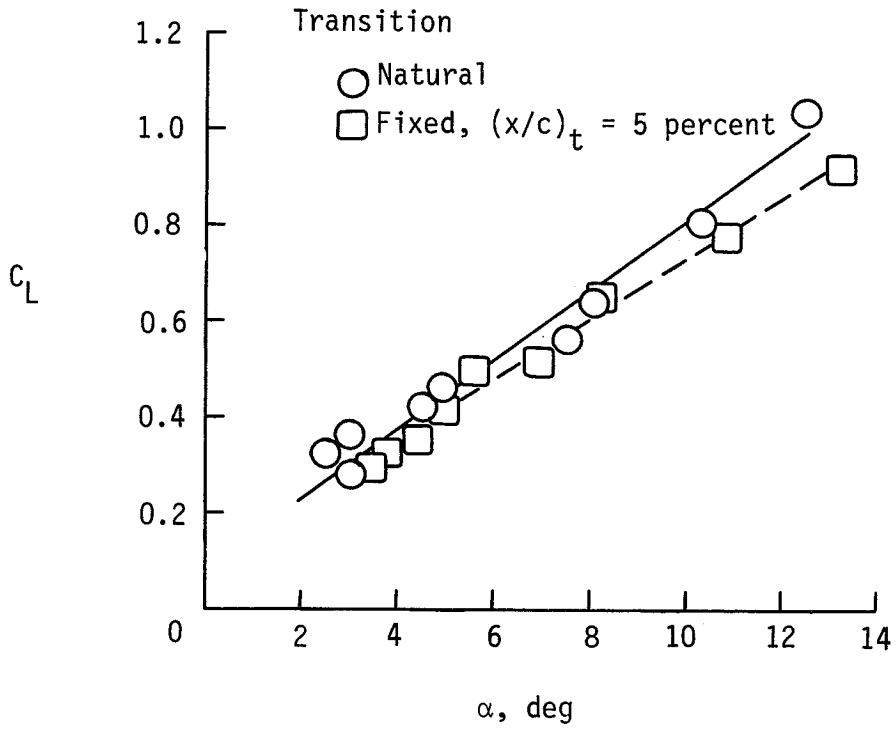

Figure 27.- Effect of fixed versus free transition on lift-curve slope for VariEze airplane.

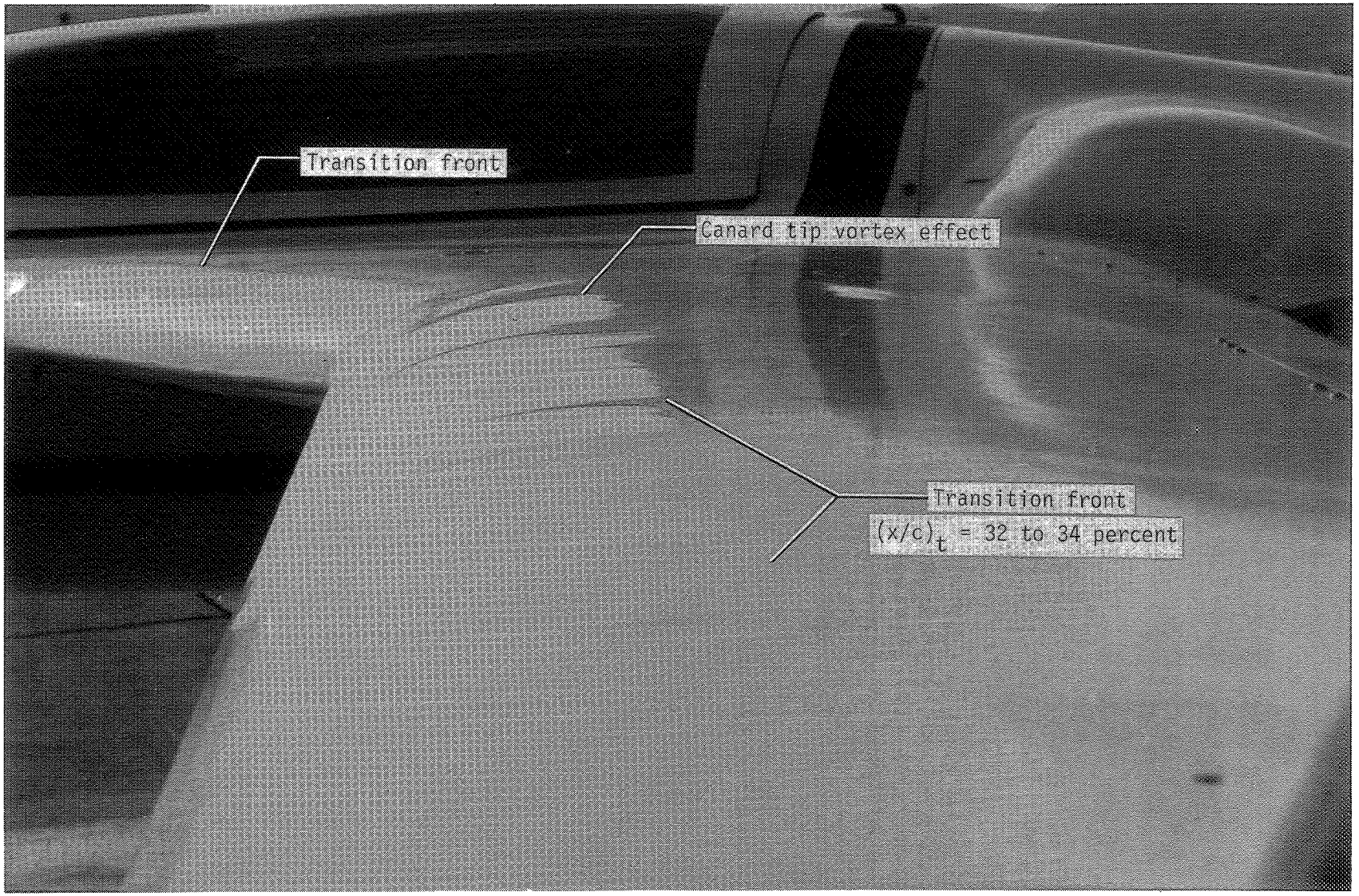

(a) Wing.

Figure 28.- Transition locations on Long-EZ airplane. $R = 1.42 \times 10^6$ ft^{-1}; $C_L = 0.16$.

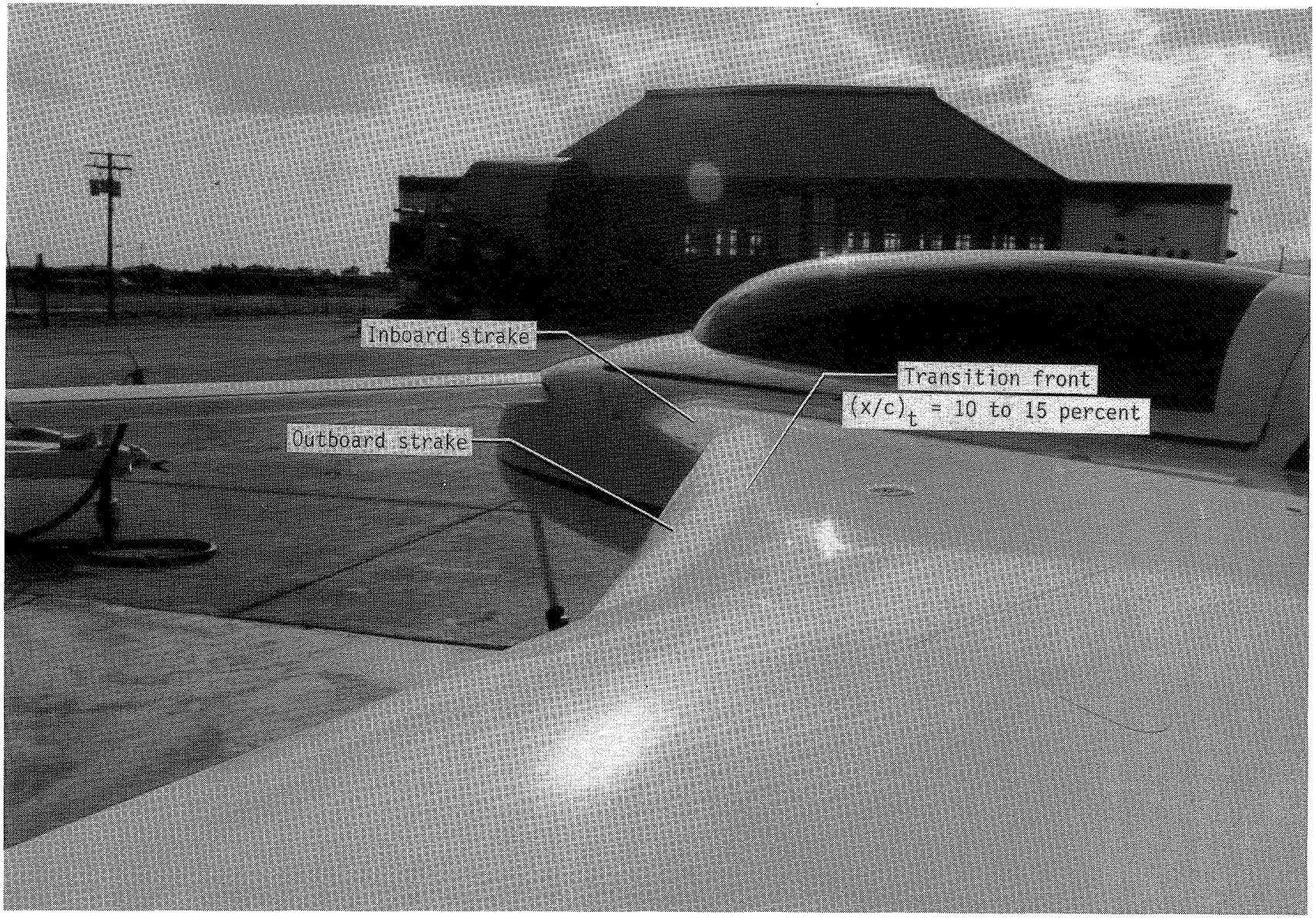

L-81-9790

(b) Strakes.

Figure 28.- Continued.

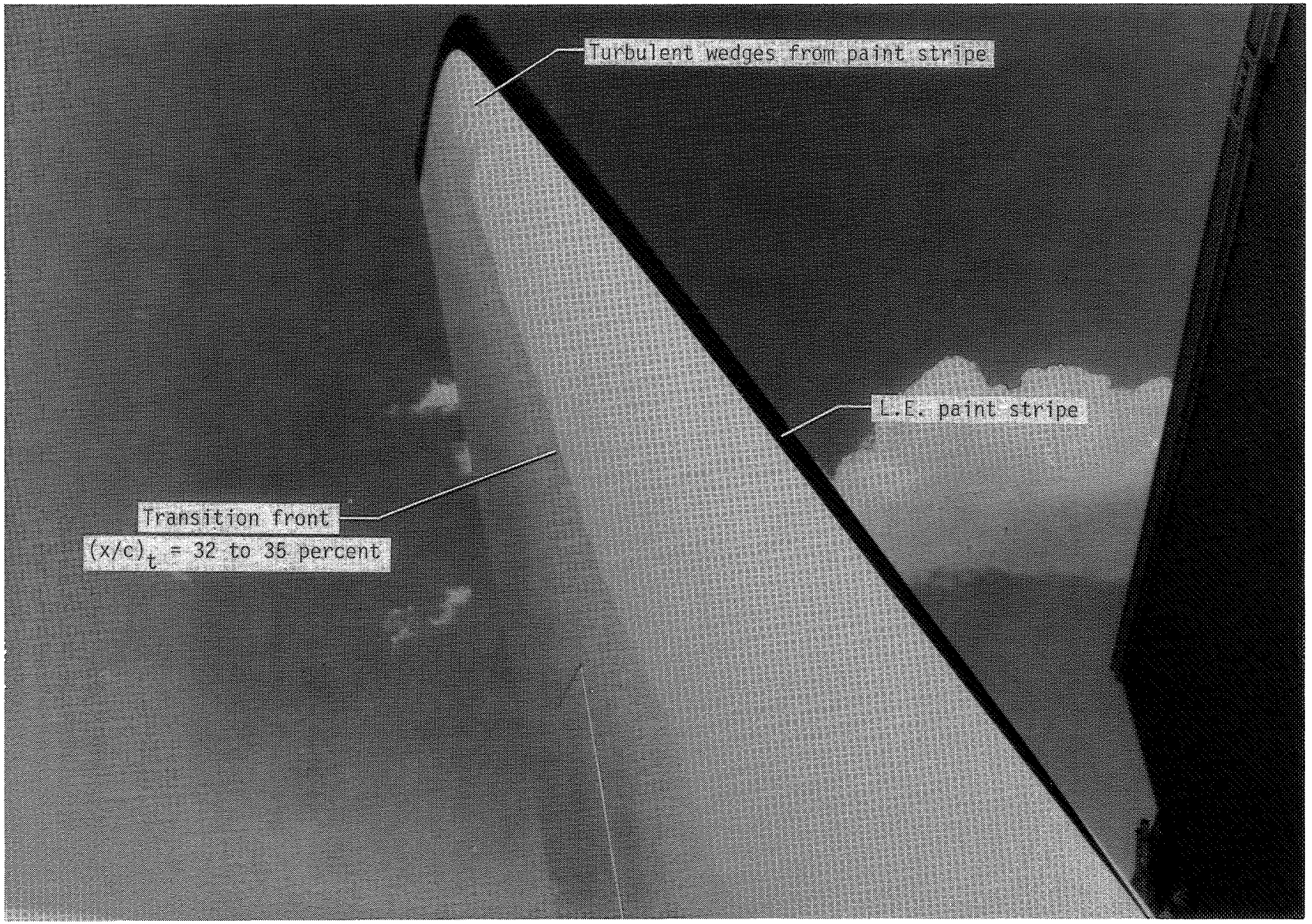

(c) Winglet.

Figure 28.- Continued.

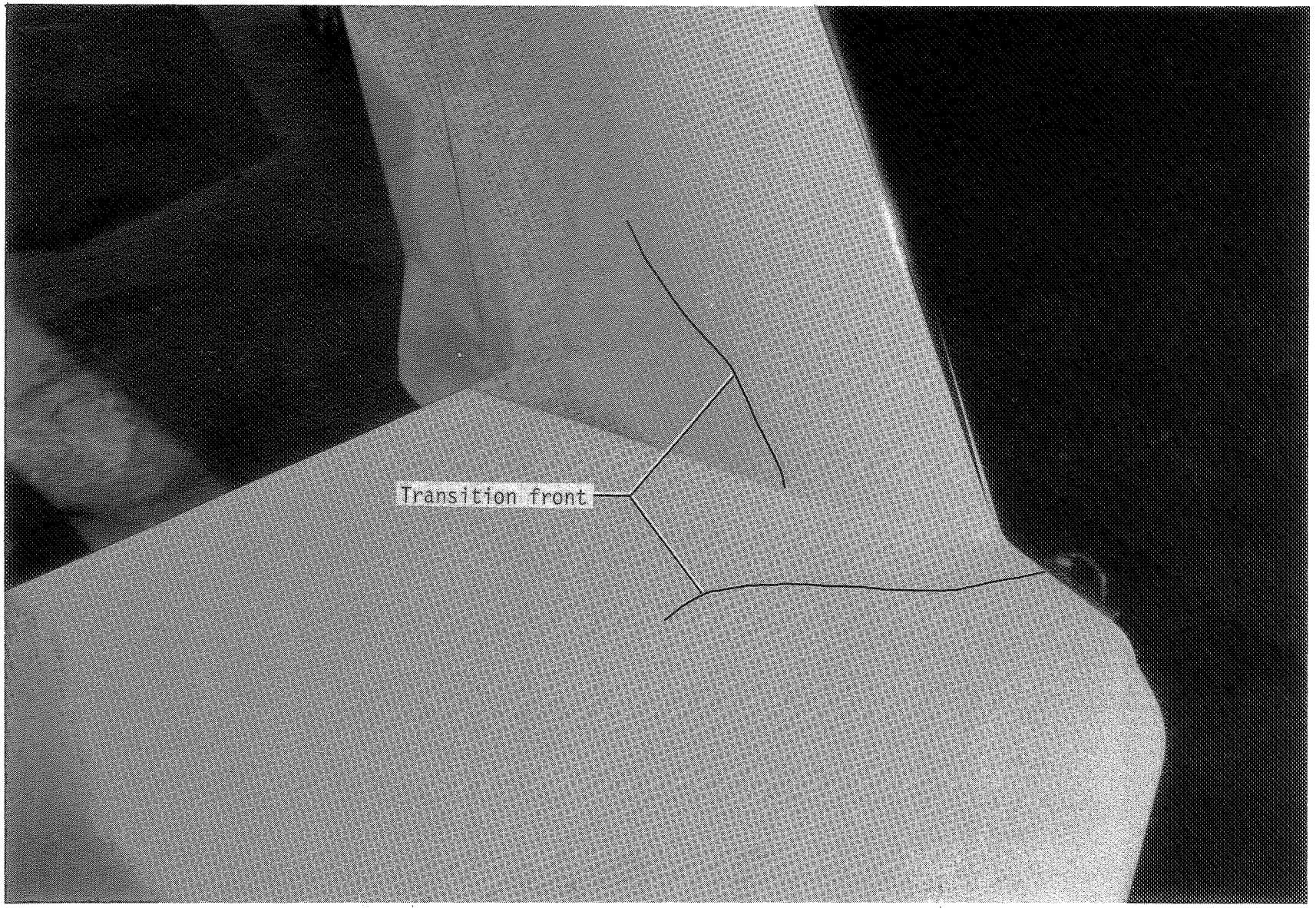

L-81-9789

(d) Wing-winglet juncture.

Figure 28.- Continued.

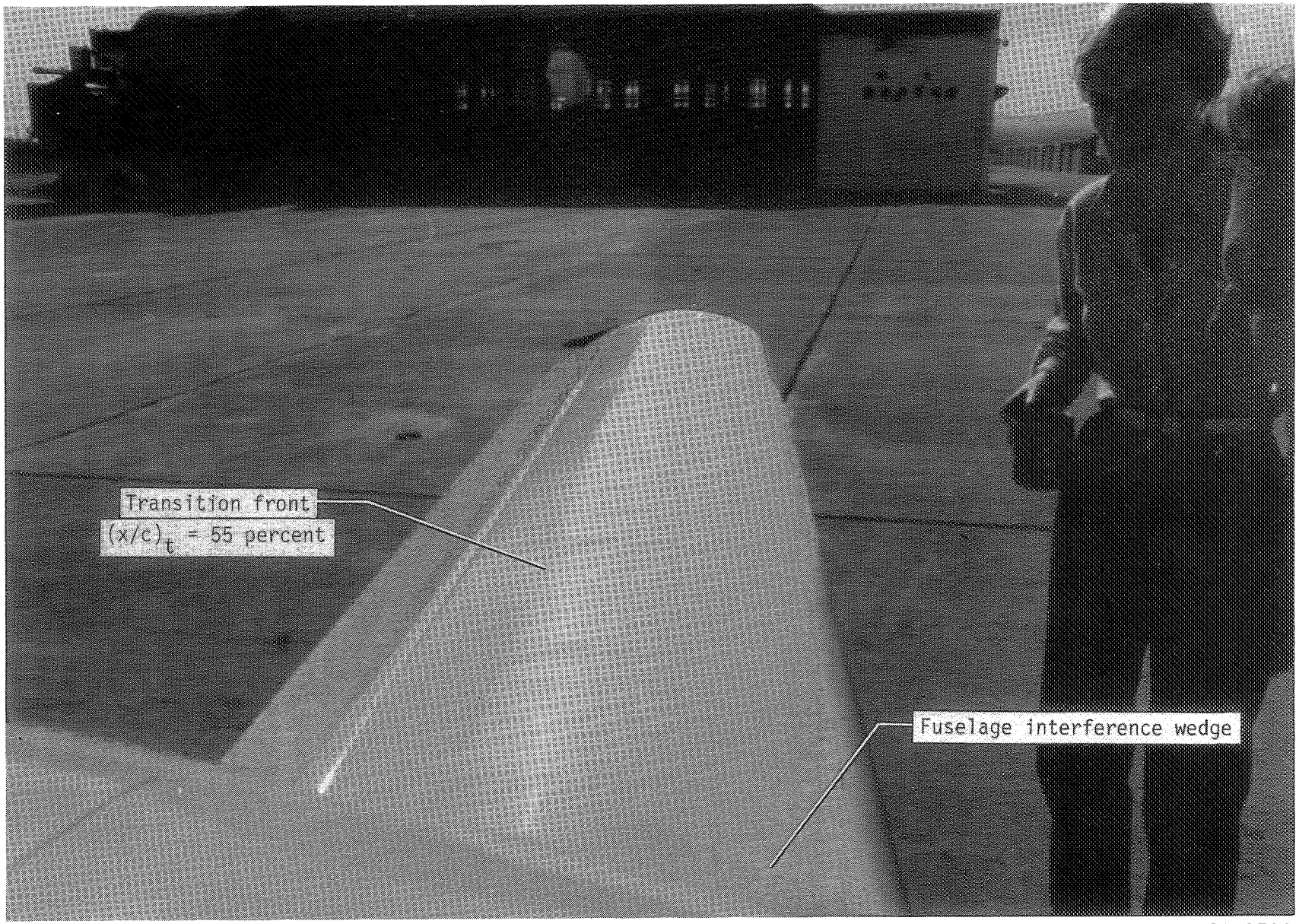

L-81-9782

(e) Canard.

Figure 28.- Continued.

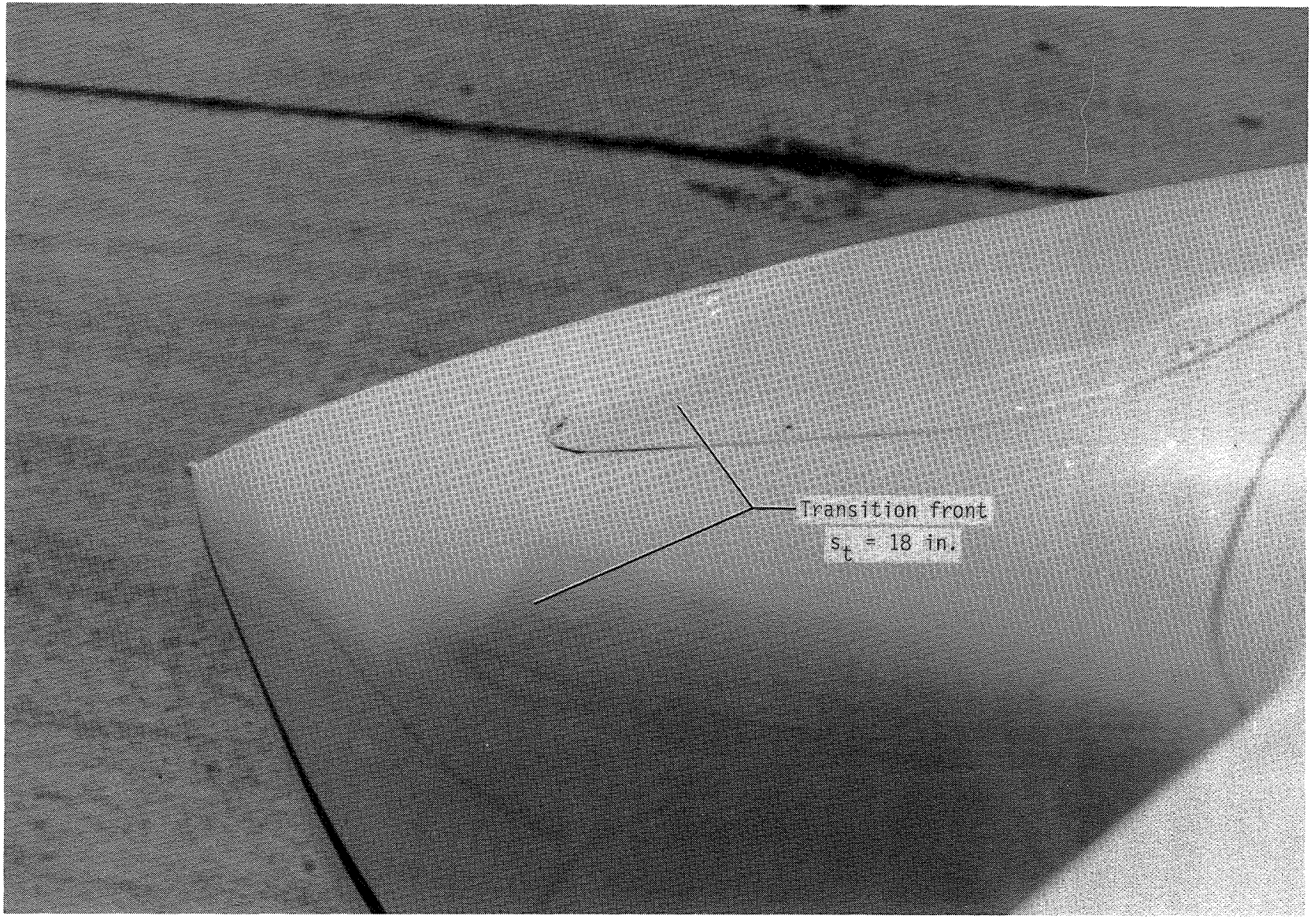

L-81-9794

(f) Fuselage nose.

Figure 28.- Continued.

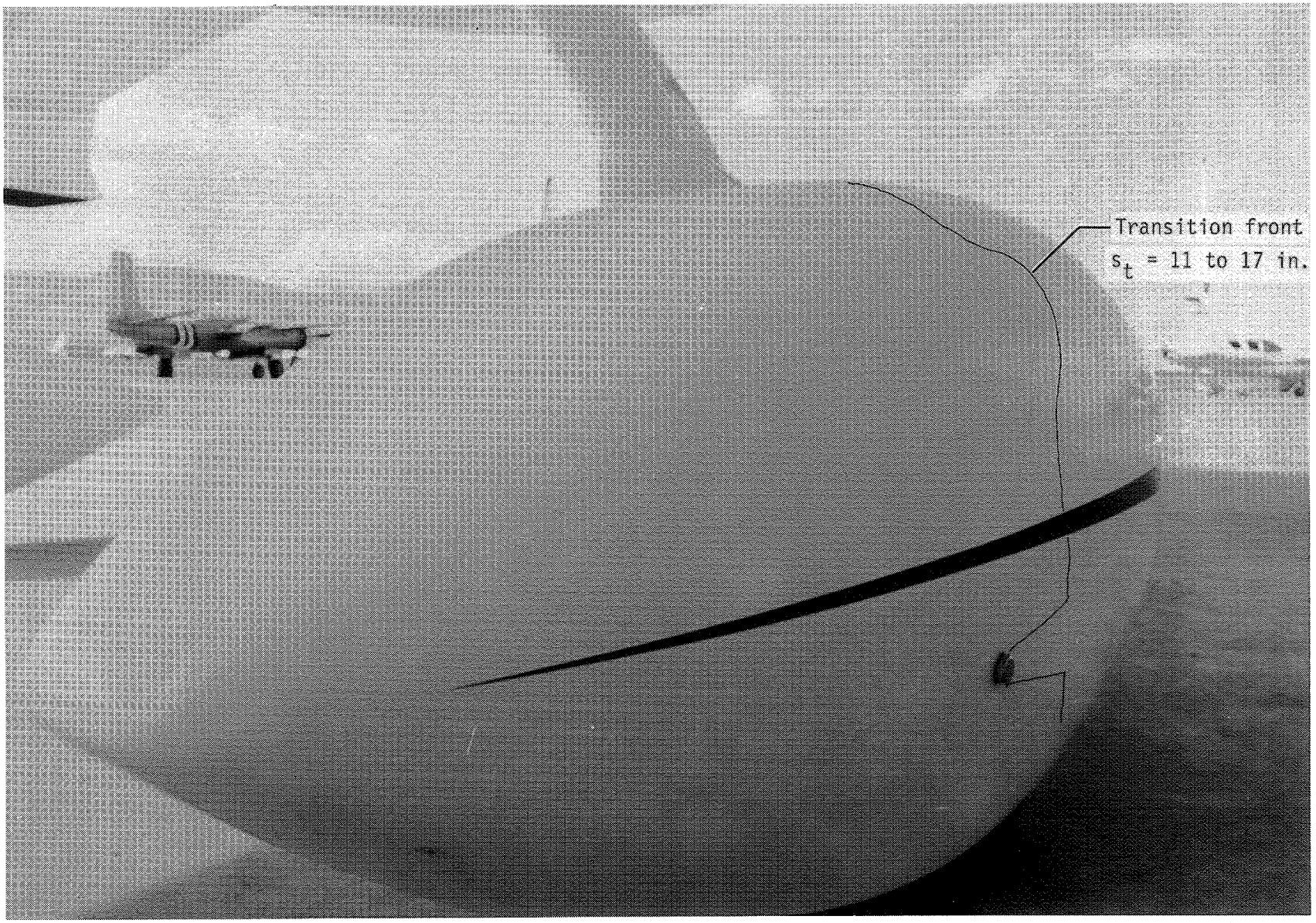

L-81-9792

(g) Wheel fairing.

Figure 28.- Concluded.

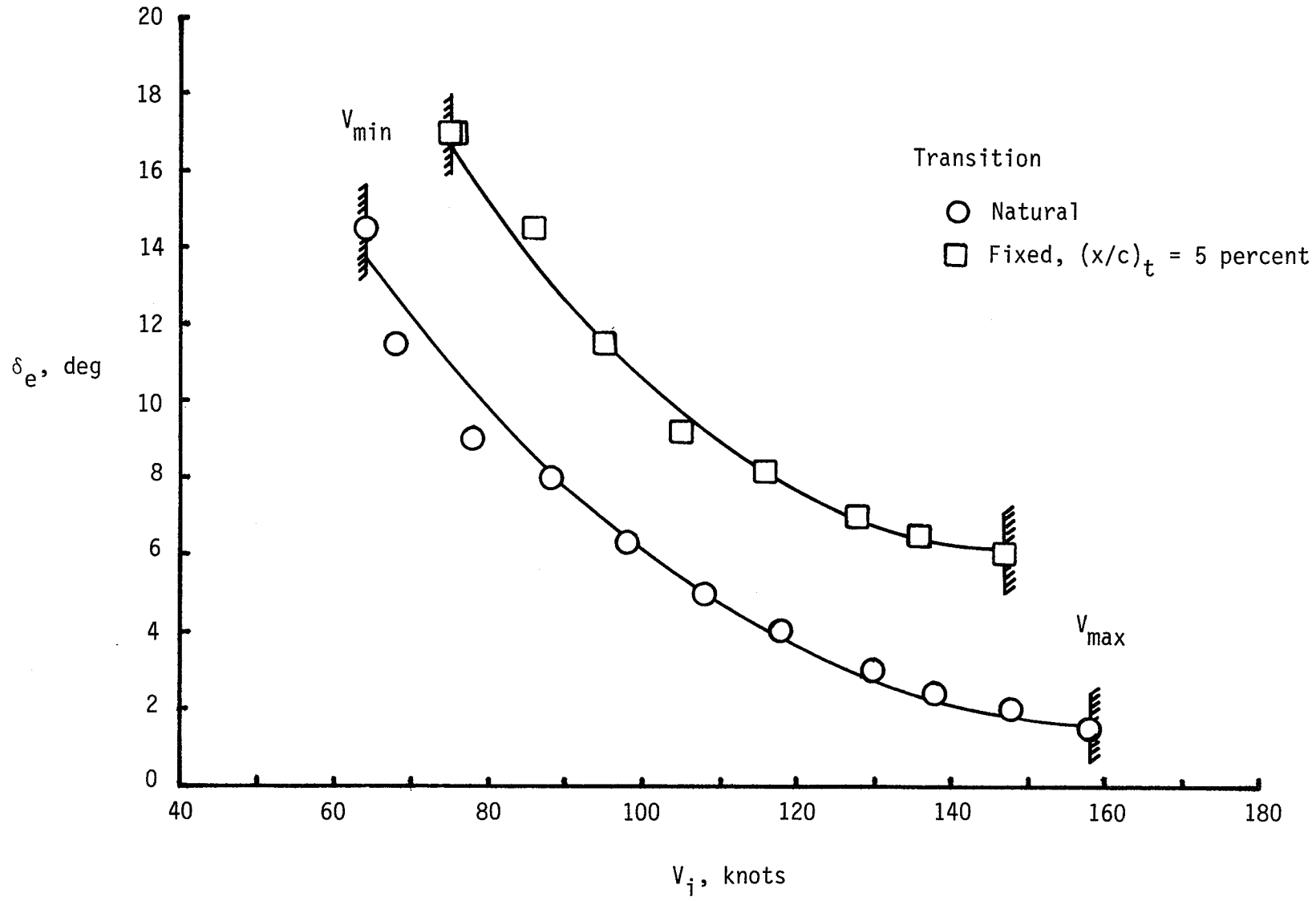

Figure 29.- Comparison of fixed- versus free-transition performance and longitudinal control characteristics for Long-EZ airplane.

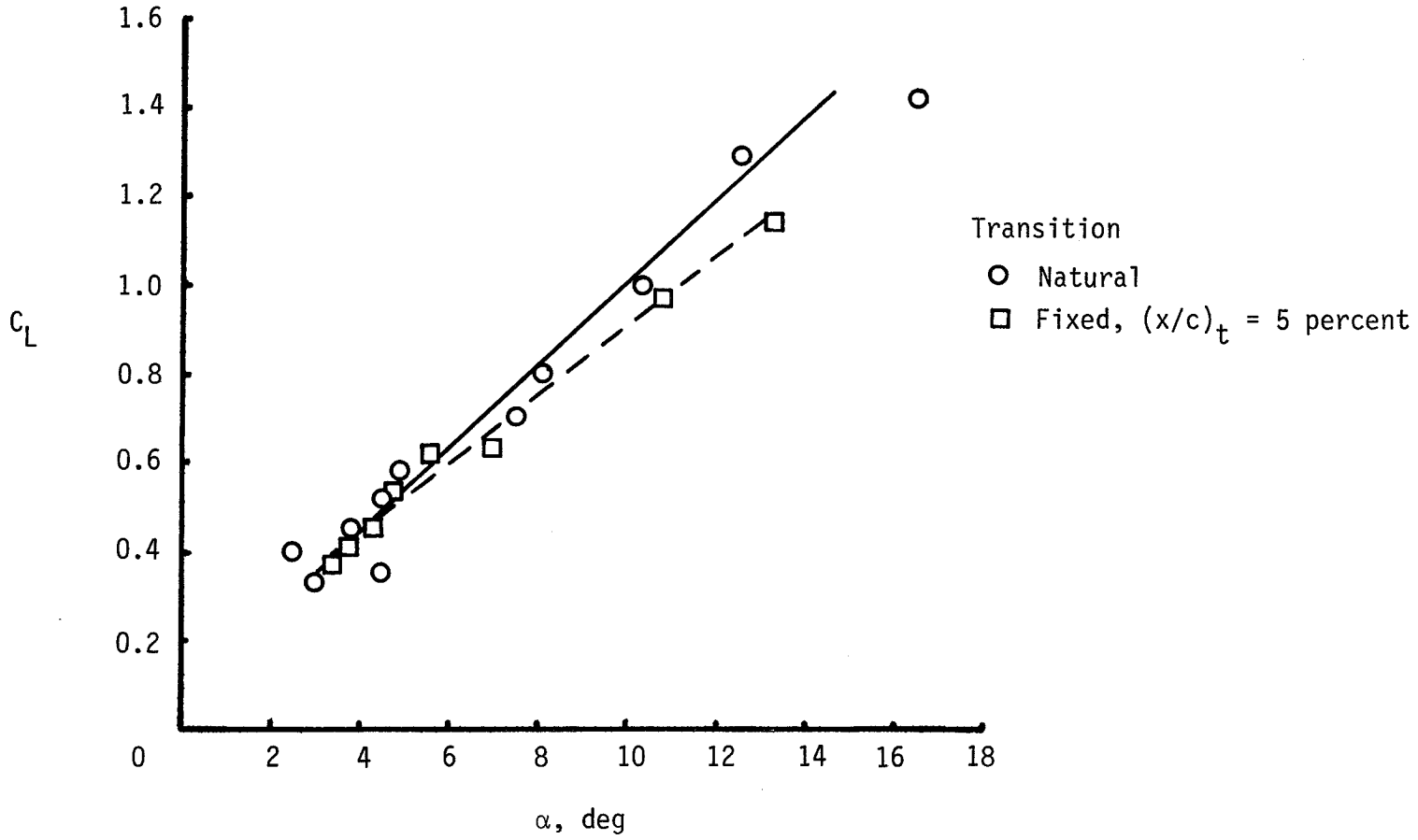

Figure 30.- Comparison of fixed- versus free-transition lift-curve slopes for Long-EZ airplane.

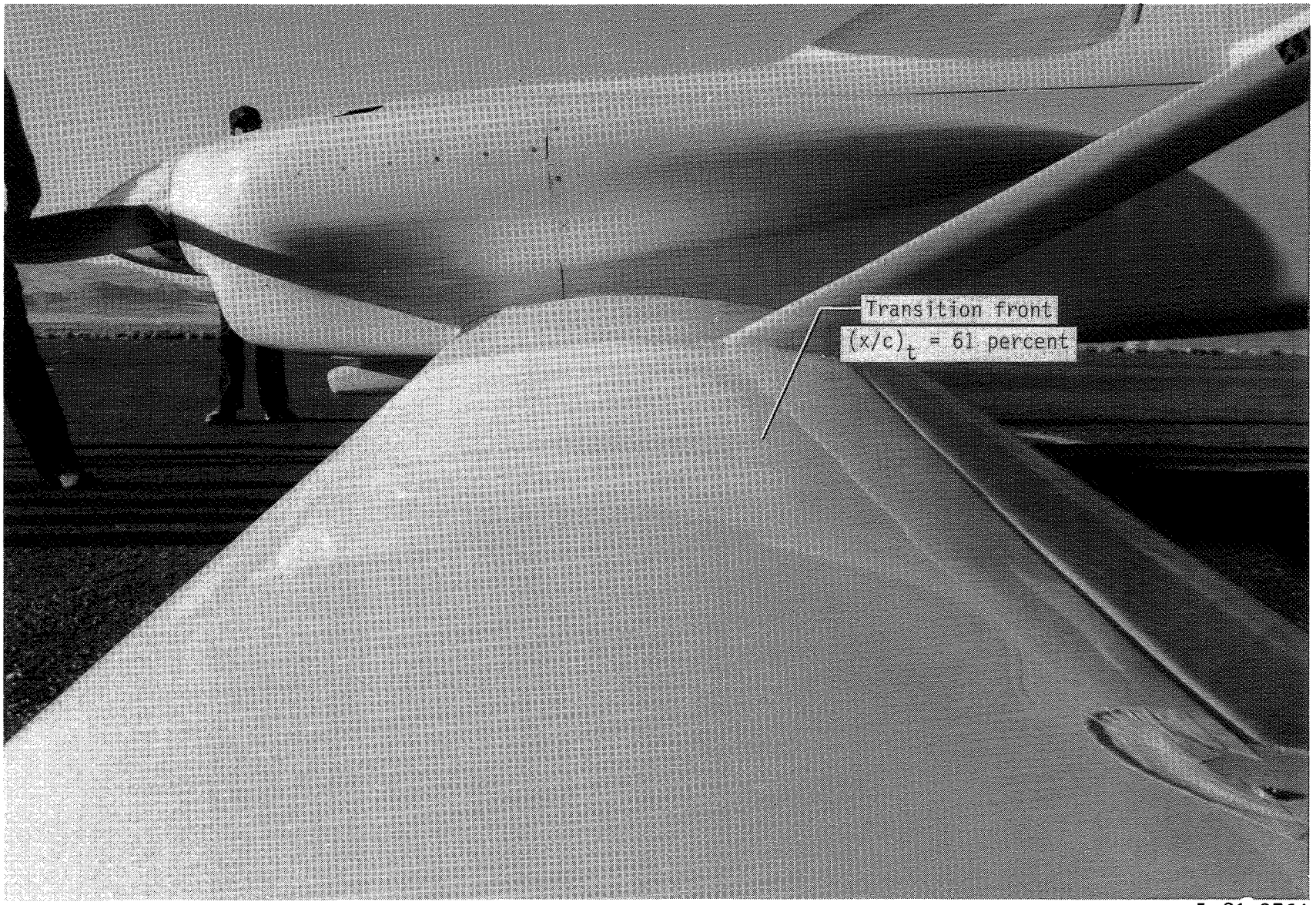

L-81-9764

(a) Lower (forward) wing.

Figure 31.- Transition on Biplane Racer. $R = 1.38 \times 10^6$ ft^{-1}; $C_L = 0.13$.

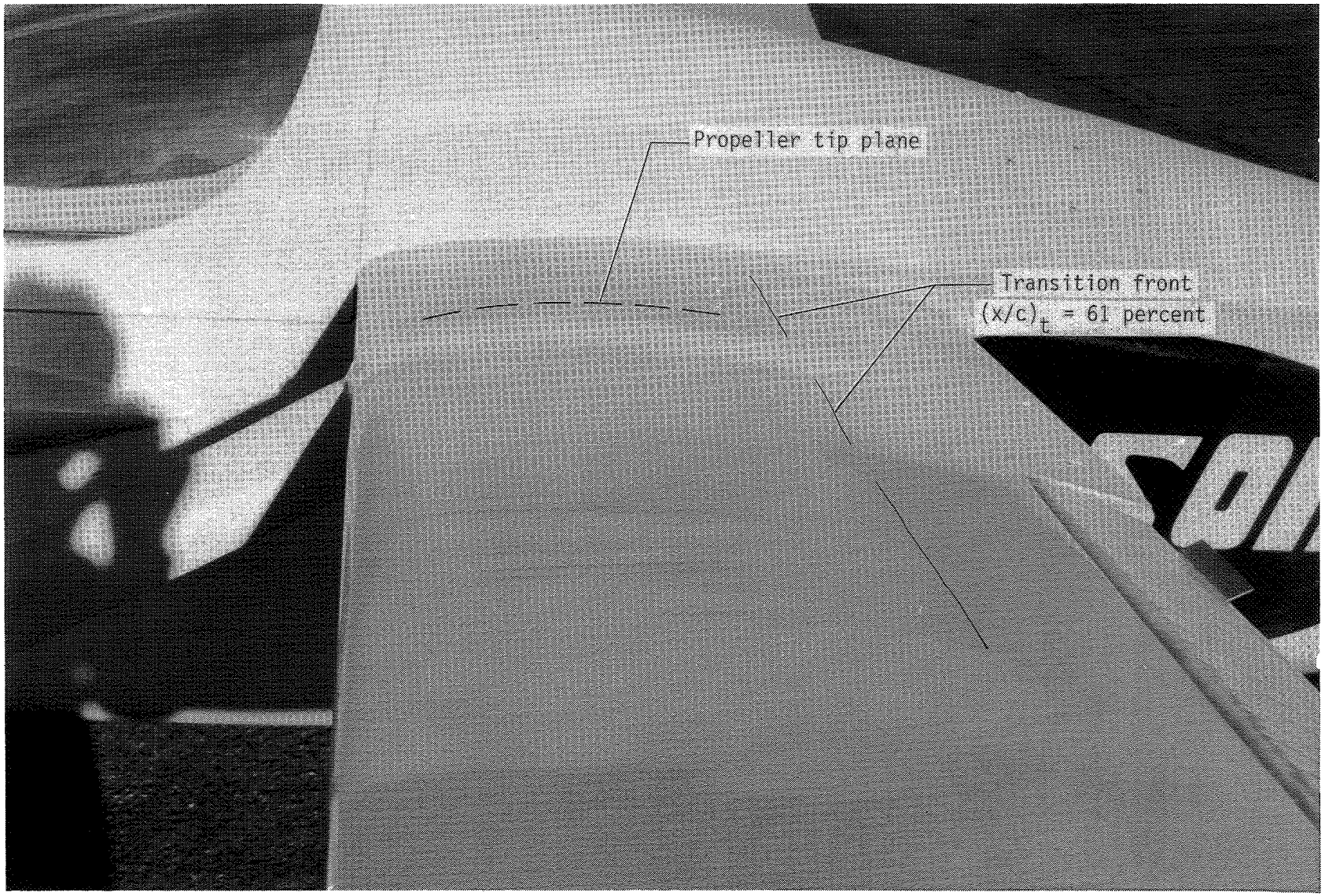

L-81-9766

(b) Upper (aft) wing.

Figure 31.- Concluded.

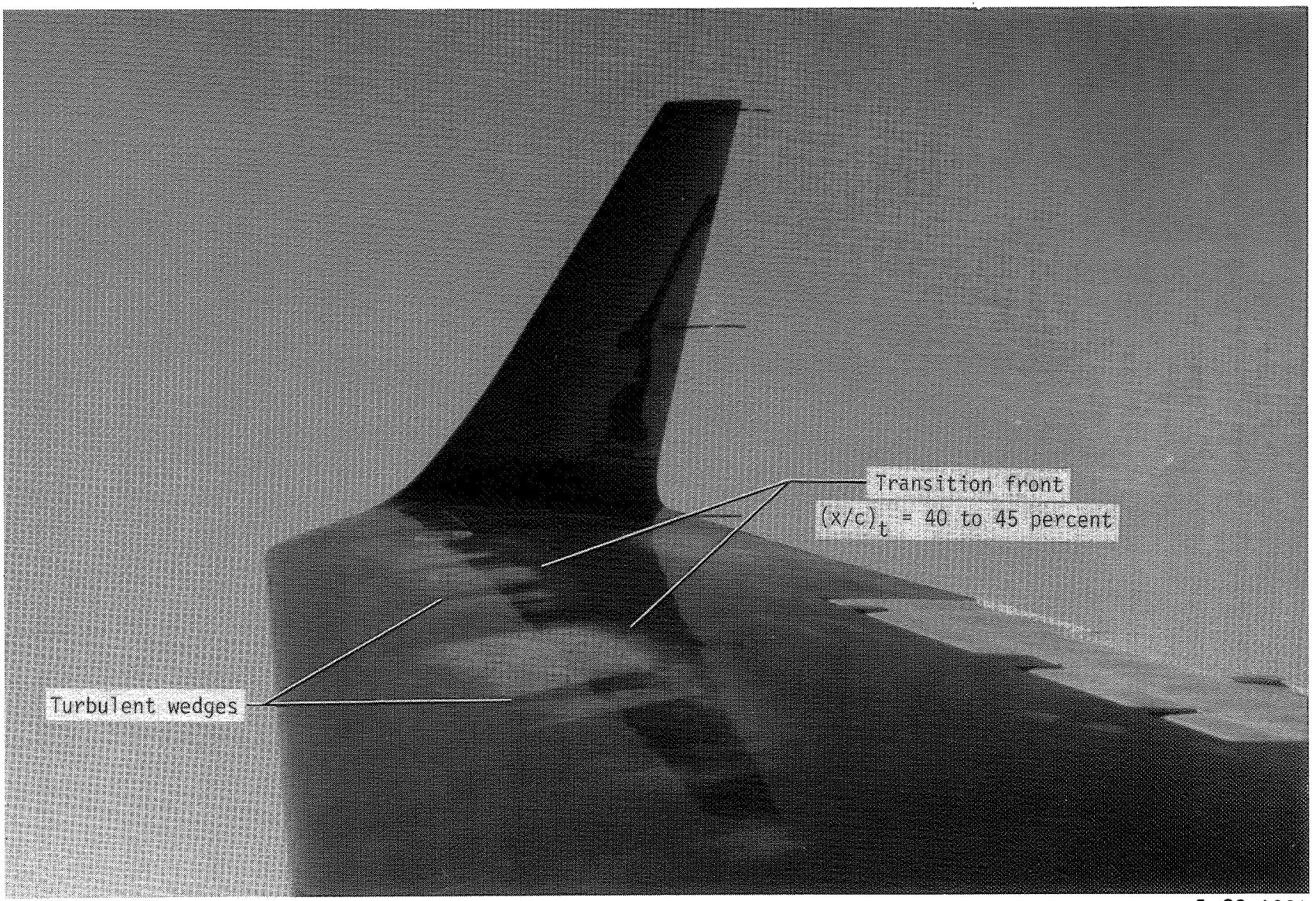

(a) Wing.

Figure 32.- Transition on Gates Learjet Model 28/29 airplane. $R = 3.08 \times 10^6$ ft^{-1}; $C_L = 0.12$; $M = 0.7$; $h_d = 16\ 500$ ft.

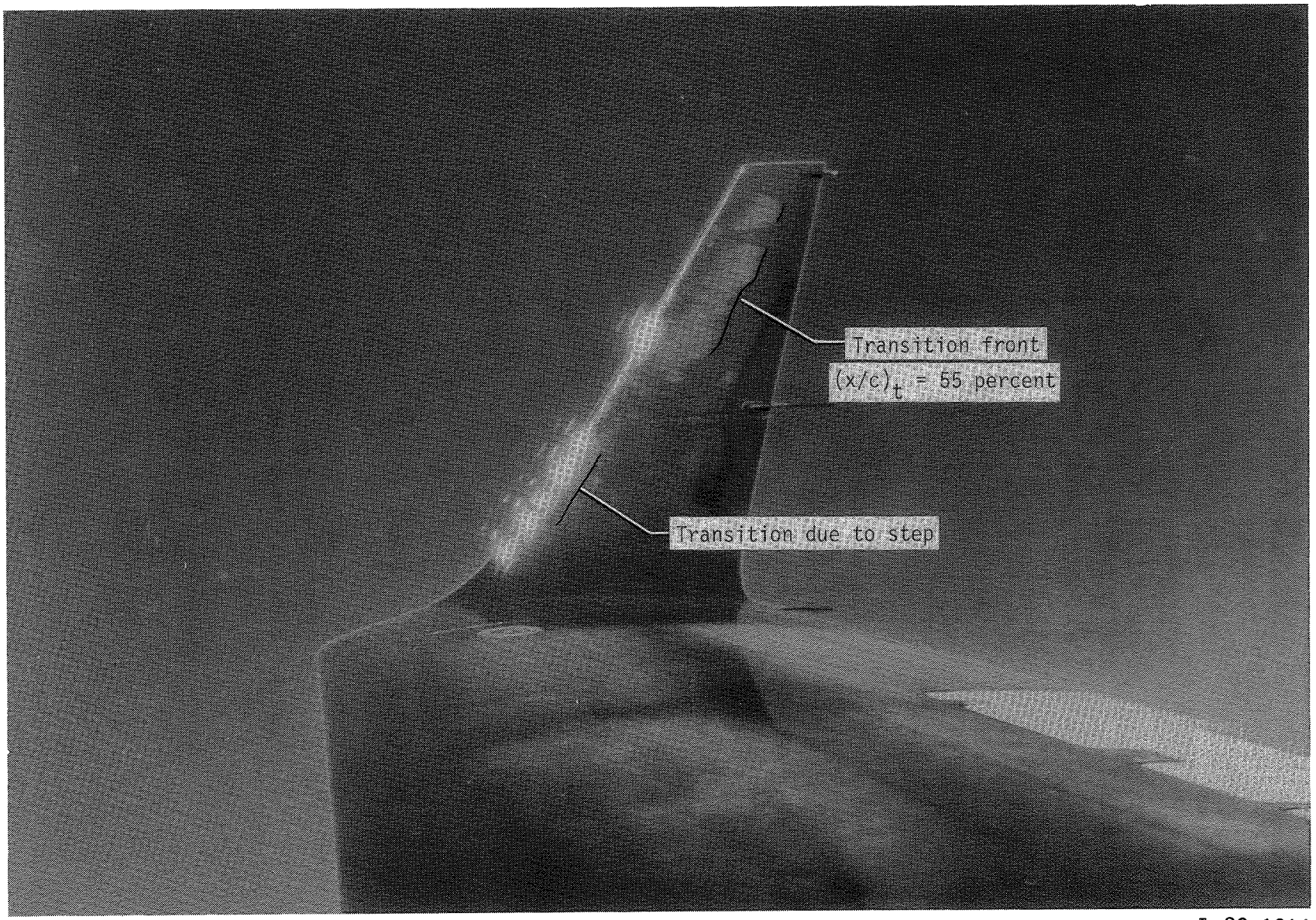

L-82-1214

(b) Winglet.

Figure 32.- Concluded.

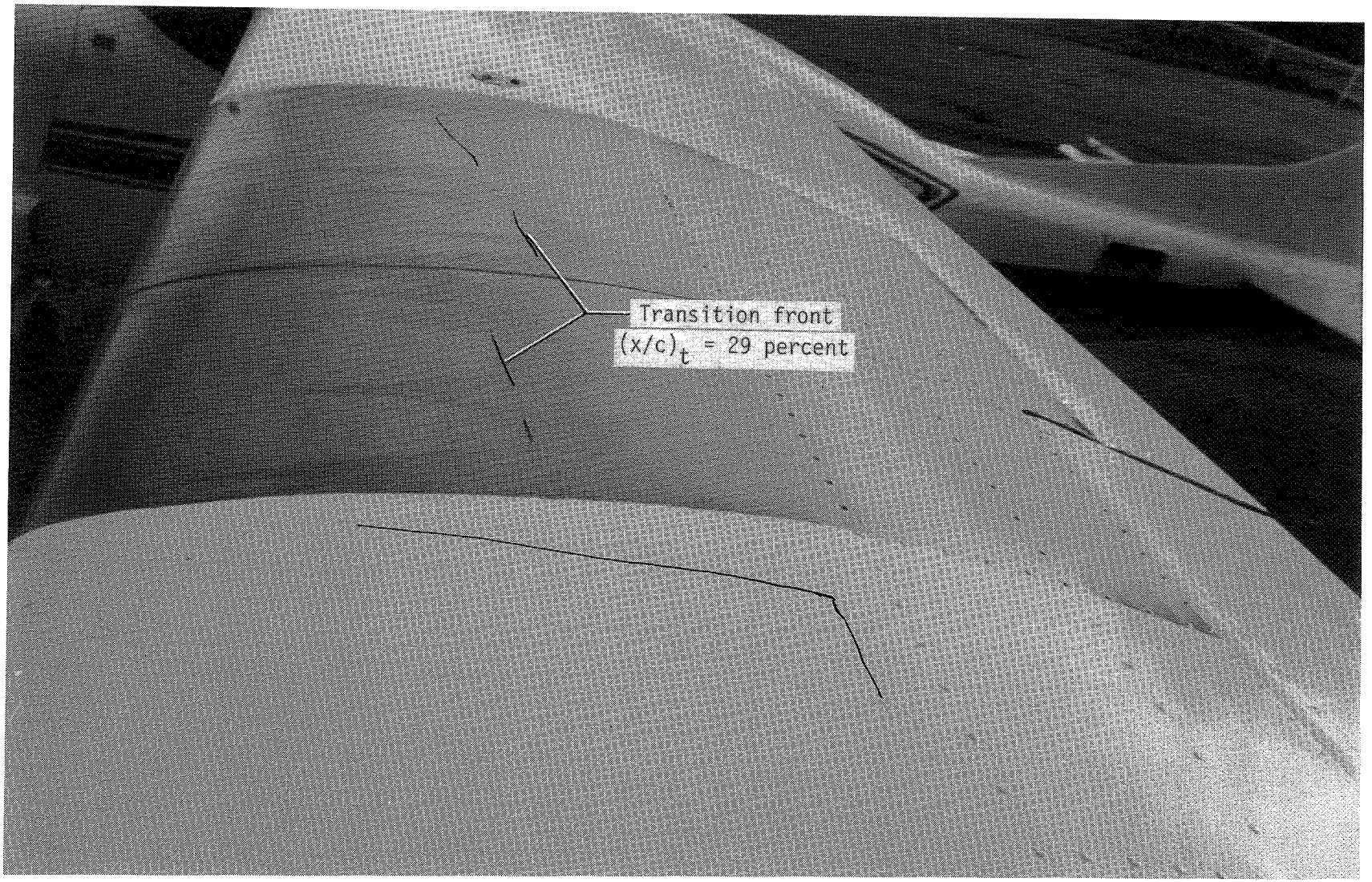

L-82-1198

(a) Wing upper surface.

Figure 33.- Transition on Cessna P-210 Centurion. $R = 1.34 \times 10^6$ to 1.48×10^6 ft^{-1}; $C_L = 0.26$ to 0.32.

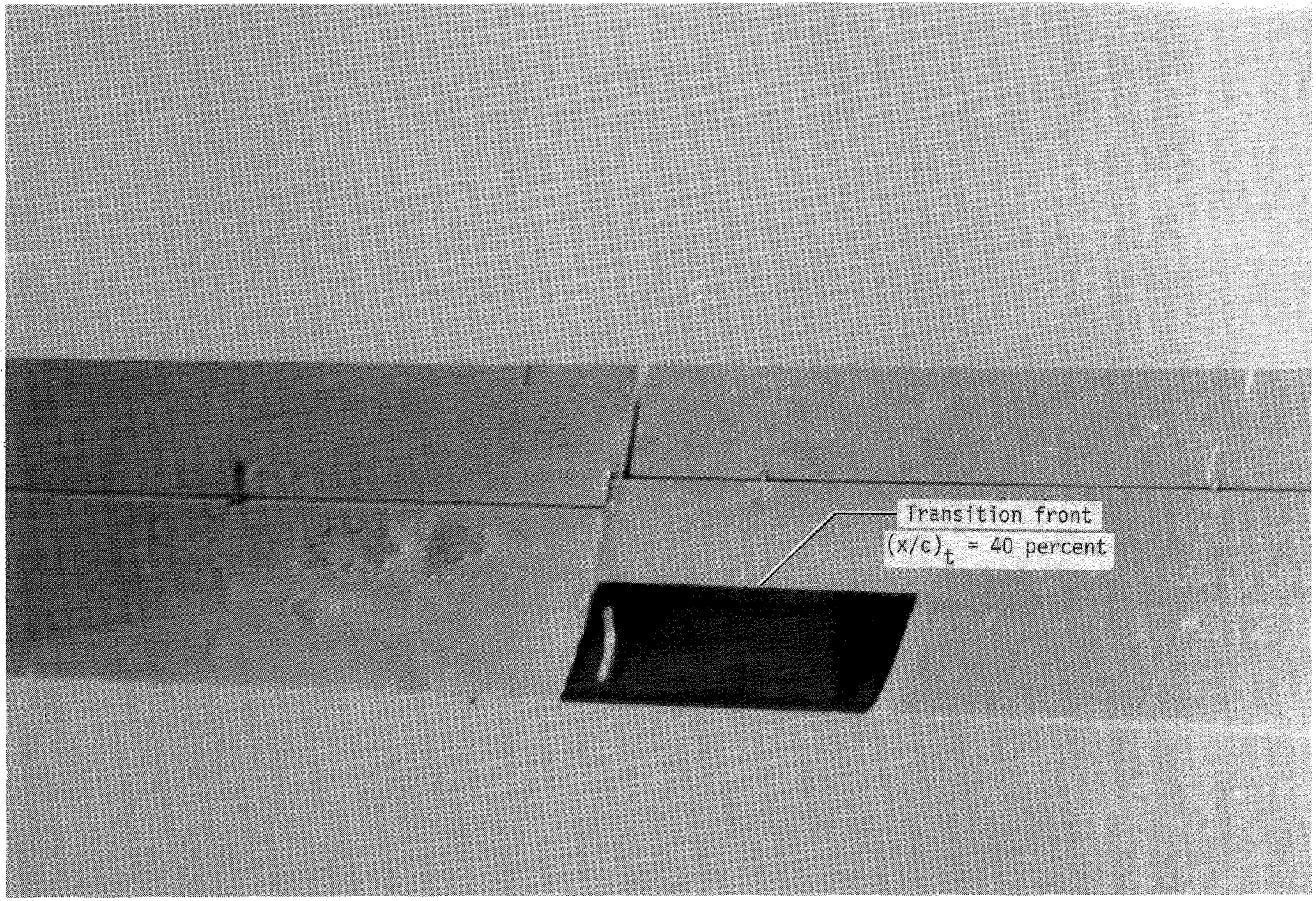

L-82-1217

(b) Wing lower surface.

Figure 33.- Continued.

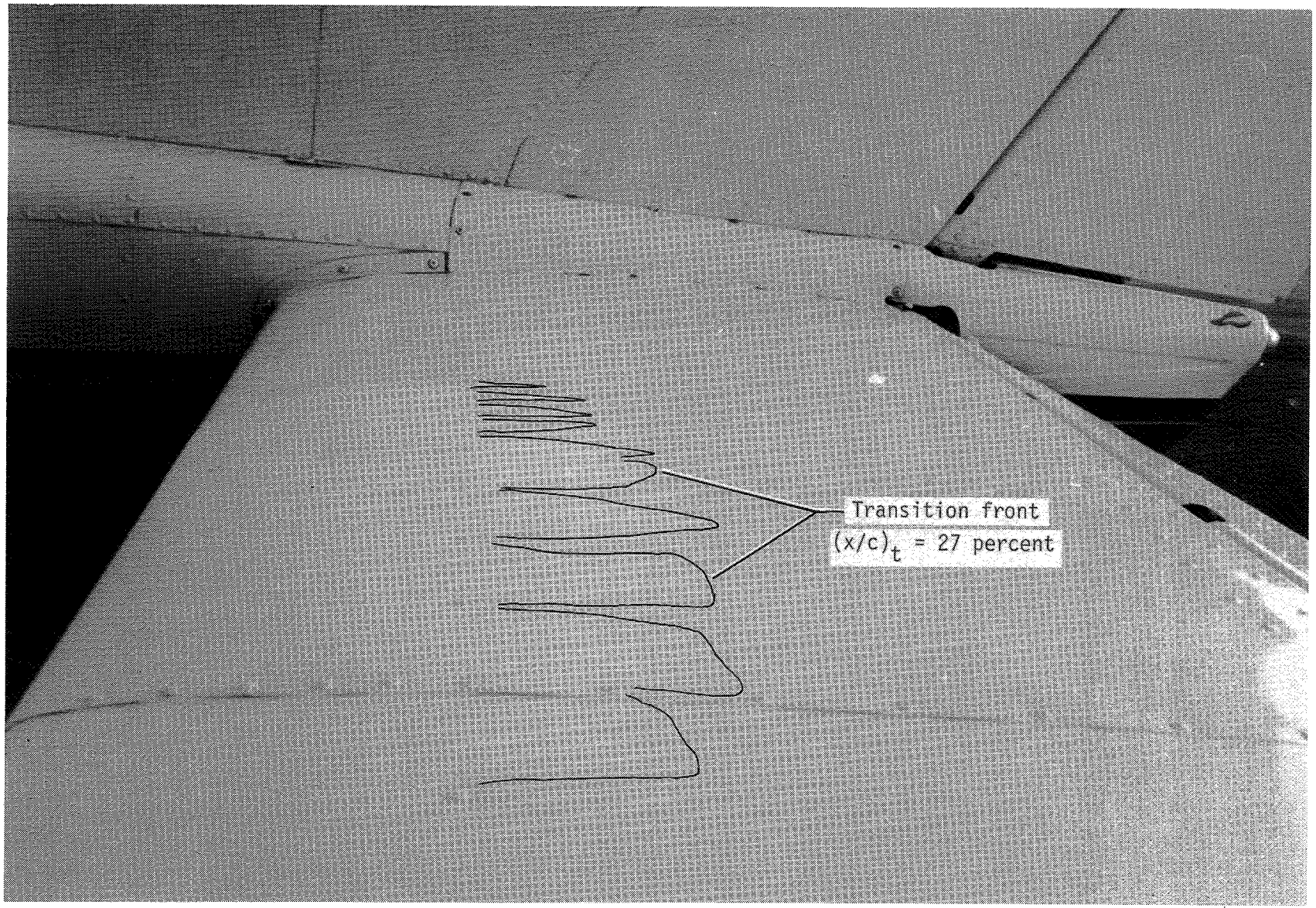

L-82-1199

(c) Horizontal stabilizer, pressure side.

Figure 33.- Continued.

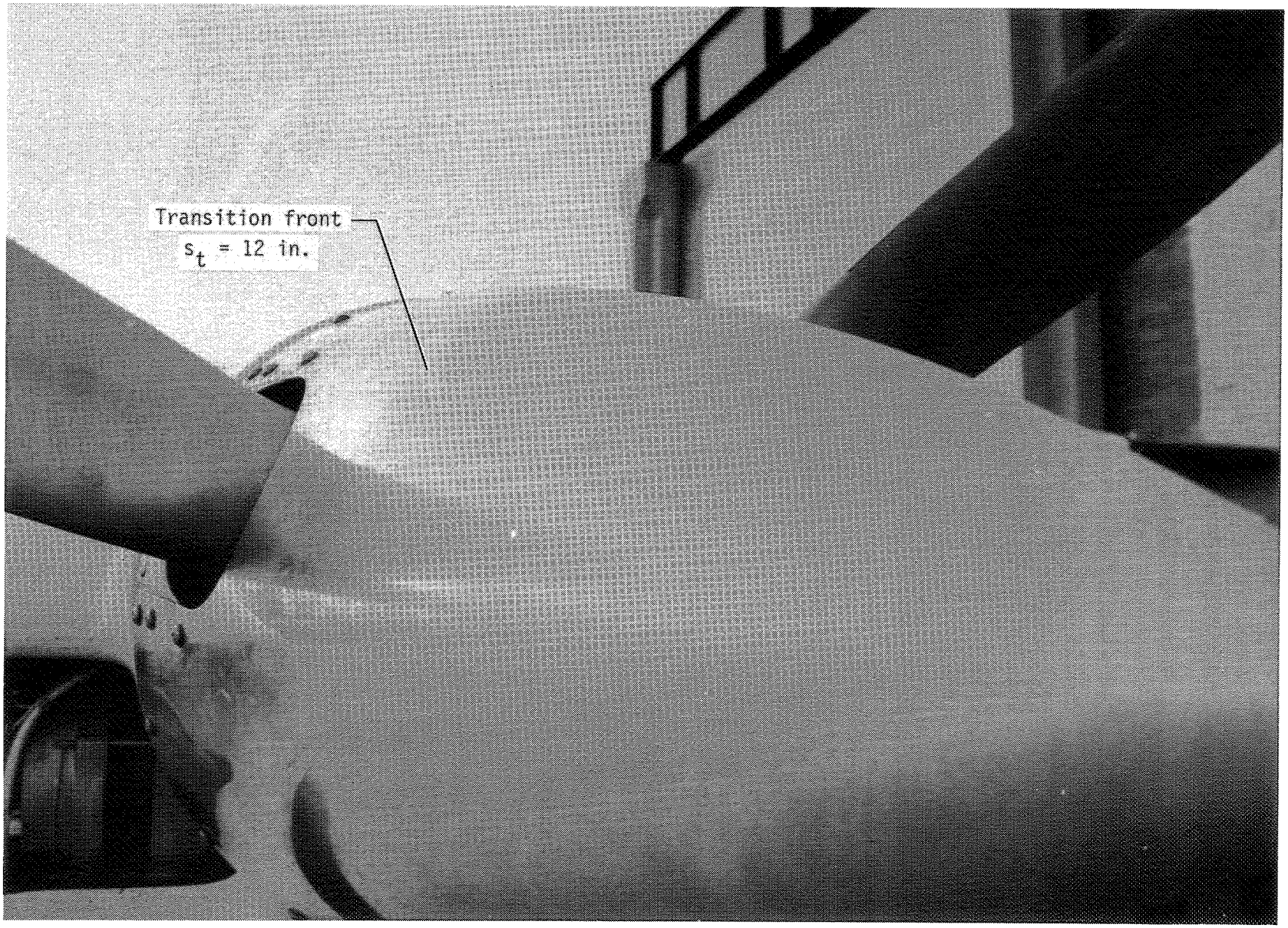

L-82-1207

(d) Propeller spinner.

Figure 33.- Concluded.

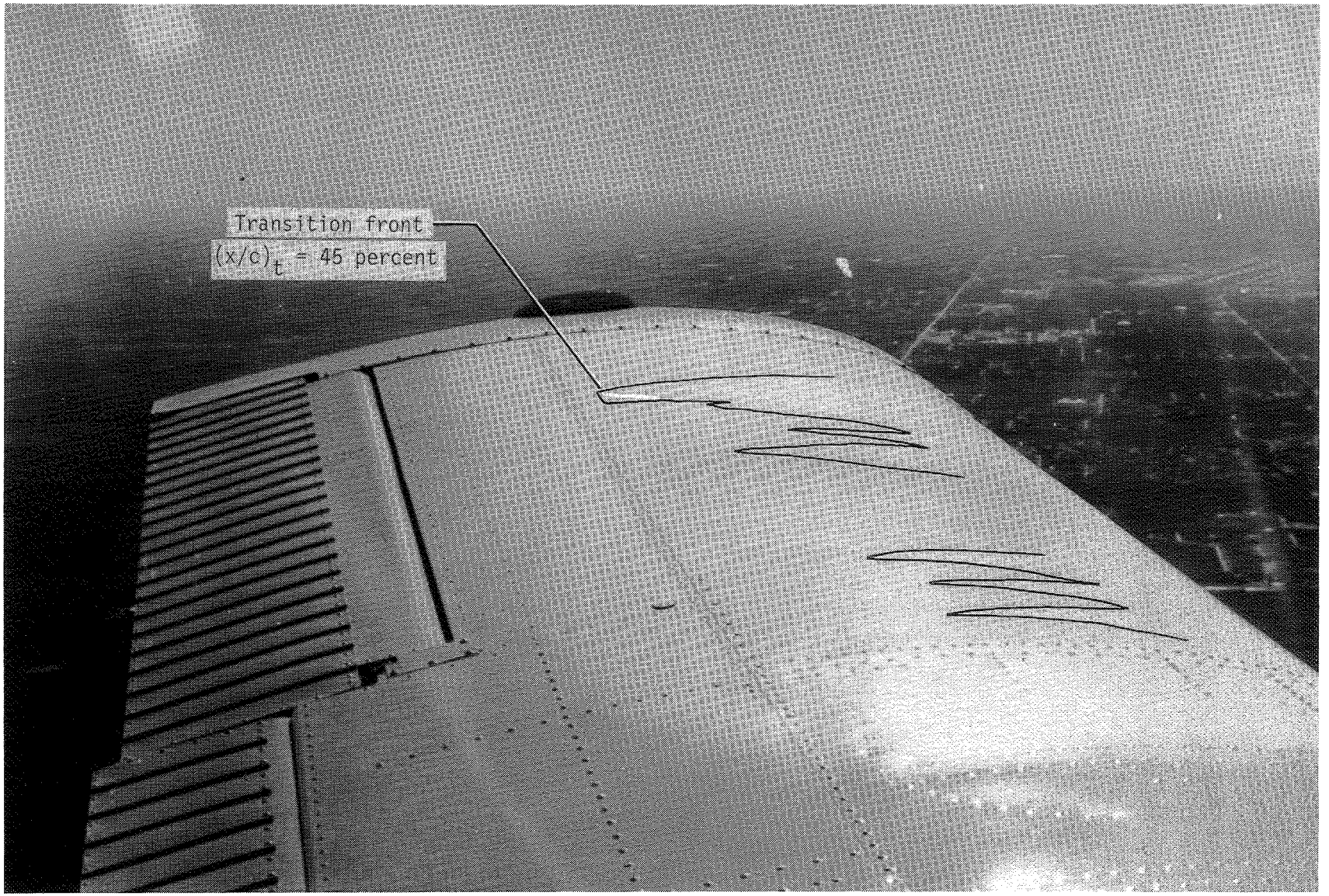

L-82-1196

(a) Wing upper surface.

Figure 34.- Transition on Beech 24R Sierra. $R = 1.38 \times 10^6$ ft^{-1}; $C_L = 0.30$.

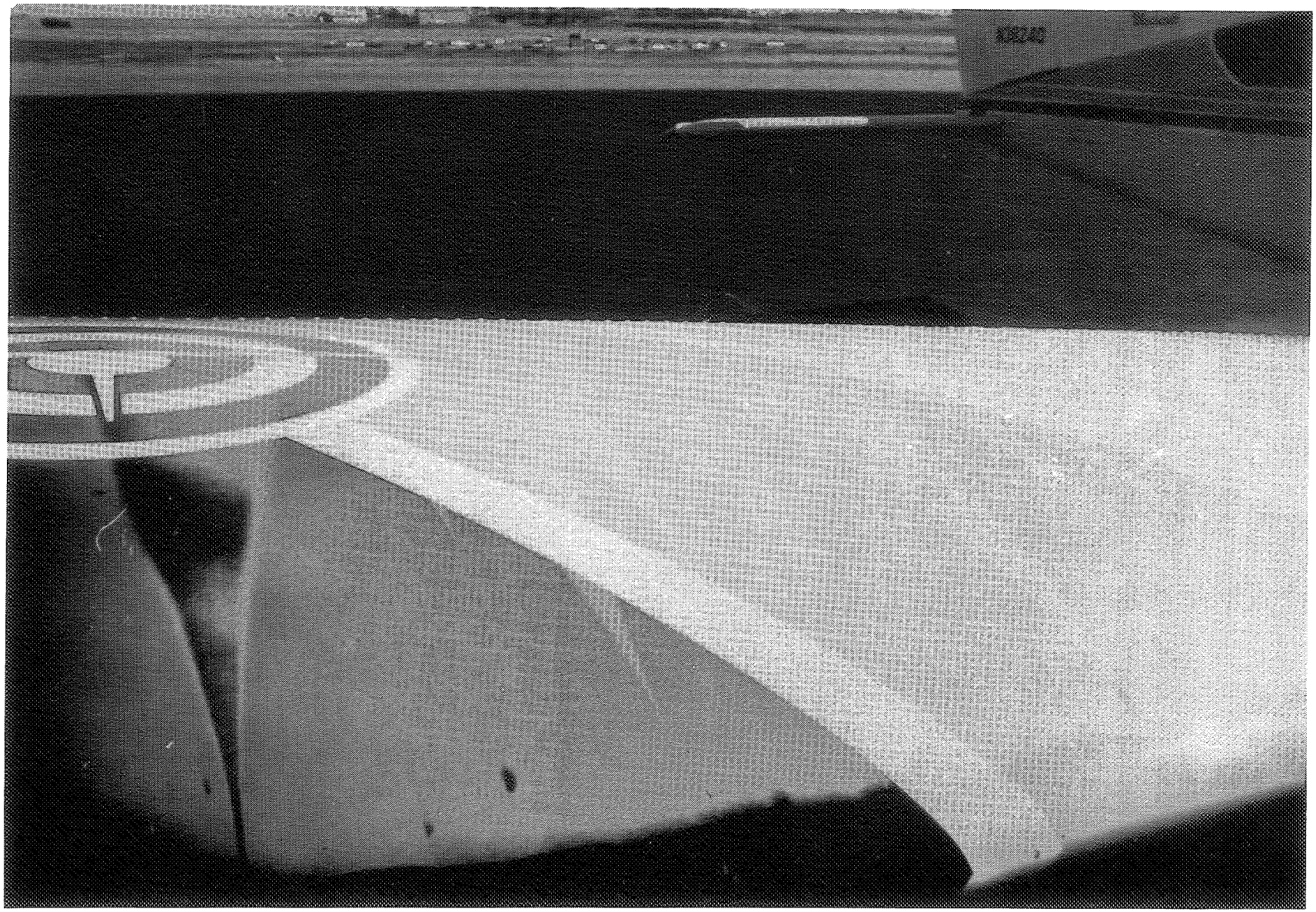

L-82-1215

(b) Turbulent wedges on wing upper surface.

Figure 34.- Continued.

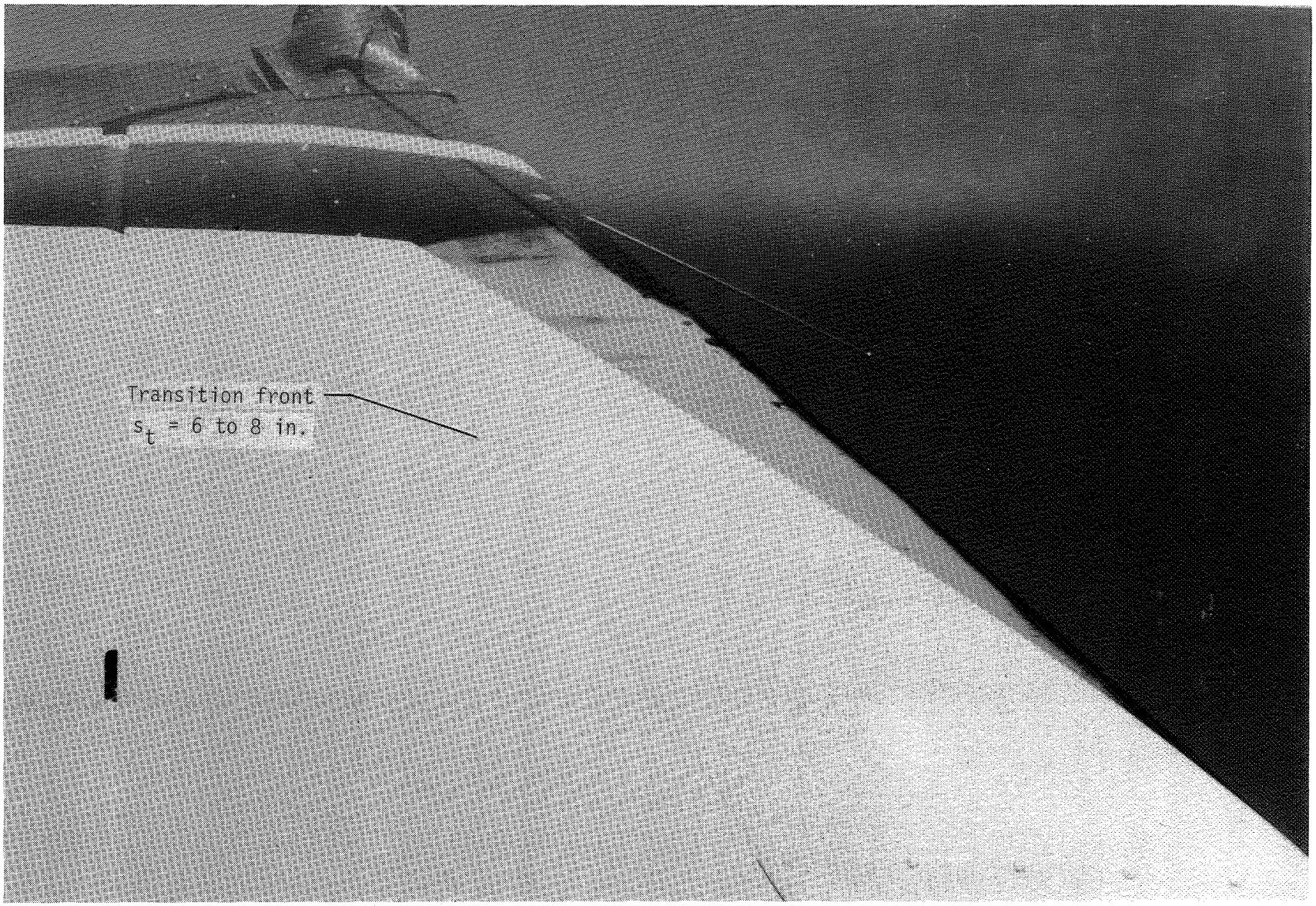

L-82-1212

(c) Vertical stabilizer.

Figure 34.- Continued.

L-82-1197

(d) Propeller, suction side.

Figure 34.- Continued.

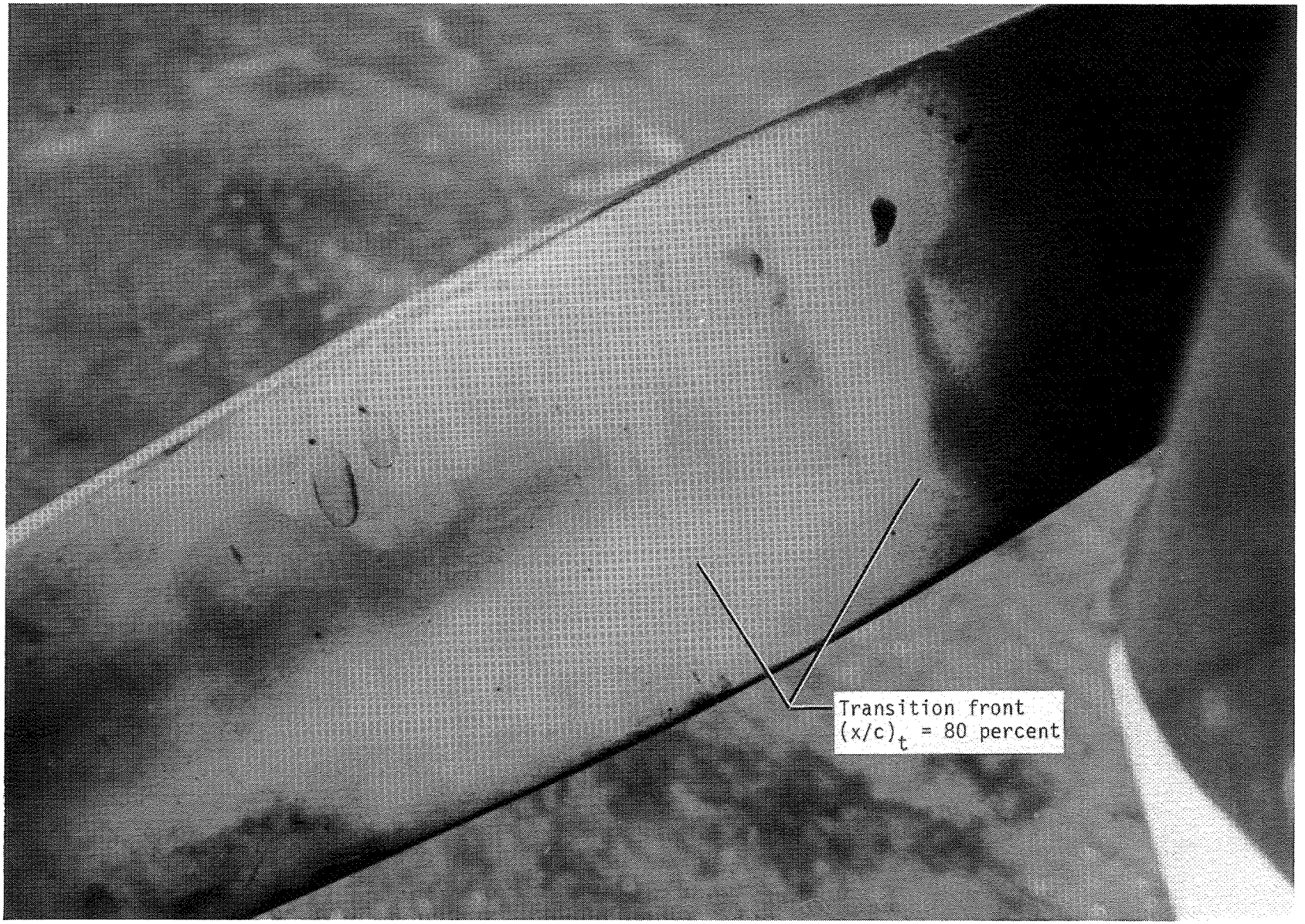

L-82-1203

(e) Propeller, pressure side.

Figure 34.- Concluded.

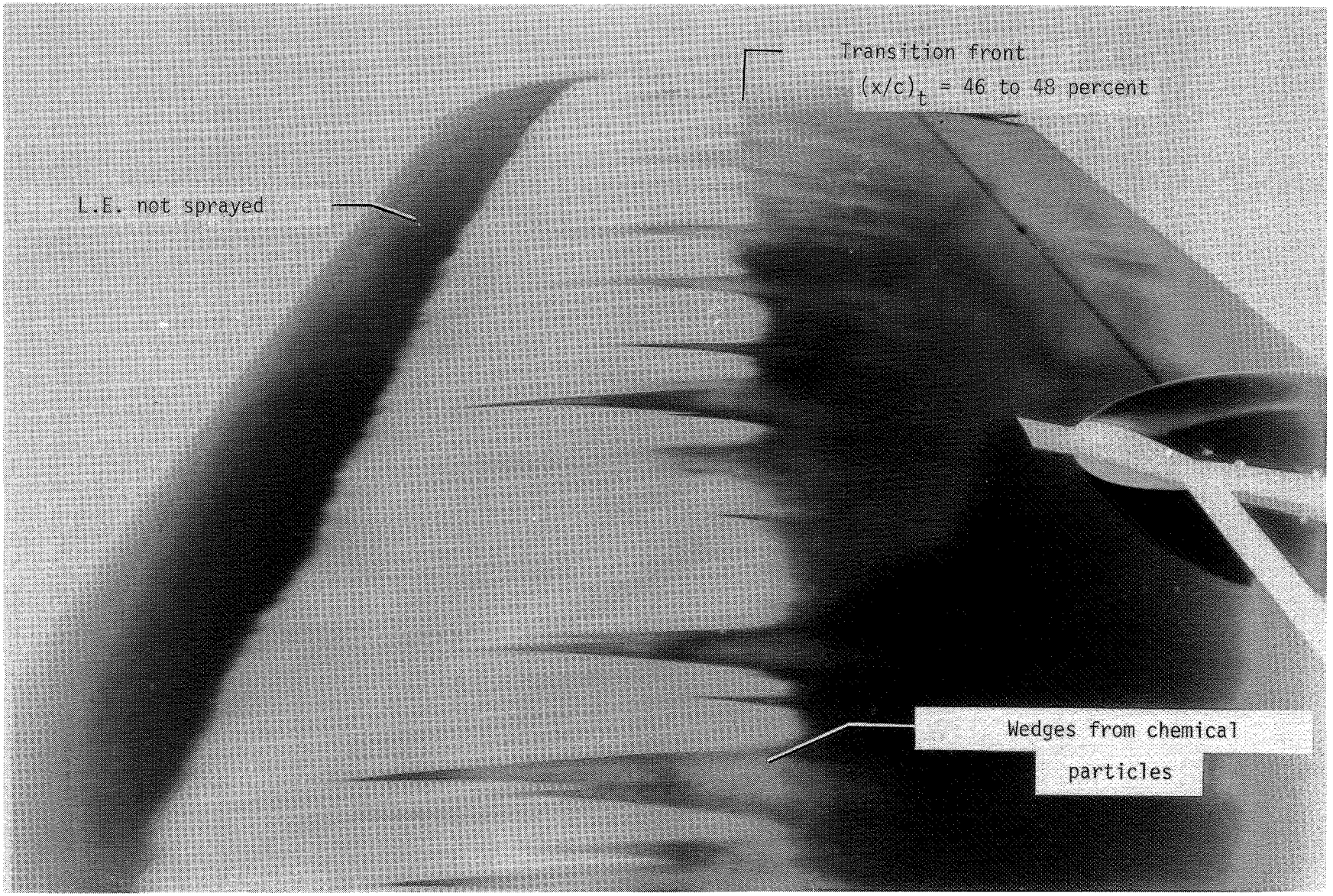

(a) Wing upper surface.

Figure 35.- Transition on Bellanca Skyrocket II. $R = 1.88 \times 10^6$ ft^{-1}; $C_L = 0.22$.

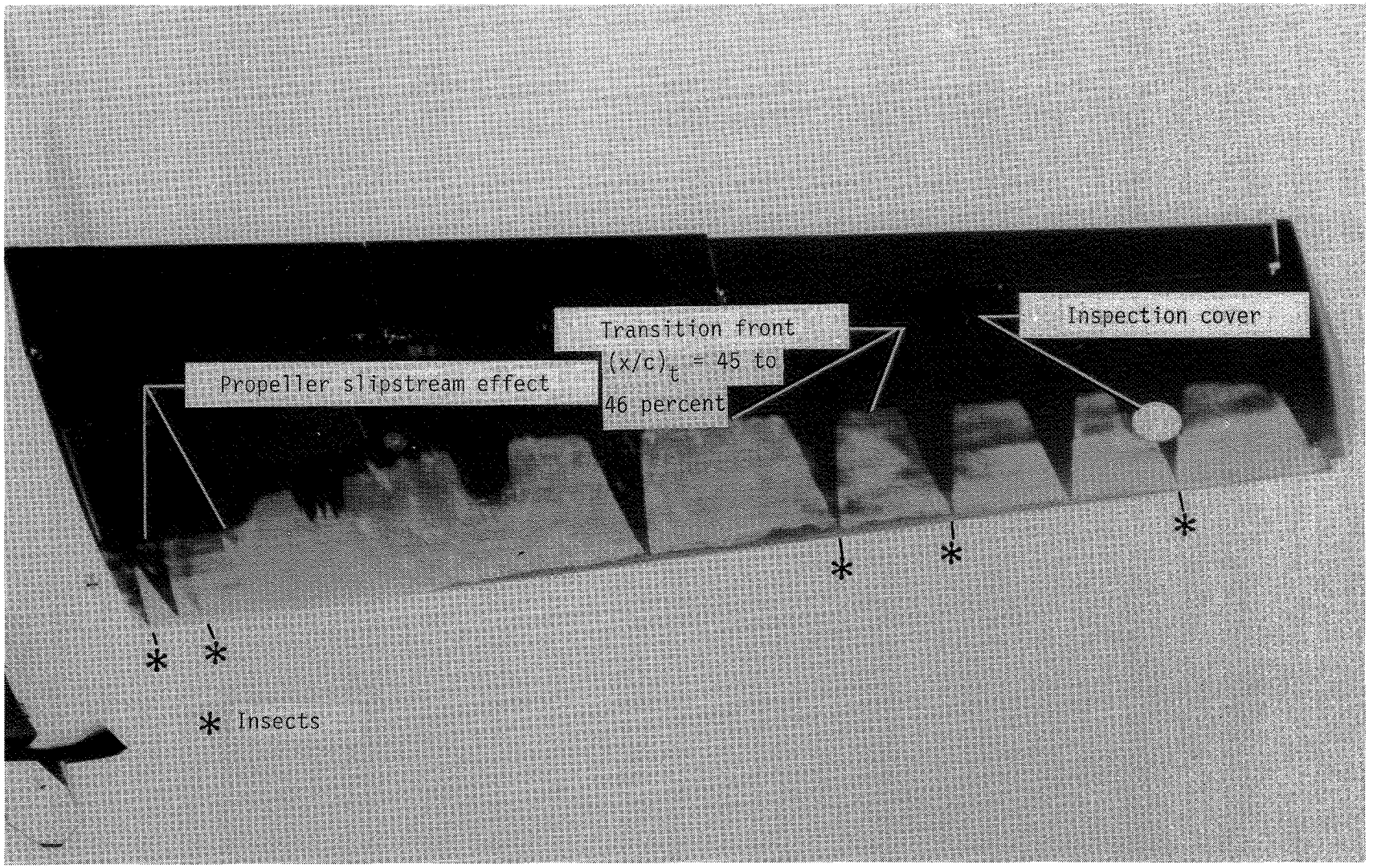

L-84-47

(b) Wing lower surface.

Figure 35.- Continued.

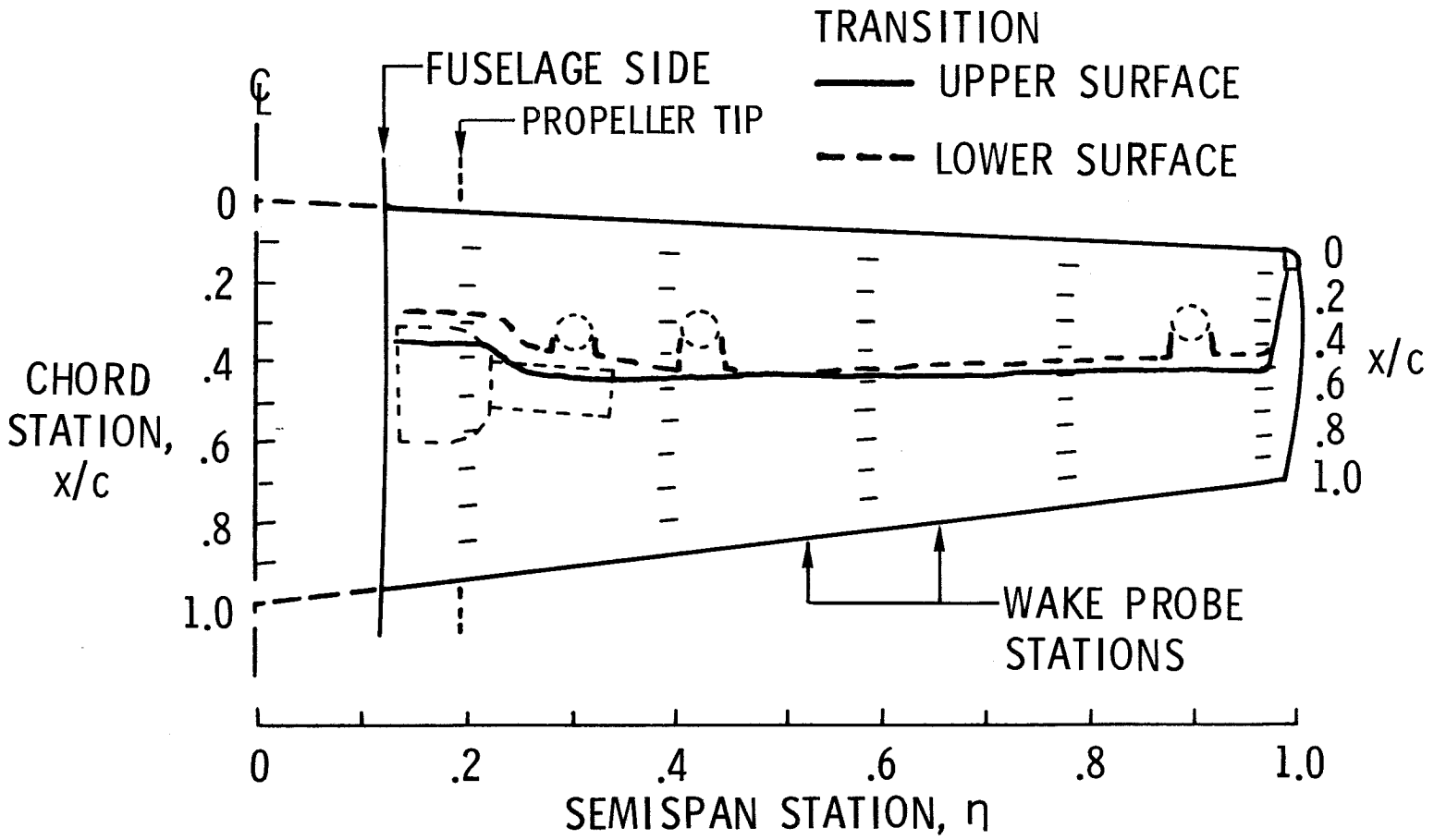

(c) Nondimensional transition locations.

Figure 35.- Concluded.

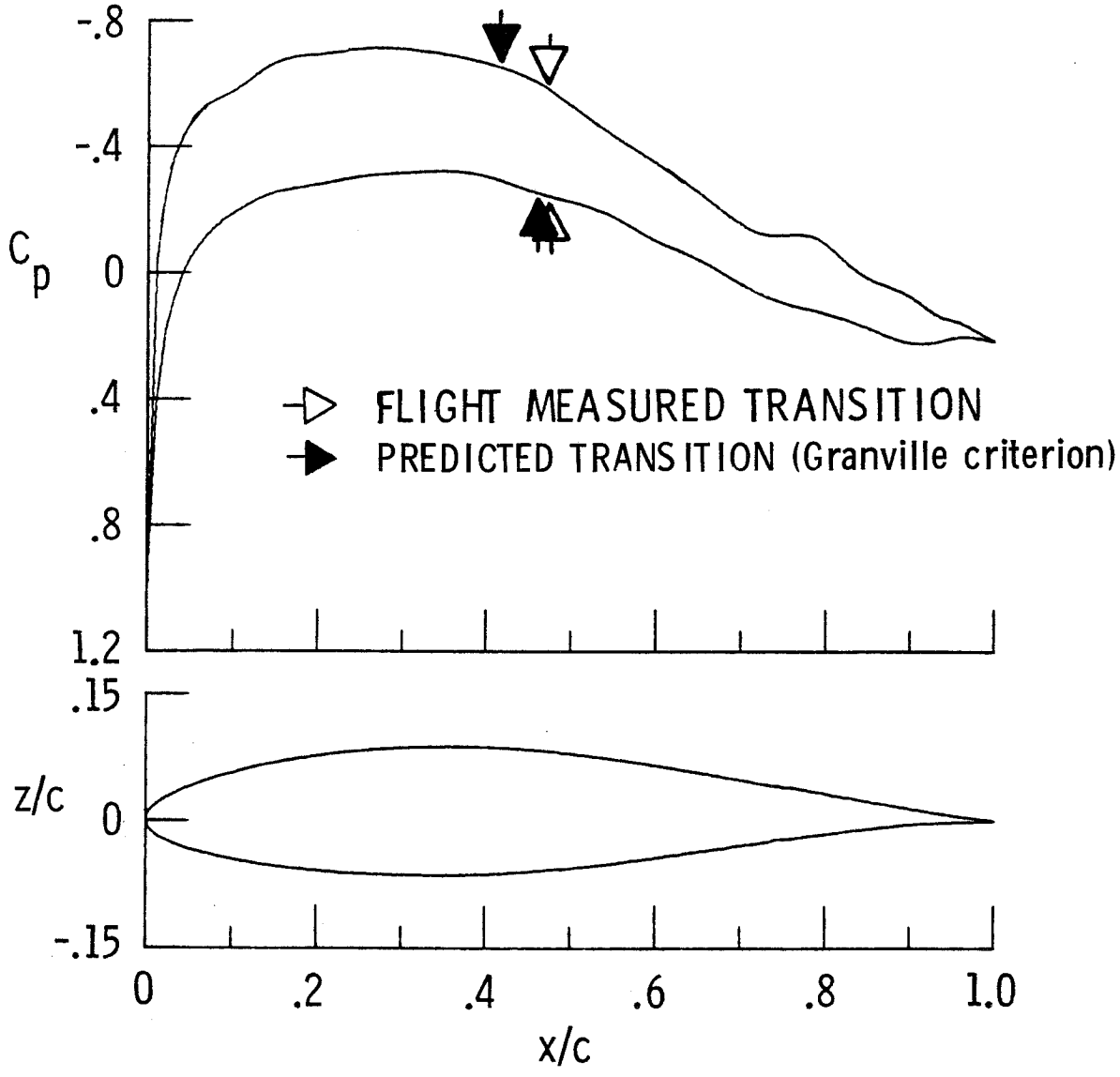

(a) Inboard wake probe station; $R_c = 9.04 \times 10^6$; $C_\ell = 0.288$; $M = 0.31$.

Figure 36.- Comparison of predicted pressure distribution with transition for Bellanca Skyrocket II (right wing).

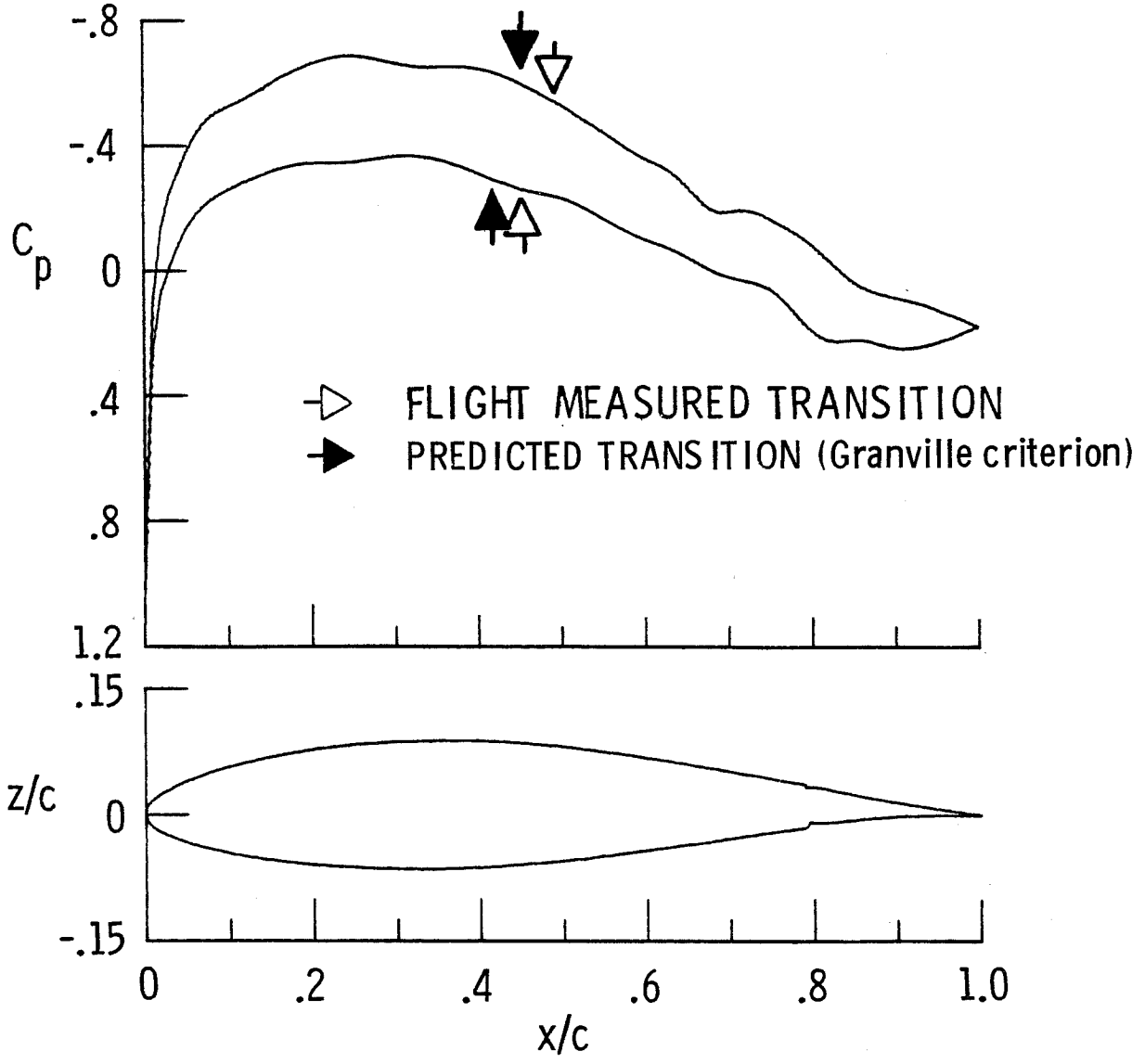

(b) Outboard wake probe station; $R_c = 8.39 \times 10^6$; $C_\ell = 0.254$; $M = 0.31$.

Figure 36.- Concluded.

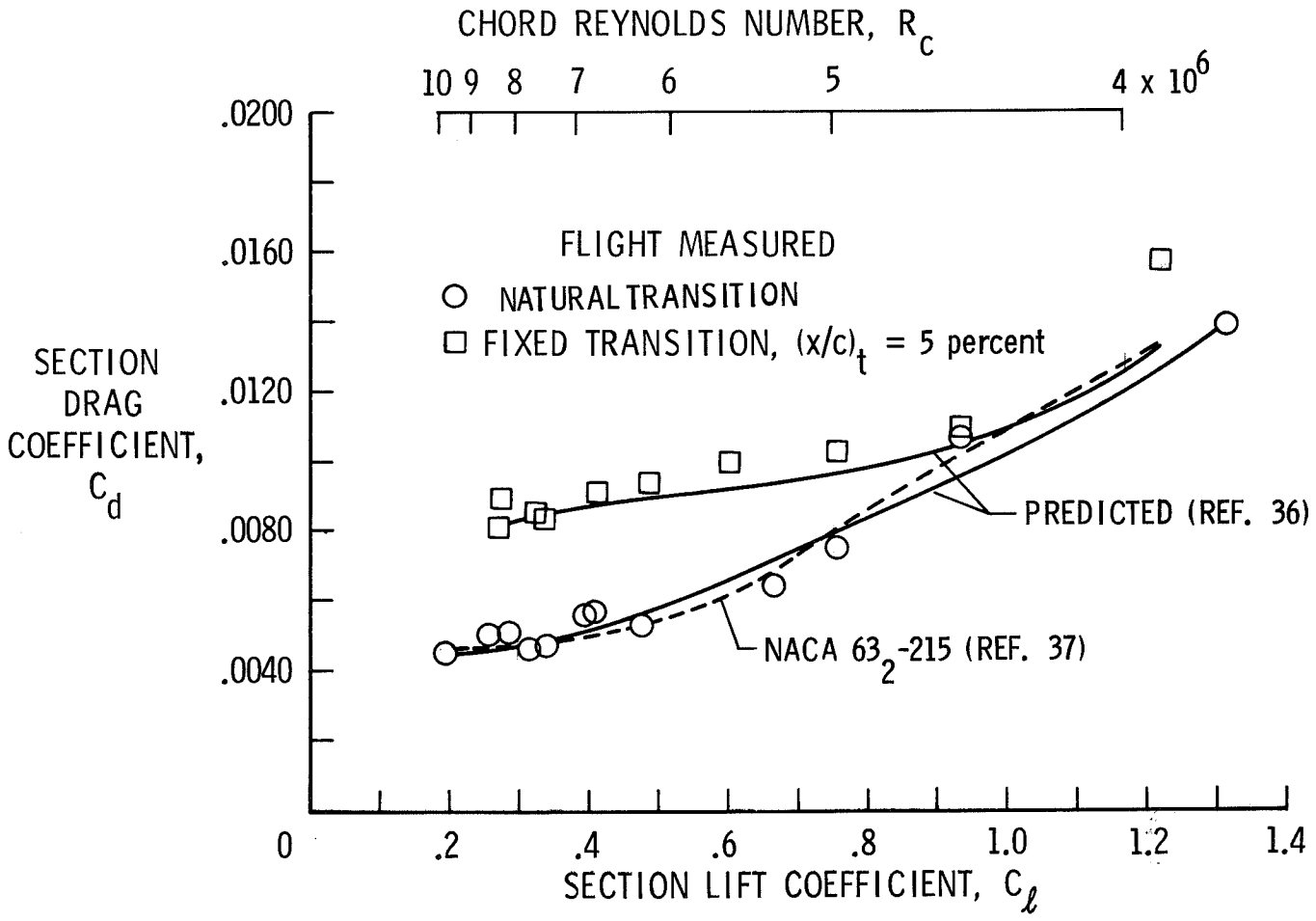

(a) Inboard wake probe station.

Figure 37.- Comparisons of flight-measured, wind-tunnel measured, and predicted section characteristics for Bellanca Skyrocket II airfoil (right wing).

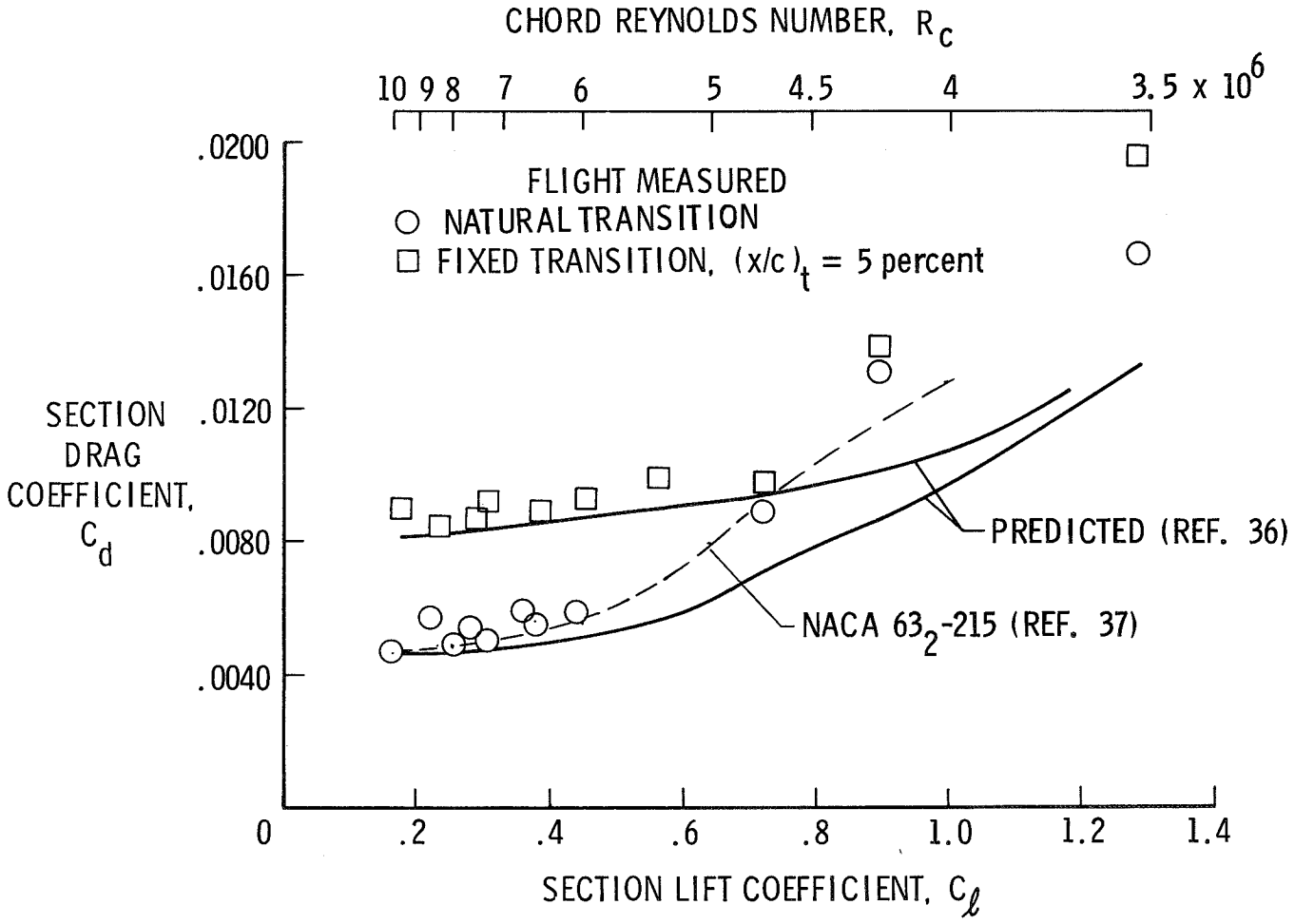

(b) Outboard wake probe station.

Figure 37.- Concluded.

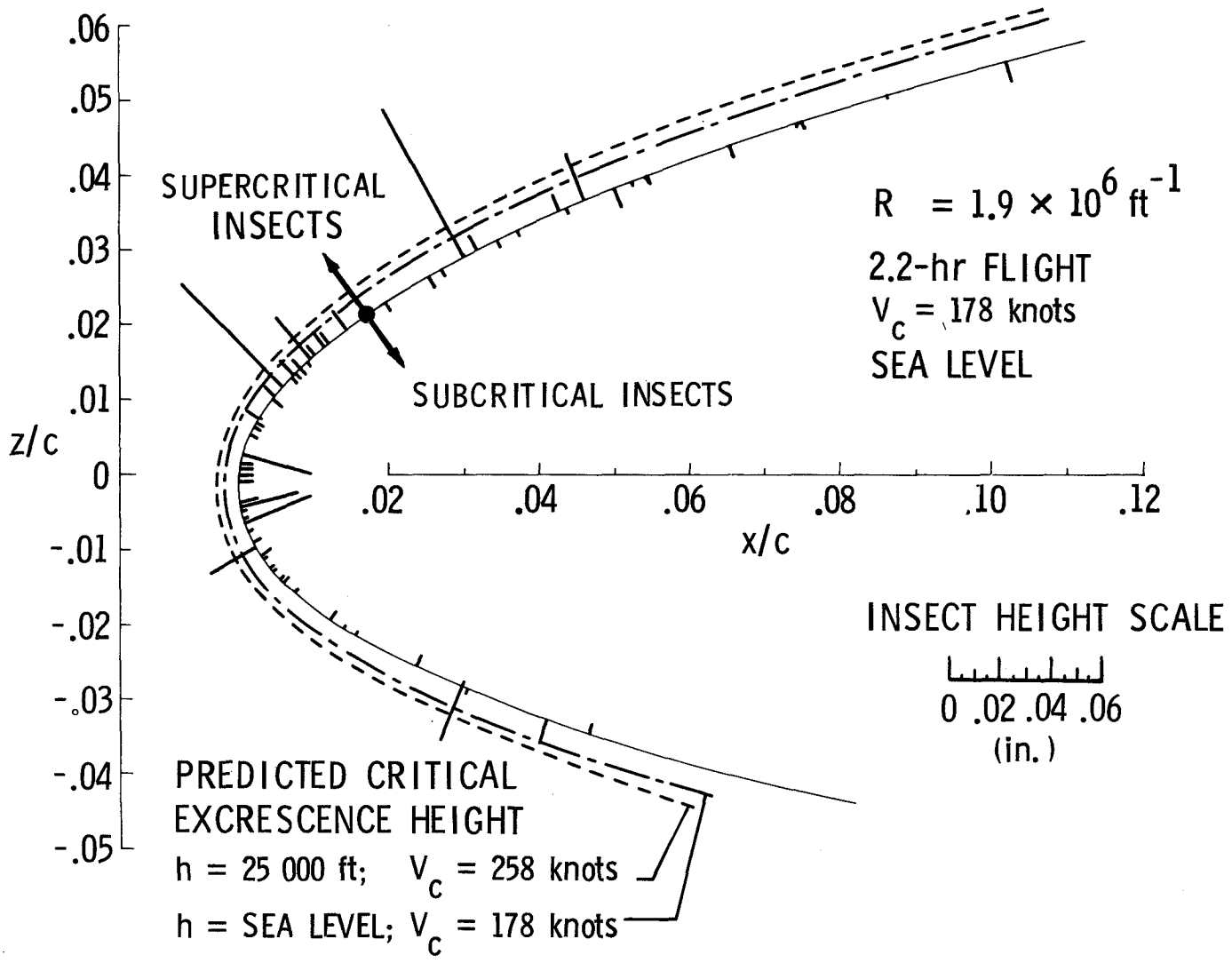

Figure 38.- Insect contamination pattern on Bellanca Skyrocket II NLF wing, accumulated in flight.

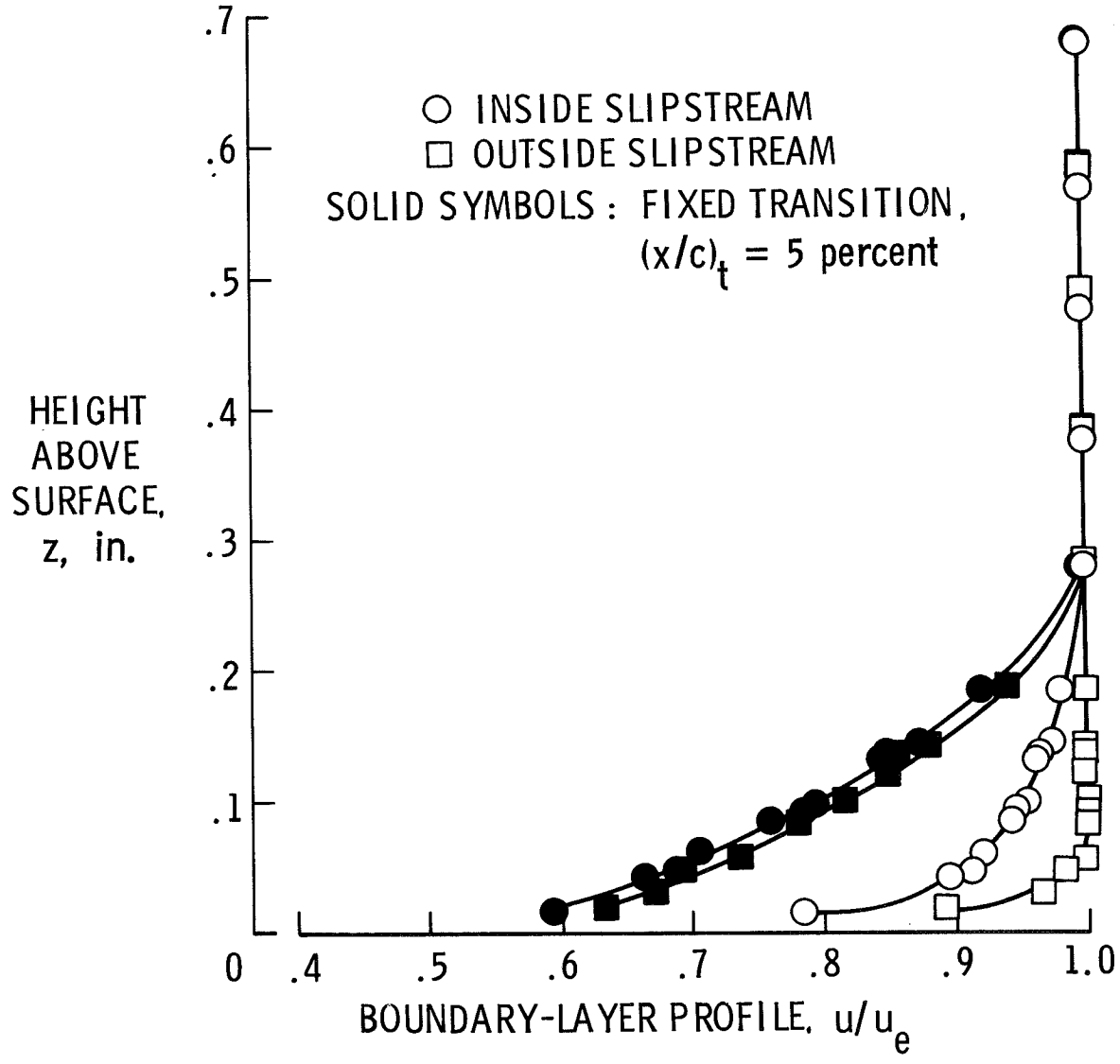

Figure 39.- Effect of propeller slipstream on Bellanca Skyrocket II boundary-layer profiles. s/c = 28.7 percent; n = 1800 rpm; V = 178 knots.

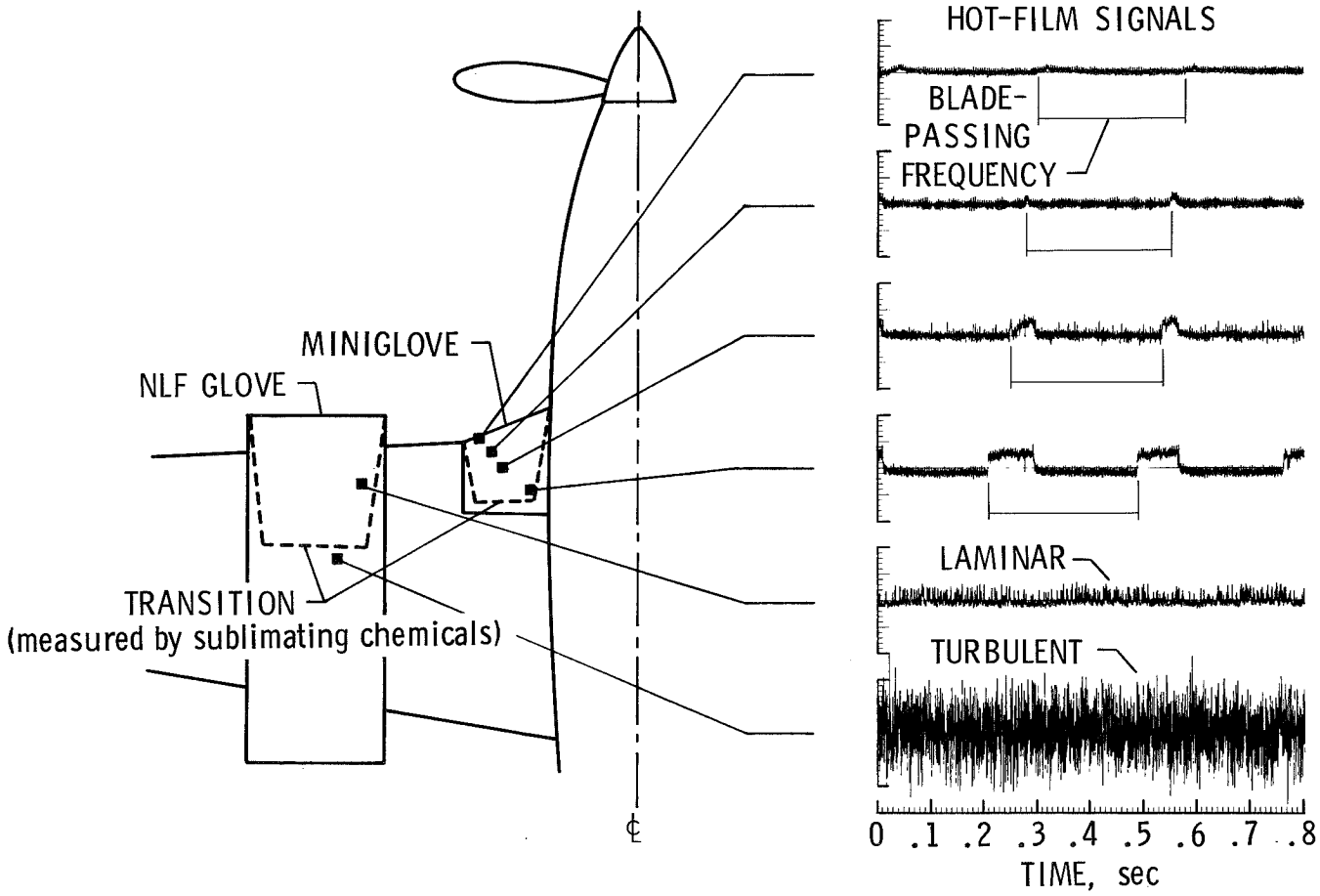

Figure 40.- In-flight, hot-film measured, time-dependent effects of propeller slipstream on laminar boundary layer (T-34C airplane). $R = 1.5 \times 10^6$ ft^{-1}; n = 150 rpm.

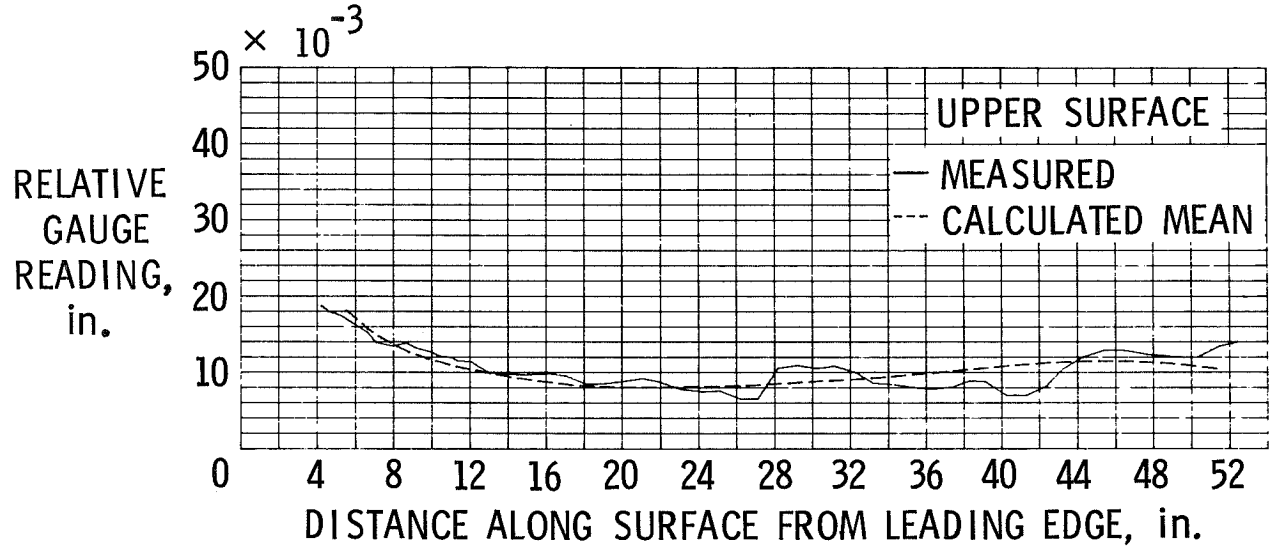

(a) King Cobra (filled and sanded wing, circa 1950).

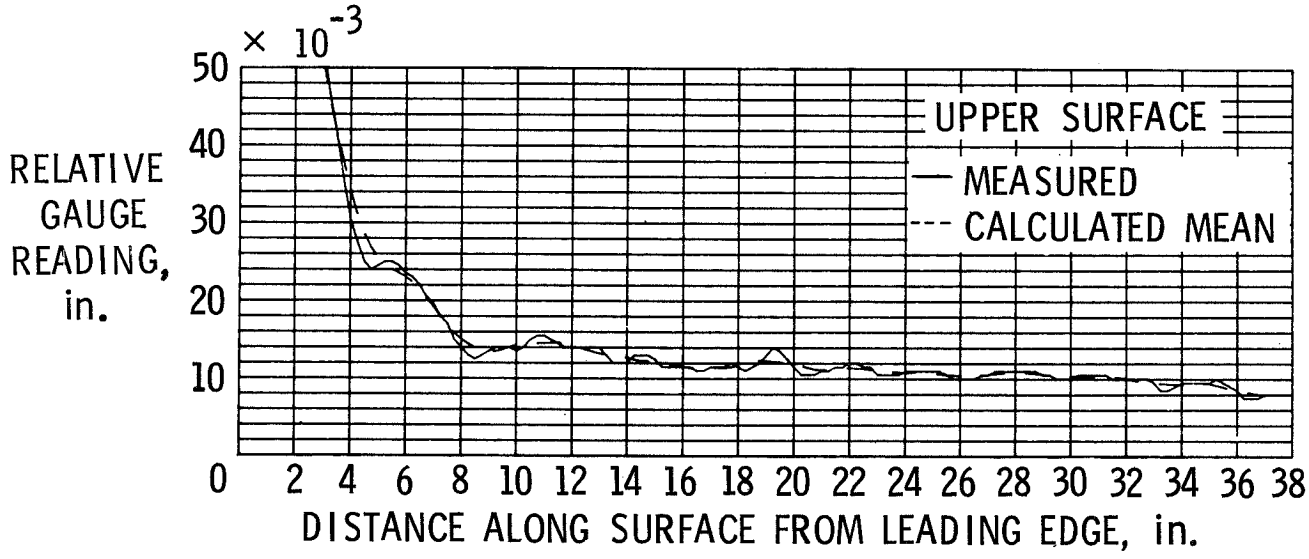

(b) Skyrocket II (as-produced composite wing, circa 1970).

Figure 41.- Indicated surface waviness for Bellanca Skyrocket II and King Cobra.

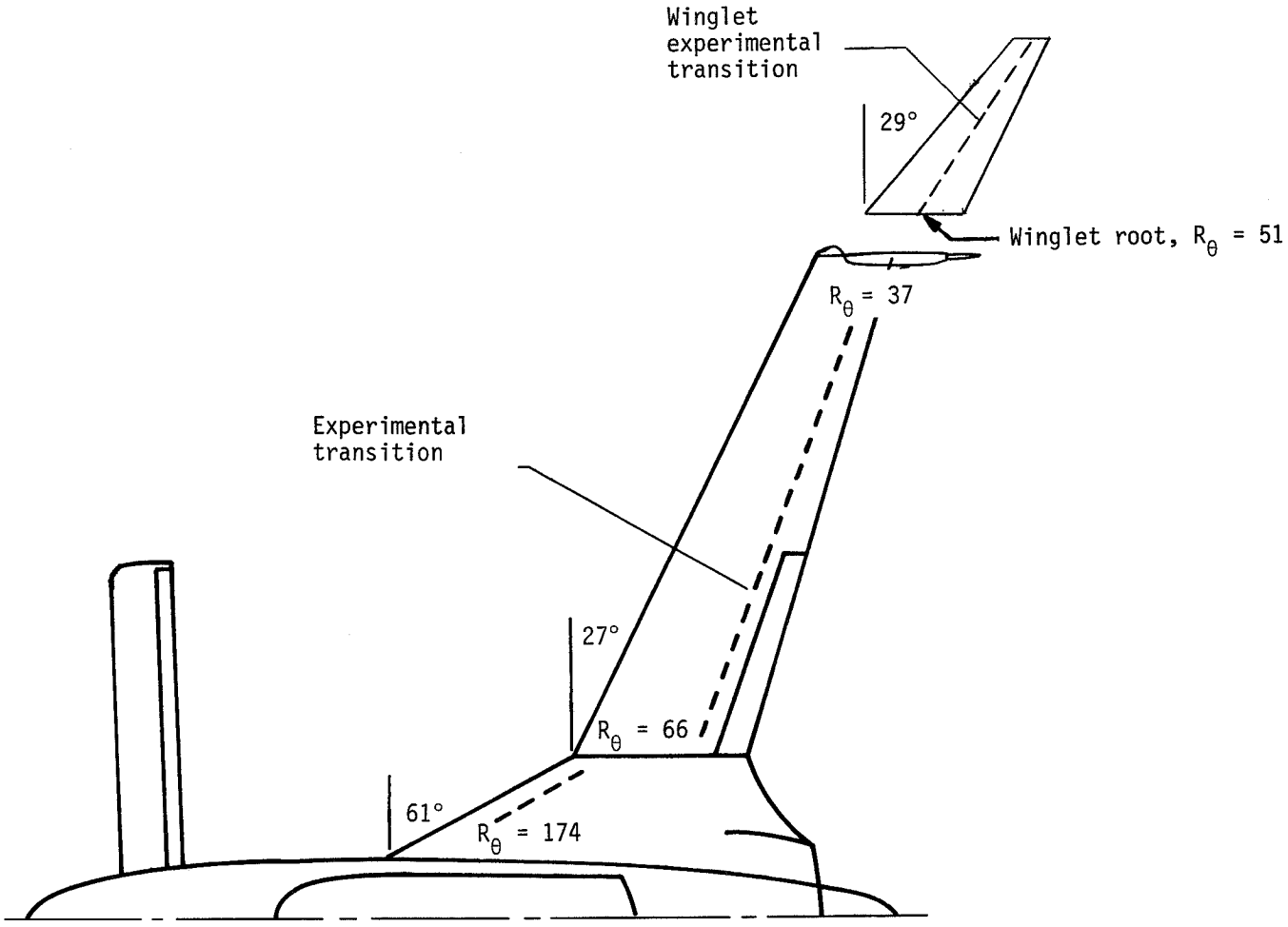

(a) VariEze.

Figure 42.- Comparison of experimental transition data with spanwise contamination criterion.

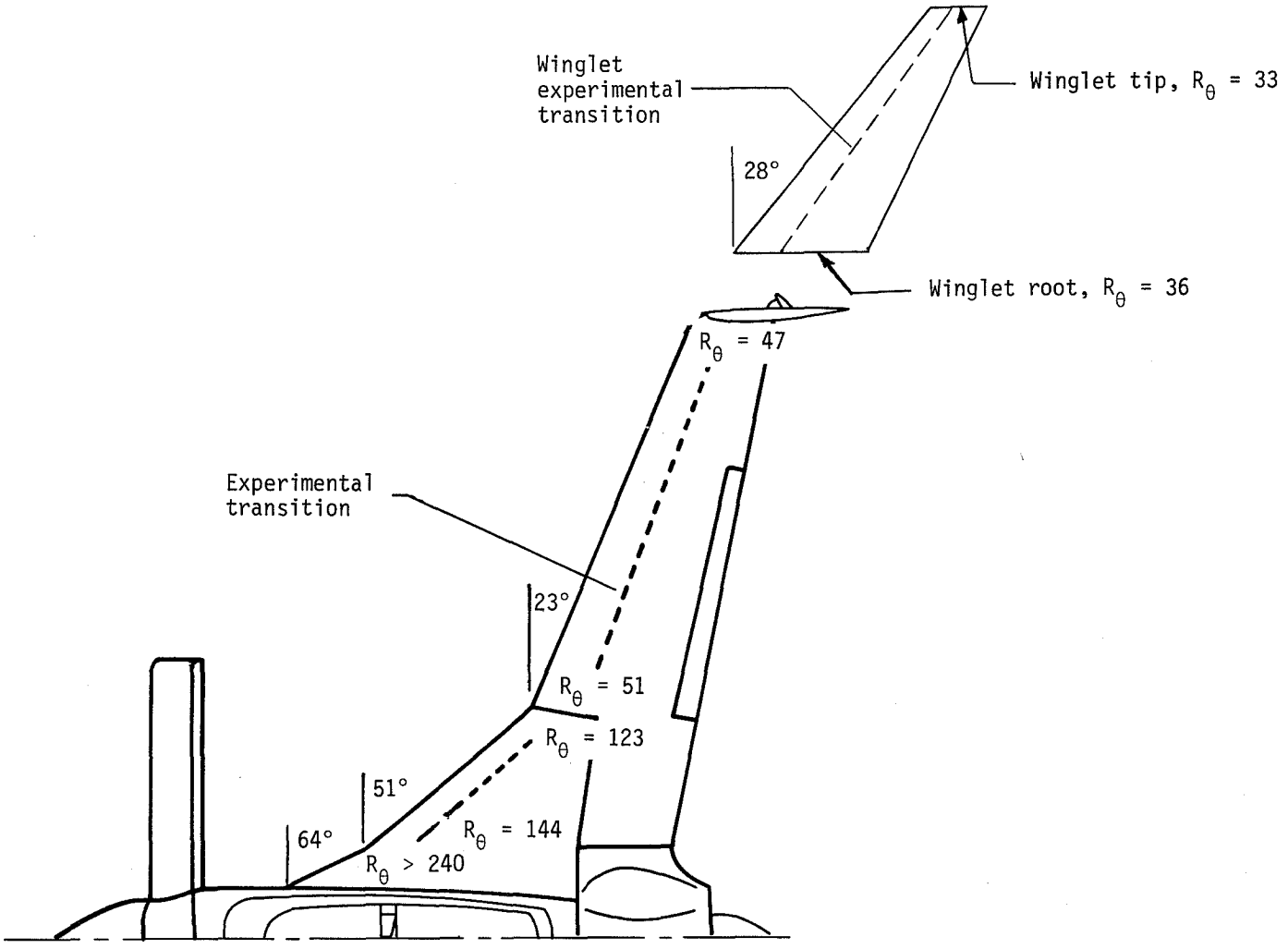

(b) Long-EZ.

Figure 42.- Concluded.

1. Report No.	2. Government Accession No.	3. Recipient's Catalog No.
NASA TP-2256		

4. Title and Subtitle	5. Report Date
NATURAL LAMINAR FLOW EXPERIMENTS ON MODERN AIRPLANE SURFACES	June 1984
	6. Performing Organization Code: 505-45-43-02
7. Author(s): Bruce J. Holmes, Clifford J. Obara, and Long P. Yip	8. Performing Organization Report No.: L-15552
	10. Work Unit No.
9. Performing Organization Name and Address: NASA Langley Research Center, Hampton, VA 23665	11. Contract or Grant No.
	13. Type of Report and Period Covered: Technical Paper
12. Sponsoring Agency Name and Address: National Aeronautics and Space Administration, Washington, DC 20546	14. Sponsoring Agency Code

15. Supplementary Notes

Bruce J. Holmes and Long P. Yip: Langley Research Center, Hampton, Virginia.
Clifford J. Obara: Kentron International, Inc., Hampton, Virginia.

16. Abstract

Flight and wind-tunnel natural laminar flow experiments have been conducted on various lifting and nonlifting surfaces of several airplanes at unit Reynolds numbers between 0.63×10^6 ft^{-1} and 3.08×10^6 ft^{-1}, at Mach numbers from 0.1 to 0.7, and at lifting surface leading-edge sweep angles from 0° to 63°. The airplanes tested were selected to provide relatively stiff skin conditions, free from significant roughness and waviness, on smooth modern production-type airframes. The observed transition locations typically occurred downstream of the measured or calculated pressure peak locations for the test conditions involved. No discernible effects on transition due to surface waviness were observed on any of the surfaces tested. None of the measured heights of surface waviness exceeded the empirically predicted allowable surface waviness. Experimental results consistent with spanwise contamination criteria were observed. Large changes in flight-measured performance and stability and control resulted from loss of laminar flow by forced transition. Rain effects on the laminar boundary layer caused stick-fixed nose-down pitch-trim changes in two of the airplanes tested. No effect on transition was observed for flight through low-altitude liquid-phase clouds. These observations indicate the importance of fixed-transition tests as a standard flight testing procedure for modern smooth airframes. The results taken as a whole indicate that significant regions of natural laminar flow exist and that this boundary-layer behavior is more durable and persistent on certain modern practical production airplane surfaces than previously expected.

17. Key Words (Suggested by Author(s))	18. Distribution Statement
Laminar flow Natural laminar flow General aviation Laminar boundary layer Flight experiments	Unclassified - Unlimited Subject Category 02

19. Security Classif. (of this report)	20. Security Classif. (of this page)	21. No. of Pages	22. Price
Unclassified	Unclassified	143	A07

For sale by the National Technical Information Service, Springfield, Virginia 22161 NASA-Langley, 1984